Studying the Indian monsoon variability over the Early Holocene and Common Era in high resolution with numerical reconstructions based on planktic foraminifera

Dissertation

der Mathematisch-Naturwissenschaftlichen Fakultät
der Eberhard Karls Universität Tübingen
zur Erlangung des Grades eines
Doktors der Naturwissenschaften
(Dr. rer. nat)

vorgelegt von
Dipl.-Geol. Philipp Moritz Munz
aus Filderstadt

Tübingen
2016

Gedruckt mit Genehmigung der Mathematisch-Naturwissenschaftlichen Fakultät der Eberhard Karls Universität Tübingen.

Tag der mündlichen Qualifikation:	13.07.2016
Dekan:	Prof. Dr. Wolfgang Rosenstiel
1. Berichterstatter:	Dr. Hartmut Schulz
2. Berichterstatter:	Prof. Dr. Michal Kucera

Abstract

The Indian Monsoon is an impressive seasonal climate phenomenon and an important driver for the inter-hemispheric transport of heat and moisture. Due to the strongly seasonal character, the Indian Monsoon is subdivided into the Indian Summer Monsoon (ISM), which is most intense from July to September, and the Indian Winter Monsoon (IWM), which generally occurs from January to March. The ISM and accompanied precipitation is an important source of freshwater, because it brings most of the annual rainfall to India and its neighbouring countries. To assess the future development of ISM variability is therefore of utmost importance for the economic prosperity and agricultural development in one of the worlds' most densely populated regions. The understanding of potential ISM response to different scenarios of future climate changes requires detailed knowledge of the monsoon history. It is therefore vital to study archives of past ISM variability on time scales that are important for societal development, i.e. years to decades. Furthermore, our understanding of the monsoon system and its potential driving forces is incomplete without better knowledge of IWM variability.

Due to the extreme seasonality of the Indian Monsoon, induced by the opposing direction of the prevailing surface winds, the monsoons exert a strong influence on the hydrography of the Arabian Sea. The ISM is characterized by intensive upwelling, associated with surface water cooling and elevated surface water productivity in the northwestern Arabian Sea. The dry and cold winds of IWM are associated with evaporative cooling of surface waters and convective deepening of the mixed-layer, which leads to nutrient entrainment and elevated surface water productivity in the northeastern part of the basin. High primary productivity and reduced ventilation of intermediate waters leads to strong and stable oxygen deficient conditions at mid-depth. The conditions within the oxygen minimum zone (OMZ) favor the removal of nitrogen via reduction of biologically available inorganic nitrogen to nitrous oxide (N_2O), which is an important greenhouse gas.

This thesis focuses on the reconstruction of both seasonal monsoon components throughout three relatively short time slices of the Holocene epoch in ultra high resolution using a collaborative multi-proxy approach. In order to study past changes of the monsoon seasons, three hemipelagic sediment cores from the Arabian Sea region were studied. One core from the northern Oman margin is deposited under the dominant influence of ISM conditions, whereas two other cores from the Pakistan margin are mainly under IWM influence. Sea surface temperatures (SST) derived from transfer functions based on census counts of planktic foraminifera were studied in comparison to geochemical proxies, alkenone biomarkers and trace elemental composition in planktic foraminiferal calcite.

During the first of the three time slices, the last 250 years, IWM conditions were coupled to large-scale oscillation patterns originating in the Pacific (El Niño-Southern Oscillation, ENSO and Pacific Decadal Oscillation, PDO) and Atlantic (North Atlantic Oscillation, NAO). The coupling, however, was not stable but weakened since the beginning of the 20th century. Phases of very intense IWM conditions were coupled to NAO, suggesting a strong extratropical link to the monsoon climate. Over the second interval, the last 2,000 years, the 'Common Era' (CE) variations of IWM conditions on centennial-scales were linked climatic warm phases of the North Atlantic region, namely the end of the 'Roman Warm Period' (at ~450 CE) and the 'Medieval Warm Period' (~950–1250 CE). The third interval during the early- to mid-Holocene is marked by more intense ISM conditions compared to modern times. The results further suggest, that, instead of water mass changes, bottom-water OMZ conditions were controlled by surface water processes during weak ISM phases.

Kurzfassung

Der Indische Monsun ist ein beeindruckendes Klimaphänomen und ein wichtiger Einflussfaktor für den interhemisphärischen Wärme- und Feuchtetransport. Aufgrund des starken saisonalen Charakters wird der Indische Monsun unterteilt in Indischen Sommermonsun (ISM), welcher von Juli bis September vorkommt, und Indischen Wintermonsun (IWM), welcher von Januar bis März vorkommt. Der ISM und die mit ihm einhergehenden Niederschläge ist eine wichtige Frischwasserquelle, da er für den größten Teil des jährlichen Niederschlages in Indien und den umliegenden Ländern verantwortlich ist. Die künftige Entwicklung der ISM Variabilität abschätzen zu können ist daher von höchster Wichtigkeit für den wirtschaftlichen Erfolg und die landwirtschaftliche Entwicklung in einer der dichtbesiedelsten Regionen der Erde. Das Verständnis potentieller Veränderungen des ISM aufgrund zukünftiger Klimaveränderungen erfordert die genaue Kenntnis der Monsungeschichte. Daher ist es entscheidend Archive vergangener ISM Variabilität auf Zeitskalen zu untersuchen, die wichtig für gesellschaftliche Entwicklungen sind, d.h. Jahre bis Dekaden. Darüberhinaus ist unser Verständnis des Monsunsystems ohne eine bessere Kenntnis der IWM Variabilität unvollständig.

Aufgrund der extremen Saisonalität des Indischen Monsuns, die durch gegensätzliche Richtungen der vorherrschenden oberflächennahen Winde hervorgerufen wird, hat der Monsun einen starken Einfluss auf die Hydrographie des Arabischen Meeres. Der ISM wird durch intensiven Auftrieb charakterisiert, der von Abkühlung des Oberflächenwassers und erhöhter Wasseroberflächenproduktivität im nordwestlichen Arabischen Meer begleitet ist. Die trockenen und kalten Winde des IWM sind verbunden mit Verdunstungskühlung des Oberflächenwassers und einer konvektiven Vertiefung der durchmischten Schicht, was zu Nährstoffeintrag und erhöhter Wasseroberflächenproduktivität im nordöstlichen Teil des Beckens führt. Hohe Primäproduktion und verminderte Durchlüftung des Zwischenschichtwassers führt zu starken und stabilen Sauerstoffmangelbedingungen in

mittleren Wassertiefen. Die Bedingungen in der Sauerstoffminimumzone (OMZ) begünstigen den Entzug von Stickstoff über die Reduktion von biologisch verfügbarem anorganischem Stickstoff zu gasförmigem Distickstoffmonoxid (N_2O), einem wichtigen Treibhausgas.

Diese Dissertation konzentriert sich auf die ultrahochauflösende Rekonstruktion beider saisonaler Monsunkomponenten während dreier relativ kurzer Zeitscheiben des Holozäns mithilfe eines gemeinschaftlichen Multi-Proxy-Ansatzes. Um die vergangenen Änderungen des Monsunsystems zu untersuchen, wurden drei hemipelagische Sedimentkerne aus der Region des Arabischen Meeres untersucht. Ein Kern vom nördlichen Kontinenthang vor Oman wurde unter dem maßgeblichen Einfluss des ISM abgelagert, wohingegen zwei weitere Kerne vor Pakistan hauptsächlich unter dem Einfluss des IWM standen. Basierend auf Zählungen planktischer Foraminiferen wurden mittels Transferfunktionen Meeresoberflächentemperaturen (SST) abgeleitet und im Vergleich zu geochemischen Proxies, Alkenon-Biomarkern und Spurenelementzusammensetzungen im Kalzit planktischer Foraminiferenschalen untersucht.

Während der ersten der drei Zeitscheiben, der letzten 250 Jahre, waren IWM Bedingungen anscheinend an groß-skalige Oszillationsmuster gekoppelt, die ihren Ursprung im Pazifik (El Niño-Southern Oscillation, ENSO und Pazifische Dekadenoszillation, PDO) und Atlantik (Nordatlantische Oszillation, NAO) haben. Die Kopplung war jedoch nicht stabil, sondern nahm seit Beginn des 20. Jahrhunderts ab. Phasen sehr intensiver IWM Bedingungen waren an NAO gekoppelt, was eine starke extratropische Verbindung des Monsunklimas andeutet. Während des zweiten untersuchten Intervals, der letzten 2.000 Jahre, die 'Common Era' (CE), waren Variationen des IWM auf hundertjährigen Zeitskalen mit Warmphasen der Nordatlantikregion verbunden, nämlich dem Ende der Römischen Warmzeit (um ~450 CE) und der Mittelalterlichen Warmzeit (~950–1250 CE). Das dritte Interval während des frühen bis mittleren Holozäns ist im Gegensatz zu heute durch intensivere ISM Bedingungen geprägt. Die Ergebnisse deuten darüberhinaus darauf hin, dass anstelle von Veränderungen der Zwischenwassermassen, die OMZ Bedingungen durch Prozesse des Oberflächenwassers während schwächerer ISM-Phasen beeinflusst wurden.

Acknowledgments

The work presented in this thesis was conducted within the collaborative research project "*Natural versus anthropogenic controls of past monsoon variability in Central Asia recorded in marine archives (CARIMA)*" funded by the German Ministry of Education and Research (BMBF). The project involved a close collaboration with colleagues from the University of Hamburg, the MARUM (University Bremen), the ZMT Bremen and the BGR Hannover. I want to thank all friends and colleagues who supported me during the time of this thesis.

First and foremost I want to thank Hartmut Schulz for giving me the chance to work on this interesting and fascinating project and for being a mentor who was always a source of advice and motivation. Thank you for the invaluable experiences and excellent support during the last four years, which I do not take for granted.

I am grateful to the support of Michal Kucera as my co-supervisor, whose suggestions and inspiration were crucial for the success of this study.

Further, I thank Annett Junginger and Hervé Bocherens, who agreed to volunteer as members of the thesis committee.

I thank all colleagues involved in the CARIMA project, especially Andreas Lückge, Stephan Steinke, Birgit Gaye, Anna Böll, Tim Rixen and Sven Forke. Further thanks go to Jeroen Groeneveld for conducting the ICP-OES analyses.

Special thanks also go to Annett Junginger for the generous support in procuring and providing further external funding. I thank everyone in the Mikropal working

group for the great time during the past years. My diligent Hiwis, Igor Cerkasin, Tatjana Epp, Dorothea Mosandl, Kristina Pascher and Patrick Schwarz, were an enormous help during the early phases of intensive lab work.

I am deeply grateful for the constant encouragement and tireless support of my beloved family. Mama and Shaby, this thesis would never have been possible without you! At last and above all, thank you Ines for your enduring and patient support and that you always believed in me.

List of Figures

List of Tables

List of publications

Contributions published in a peer-reviewed journal or in preparation for submission to fulfil the requirements of a cumulative dissertation. Percentages of own contributions are given in the following order: original idea/data collection/data analysis/writing.

Paper I (page 43): Munz, P. M., A. Lückge, M. Siccha, A. Böll, S. Forke, M. Kucera, and H. Schulz: ´The Indian winter monsoon and its response to external forcing over the last two and a half centuries´. Submitted to *Climate Dynamics*.

Status: revise (minor revisions)
Own contributions: 70/80/100/80

Paper II (page 69): Böll, A., A. Lückge, **P. Munz**, S. Forke, H. Schulz, V. Ramaswamy, T. Rixen, B. Gaye, and K.-C. Emeis (2014): ´Late Holocene primary productivity and sea surface temperature variations in the northeastern Arabian Sea: Implications for winter monsoon variability´. *Paleoceanography* 29(8), 778–794. doi:10.1002/2013PA002579.

Status: published
Own contributions: 0/20/20/10

Paper III (page 105): Munz, P. M., M. Siccha, A. Lückge, A. Böll, M. Kucera, and H. Schulz (2015): ´Decadal-resolution record of winter monsoon intensity over the last two millennia from planktic foraminiferal assemblages in the northeastern Arabian Sea´. *The Holocene* 25(11), 1756–1771. doi:10.1177/0959683615591357.

Status: published
Own contributions: 60/80/100/80

Paper IV (page 145): Munz, P. M., S. Steinke, A. Böll, A. Lückge, J. Groeneveld, M. Kucera, and H. Schulz: ´Variability of the Indian summer monsoon during early- to mid Holocene and its relation to bottom-water conditions at the northern Oman margin´. *in preparation*.

Status: in preparation
Own contributions: 60/80/80/70

Contents

PART I

Synopsis

CHAPTER 1

Introduction

1.1 Background of the study

The Indian monsoon is the main promoter of inter-hemispheric moisture and heat transport and clearly one of the worlds most important and spectacular climate phenomena. It is subdivided into a summer and winter monsoon component. The summer monsoon brings most of the annual rainfall to India and its neighbouring countries. Therefore, the timing, onset, strength and intensity fluctuations of the summer monsoon largely determine the agricultural and economic prosperity in one of the most densely populated regions (e.g., Sivakumar and Stefanski, 2010). Observations from instrumental data over the past century indicate that the Indian summer monsoon has fluctuated on annual to decadal time scales (Sontakke and Singh, 1996). Relationships of recent monsoonal intensity fluctuations involves internal and external climate forcing (e.g., Wang et al., 2005). However, the magnitude of external natural (e.g., solar activity) and anthropogenic (e.g., greenhouse gas emissions, aerosols, land use changes) impact and internal modulations of global atmospheric oscillation systems on inter-annual- (e.g. El Niño-Southern Oscillation, ENSO) and decadal time scale (e.g. Indian Ocean Dipole, IOD; Atlantic Multidecadal Oscillation, AMO; Pacific Decadal Oscillation, PDO) are poorly understood.

The monsoonal precipitation has a strong impact on the global carbon cycle, by affecting continental erosion, silicate weathering on land and carbon burial (e.g., Galy et al., 2007; Hren et al., 2007). Moreover, high surface water productivity with associated respiration and oxygen consumption in the water column, leads to strong oxygen deficient conditions at mid depth. The strong hypoxia within

the OMZ favor the production of nitrous oxide (N_2O), an important greenhouse gas, through the process of denitrification. Better knowledge of the role and impact of these processes on the climate system has become an important task in the last decade, as to the alarming risk of global sea-level rise and warming. Studying the decadal- to centennial scale variability of the monsoon system with long records beyond the instrumental period, quantitatively tracing summer and winter conditions independently, is therefore vital to understand the response to short-term climate fluctuations and involved feedback mechanisms.

1.2 The seasonal cycle of the Indian monsoon and its controlling mechanisms

The general setting of the northern Indian Ocean is substantially different from the other two major oceanic basins, the Atlantic and the Pacific. North of ~25 °N, the Indian Ocean is confined by the landmass of the Eurasian continent, making it essentially a tropical basin. Seasonally changing insolation determined by the solar zenith angle induces an alternating land–sea thermal contrast, which drives a large-scale atmospheric thermal circulation and induces strong seasonality in the wind direction and precipitation patterns (Meehl, 1994; Webster et al., 1998). Ascending warm air masses over the continent lead to a latitudinal northward displacement of the low-pressure cell associated with the Intertropical Convergence Zone (ITCZ) during Northern Hemisphere summer (Figure 1.1 a), often referred to as the 'Monsoon trough' (Wang, 2006). It is currently debated whether the summer monsoonal circulation is driven by elevated surface sensible heating of the mountain plateaus in Central Asia, which acts as a sensible heat-driven air-pump (Wu et al., 2012, and references therein), or if thermal insulation provided by the Himalayas mountain ranges blocks the intrusion of cold air masses from the north, leading to peak upper tropospheric temperatures south of the plateau (Boos and Kuang, 2010). Southwesterly summer monsoonal winds are drawn northward to compensate for the near-surface pressure gradient between the Indian Ocean High and the Tibetan Low (Figure 1.1 a). This is associated with intense interhemispheric convergence of warm and moist surface winds over continental South Asia.

During Northern Hemisphere winter, the maximum solar insolation and associated low-pressure zone is located south of the equator in the northern Australian

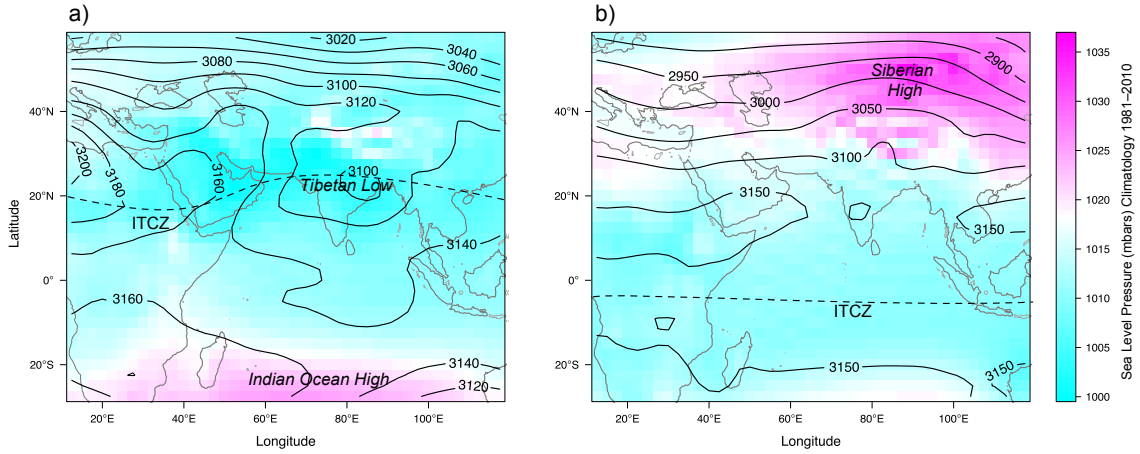

Figure 1.1: Atmospheric setting over the Indian Ocean and the adjacent continents, indicating the pressure gradients during **(a)** boreal summer (July–September) and **(b)** winter (January–March) season. Contour lines indicate the geopotential height at the 700 millibar level, coloured grid gives the long-term mean of sea-level pressure in millibars. The dashed line indicates the approximate position of the low-pressure belt of the Intertropical Convergence Zone (ITCZ). Data are derived from long-term monthly means (1981–2010) from NCEP/NCAR Reanalysis 1 (Kalnay et al., 1996) available from the NOAA Earth System Research Laboratory (http://www.esrl.noaa.gov/)

region (Figure 1.1 b). Cold air accumulates over northern continental Eurasia, building a very strong anticyclonic high-pressure cell referred to as the Siberian High (Ding, 1994). This induces divergence of dry and cold air with low-level northeasterly winter winds, providing an atmospheric link between the tropics and extratropical climate of the northern high latitudes (Ding, 1990).

In addition to the above mentioned solar insolation control on the land-ocean pressure gradient, there is apparently some degree of internal feedback mechanism e.g., through release of latent heat by precipitation and thus internal reinforcement of the atmospheric circulation (Webster et al., 1998). Although climate models suggest an intensification of monsoon winds and precipitation under a global warming scenario (Meehl and Washington, 1993; Wang et al., 2013), such internal feedbacks could lead the monsoon system to cross a critical tipping point, potentially triggered by aerosol pollution (Levermann et al., 2009).

1.3 Modern hydrographic conditions of Arabian Sea surface waters during an annual cycle

During summer (SW Monsoon), winter (NE Monsoon), as well as the spring and fall intermonsoon seasons, the alternating monsoonal circulation has a considerable impact on the physical hydrography in the Arabian Sea (Wyrtki, 1973). The cross-equatorial surface winds during SW Monsoon from June to September, referred to as the Somali or Findlater Jet (Findlater, 1969), reach wind speeds of more than 15 m/s (Figure 1.2 a). Frictional wind stress drives an anticyclonic circulation pattern in the Arabian Sea, where surface water masses are transported northeastwards along the coast of Somalia and Oman. Ekman transport along the coast and along the axis of the jet leads to offshore-directed deflection of the surface flow, which is compensated by upwelling. The process of upwelling induces vertical mixing of colder, nutrient-rich intermediate water masses, thereby decreasing sea surface temperatures (SST), increasing nutrient availability in the photic zone and nourishing primary productivity (Hastenrath and Lamb, 1979).

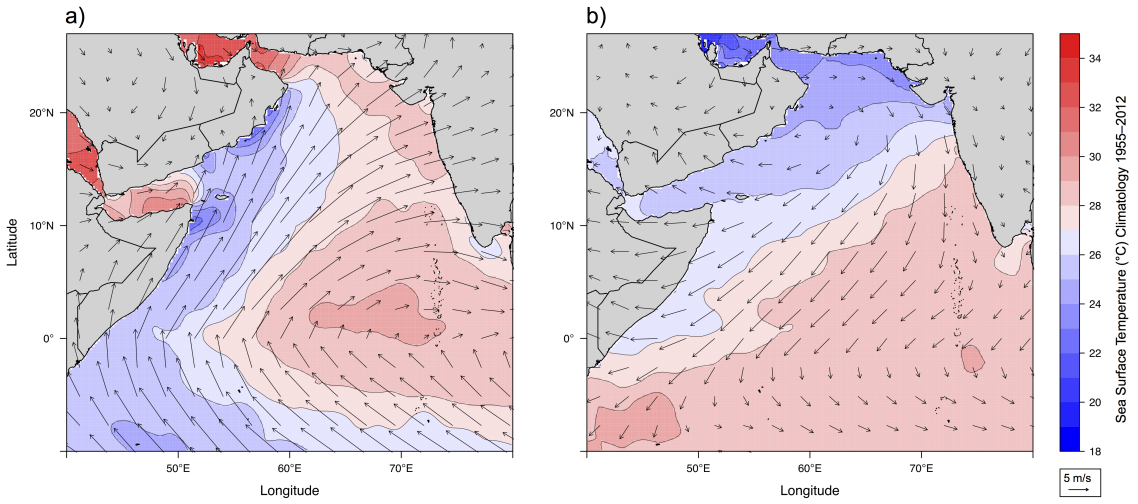

Figure 1.2: Sea surface temperature and prevailing winds at sea level pressure in the Arabian Sea region during **(a)** summer (July–September) and **(b)** winter (January–March). Sea surface temperature data are obtained from the World Ocean Atlas 2013 v2 (Locarnini et al., 2013) averaged over the available decades (1955–2012). Wind data are derived from long-term monthly means (1981–2010) from NCEP/NCAR Reanalysis 1 (Kalnay et al., 1996) available from the NOAA Earth System Research Laboratory (http://www.esrl.noaa.gov/).

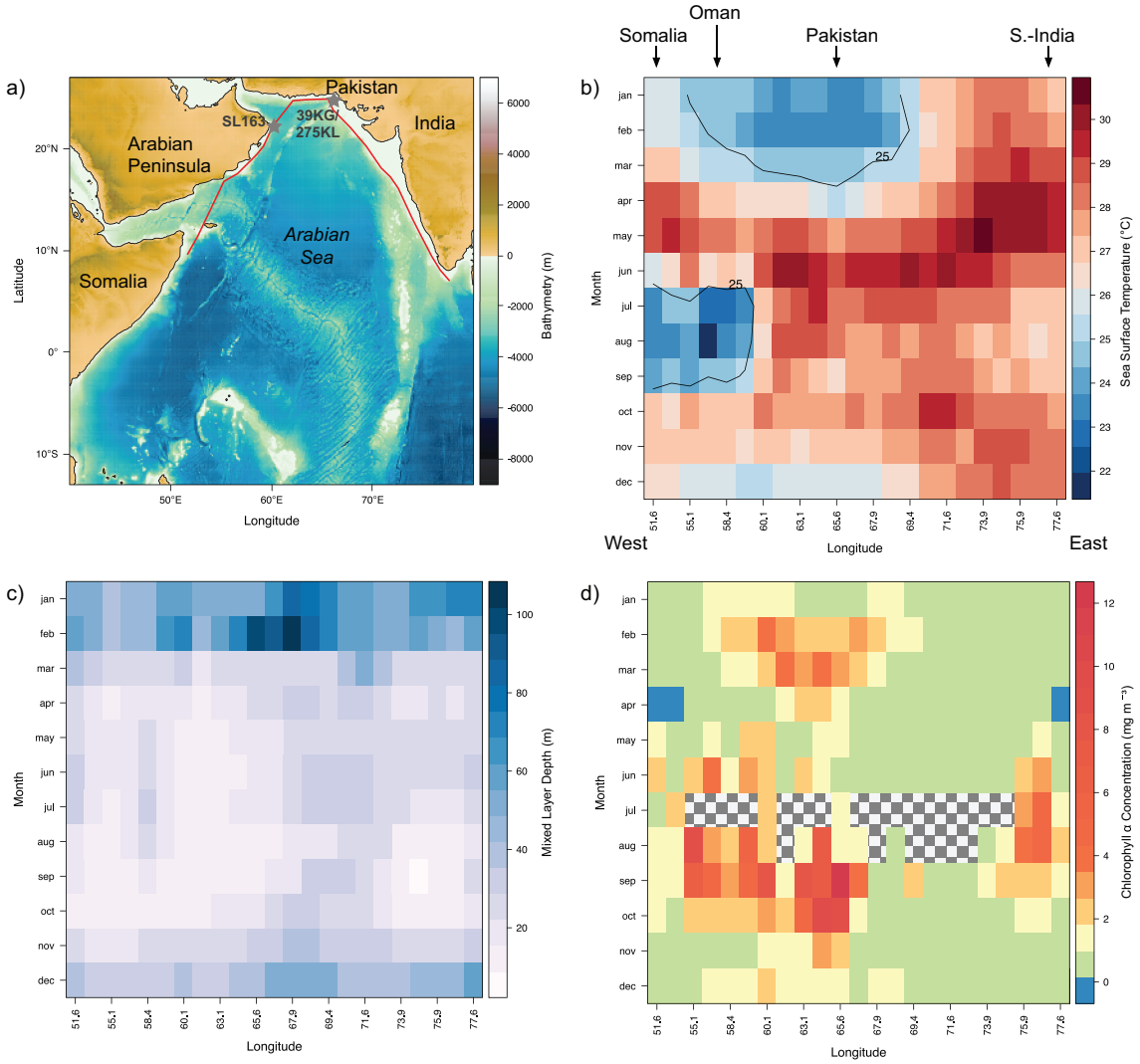

Figure 1.3: (a) shows a bathymetric map of the Arabian Sea with stars indicating the locations and names of the studied sediment cores at the northern Oman margin and the Pakistan margin. Along the path of the red line, monthly surface water properties were extracted and plotted in Hovmöller-like diagrams: the annual time evolution of sea surface temperature **(b)**, mixed-layer depth **(c)** and chlorophyll α **(d)**. Coldest temperatures are found during January and February in the northeastern Arabian Sea and during July to September in the western Arabian Sea (b; the 25 °C contour line is indicated). Winter cooling at $65 - 68$ °E is associated with a deepening of the mixed layer (c). Satellite-derived chlorophyll α measurements show enhanced winter productivity in the northeastern Arabian Sea from February to March (d). Summer productivity is partially obscured by cloud cover (chessboard pattern), but still indicates that productivity onset starts in June at the Oman margin and maximum productivity is found during late summer at the Pakistan margin. Data of (b) are from the World Ocean Atlas 2013 v2 (Locarnini et al., 2013), for (c) from the World Ocean Atlas 1994 (Monterey and Levitus, 1997) and for (d) from the monthly climatology of SeaWiFS and Aqua-MODIS sensors (NASA Goddard Space Flight Center, 2014).

Because Ekman transport is confined to the left side of the surface flow direction, coldest summer SST are being observed in the western Arabian Sea and at the southern tip of the Indian peninsula (Figure 1.2 a). During boreal winter (November to February), lower solar radiation and dry continental air masses associated with the NE Monsoon (Figure 1.2 b) increase salinity and evaporative cooling of surface waters (Prasanna Kumar and Prasad, 1996). Through a reduction of the vertical density stratification, mixed-layer deepening enables mixing of nutrients from deeper waters into the photic zone, leading to increased primary productivity during winter (Madhupratap et al., 1996; Morrison et al., 1998; Prasanna Kumar et al., 2000; Wiggert et al., 2002). To visualize the seasonal succession of physical and biological sea surface parameters in the Arabian Sea in more detail, a monthly grid of measurements along an arch-shaped transect from the eastern margin of Somalia and Arabia to the western margin of India was produced (Figure 1.3 a). The monthly distribution of sea surface temperature (SST), mixed-layer depth and chlorophyll-α is described below.

1.3.1 Temperature

Upwelling along the western boundary of the Arabian Sea, induced by strong southwesterly monsoonal winds, leads to SST below 25 °C off the continental margin of Somalia (51.5 °E) and Oman (57 − 60 °E) (Figure 1.3 b). Winter cooling at these locations is less intense compared to the Pakistan Margin (65.5 °E), where the seasonal distribution of minimum SST is opposite to the Somali-/Oman Margin. Along the Pakistan Margin, no upwelling occurs during summer and temperatures are above 27 °C from June to August. However, coldest SST below 25 °C found during January and February are associated with the Northeast Monsoon (Banse, 1968). In comparison to the northwestern Arabian Sea, the southeastern Arabian Sea at the southern tip of India is less affected by cold summer upwelling temperatures. All locations of the transect are marked by an annual temperature maximum during the inter-monsoon seasons during boreal spring (April–June) and fall (October–November)

1.3.2 Mixed-layer depth

The topmost oceanic layer, the mixed-layer, is defined by a relatively homogeneous density profile. Its depth is determined by the absence of steep physical gradients and it is thus used as a measure of stability of the upper water column. Over the

entire near-coastal transect in the Arabian Sea, a relatively shallow mixed-layer above 30 m can be observed from March to November (Figure 1.3 c). During the summer months, a small deepening occurs along the Somali- and Oman Margin as a consequence of the upwelling process, as well as in the eastern part of the basin. However, during winter (December–February) a substantial deepening is noticeable at all stations, with maximum depths found between 80–100 m offshore Pakistan during February. In the northern Arabian Sea, excess evaporation over precipitation during winter leads to evaporative heat loss and the formation of high salinity surface waters, which enables convective deep mixing (Prasanna Kumar and Prasad, 1996, 1999).

1.3.3 Chlorophyll α

Satellite-derived measurements of surface water properties are available in a wide range of compositing time periods from a few days to several years (NASA Goddard Space Flight Center, 2014). In the Arabian Sea, even the measurements binned over the entire mission partially suffer from extensive cloud cover during the summer monsoon. Although this results in a number of data gaps during July and August in Figure 1.3 d, it is still apparent that maximum chlorophyll α concentrations are found during the summer months. In the northwestern Arabian Sea, primary productivity peaks from June to September, whereas in the northeastern part a second productivity maximum occurs from February to March. The southeastern part of the basin is apparently not affected by increased winter productivity. Although the pattern of seasonal SST distribution in Figure 1.3 b revealed that no upwelling occurs off Pakistan during the summer monsoon, chlorophyll α measurements indicate that primary productivity is even higher at this site during September and October compared to the northwestern Arabian Sea. In surface waters of a tropical basin, like the Arabian Sea, nutrient availability instead of lighting conditions is the major limiting factor for biological productivity. It has been suggested that summer productivity in the northeastern Arabian Sea is fuelled by lateral advection of highly productive surface waters from the upwelling regions off Arabia (Andruleit et al., 2000; Schulz et al., 1996). Apparently, the vigorous surface currents in the western part of the basin lead to a quick removal of nitrate-rich upwelling waters before the nutrients can be fully utilized (Prasanna Kumar et al., 2000, 2001). Lateral transport of unutilized nutrients to the northeast during summer thus leads to higher chlorophyll α and primary productivity values

offshore Pakistan and northwest India than in the actual near-coastal upwelling cells.

1.4 State of the art

Research over the past decades (Table 1.1) has shown that past changes of summer monsoon intensity on Milankovitch timescales have been related to Northern Hemisphere summer insolation changes induced by the long-term pattern from the earths' precessional variability (Caley et al., 2011; Clemens and Prell, 2003; Kutzbach and Guetter, 1984). Furthermore, proxy records of summer monsoon variability within the Milankovitch time scales indicate, that shorter fluctuations on millennial- to centennial-scale climate variability are in correspondence with Dansgaard-Oeschger cycles recorded in the Greenland ice cores (Altabet et al., 2002; Bolton et al., 2013; Jung et al., 2009; Kudrass et al., 2001; Schulz et al., 1998; Singh et al., 2011; Sirocko et al., 1993). During the Holocene, evidence for a persistent teleconnection of the summer monsoon to millennial-scale climate comes from records that reveal a dominant ~1470 year cylicity (Gupta et al., 2003; Neff et al., 2001), a cycle that is known from North Atlantic drift ice records (Bond et al., 2001). It is, however, debated whether atmospheric (Marzin et al., 2013; Reichart et al., 2002; Schulz et al., 1998) or oceanic (Hong et al., 2003; Schulte and Müller, 2001) linkages are responsible for the teleconnection between the summer monsoon and North Atlantic climate. Additionally, centennial-scale monsoonal fluctuations are also observed in proxy records from Oman and have been related to solar irradiation changes (Gupta et al., 2005; Neff et al., 2001). Higher frequency variability on decadal to inter-annual timescales of surface water properties in the equatorial Indian Ocean is apparently linked to AMO (Goswami et al., 2006), IOD (Ashok et al., 2001; Saji et al., 1999; Webster et al., 1999) and ENSO (Krishna Kumar et al., 1999), also affecting the Indian monsoonal system (e.g., Gadgil, 2003, 2004). Most proxy evidence for decadal-scale monsoon variability during the Holocene comes from terrestrial precipitation records, such as cave speleothems from the Oman Peninsula and Andaman Islands (e.g., Fleitmann et al., 2007; Laskar et al., 2013). However, despite that cave $\delta^{18}O$ values can only infer a semi-quantitative measure of the past hydrological cycle, they may further be controlled by a combination of several different processes other than precipitation, as it was suggested for Chinese caves (e.g., Maher, 2008).

Our knowledge of the Indian monsoon system is, however, incomplete without

records of the winter monsoon component. Such records are scarce (Table 1.1), partly due to the lack of appropriate archives recording winter monsoon conditions quantitatively and independent from the summer monsoon. Studying winter monsoon variations prior to the instrumental era is vital to understand the overall development of the monsoon system and better predict future variation.

Table 1.1: Comparison of time range and resolution of published quantitative paleoclimate reconstructions of the marine Indian monsoon realm.

Reconstructed parameter	Season	Proxy	Area of investigation	Time range	Resolution (years)	Reference
SST	annual	Mg/Ca, $\delta^{18}O$	Entire Arabian Sea	0–20 ka	6,300	Dahl and Oppo, (2006)
SST	annual	Alkenone $U^{K'}_{37}$	Oman margin	0–500 ka	2,000	Emeis et al., (1995)
SST	seasonal	Mg/Ca, $\delta^{18}O$	Somali margin	0–20.7 ka	6,000	Ganssen et al., (2011)
SST	annual	Alkenone $U^{K'}_{37}$	Eastern Arabian Sea	0–240 ka	1,500	Rostek et al., (1997)
SST,SSS	annual	Mg/Ca, $\delta^{18}O$	Equatorial Indian Ocean	0–137 ka	1,000	Saraswat et al., (2012, 2005)
SST	annual	Alkenone $U^{K'}_{37}$	Eastern Arabian Sea	0–65 ka	800	Schulte and Müller, (2001)
SST,SSS	annual	Mg/Ca, $\delta^{18}O$	Eastern Arabian Sea	0–100 ka	700	Banakar et al., (2010)
SST,SSS	annual and summer	Mg/Ca, $\delta^{18}O$	Eastern and western Arabian Sea	0–35 ka	550 and 1,100	Anand et al., (2008)
SST,PP	annual	Alkenone $U^{K'}_{37}$ Foraminiferal TF	Eastern Arabian Sea	0–~25 ka	540	Cayre and Bard, (1999)
SST,SSS	annual	Mg/Ca, $\delta^{18}O$	Bay of Bengal	0–25 ka	500	Rashid et al., (2007)
SST,SSS	annual	Mg/Ca, $\delta^{18}O$	Bay of Bengal	0–32 ka	500	Govil and Naidu, (2010)
SST	annual and seasonal	Foraminiferal TF	Oman Margin	0–22 ka	300	Naidu and Malmgren, (2005)
SST	seasonal	Foraminiferal TF	Oman Margin	0–22 ka	300	Godad et al., (2011)
SST	seasonal	Foraminiferal TF	Western Arabian Sea	0–22 ka	300	Schulz, (1995)
SST	annual	Alkenone $U^{K'}_{37}$, TEX_{86}	Western Arabian Sea	0–23 ka	200	Huguet et al., (2006)
SST	annual	Mg/Ca, $\delta^{18}O$	Western Arabian Sea	3–30 ka	200	Saher et al., (2007)
SST	annual	Alkenone $U^{K'}_{37}$	Eastern and western Arabian Sea	0–25 ka	160 and 300	Böll et al., (2015)
SST	annual	Mg/Ca, $\delta^{18}O$	Southeastern Arabian Sea	0–32 ka	140	Saraswat et al., (2013)
SSS	annual	$\delta^{18}O$, Alkenone $U^{K'}_{37}$	Bay of Bengal	0–100 ka	100	Kudrass et al., (2001)
SST	annual	Alkenone $U^{K'}_{37}$	Eastern Arabian Sea	0–2 ka	25	Böll et al., (2014) *
SST	winter	Foraminiferal TF	Eastern Arabian Sea	0–2 ka	9	Munz et al., (2015) *

SST=sea surface temperature, SSS=sea surface salinity, PP=primary production, TF=transfer function methods, *=this study.

1.5 Quantitative environmental reconstructions

Geochemical proxies

Alkenones are long-chained unsaturated ketones, produced by the two haptophytes species *Emiliania huxleyi* and *Gephyrocapsa oceanica*. Culture experiments revealed a linear relationship of the relative abundances of C_{37} alkenones ($U_{37}^{K'}$) with temperature (Prahl et al., 1988). Like all paleotemperature proxies, alkenone-based reconstructions are involved in biological processes and therefore suffer from a number of biases (e.g., Mix et al., 2001, and references therein). For example, the interpretation of alkenone-derived paleotemperatures, usually on the basis of annual mean SST, depend on the growing season of the alkenone producers, which could be biased in environments of strong seasonality (Prahl et al., 2001). Furthermore, organic biomarkers and other small proxies like coccoliths or TEX_{86} hold a potential risk for being redistributed prior to their final deposition on the sea floor. Mollenhauer et al., (2003) compared radiocarbon ages of alkenones and planktic foraminifera from sediments below the upwelling systems off Namibia and found that alkenone ages were substantially older, which was probably an effect of redistribution caused by strong bottom currents.

Foraminifera are a group of single-celled eukaryotic marine Protozoa belonging to the phylum Rhizaria (Cavalier-Smith, 2004). According to their preferred mode of life, they are usually subgrouped into planktic (floating in the water column) and benthic foraminifera (living attached to plants, on or in the substrate). With ca. 50 known modern species of planktic foraminifera (e.g., Kucera, 2007), the diversity is much lower compared to several thousand species of benthic foraminifera. However, there is apparently a yet unknown degree of cryptic diversity within the group of planktic foraminifera (Kucera and Darling, 2002). With ca. 20 species commonly used for paleoceanographic applications, planktic foraminifera are relatively easily distinguishable from other elements in the washed sediment samples. An enourmous body of studies investigated the potential of planktic foraminifera as an indicator, or proxy, for paleoceanographic conditions (e.g., Kucera, 2007, and references therein).

A wide range of proxies make use of the chemical properties of their calcite shells, i.e. by using isotopic compositions or elemental ratios. Oxygen stable isotopes ($\delta^{18}O$) of foraminiferal calcite is commonly used to infer changes of water masses or to correlate sediment cores e.g., with the global ice volume (Shackleton, 1967).

However, the stable isotopic composition is controlled by several factors, including the temperature and salinity, as well as the isotopic composition of the ambient seawater, complicating paleoenvironmental reconstructions based solely on $\delta^{18}O$ (reviewed by Ravelo and Hillaire-Marcel, 2007).

Another approach is followed by measuring trace elemental compositions in planktic foraminiferal calcite. In seawater, there is apparently a thermodynamic response on the inorganic precipitation of magnesium (Mg) in calcite with warmer temperatures (e.g., Mucci, 1987). In laboratory experiments, this relationship was found to be exponential for planktic foraminiferal calcite (Lea et al., 1999; Mashiotta et al., 1999; Nürnberg et al., 1996). In environments, where the succession of planktic foraminiferal species is strongly coupled to the seasonal cycle, this finding offers the potential of reconstructing seasonal SST from monospecific populations (e.g., Anand et al., 2008; Saher et al., 2007). However, a number of potential restrictions might be complicating the use of Mg/Ca ratios for paleoceanographic reconstructions. One serious disadvantage of this technique arises from the heterogeneous distribution of Mg in the tests and individual chambers (e.g., Sadekov and Eggins, 2005). This, at least, requires the calibration and the fossil application to be conducted on foraminiferal shells from the same sharply confined size ranges. Cultural studies further revealed that, apart from the strong temperature effect, also pH and salinity are secondarily affecting the Mg/Ca composition (e.g., Lea et al., 1999). The use of Mg/Ca as a paleoceanographic indicator in environments of strong postdepositional dissolution might be biased by partial removal of more solution-susceptible Mg-rich calcite (Brown and Elderfield, 1996; Dekens et al., 2002; Rosenthal et al., 2000). This can especially be expected in sediments below high-productivity areas where supralysoclinal calcite dissolution is produced by metabolic release of CO_2 during remineralisation of organic matter. However, the actual mechanism of Mg incorporation during foraminiferal shell calcification is still poorly understood (Nehrke et al., 2013).

Reconstructions based on planktic foraminiferal census counts

Paleoenvironmental reconstructions based on assemblage compositions of planktic foraminifera potentially bear the advantage to extract a seasonal signal, if it can be assumed that the respective seasons had the same strong determination on the species assemblage during the deposition of the fossil record as it is observed in the modern environment (Kucera et al., 2005). A further advantage of using

planktic foraminifera as a proxy for paleoceanographic conditions in the northern Arabian Sea, is their numerous occurrence even in a small amount of sediment. Using smaller sample sizes, for instance cutting thinner sections from a U-Channel, enables a higher sampling rate and study the covered interval in more detail.

So-called transfer functions for quantitative paleoenvironmental reconstructions are a suite of tools that can be used to infer past changes in the physical environment of species, in our case planktic foraminifera, based on modern observations. The methodology was first introduced by Imbrie and Kipp, (1971) and has ever since experienced widely increased development, applied to a multitude of different biota, sites and proxies. A transfer function is ideally a mathematical equation that relates changes of an observed modern species abundance matrix (Y_m) to a set of driving environmental parameters (X_m) to calculate past environmental conditions from fossil species abundances: $Y_m = f(X_m) + \text{error}$ (e.g., Juggins and Birks, 2012). As we usually lack *a priori* a mechanistic understanding which factors influence the abundance pattern of biological species, the function $f()$ has to be derived from an empirical calibration. This is usually accomplished by the compilation of a modern calibration data set that combines species counts with measured environmental parameters.

The concept of paleoecological transfer functions is based on several general assumptions and prerequisites (Birks, 1995). The first prerequisite involves the design and development of a calibration data set. This data set should cover the entire range of the environmental parameters in question, which is expected to also have influenced the fossil assemblages (Birks, 1998; Kucera et al., 2005). However, a larger coverage also introduces several sources for noise in the data set, such as a potential increasing influence of cryptic species or the introduction of secondary gradients beyond the scope of the application to the fossil abundances (Kucera et al., 2005). Using samples from the sediment surface for calibration, so-called core tops, bears the advantage that calibration samples are likely affected by the same taphonomic pathways as the fossil samples and involve the same preparation techniques. Another general assumption is based on the causality between the species and the environment, stating that the reconstructed environmental variable is the most important determinant of the ecological system and all other variables are negligible (Birks, 1995). To test whether any of the measured and, if so, which environmental variable meets this criterion, canonical ordination methods like redundancy analysis, are commonly applied. These methods constrain an

ordination to explain the maximum variation of the species abundance data with a set of measured environmental variables (e.g., Legendre and Birks, 2012).

After a calibration data set is properly designed to meet the defined prerequisites, one or more numerical methods are used to perform a predictive regression. The use of modern species–environment relationships to delineate changes of fossil assemblages refers to the principle of uniformitarianism (Birks, 2010), which basically means that fossil and modern species assemblages are affected in the same way by the same environmental gradients. Several methods exist to model environmental parameters from biological abundance data, which have certain advantages and disadvantages (reviewed by Juggins and Birks, 2012). As there is no direct way to assess whether a certain model makes paleoecological sense, the divergence of estimates from a group of methods can be used to assess a model-specific bias (Kucera et al., 2005).

The general performance of a transfer function model is usually validated by the prediction error, an uncertainty estimation based on new data, which was not previously used for calibration. To this end, the data set has to be subsampled to form an independent group of test samples for cross-validation. This is commonly achieved either by using a certain proportion of the data set (k-fold leave-out) or by bootstrapping, a method which replaces with randomly selected samples and iterates this process several hundred times. Although this type of cross-validation is based on a test set which is somehow statistically independent from the training set, the amount of error is still likely under-estimated due to spatial auto-correlation. This effect is based on the tendency of assemblages from geographically close sites to be more similar to each other than assemblages from randomly selected sites (Telford and Birks, 2005, 2009).

Any transfer function will likely produce an arbitrary paleoecological estimate if it is calculated from a random assemblage. Even a robust error estimate does not validate if such a model has statistical relevance. The significance of a reconstruction must therefore be assessed, which can be achieved by comparing the variance of the fossil data explained by a number of random environmental variables with the variance explained by the actual environmental variable in question (Telford and Birks, 2011).

1.6 Research objectives

In order to reconstruct the Indian summer and winter monsoon component independently and address open questions the study has the following research objectives:

- To assess the applicability of a regionally validated transfer function to a fossil dataset of planktic foraminiferal assemblages with the unique preservation potential found in annually laminated sediments.
- To use this transfer function to quantify changes of the intensity of the Indian monsoon, independently for the winter and summer component, over several time slices of the Holocene epoch in high resolution (years to decades) that can be relevant for societies.
- To evaluate potential driving mechanisms of anthropogenic and natural solar origin or large scale circulation patterns using advanced spectral methods.
- To test a potential link between early- to mid Holocene changes of surface and deep-water masses and processes controlling oxygen deficient conditions.

CHAPTER 2

Material and methods

2.1 Selection of samples and stratigraphy

Sediments from the Indian-Pakistani continental slope often show exceptionally well preserved "varve-like", annually laminated sediments (Schulz et al., 1996; von Rad et al., 1999; von Stackelberg, 1972). The preservation of laminae is enabled by absence of bioturbation, due to strongly oxygen depleted bottom-water masses within the permanent oxygen minimum zone (OMZ). Oxygen minimum conditions form due to the combined effect of high rates of decaying organic matter associated with elevated surface water productivities during summer and winter, lateral advection of already low-oxygenated subsurface waters, as well as the prevention of mixing due to the lateral subsurface injection of high-salinity waters originating in the Red Sea and Persian Gulf (Pichevin et al., 2007; Schulz et al., 1996). The OMZ usually impinges on the slope in water depths between roughly 200–1200 m (von Rad et al., 1995). The formation of the distinct hemipelagic laminae in sediments from the Makran continental slope is considered to be linked to the semi-annually alternating monsoonal influence (Lückge et al., 2001; Schulz and von Rad, 2014; Schulz et al., 1996; von Rad et al., 1999). Accordingly, high rates of resuspended fine-grained terrigeneous matter during winter forms typically light-gray, well-sorted, carbonate- and organic carbon-poor, but mica-, chlorite-, and quartz-rich winter laminae. Laminae formed during summer are usually dark, olive-gray, poorly sorted and rich in carbonate- and organic carbon (ca. 3 % C_{org}). Turbulent mixing and resuspension of fine-grained sediments deposited by perennial rivers on the Makran shelf and coastal plains, episodically leads to the formation of suspensate event-deposits (von Rad et al., 1999, and references

therein). These allochthonous deposits are either reddish-brown ("F-layers") or light-gray ("C-layers"), but usually thicker (>1.5 mm, can reach up to 80 mm) compared to the likewise light-gray hemipelagic winter laminae (0.3–0.5 mm). A quick identification of these lithotypes enables to use them as distinct marker horizons (Schulz and von Rad, 2014; von Rad et al., 1999).

For the purpose of this study, two sediment cores from the Makran continental slope off Pakistan and one core from the northern Oman margin were used (Figure 1.3 a). The cores from the Pakistan margin were stored at the core repository of the Bundesanstalt für Geowissenschaften und Rohstoffe in Hannover/Germany. It includes the uppermost 1.8 m of piston core SO130-275KL, retrieved in 1998 from 782 m water depth at the position 24 °49.31'N; 065 °54.60'E (von Rad et al., 1998) and box core SO90-39KG, which was retrieved five years earlier from the same position. One of the advantages of using these cores is that they run parallel to the already well-studied core SO90-56KA, previously dated using varve counts and AMS ^{14}C datings (von Rad et al., 1999). Correlation of both cores using a layer-by-layer tracking of 52 C- and F-layers as marker horizons between 56KA and 275KL (Figure 2.1) provided detailed age control for core 275KL. The uppermost 188 cm of core 275KL are accordingly covering the interval from 403 BCE until 1893 CE and the 44 cm long core 39KG covered the partly overlapping interval 1738 CE until 1993 CE.

The sediment core from the summer upwelling region off the Oman margin is gravity core M74/1b-SL163, which was recovered in 2007 from 650 m water depth at the position 21 °55.97'N, 059 °48.15'E (Bohrmann et al., 2010) and stored at the core repository of the University of Tübingen/Germany.

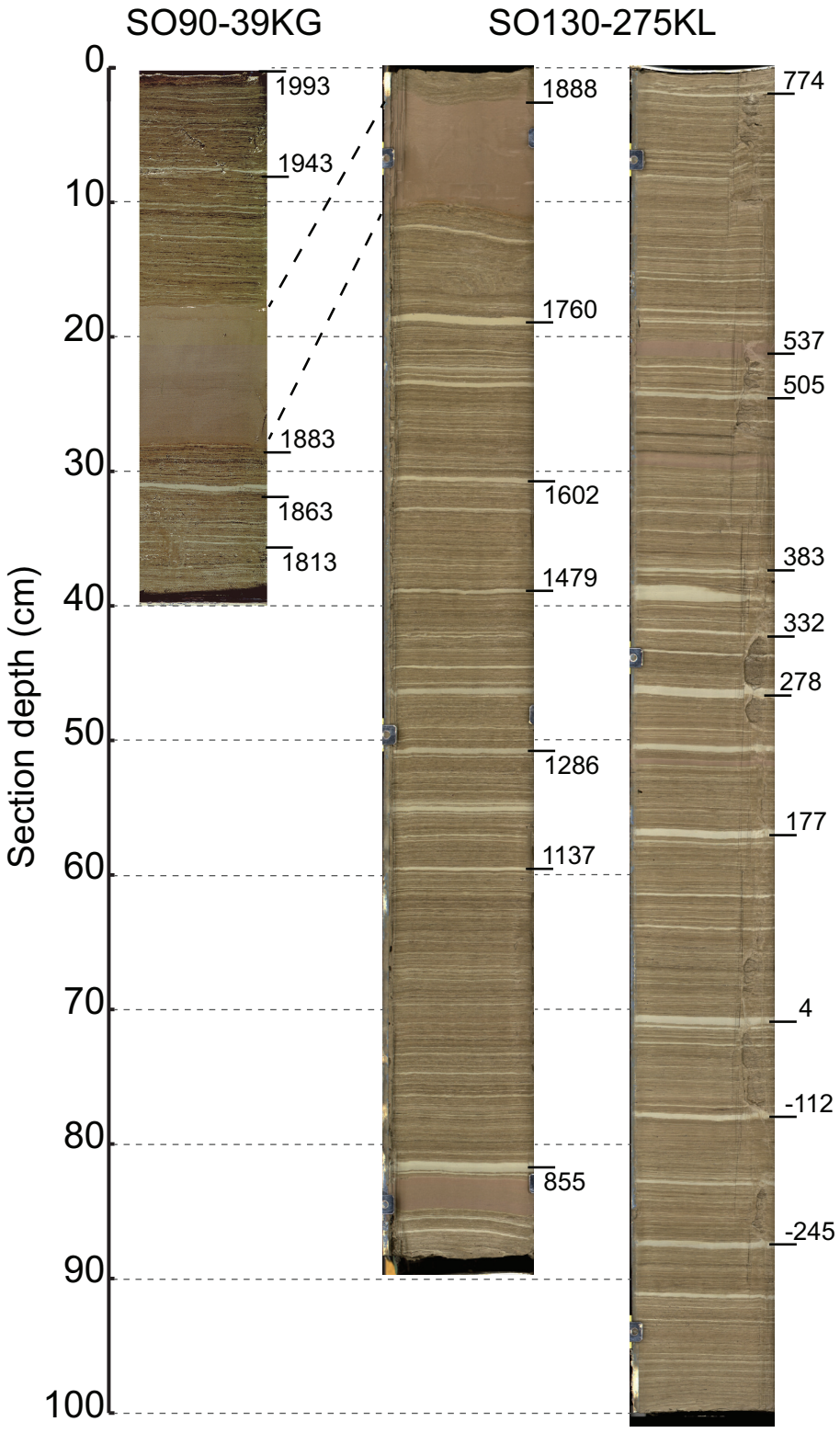

Figure 2.1: Core photographs of the sediment cores SO90-39KG and SO130-275KL recovered from the same position on the Pakistan margin. The numbers indicate the age of the event deposits according to von Rad et al., (1999). Core 275KL was correlated with the adjacent core SO90-56KA by a layer-by-layer tracking of the prominent light- and red-coloured event deposits (C- and F-layers). The oblique dashed lines indicate the top and bottom of a 10 cm-thick F-layer (F_1) that ties 39KG on top of 275KL.

2.2 Calculation of accumulation rates in laminated sediments

The determination of flux rates of sedimentary components, like organic carbon, carbonate, opal, eolian dust particles or individual foraminiferal species, is ultimately based on the precision of the age model. The counting of semi-annually deposited, distinctly alternating light- and dark laminae couplets, provides a very precise relative age control of the sequence. Thus, the sedimentary accumulation rate is exemplarily determined by the thickness of the sample slice divided by the number of varve couplets. This is, however, partly hampered by the presence of allochthonous deposits, accumulating an enormous amount of solely land-derived sediment in a very short amount of time (i.e. less than one year), thereby diluting the hemipelagic sediment content. If a sample contains such a deposit, the dilution is ideally compensated by the proportionately higher sedimentary accumulation rate.

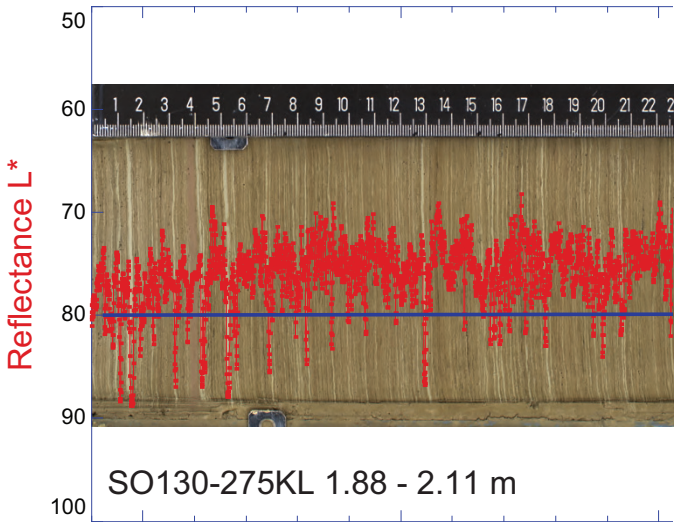

Fig. 2.2: A 23 cm long section of core 275KL to exemplarily demonstrate the photometric identification of event deposits. A threshold of 80 for the reflectance L* was used to identify the onset and thickness of the light-coloured C-layers on a sub-millimeter scale.

The actual duration of the depositional time of a sample from core 275KL was determined from the varve thickness data of von Rad et al., (1999), which is available from the adjacent core 56KA for every year from 1993 CE until 4.9 ka BP. However, the thickness data is cleaned from event deposits, making it mandatory to precisely determine the position of the events for comparison with core 275KL. Whether part of a sample from 275KL consisted either of a C- or F-layer, thus increasing the thickness of the sample disproportionate to the age of the succession, was determined by using a threshold from the L*a*b* color space of the color-scan profile (Figure 2.2). Careful comparison of the results with the core photograph indicated that a threshold of a lightness value (L*) of 80 for C-Layers and 1.5

(a*) for F-Layers was most practicable. This enabled to calculate event layer-free sedimentary accumulation rates.

2.3 Sample preparation and census counts of planktic foraminifera

The samples for coarse-fraction analysis of core 275KL were sampled in a continuous 5-mm scheme. A pre-study with bulk sediment from this core, indicated that this amount of sediment, corresponding to ca. 1.5 g dry weight, yields a minimum of 300 individuals of planktic foraminifera for counting in accordance to the MARGO recommendations (Kucera et al., 2005). However, samples that were diluted with fine-grained sediments of an event deposit, had to be combined with adjacent samples to yield this minimum amount of counted individuals. This was done for 89 samples, representing 27 % of the data set of core 275KL. Because event deposits are solely land-derived and finer than the sand fraction (>63 µm), admixture dilutes the hemipelagic content of a sample, but merging of samples is not decreasing the actual resolution of the marine deposition. The sampling scheme after merging therefore corresponds to an average sample spacing of 9 years. The samples were cut from U-channels, freeze-dried and washed with tap water over a 63-µm screen. After drying in an oven at 40 °C, the residue was further sieved to the size fractions 63–150 µm and >150 µm. To enable comparison with other paleoceanographic studies, the latter size fraction was used for the determination of planktic foraminiferal species under a stereo dissecting microscope, following the taxonomy of (Bé, 1967; Hemleben et al., 1989; Parker, 1962). Coarse fraction samples from the cores 39KG and SL163 were already available from previous studies and did not require further preprocessing. For counting purposes, samples from the latter two cores were split with an Otto microsplitter and analyses were conducted on smaller aliquots of the >150 µm size fraction, containing a minimum of 300 individuals of planktic foraminifera.

2.4 Quantitative reconstructions

Transfer function analyses

To increase the signal-to-noise ratio for quantitative paleoenvironmental estimates, samples from diverging oceanic environments were excluded by subsetting the

calibration data set to a predefined region. This region was constrained by a box extending from 30 °N to 30 °S and from 30 ° to 120 °E, furthermore excluding the Red Sea and the Bay of Bengal. Calibration samples originating from a position inside the box were compiled from a published data base of core tops (Barrows and Juggins, 2005) and significantly extended by previously unpublished data. To further exclude any potential ecological gradients that are outside of the range of the fossil data, the calibration samples from within the box and the fossil samples were analyzed together in a joint principle component analysis (PCA). Along the first and second axis of the joint PCA, the scatter of the fossil samples spans a convex hull. Thus, calibration samples that also plot within this hull are most similar to the fossil samples along the first two principal components. These samples are expected to record the conditions in the same range of variation as the fossil samples and were therefore used for training the transfer functions. Quantitative estimates were conducted using a suite of functions available in the *R* statistical software package *rioja* ver. 0.9-5 (Juggins, 2015), as well as with the BioComp™ software NeuroGeneticOptimizer™ ver. 2.6.142.

Trace elemental composition of planktic foraminiferal calcite

Sample preparation and analyses of trace elemental composition on planktic foraminiferal calcite of the species *Globigerina bulloides* and *Globigerinoides sacculifer* from the Oman core SL163 were carried out at the facilities of the MARUM Center for Marine Environmental Sciences in Bremen/Germany. After carefully opening the chambers of ca. 30 individuals of the two species under a microscope by crushing them gently between two glass plates with Seralpur™ water, cleaning procedures followed the protocol of Barker et al., (2003).

CHAPTER 3

Summary and concluding remarks

3.1 Main results

The research presented in this doctoral thesis aims at the reconstruction of monsoon intensity fluctuations on decadal- to subdecadal time scales during three phases of the Holocene epoch. The first of these phases is the timespan over the last 250 years. We have a rather good knowledge of short-term climate fluctuations during part of this period, owing to the increasing systematical development of comprehensive weather observations, starting at around 150 years ago (Sontakke and Singh, 1996). Furthermore, detailed knowledge about potential external forcing exists, e.g. volcanic eruptions and solar variability (e.g., Ammann et al., 2007; Jungclaus et al., 2010). The timespan over the last 2,000 years has recently gained broad interest of the scientific community (PAGES 2k Consortium, 2013). This phase includes several centennial-scale hemispheric climate excursions, like the so-called "Medieval Warm Period" or the "Little Ice Age", evident from a wide range of proxy data (Jones and Mann, 2004). It also holds the potential to disentangle natural from anthropogenic factors influencing the climate. The third phase is the early- to mid-Holocene epoch, which is a period prior to the influence of anthropogenic greenhouse gas emissions. However, in the Northern Hemisphere the perihelion during the early Holocene was close to the summer solstice, which allows to test if climate fluctuations were more sensitive to changes of incoming irradiation during this period.

Last two an a half centuries

Paper I is based on a study of planktic foraminiferal assemblages of core 39KG over the last ~250 years in quasi-biennial (2.55 year) resolution. The preservation of varve-like laminae under the absence of bioturbation enables to study the variability of the faunal assemblages in very high detail. Over the last ~150 years, the record overlaps with instrumental temperature measurements, which allows to evaluate the faunal record as the response to local winter temperatures. The species data was found to correlate best with January temperatures, which is in good agreement with the results of Paper III, where a core top study also revealed a strong influence of winter temperatures on the faunal composition. It also shows that the site at the Pakistan margin might be well suited to reconstruct winter monsoonal conditions independently from the influence of the summer monsoon. This relationship was used to extend the instrumental record into pre-industrial times and to significantly assess long-term trends of winter monsoon conditions. The results indicate that winter conditions are modulated in accordance with large-scale oscillations patterns originating in the Pacific, namely ENSO and PDO. However, this teleconnection might not have been stable over the last 250 years, but might have been decoupling since the beginning of the 20^{th} century. An interesting new finding is, that strong cooling and intensification of winter conditions was apparently linked to the NAO, potentially through strengthening of the Siberian High. These findings shed new light on the coupling of local winter monsoon conditions to continental-scale and intra-basin wide climate oscillation modes.

Last two millennia

In a first collaborative study presented in Paper II, we aimed at the reconstruction of annual mean SST based on alkenones, in comparison to organic carbon content and δ^{15}N as productivity proxies, from cores 39KG and 275KL. Winter monsoon conditions from quantitative reconstructions in this area of the NE Arabian Sea were previously unknown. The study revealed that winter conditions were not stable over most parts of the last two millennia. Instead, the results showed an overall cooling trend together with several centennial-scale fluctuations of slightly warmer and colder SST, although the range of annual temperatures was low during the last ~2,500 years ($< 1.5\,^{\circ}$C). Exceptionally strong winter conditions, indicated by colder than average annual SST in concert with increased productivity indices, were observed from 1500–1900 CE, which let to the conclusion that this

feature could be linked to the continental-scale cooling in the northern hemisphere, referred to as the Little Ice Age.

However, a sediment trap study presented in Paper II indicated a high seasonality of alkenone fluxes at the Pakistan margin, which might potentially introduce a temperature bias in the signal of annual mean SST. Paper III therefore again addressed the winter monsoon climate in the NE Arabian Sea, by comparing the alkenone-based record of annual mean SST to a record of seasonal winter SST based on planktic foraminiferal census counts. To this end, a new transfer function was compiled and potential environmental driving forces were evaluated on a modern set of core top samples, which were most similar to the fossil samples of cores 39KG and 275KL. The analysis indicated that winter SST is the strongest determinant in the species assemblage data of the modern samples. Reconstructions of winter SST based on this relationship fluctuate on a range of 2.5 °C over the last two millennia and also reveal a long-term trend of more intensified winter conditions towards the present. The main feature of the time series of winter SST is a sharp drop of temperatures at 450 CE, which is ~250 years later relative to the alkenone-based annual SST record. The higher resolution of the foraminiferal record in comparison to the alkenone record further revealed significant cyclicities underlying the winter SST record on 75-, 40-, 37-, and 31-years per cycle. These periodicities were previously found in proxies recording Indian summer monsoon conditions, providing evidence that winter and summer monsoon are modulated by the same driving forces. An apparent significant coherency on centennial bandwidth with the Lake Huguang Maar record, expected to be influenced by the East Asian monsoon, ends abruptly at ~1000 CE, indicating a decoupling of East Asian and Indian winter monsoon conditions in medieval times.

Early to mid Holocene

In Paper IV, the early- to mid Holocene epoch ISM intensities were studied independently using planktic foraminiferal assemblages with transfer functions calibrated to summer SST and Mg/Ca ratios of the upwelling species *Globigerina bulloides*. Upwelling and summer SST fluctuated coherently with sunspot cycles, on frequencies previously identified by other studies. It could be shown that phases of diminished OMZ intensitiy were linked to phases of low surface water productivity. Moreover, these phases were linked to warmer upwelling- and summer SST proxies, indicating that surface water properties, instead of better

ventilated water masses, are controlling bottom water conditions in the upwelling areas of the northwestern Arabian Sea on decadal time scales.

3.2 Outlook for future studies

The studies presented in this doctoral thesis provide new evidence for the coupling of the Indian winter monsoon with external forcing mechanisms on decadal time scales. In order to better understand the factors influencing winter monsoon conditions on longer time scales, i.e. hundreds of years to millennia, longer records are needed. The transfer function presented in this study, however, holds the potential to be applied on planktic foraminiferal assemblages from the Holocene and earlier glacial intervals. From such data it would be possible to obtain independent information on the glacial/interglacial variability of the winter monsoon and resolve its relationship with the summer monsoon on millennial scales.

The new record of assemblage-based winter SST could be supplemented with other independent proxies providing a seasonal temperature dependence. This could be best established by Mg/Ca measurements of the 'winter monsoon species' *Globigerina falconensis* in sediments from the northeastern Arabian Sea. An appropriate Mg/Ca–temperature calibration for this species, however, is currently not available and would be crucial for this approach.

References

Altabet, M. A., M. J. Higginson, and D. W. Murray (2002): 'The effect of millennial-scale changes in Arabian Sea denitrification on atmospheric CO2.' *Nature*, vol. 415(6868): pp. 159–162.

Ammann, C. M., F. Joos, D. S. Schimel, B. L. Otto-Bliesner, and R. A. Tomas (2007): 'Solar influence on climate during the past millennium: results from transient simulations with the NCAR Climate System Model.' *Proceedings of the National Academy of Sciences*, vol. 104(10): pp. 3713–3718.

Anand, P., D. Kroon, A. D. Singh, and G. Ganssen (2008): 'Coupled sea surface temperature-seawater δ^{18}O reconstructions in the Arabian Sea at the millennial scale for the last 35 ka'. *Paleoceanography*, vol. 23: PA4207.

Andruleit, H. A., U. von Rad, A. Brans, and V. Ittekkot (2000): 'Coccolithophore fluxes from sediment traps in the northeastern Arabian Sea off Pakistan'. *Marine Micropaleontology*, vol. 38(3-4): pp. 285–308.

Ashok, K., Z. Guan, and T. Yamagata (2001): 'Impact of the Indian Ocean dipole on the relationship between the Indian monsoon rainfall and ENSO'. *Geophysical Research Letters*, vol. 28(23): pp. 4499–4502.

Banakar, V. S., B. S. Mahesh, G. Burr, and A. R. Chodankar (2010): 'Climatology of the Eastern Arabian Sea during the last glacial cycle reconstructed from paired measurements of foraminiferal δ^{18}O and Mg/Ca'. *Quat. Res.* Vol. 73: pp. 535–540.

Banse, K. (1968): 'Hydrography of the Arabian Sea Shelf of India and Pakistan and effects on demersal fishes'. *Deep sea research and oceanographic Abstracts*, vol. 15(1): pp. 45–79.

Barker, S., M. Greaves, and H. Elderfield (2003): 'A study of cleaning procedures used for foraminiferal Mg/Ca paleothermometry'. *Geochemistry, Geophysics, Geosystems*, vol. 4(9).

Barrows, T. T. and S. Juggins (2005): 'Sea-surface temperatures around the Australian margin and Indian Ocean during the Last Glacial Maximum'. *Quaternary Science Reviews*, vol. 24(7): pp. 1017–1047.

Bé, A. (1967): 'Foraminifera families: *Globigerinidae* and *Globorotalidae*'. *Fiches d´Identification du Zooplankton*. Ed. by Fraser, J. H. Vol. Sheet 108. Charlottenlund, Denmark: Conseil Perm. Internat. Explor. Mer: pp. 1–8.

Birks, H. J. B. (2010): 'Numerical methods for the analysis of diatom assemblage data'. *The diatoms - applications for the environmental and earth sciences*. Ed. by Smol, J. P. and E. F. Stoermer. Cambridge University Press: pp. 23–54.

Birks, H. (1995): 'Quantitative palaeoenvironmental reconstructions'. *Statistical Modelling of Quaternary Science Data*. Ed. by Maddy, D. and J. S. Brew. Technical guide 5. Cambridge: Quaternary Research Association: pp. 161–254.

Birks, H. (1998): 'Numerical tools in palaeolimnology–Progress, potentialities, and problems'. *Journal of Paleolimnology*, vol. 20: pp. 307–322.

Bohrmann, G., N. Lahajnar, B. Gaye, V. Spiess, and C. Betzler (2010): *Nitrogen Cycle, Cold Seeps, Carbonate Platform Development in the Northwestern Indian Ocean, Cruise No.74, August 31 - December 22, 2007*. 10-3. University of Hamburg. Hamburg.

Böll, A., A. Lückge, P. Munz, S. Forke, H. Schulz, V. Ramaswamy, T. Rixen, B. Gaye, and K.-C. Emeis (2014): 'Late Holocene primary productivity and sea surface temperature variations in the northeastern Arabian Sea: Implications for winter monsoon variability'. *Paleoceanography*, vol. 29(8): pp. 778–794.

Böll, A., H. Schulz, P. M. Munz, T. Rixen, B. Gaye, and K.-C. Emeis (2015): 'Contrasting sea surface temperature of summer and winter monsoon variability in the northern Arabian Sea over the last 25ka'. *Palaeogeography, Palaeoclimatology, Palaeoecology*, vol. 426: pp. 10–21.

Bolton, C. T., L. Chang, S. C. Clemens, and K. Kodama (2013): 'A 500,000 year record of Indian summer monsoon dynamics recorded by eastern equatorial Indian Ocean upper water-column structure'. *Quaternary Science Reviews*, vol. 77: pp. 167–180.

Bond, G., B. Kromer, J. Beer, R. Muscheler, M. N. Evans, W. Showers, S. Hoffmann, R. Lotti-Bond, I. Hajdas, and G. Bonani (2001): 'Persistent solar influence on North Atlantic climate during the Holocene.' *Science*, vol. 294(5549): pp. 2130–2136.

Boos, W. R. and Z. Kuang (2010): 'Dominant control of the South Asian monsoon by orographic insulation versus plateau heating'. *Nature*, vol. 463(7278): pp. 218–222.

Brown, S. J. and H. Elderfield (1996): 'Variations in Mg/Ca and Sr/Ca ratios of planktonic foraminifera caused by postdepositional dissolution: Evidence of shallow Mg-dependent dissolution'. *Paleoceanography*, vol. 11(5): pp. 543–551.

Caley, T., B. Malaizé, S. Zaragosi, L. Rossignol, J. Bourget, F. Eynaud, P. Martinez, J. Giraudeau, K. Charlier, and N. Ellouz-Zimmermann (2011): 'New Arabian Sea records help decipher orbital timing of Indo-Asian monsoon'. *Earth and Planetary Science Letters*, vol. 308(3): pp. 433–444.

Cavalier-Smith, T. (2004): 'Only six kingdoms of life'. *Proceedings of the Royal Society B: Biological Sciences*, vol. 271(1545): pp. 1251–1262.

Cayre, O. and E. Bard (1999): 'Planktonic foraminiferal and alkenone records of the last deglaciation from the Eastern Arabian Sea'. *Quat. Res.* Vol. 52: pp. 337–342.

Clemens, S. C. and W. L. Prell (2003): 'A 350,000 year summer-monsoon multi-proxy stack from the Owen Ridge, Northern Arabian Sea'. *Marine Geology*, vol. 201(1-3): pp. 35–51.

Dahl, K. A. and D. W. Oppo (2006): 'Sea surface temperature pattern reconstructions in the Arabian Sea'. *Paleoceanography*, vol. 21(1).

Dekens, P. S., D. W. Lea, D. K. Pak, and H. J. Spero (2002): 'Core top calibration of Mg/Ca in tropical foraminifera: Refining paleotemperature estimation'. *Geochemistry, Geophysics, Geosystems*, vol. 3(4): pp. 1–29.

Ding, Y. H. (1990): 'Buildup, Air-Mass Transformation and Propagation of Siberian High and Its Relations to Cold Surge in East-Asia'. *Meteorology and Atmospheric Physics*, vol. 44(1-4): pp. 281–292.

Ding, Y. H. (1994): *Monsoons over China*. Vol. 16. Springer Netherlands.

Emeis, K.-C., D. M. Anderson, D. Kroon, and D. Schulz-Bull (1995): 'Sea-surface temperatures and history of monsoon upwelling in the Northeastern Arabian Sea during the last 500,000 years'. *Quat. Res.* Vol. 43: pp. 355–361.

Findlater, J. (1969): 'A major low-level air current near the Indian Ocean during the northern summer'. *Quarterly Journal of the Royal Meteorological Society*, vol. 95(404): pp. 362–380.

Fleitmann, D., S. J. Burns, A. Mangini, and M. Mudelsee (2007): 'Holocene ITCZ and Indian monsoon dynamics recorded in stalagmites from Oman and Yemen (Socotra)'. *Quaternary Science Reviews*, vol. 26(1-2): pp. 170–188.

Gadgil, S. (2003): 'The Indian monsoon and its variability'. *Annual Review of Earth and Planetary Sciences*, vol. 31(1): pp. 429–467.

Gadgil, S. (2004): 'Extremes of the Indian summer monsoon rainfall, ENSO and equatorial Indian Ocean oscillation'. *Geophysical Research Letters*, vol. 31(12): pp. L12213–4.

Galy, V., C. France-Lanord, O. Beyssac, P. Faure, H. Kudrass, and F. Palhol (2007): 'Efficient organic carbon burial in the Bengal fan sustained by the Himalayan erosional system'. *Nature*, vol. 450(7168): pp. 407–410.

Ganssen, G. M., F. J. C. Peeters, B. Metcalfe, P. Anand, S. J. A. Jung, D. Kroon, and G. J. A. Brummer (2011): 'Quantifying sea surface temperature ranges of the Arabian Sea for the past 20 000 years'. *Climate of the Past*, vol. 7(4): pp. 1337–1349.

Godad, S. P., P. D. Naidu, and B. A. Malmgren (2011): 'Sea surface temperature changes during May and August in the western Arabian Sea over the last 22kyr: Implications as to shifting of the upwelling season'. *Marine Micropaleontology*, vol. 78(1): pp. 25–29.

Goswami, B. N., M. S. Madhusoodanan, C. P. Neema, and D. Sengupta (2006): 'A physical mechanism for North Atlantic SST influence on the Indian summer monsoon'. *Geophysical Research Letters*, vol. 33(2): p. L02706.

Govil, P. and P. D. Naidu (2010): 'Evaporation-precipitation changes in the eastern Arabian Sea for the last 68 ka: Implications on monsoon variability'. *Paleoceanography*, vol. 25(1): PA1210.

Gupta, A. K., D. M. Anderson, and J. T. Overpeck (2003): 'Abrupt changes in the Asian southwest monsoon during the Holocene and their links to the North Atlantic Ocean'. *Nature*, vol. 421: pp. 354–357.

Gupta, A. K., M. Das, and D. M. Anderson (2005): 'Solar influence on the Indian summer monsoon during the Holocene'. *Geophysical Research Letters*, vol. 32(17): p. L17703.

Hastenrath, S. and P. J. Lamb (1979): *Surface climate and atmospheric circulation. Climatic atlas of the Indian Ocean. Part-I*. University of Wisconsin Press.

Hemleben, C., M. Spindler, and O. R. Anderson (1989): *Modern planktonic foraminifera*. Springer Berlin Heidelberg.

Hong, Y. T., B. Hong, Q. H. Lin, Y. X. Zhu, Y. Shibata, M. Hirota, M. Uchida, X. T. Leng, H. B. Jiang, H. Xu, H. Wang, and L. Yi (2003): 'Correlation between Indian Ocean summer monsoon and North Atlantic climate during the Holocene'. *Earth and Planetary Science Letters*, vol. 211(3-4): pp. 371–380.

Hren, M. T., C. P. Chamberlain, G. E. Hilley, P. M. Blisniuk, and B. Bookhagen (2007): 'Major ion chemistry of the Yarlung Tsangpo–Brahmaputra river: Chemical weathering, erosion, and CO_2 consumption in the southern Tibetan plateau

and eastern syntaxis of the Himalaya'. *Geochimica et Cosmochimica Acta*, vol. 71(12): pp. 2907–2935.

Huguet, C., J.-H. Kim, J. S. Sinninghe Damsté, and S. Schouten (2006): 'Reconstruction of sea surface temperature variations in the Arabian Sea over the last 23 kyr using organic proxies (TEX 86 and $U_{37}^{K'}$)'. *Paleoceanography*, vol. 21(3).

Imbrie, J. and N. G. A. Kipp (1971): 'New micropaleontologic method for quantitative paleoclimatology: application to Late Pleistocene Carribean core'. *The Late Cenozoic Glacial Ages*. Ed. by Turekian, K. K. New Haven, Conn.: pp. 71–182.

Jones, P. D. and M. E. Mann (2004): 'Climate over past millennia'. *Reviews of Geophysics*, vol. 42(2): RG2002.

Juggins, S. (2015): *rioja: Analysis of Quaternary Science Data*. R package version (0.8-7).

Juggins, S. and H. Birks (2012): 'Quantitative environmental reconstructions from biological data'. *Tracking environmental change using lake sediments*. Ed. by Birks, H. J. B., A. F. Lotter, S. Juggins, and J. P. Smol. Developments in Paleoenvironmental Research 5. Springer Netherlands.

Jung, S., D. Kroon, G. Ganssen, and F. Peeters (2009): 'Enhanced Arabian Sea intermediate water flow during glacial North Atlantic cold phases'. *Earth and Planetary Science Letters*, vol. 280(1-4): pp. 220–228.

Jungclaus, J. H. et al. (2010): 'Climate and carbon-cycle variability over the last millennium'. *Climate of the Past*, vol. 6(5): pp. 723–737.

Kalnay, E. et al. (1996): 'The NCEP/NCAR 40-Year Reanalysis Project'. *Bulletin of the American Meteorological Society*, vol. 77(3): pp. 437–471.

Krishna Kumar, K., B. Rajagopalan, and M. Cane (1999): 'On the weakening relationship between the Indian monsoon and ENSO'. *Science*, vol. 284(5423): pp. 2156–2159.

Kucera, M. (2007): 'Planktonic Foraminifera as Tracers of Past Oceanic Environments'. *Proxies in Late Cenozoic Paleoceanography*. Ed. by Hillaire-Marcel, C. and A. De Vernal. Vol. 1. Developments in Marine Geology. Elsevier: pp. 213–262.

Kucera, M. and K. F. Darling (2002): 'Cryptic species of planktonic foraminifera: their effect on palaeoceanographic reconstructions'. *Philosophical Transactions of the Royal Society A*, vol. 360(1793): pp. 695–718.

Kucera, M., M. Weinelt, T. Kiefer, U. Pflaumann, A. Hayes, M. Weinelt, M.-T. Chen, A. C. Mix, T. T. Barrows, E. Cortijo, J. Duprat, S. Juggins, and C. Waelbroeck (2005): 'Reconstruction of sea-surface temperatures from assemblages of planktonic foraminifera: multi-technique approach based on geographically con-

strained calibration data sets and its application to glacial Atlantic and Pacific Oceans'. *Quaternary Science Reviews*, vol. 24(7-9): pp. 951–998.

Kudrass, H. R., A. Hofmann, H. Doose, K. Emeis, and H. Erlenkeuser (2001): 'Modulation and amplification of climatic changes in the Northern Hemisphere by the Indian summer monsoon during the past 80 k.y'. *Geology*, vol. 29(1): p. 63.

Kutzbach, J. E. and P. J. Guetter (1984): 'The Sensitivity of Monsoon Climates to Orbital Parameter Changes for 9,000 Years BP : Experiments with the NCAR General Circulation Model'. *Milankovitch and Climate*. Dordrecht: Springer Netherlands: pp. 801–820.

Laskar, A. H., M. G. Yadava, and R. Ramesh (2013): 'A 4 kyr stalagmite oxygen isotopic record of the past Indian Summer Monsoon in the Andaman Islands'. *Geochemistry*, vol. 14(9): pp. 3555–3566.

Lea, D. W., T. A. Mashiotta, and H. J. Spero (1999): 'Controls on magnesium and strontium uptake in planktonic foraminifera determined by live culturing'. *Geochimica et Cosmochimica Acta*, vol. 63(16): pp. 2369–2379.

Legendre, P. and H. Birks (2012): 'From classical to canonical ordination'. *Tracking environmental change using lake sediments*. Ed. by Birks, H. J. B., A. F. Lotter, S. Juggins, and J. P. Smol. Developments in Paleoenvironmental Research 5. Springer Netherlands: pp. 201–248.

Levermann, A., J. Schewe, V. Petoukhov, and H. Held (2009): 'Basic mechanism for abrupt monsoon transitions'. *Proceedings of the National Academy of Sciences*, vol. 106(49): pp. 20572–20577.

Locarnini, R. A., A. V. Mishonov, J. I. Antonov, T. P. Boyer, H. E. Garcia, O. K. Baranova, M. M. Zweng, C. R. Paver, J. R. Reagan, D. R. Johnson, M. Hamilton, and D. Seidov (2013): 'World Ocean Atlas 2013, Volume 1: Temperature'. *A. Mishonov Technical Ed.* Ed. by Levitus, S. NOAA Atlas NESDIS 73: p. 40.

Lückge, A., H. Doose-Rolinski, A. A. Khan, H. Schulz, and U. von Rad (2001): 'Monsoonal variability in the northeastern Arabian Sea during the past 5000 years: Geochemical evidence from laminated sediments'. *Palaeogeography, Palaeoclimatology, Palaeoecology*, vol. 167(3-4): pp. 273–286.

Madhupratap, M., S. Prasanna Kumar, P. M. A. Bhattathiri, M. Dileep Kumar, S. Raghukumar, K. K. C. Nair, and N. Ramaiah (1996): 'Mechanism of the biological response to winter cooling in the northeastern Arabian Sea'. *Nature*, vol. 384: pp. 549–552.

Maher, B. A. (2008): 'Holocene variability of the East Asian summer monsoon from Chinese cave records: a re-assessment'. *The Holocene*, vol. 18(6): pp. 861–866.

Marzin, C., N. Kallel, M. Kageyama, J. C. Duplessy, and P. Braconnot (2013): 'Glacial fluctuations of the Indian monsoon and their relationship with North Atlantic climate: new data and modelling experiments'. *Climate of the Past*, vol. 9(5): pp. 2135–2151.

Mashiotta, T. A., D. W. Lea, and H. J. Spero (1999): 'Glacial–interglacial changes in Subantarctic sea surface temperature and δ^{18}O-water using foraminiferal Mg'. *Earth and Planetary Science Letters*, vol. 170(4): pp. 417–432.

Meehl, G. A. (1994): 'Influence of the land surface in the Asian summer monsoon: external conditions versus internal feedbacks'. *Journal of Climate*, vol. 7: pp. 1033–1049.

Meehl, G. A. and G. W. M. Washington (1993): 'South Asian monsoon variability in a model with doubled atmospheric carbon dioxide concentration'. *Science*, vol. 260: pp. 1101–1104.

Mix, A. C., E. Bard, and R. Schneider (2001): 'Environmental processes of the ice age: land, oceans, glaciers (EPILOG)'. *Quaternary Science Reviews*, vol. 20(4): pp. 627–657.

Mollenhauer, G., T. I. Eglinton, and N. Ohkouchi (2003): 'Asynchronous alkenone and foraminifera records from the Benguela Upwelling System'. *Geochimica et Cosmochimica Acta*, vol. 67(12): pp. 2157–2171.

Monterey, G. and S. Levitus (1997): *Climatological cycle of mixed layer depth in the world ocean*. Tech. rep. U.S. Gov. Printing Office, NOAA NESDIS.

Morrison, J. M., L. A. Codispoti, S. Gaurin, and B. Jones (1998): 'Seasonal variation of hydrographic and nutrient fields during the US JGOFS Arabian Sea Process Study'. *Deep Sea Research*, vol. 45(10–11): pp. 2053–2101.

Mucci, A. (1987): 'Influence of temperature on the composition of magnesian calcite overgrowths precipitated from seawater'. *Geochimica et Cosmochimica Acta*, vol. 51(7): pp. 1977–1984.

Munz, P. M., M. Siccha, A. Lückge, A. Böll, M. Kucera, and H. Schulz (2015): 'Decadal-resolution record of winter monsoon intensity over the last two millennia from planktic foraminiferal assemblages in the northeastern Arabian Sea'. *The Holocene*, vol. 25(11): pp. 1756–1771.

Naidu, P. D. and B. A. Malmgren (2005): 'Seasonal sea surface temperature contrast between the Holocene and last glacial period in the western Arabian Sea (Ocean Drilling Project Site 723A): Modulated by monsoon upwelling'. *Paleoceanography*, vol. 20(1):

NASA Goddard Space Flight Center (2014): *Sea-viewing Wide Field-of-view Sensor (SeaWiFS) Ocean Color Data*. Accessed 2015/10/02. Ocean Biology Distributed Active Archive Center. Greenbelt, MD, USA.

Neff, U., S. J. Burns, A. Mangini, M. Mudelsee, D. Fleitmann, and A. Matter (2001): 'Strong coherence between solar variability and the monsoon in Oman between 9 and 6 kyr ago.' *Nature*, vol. 411(6835): pp. 290–293.

Nehrke, G., N. Keul, G. Langer, L. J. d. Nooijer, J. Bijma, and A. Meibom (2013): 'A new model for biomineralization and trace-element signatures of Foraminifera tests'. *Biogeosciences*, vol. 10(10): pp. 6759–6767.

Nürnberg, D., J. Bijma, and C. Hemleben (1996): 'Assessing the reliability of magnesium in foraminiferal calcite as a proxy for water mass temperatures'. *Geochimica et Cosmochimica Acta*, vol. 60(5): pp. 803–814.

PAGES 2k Consortium (2013): 'Continental-scale temperature variability during the past two millennia'. *Nature Geoscience*, vol. 6: pp. 339–346.

Parker, F. L. (1962): 'Planktonic foraminiferal species in Pacific sediments'. *Micropaleontology*, vol. 8: pp. 219–254.

Pichevin, L., E. Bard, P. Martinez, and I. Billy (2007): 'Evidence of ventilation changes in the Arabian Sea during the late Quaternary: Implication for denitrification and nitrous oxide emission'. *Global Biogeochemical Cycles*, vol. 21(4).

Prahl, F. G., C. H. Pilskaln, and M. A. Sparrow (2001): 'Seasonal record for alkenones in sedimentary particles from the Gulf of Maine'. *Deep Sea Research Part I: Oceanographic Research Papers*, vol. 48(2): pp. 515–528.

Prahl, F. G., L. A. Muehlhausen, and D. L. Zahnle (1988): 'Further evaluation of long-chain alkenones as indicators of paleoceanographic conditions'. *Geochimica et Cosmochimica Acta*, vol. 52(9): pp. 2303–2310.

Prasanna Kumar, S., M. Madhupratap, M. Dileep Kumar, M. Mangesh Gauns, P. M. Muraleedharan, V. V. S. S. Sarma, and S. N. De Souza (2000): 'Physical control of primary productivity on a seasonal scale in central and eastern Arabian Sea'. *Journal of Earth System Science*, vol. 109(4): pp. 433–441.

Prasanna Kumar, S., M. Madhupratap, M. Dileep Kumar, P. M. Muraleedharan, S. N. DeSouza, M. Mangesh Gauns, and V. V. S. S. Sarma (2001): 'High biological productivity in the central Arabian Sea during the summer monsoon driven by Ekman pumping and lateral advection'. *Current Science*, vol. 81(12).

Prasanna Kumar, S. and T. G. Prasad (1996): 'Winter cooling in the northern Arabian Sea'. *Current Science*, vol. 71(11).

Prasanna Kumar, S. and T. G. Prasad (1999): 'Formation and spreading of Arabian Sea high-salinity water mass'. *Journal of Geophysical Research*, vol. 104(C1): pp. 1455–1464.

Rashid, H., B. P. Flower, R. Z. Poore, and T. M. Quinn (2007): 'A ~25 ka Indian Ocean monsoon variability record from the Andaman Sea'. *Quaternary Science Reviews*, vol. 26(19–21): pp. 2586–2597.

Ravelo, A. C. and C. Hillaire-Marcel (2007): 'The Use of Oxygen and Carbon Isotopes of Foraminifera in Paleoceanography'. *Proxies in Late Cenozoic Paleoceanography*. Vol. 1. Developments in Marine Geology. Elsevier. Chap. 18: pp. 735–764.

Reichart, G.-J., S. J. Schenau, G. J. De Lange, and W. J. Zachariasse (2002): 'Synchroneity of oxygen minimum zone intensity on the Oman and Pakistan Margins at sub-Milankovitch time scales'. *Marine Geology*, vol. 185(3): pp. 403–415.

Rosenthal, Y., G. P. Lohmann, K. C. Lohmann, and R. M. Sherrell (2000): 'Incorporation and preservation of Mg in *Globigerinoides sacculifer*: implications for reconstructing the temperature and $^{18}O/^{16}O$ of seawater'. *Paleoceanography*, vol. 15(1): pp. 135–145.

Rostek, F., E. Bard, L. Beaufort, C. Sonzogni, and G. Ganssen (1997): 'Sea surface temperature and productivity records for the past 240 kyr in the Arabian Sea'. *Deep Sea Res. II*, vol. 44(6–7): pp. 1461–1480.

Sadekov, A. Y. and S. M. Eggins (2005): 'Characterization of Mg/Ca distributions in planktonic foraminifera species by electron microprobe mapping'. *Geochemistry*, vol. 6(12).

Saher, M. H., S. J. A. Jung, H. Elderfield, M. J. Greaves, and D. Kroon (2007): 'Sea surface temperatures of the western Arabian Sea during the last deglaciation'. *Paleoceanography*, vol. 22(2):

Saji, N. H., B. N. Goswami, P. N. Vinayachandran, and T. Yamagata (1999): 'A dipole mode in the tropical Indian Ocean.' *Nature*, vol. 401(6751): pp. 360–363.

Saraswat, R., D. W. Lea, R. Nigam, and A. Mackensen (2013): 'Deglaciation in the tropical Indian Ocean driven by interplay between the regional monsoon and global teleconnections'. *Earth and Planetary Science Letters*, vol. 375: pp. 166–175.

Saraswat, R., R. Nigam, A. Mackensen, and S. Weldeab (2012): 'Linkage between seasonal insolation gradient in the tropical Northern Hemisphere and the sea surface salinity of the equatorial Indian Ocean during the last glacial period'. *Acta Geologica Sinica-English Edition*, vol. 86(5): pp. 1265–1275.

Saraswat, R., R. Nigam, S. Weldeab, A. Mackensen, and P. Naidu (2005): 'A first look at past sea surface temperatures in the equatorial Indian Ocean from Mg/Ca in foraminifera'. *Geophys. Res. Lett.* Vol. 32: p. L24604.

Schulte, S. and P. J. Müller (2001): 'Variations of sea surface temperature and primary productivity during Heinrich and Dansgaard-Oeschger events in the northeastern Arabian Sea'. *Geo-Marine Letters*, vol. 21(3): pp. 168–175.

Schulz, H. (1995): 'Meeresoberflächentemperaturen vor 10,000 Jahren–Auswirkungen des frühholozänen Insolationsmaximums'. PhD thesis. Germany: Geol.-Paläontol. Inst. Univ. Kiel.

Schulz, H. and U. von Rad (2014): 'Vertical and lateral flux on the continental slope off Pakistan: correlation of sediment core and trap results'. *Biogeosciences*, vol. 11(12): pp. 3107–3120.

Schulz, H., U. von Rad, and H. Erlenkeuser (1998): 'Correlation between Arabian Sea and Greenland climate oscillations of the past 110,000 years'. *Nature*, vol. 393(6680): pp. 54–57.

Schulz, H., U. von Rad, and U. von Stackelberg (1996): 'Laminated sediments from the oxygen-minimum zone of the northeastern Arabian Sea'. *Paleoclimatology and Paleoceanography from Laminated Sediments*. Ed. by Kemp, A. E. S. London: Geological Society Special Publication: pp. 185–207.

Shackleton, N. (1967): 'Oxygen Isotope Analyses and Pleistocene Temperatures Re-assessed'. *Nature*, vol. 215(5096): pp. 15–17.

Singh, A. D., S. J. A. Jung, K. Darling, R. Ganeshram, T. Ivanochko, and D. Kroon (2011): 'Productivity collapses in the Arabian Sea during glacial cold phases'. *Paleoceanography*, vol. 26(3).

Sirocko, F., M. Sarnthein, H. Erlenkeuser, H. Lange, M. Arnold, and J. C. Duplessy (1993): 'Century-scale events in monsoonal climate over the past 24,000 years'. *Nature*, vol. 364(6435): pp. 322–324.

Sivakumar, M. V. K. and R. Stefanski (2010): 'Climate Change in South Asia'. *Climate Change and Food Security in South Asia*. Dordrecht: Springer Netherlands: pp. 13–30.

Sontakke, N. A. and N. Singh (1996): 'Longest instrumental regional and all-India summer monsoon rainfall series using optimum observations: reconstruction and update'. *The Holocene*, vol. 6(3): pp. 315–331.

Telford, R. J. and H. J. B. Birks (2005): 'The secret assumption of transfer functions: problems with spatial autocorrelation in evaluating model performance'. *Quaternary Science Reviews*, vol. 24(20): pp. 2173–2179.

Telford, R. J. and H. J. B. Birks (2009): 'Evaluation of transfer functions in spatially structured environments'. *Quaternary Science Reviews*, vol. 28(13): pp. 1309–1316.

Telford, R. J. and H. J. B. Birks (2011): 'A novel method for assessing the statistical significance of quantitative reconstructions inferred from biotic assemblages'. *Quaternary Science Reviews*, vol. 30(9): pp. 1272–1278.

von Rad, U., H. Doose, and cruise participants (1998): *SONNE Cruise SO 130 Cruise Report MAKRAN II*. Hannover: Bundesanstalt für Geowissenschaften und Rohstoffe.

von Rad, U., M. Schaaf, K. H. Michels, H. Schulz, W. H. Berger, and F. Sirocko (1999): 'A 5000-yr record of climate change in varved sediments from the oxygen minimum zone off Pakistan, northeastern Arabian sea'. *Quaternary Research*, vol. 51(1): pp. 39–53.

von Rad, U. et al. (1995): 'Sampling the oxygen minimum zone off Pakistan: glacial-interglacial variations of anoxia and productivity (preliminary results, sonne 90 cruise)'. *Marine Geology*, vol. 125(1-2): pp. 7–19.

von Stackelberg, U. (1972): *Faziesverteilung in Sedimenten des indisch-pakistanischen Kontinentalrandes (Arabisches Meer)*. C 9. "Meteor" - Forschung-Ergebnisse.

Wang, B. (2006): *The Asian Monsoon*. Springer Praxis Books. Springer-Verlag Berlin Heidelberg.

Wang, B., S.-Y. Yim, J.-Y. Lee, J. Liu, and K.-J. Ha (2013): 'Future change of Asian-Australian monsoon under RCP 4.5 anthropogenic warming scenario'. *Climate Dynamics*, vol. 42(1-2): pp. 83–100.

Wang, P., S. Clemens, L. Beaufort, and P. Braconnot (2005): 'Evolution and variability of the Asian monsoon system: state of the art and outstanding issues'. *Quaternary Science Reviews*, vol. 24(5): pp. 595–629.

Webster, P. J., V. O. Magana, T. N. Palmer, J. Shukla, R. A. Tomas, M. Yanai, and Y. T (1998): 'Monsoons: Processes, predictability, and the prospects for prediction'. *Journal of Geophysical Research*, vol. 103(C7): pp. 14451–14510.

Webster, P. J., A. M. Moore, J. P. Loschnigg, and R. R. Leben (1999): 'Coupled ocean-atmosphere dynamics in the Indian Ocean during 1997-98.' *Nature*, vol. 401(6751): pp. 356–360.

Wiggert, J. D., R. G. Murtugudde, and C. R. McClain (2002): 'Processes controlling interannual variations in wintertime (Northeast Monsoon) primary productivity in the central Arabian Sea'. *Deep Sea Research Part II: Topical Studies in Oceanography*, vol. 49(12): pp. 2319–2343.

Wu, G., Y. Liu, B. He, Q. Bao, A. Duan, and F.-F. Jin (2012): 'Thermal Controls on the Asian Summer Monsoon'. *Scientific Reports*, vol. 2: pp. 1–7.

Wyrtki, K. (1973): 'Physical Oceanography of the Indian Ocean'. *The Biology of the Indian Ocean*. Ed. by Zeitschel, B. New York: pp. 18–36.

PART II

Manuscripts

The Indian winter monsoon and its response to external forcing over the last two and a half centuries

Climate Dynamics

Submitted Manuscript

Philipp M. Munz[1], Andreas Lückge[2], Michael Siccha[3], Anna Böll[4], Sven Forke[5], Michal Kucera[3] and Hartmut Schulz[1]

[1]*Department of Geosciences, University of Tübingen, Germany;*
[2]*Bundesanstalt für Geowissenschaften und Rohstoffe (BGR), Germany;*
[3]*MARUM – Center for Marine Environmental Sciences, Germany;*
[4]*Institute of Geology, University of Hamburg, Germany;*
[5]*ZMT – Leibniz Center for Tropical Marine Ecology, Bremen, Germany;*

Keywords: Indian winter monsoon; Mid-latitude climate interaction; El Niño Southern Oscillation; Pacific Decadal Oscillation; North Atlantic Oscillation

Abstract

The Indian winter monsoon is a key component of the seasonally changing monsoon system that affects the densely populated regions of South Asia. Cold northeasterly winds originating in high northern latitudes provide a link of continental-scale Northern Hemisphere climate to the tropics. It is vital to understand the mechanisms and teleconnections that influence its variability to better predict changes in future climate. Here we present a study of regionally calibrated winter (January) temperatures and according Indian winter monsoon (IWM) intensities, based on a planktic foraminiferal record with biennial (2.55 years) resolution. Over the last ~250 years, IWM intensities gradually weakened, based on the long-term trend of reconstructed January temperatures. Furthermore the results indicate that IWM is connected on interannual- to decadal time scales to climate variability of the tropical and extratropical Pacific, via El Niño Southern Oscillation (ENSO) and Pacific Decadal Oscillation (PDO). However, our findings suggest that this relationship appeared to begin to decouple since the beginning of the 20th century. Cross-spectral analysis revealed that several distinct decadal-scale phases of colder climate and accordingly more intense winter monsoon centered at the years ~1800, ~1890 and ~1930 can be linked to changes of the North Atlantic Oscillation (NAO).

Introduction

The Indian monsoon, as the western branch of the Asian monsoon system, is the leading mode of seasonally changing temperature and precipitation in one of the world's most densely populated regions. During boreal winter, the winter monsoonal winds provide a connection of the high northern latitudes to the tropics, when cold air masses originating from the Siberian High are moving southwards (Wang et al., 2003; Wang et al., 2012). Westerlies associated with the Indian winter monsoon (IWM) transport moisture from the Mediterranean to Central Asia and contribute significantly to annual precipitation in the Himalaya region (Dimri, 2013) and southern India (Bhanu Kumar et al., 2004). Moreover, winter temperatures in the Arabian Sea have shown to be related to the subsequent summer rainfall (Clark et al., 2000). To better understand how the monsoon system may change in response to future climate development, it is vital to study how monsoon climate changed through time and what underlying mechanisms are controlling it.

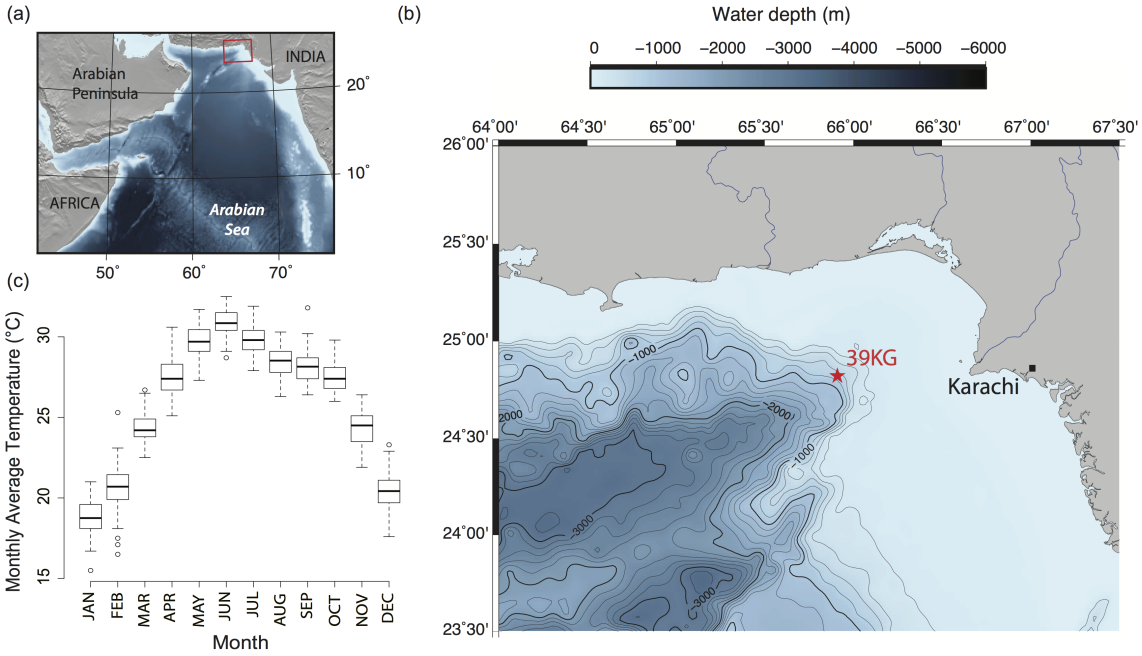

Figure I.1: (a) and **(b)** indicates the location of core SO90-39KG (N24 ° 49′ 18.599"; E065 ° 54′ 36″) in the northeastern Arabian Sea in 704 m water depth and ~160 nm west of Karachi. **(c)** Boxplot of monthly temperatures measured at Karachi weather stations (Karachi Manora and Karachi Airport, average where both stations are available) between 1878 and 1993 (data obtained from http://www.metoffice.gov.uk/research/climate/climate-monitoring/land-and-atmosphere/surface-station-records). January temperatures are continuously lowest during the annual cycle.

Apart from a dominant solar control on the Indian monsoon climate (Agnihotri et al., 2002; Gupta et al., 2005), variability of the monsoon system on millennial- and centennial timescales is likely linked to changes of North Atlantic climate (Böll et al., 2015), potentially through atmospherical reorganizations (Mohtadi et al., 2014). On decadal to interannual time scales, relationships between the North Atlantic Oscillation (NAO) and summer climate in Asia have been suggested (Liu and Yin, 2001). There is abundant evidence that interannual- to decadal variability of the summer rainfall in India and East Asia is linked to tropical Indo-Pacific climate and modulated by perturbations of the Walker circulation associated with the state of ENSO (Ashok and Saji, 2007; Krishna Kumar et al., 2006; Song and Zhou, 2015; Terray et al., 2005; Webster et al., 1998), the phase of the PDO (Krishnamurthy and Krishnamurthy, 2014; Krishnan and Sugi, 2003; Song and Zhou, 2015), and the Indian Ocean Dipole (Ashok et al., 2004; Song and Zhou, 2015; Ummenhofer et al., 2013). An intensification of the ENSO-summer monsoon relationship can be

related to the phase of the PDO, where severe drought (flooding) is associated with the co-occurrence of El Niño (La Niña) with warm (cold) PDO modes. However, because of the strong impact of the summer season, proxy data of the winter monsoon are generally scarce and previously misinterpreted. Shen et al., (2013) for example showed for Lake Huguangyan, that Ti input and diagenetic conditions are controlled by vegetation density and therefore are, instead of East Asian winter monsoon, likely a function of summer precipitation. This demonstrates the need for long, quantitative high-resolution proxy data solely recording winter monsoon conditions, enabling to rigorously investigate internal and external forcing mechanisms.

During boreal winter, surface water hydrography in the northeastern Arabian Sea is associated with evaporative cooling, convective deepening of the mixed layer and entrainment of nutrients into the photic zone (Barber et al., 2001; Prasanna Kumar and Prasad, 1999) induced by dry and cold northeasterly monsoonal winds. Planktic foraminifera are an especially valuable and widely used tool in paleoceanography (Kucera et al., 2005) reflecting trophic and thermal states of the upper water column by a variety of different proxies in the NE Arabian Sea (Schiebel et al., 2004; Schulz et al., 2002) with assemblage compositions primarily sensitive to winter sea-surface temperature (Munz et al., 2015). Here we present the first biennial resolution study of IWM intensity from a laminated marine sedimentary record off Pakistan (Figure I.1a-b) spanning the last ~250 years. During winter season, the region is under influence of northeasterly monsoonal winds that induce cold temperatures culminating in January (Figure I.1c). The winter temperature signals from PF assemblage compositions are first evaluated as the response to local winter temperatures from the instrumental temperature record. Reconstructed temperatures were then used to extend the record prior to 1850 into pre-industrial times to assess the evolution of IWM intensities and eventually identify significant long-term variability. This results in new evidence for the relationship of IWM with ENSO and PDO, which may have not been stable during the late Holocene but may have changed since the beginning of the 20th century. However, decadal-scale episodes of intensive IWM may instead have been related to positive changes of NAO.

Material and methods

Planktic foraminiferal record

Core 39KG was recovered on R/V SONNE's cruise SO90 in 1993 (von Rad et al., 1995) from the stable mid-depth oxygen minimum zone in 704 m water depth approximately 160 nm west of Karachi (Figure I.1b). Coarse fraction samples of a continuous 3-mm sampling scheme were available from a previous study (Doose-Rolinski et al., 2001). Determination of planktic foraminiferal assemblage compositions was described in (Munz et al., 2015). We used a precise age control of absolute dates established from counting annual layers of the 'varve-like' laminated sediments (von Rad et al., 1999). The average age difference between the samples of core 39KG from the 3-mm resolution is 2.55 years.

To detect major trends in the PF faunal records, correspondence analysis (CA) was calculated with the statistical programming environment *R* ver. 3.2.1 (R Core Team, 2015) and the package *vegan* ver. 2.3-1 (Oksanen et al., 2015). CA was carried out on the raw counts of species having an overall relative abundance of >0.5%. 11 out of 20 species occurred in very low frequencies (<0.5%) and were excluded from further analyses to obtain a more robust signal-to-noise ratio (Kucera et al., 2005).

Observational data

Historical temperature data was obtained from the HadCRUT4 dataset infilled by kriging interpolation (Cowtan and Way, 2014). HadCRUT4 is a monthly observational dataset that combines sea surface temperature and land surface air temperature anomalies (Morice et al., 2012) in order to cover regional winter climate of the area. The dataset covers the continuous period from 1850 to present and is available on a 5 °x5 ° grid. The monthly mean temperature anomalies were extracted from the grid cell surrounding the core location ($20-25\,^{\circ}$N; $65-70\,^{\circ}$E). Data were accessed through the KNMI climate explorer website (http://climexp.knmi.nl).

Data analysis and reconstructions

Winter temperature reconstructions were carried out using weighted averaging partial least-squares (WA-PLS) regression (Ter Braak et al., 1993) implemented in the package *rioja* (Juggins, 2015) for *R*. Biological abundance data was expressed as

relative percentages of the nine most common species converted from raw counts. WA-PLS is a common palaeoecological reconstruction method, as it combines several advantages compared to other methods (Birks et al., 2010). The selection criterion on model complexity was based on the respective minimum root means squared error of prediction (RMSEP). Sample-specific errors of the reconstruction period and RMSEP were assessed via bootstrapping over 999 cycles. Spectral analyses were performed using the multitaper method MTM (Mann and Lees, 1996) with a red-noise null hypothesis (Ghil et al., 2002) implemented in the *SpectraWorks* software kSpectra™ ver. 3.4.5. Wavelet coherence analysis (Grinsted et al., 2004) was conducted with the MATLAB software and the package provided by Aslak Grinsted on the website http://noc.ac.uk/using-science/crosswavelet-wavelet-coherence. Time-series were detrended and resampled to an equal-distant average spacing (2.55 yrs.) using piecewise cubic hermitean interpolation polynomials (PCHIP function of the *pracma* package ver. 1.6.4 for *R*) prior to MTM and wavelet coherence analyses.

Simulated temperature data

Monthly simulated January temperatures of climate model experiments were extracted from the $5\,^{\circ}x5\,^{\circ}$ grid cell surrounding the core location ($20-25\,^{\circ}$N; $65-70\,^{\circ}$E) from an ensemble of the Coupled Intercomparison Project 5 (http://cmip-pcmdi.llnl.gov/). Atmospheric and ocean output (Amon and Omon), as well as all available runs and model versions of the different models were averaged over the grid cell. Continuous time series were produced by combining results of each models last millennium (past1000) and the historical experiments. Temperatures are expressed as anomalies relative to each model's average over the period 1700–1999.

Results

Over the entire record of core 39KG, the PF fauna of the nine species having an average abundance >0.5% (Figure I.2a) is dominated by *Globigerina falconensis* (29%) and *Globigerinoides ruber* (28%) followed by *Globigerina bulloides* (19%) and *Globigerinita glutinata* (15%). Minor abundances are shown by *Globoturborotalita tenella* (3.5%), *Globigerinella siphonifera* (2%), *Neogloboquadrina dutertrei* (2%), *Globoturborotalita rubescens* (1.5%) and *Globigerinoides sacculifer* (0.5%). An advantage of ordination methods like CA is the reduction of dimensionality of the original

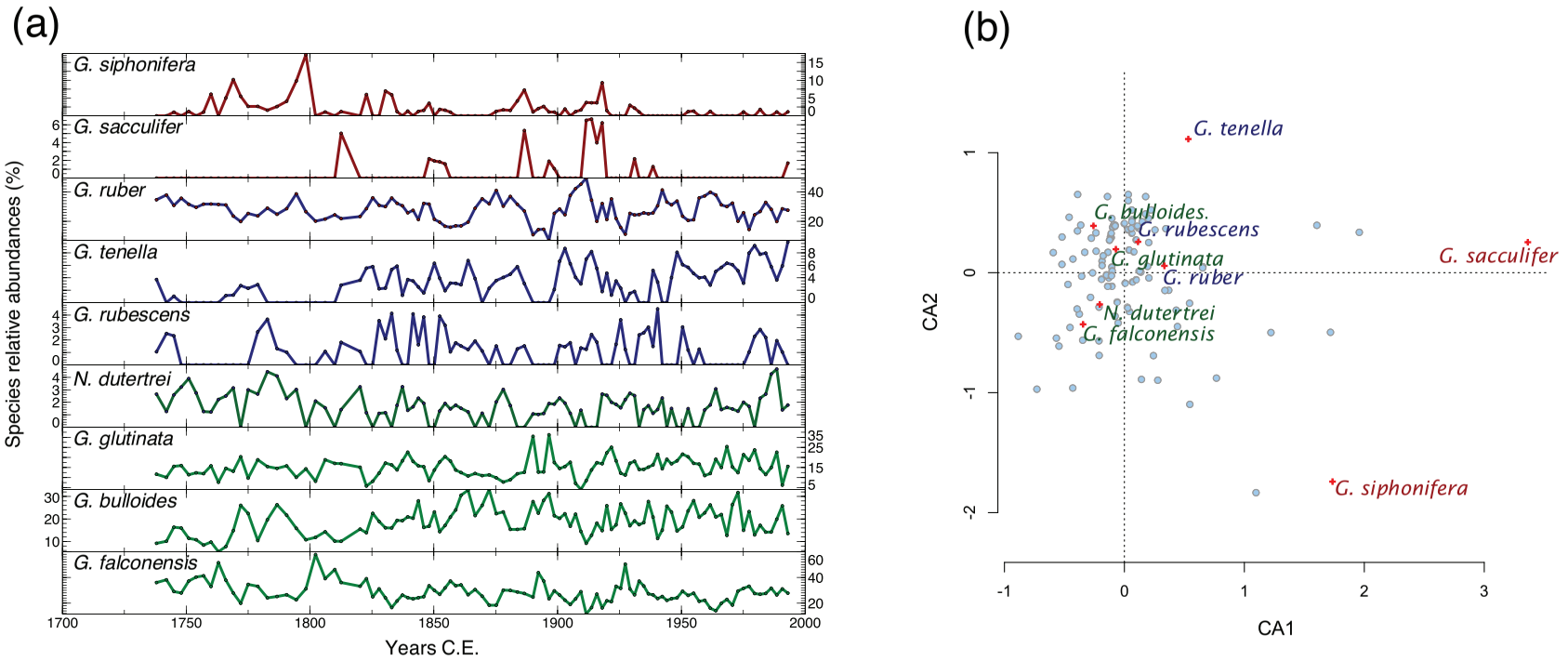

Figure I.2: (a) Relative frequencies of the nine species showing >0.5% average abundance that were used for further analyses. Colours indicate relative positioning along the first correspondence analysis axis in Fig. I.2b. **(b)** Scatter bi-plot of the first and second correspondence analysis (CA) axes with sample (blue dots) and species (red cross) scores. Sample and site species scores are symmetrically scaled by the square root of their eigenvalues. The first axis explains 26.6% of the variance of the foraminiferal assemblage, the second axis 19.8%.

dataset to a lower number of synthetic variables, which explain as much of the variance of the original data as possible. The first and second CA axes together describe almost half (46.3%) of the information of the PF faunal dataset (Table I.1). The first CA axis (CA1) separates *G. sacculifer* on the positive side from *G. falconensis* and *G. bulloides* on the negative side, whereas along the second axis (CA2) *G. tenella* is associated with positive and *G. siphonifera* with negative scores (Figure I.2b).

To identify any potential relationship between the PF faunal abundance data and historical temperature recordings, we regressed the HadCRUT4 monthly temperature data to CA1 and CA2 scores of samples overlapping with the instrumental temperature record (1852–1993). The sedimentary record of core 39KG accumulated on the sea floor over an average period of 2.55 ± 0.8 years, integrating the proxy signal of PF assemblages over this time span. A low-pass filter was therefore applied to the monthly instrumental record with a 5-year cutoff frequency, to compensate for interannual variability during the proxy generation. From the monthly linear regression analyses (Figure I.3) we found that correlations are highest with January temperatures (CA1: $r = 0.34$, $p = 0.006$; CA2: $r = 0.50$, $p < 0.0001$). This means that high (low) abundances of *G. falconensis* and *G. siphonifera* are related to colder (warmer) January temperatures and vice versa for *G. sacculifer* and *G. tenella*. This relationship of *G. falconensis* and *G. sacculifer* is in good agreement with a recent study (Munz et al., 2015), where we used redundancy analysis to characterize species response to environmental gradients on a surface sample dataset from the Arabian Sea. To discover the long-term temperature evolution

Table I.1: Eigenvalues and cumulative variance explained by the correspondence analysis based on nine species that showed an overall minimum abundance of 0.5 %.

	Eigenvalue	Cumulative variance explained (%)
CA1	0.047	26.6
CA2	0.035	46.3
CA3	0.030	63.3
CA4	0.023	76.3
CA5	0.016	85.3
CA6	0.013	92.7
CA7	0.009	97.7
CA8	0.004	100

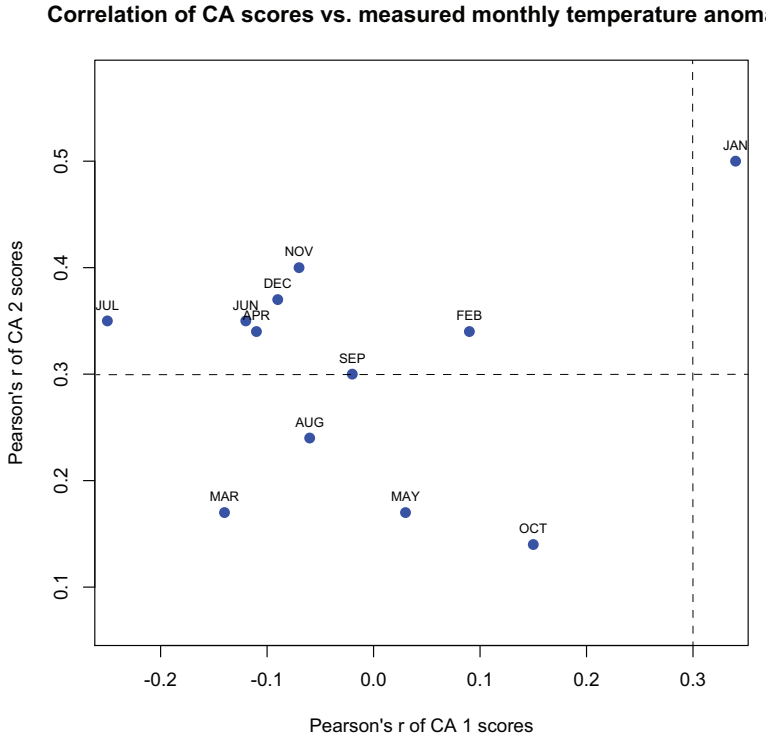

Figure I.3: Correlations of the first and second correspondence analysis (CA) scores of the planktic foraminiferal assemblages and the monthly temperatures from the HadCRUT4 dataset of the $5° \times 5°$ grid cell containing the core station of core 39KG ($20 - 25$ °N, $65 - 70$ °E). January temperatures showed highest correlation coefficients with CA1 ($r = 0.34$, $p = 0.006$) and CA2 ($r = 0.50$, $p < 0.0001$). Correlation coefficients of 0.3 are indicated by dashed lines.

and enable comparison with other calibrated proxy records we therefore used this relationship to reconstruct January temperatures prior to the instrumental period. Samples overlapping with the HadCRUT4 record (1852–1993, $n = 64$) were used for calibrating the transfer function by allocating the 5-year low-pass filtered temperature values to the respective samples of the foraminiferal record. $N = 36$ samples during 1738–1850 were used for reconstruction. A WA-PLS model with two components yielded the lowest prediction error (Table I.2) and was chosen for quantitative reconstructions.

As long as monthly temperature measurements are available, January temperatures in Karachi are constantly recorded lowest during the annual cycle (Figure I.1c) and therefore leave a strong signal in the planktic foraminiferal fauna. Reconstructed temperatures are significantly correlated with CA scores (CA1: $r = 0.28$, $p < 0.01$; CA2: $r = 0.88$, $p < 2.2E - 16$), indicating that changes of the domi-

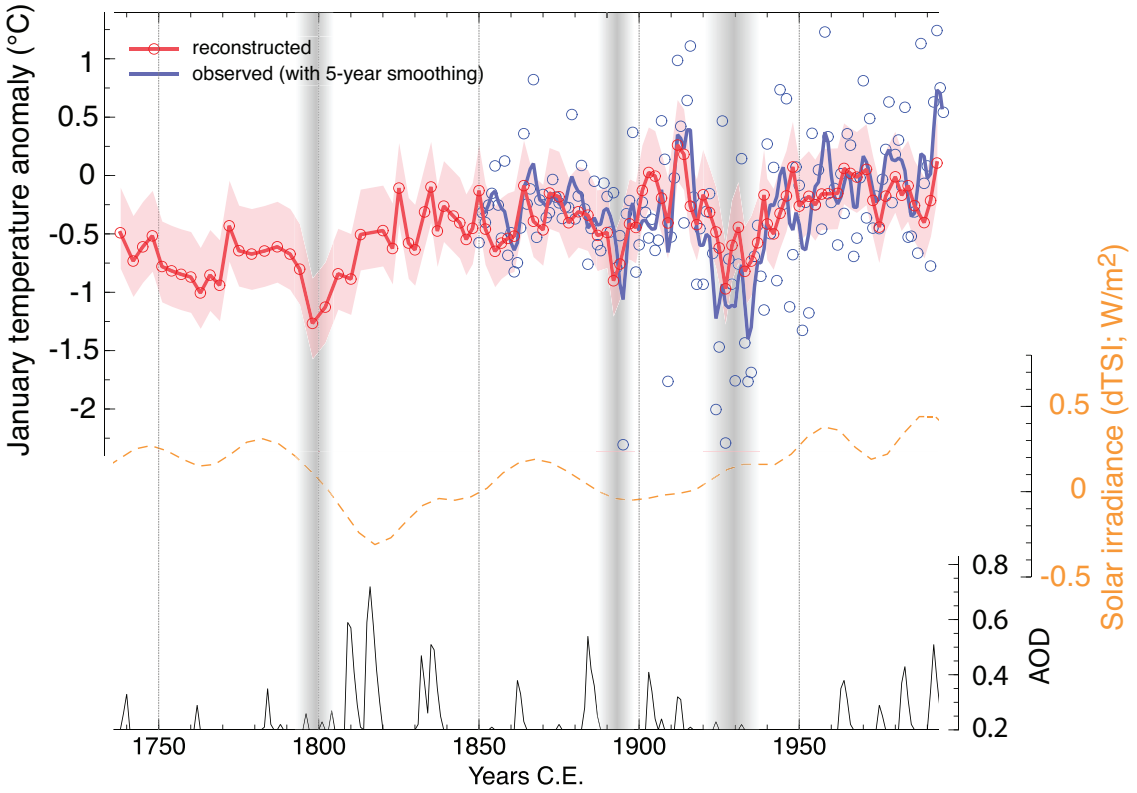

Figure I.4: Reconstructed (red line) and observed (blue circles) January temperature anomalies. Red shading indicates reconstruction uncertainty based on bootstrapping (RMSEP). Observed temperatures were smoothed with a low-pass filter (5-year cutoff frequency) to compensate for high interannual variability (blue line). Orange dashed line is the reconstructed solar irradiance of (Steinhilber et al., 2009). Black graph shows the reconstructed global volcanic aerosol optical depth (AOD) from Crowley and Unterman, (2013). Grey shaded vertical bars indicate three decadal-scale cold episodes from the reconstructed and observed temperature records. Black trend line indicates the ~0.6 °C overall warming trend between 1738 and 1993.

nant foraminiferal taxa are primarily driven by the reconstructed temperatures (Juggins and Birks, 2012). This is a valuable information, since the historical records contain measurements of surface temperatures (land surface, 0 m sea surface) and PF assemblages can potentially be more sensitive to sub-surface water conditions (Telford et al., 2013), which might then not be recording sea surface-atmosphere conditions correctly. The low-pass filtered instrumental temperatures plot generally within the uncertainty range of the reconstructions (Figure I.4) and both time series covary significantly (> 99% confidence level) on sub-decadal to multi-decadal time scales (Figure I.5). This underlines that the foraminiferal-based reconstructions can be used as a valid tool to extend the historical record of regional winter temperature anomalies to pre-industrial times.

Table I.2: Transfer function performance measures based on the root mean squared error (RMSE), the coefficients of determination and the cross-validated root mean squared error of prediction ($RMSEP_{boot}$). Cross-validation is based on bootstrapping over 999 cycles. A transfer function model with two components yielded the lowest prediction error (highlighted).

	RMSE	cross.-val. R^2	$RMSEP_{boot}$
Component1	0.340	0.222	0.372
Component2	0.314	0.285	**0.366**
Component3	0.310	0.291	0.367
Component4	0.309	0.277	0.376
Component5	0.309	0.268	0.382

A noticeable feature from the record of reconstructed January temperatures is a long-term warming trend of ~+0.6 °C towards the present (Figure I.4). This indicates that winter monsoon intensity, reflected by January temperatures, is gradually weakening towards the present and that this trend likely started prior to 1750. The record further reveals three prominent decadal-scale episodes of very low temperatures, i.e. strong IWM intensities. The first, not covered by instrumental observations, from 1795 to 1805, as well as a second one from 1892 to 1894 and a third one from 1925 to 1935. Based on the calibrated relationship of the planktic foraminifera fauna and modern temperatures, the first and most severe cooling was −1.3 °C colder than the reference period (1961–1990), the second (−0.9 °C) and third (−1.0 °C) are almost equally intense. Reconstructed January temperatures were warmest in 1912 during the 'calibration period'. This warming was, however, unprecedented prior to 1850.

Discussion

Cold winter conditions and their relationship to incoming solar radiation

The first of the three cooling episodes shown in Figure I.4 falls together with the beginning of the Dalton solar minimum, lasting from 1780 to 1840 (Anet et al., 2014). Coldest temperatures, however, were recorded asynchronous to periods of minimum irradiance forcing. Similar to basin-wide studies of tropical Indian Ocean springtime sea surface temperatures (Tierney et al., 2015) this may indicate, that solar irradiance is not the main driver of colder winter conditions.

Short-term anomalies of tropical (Tierney et al., 2015; Winter et al., 2015) and European (Sigl et al., 2015) summer climate was also affected by strong volcanic

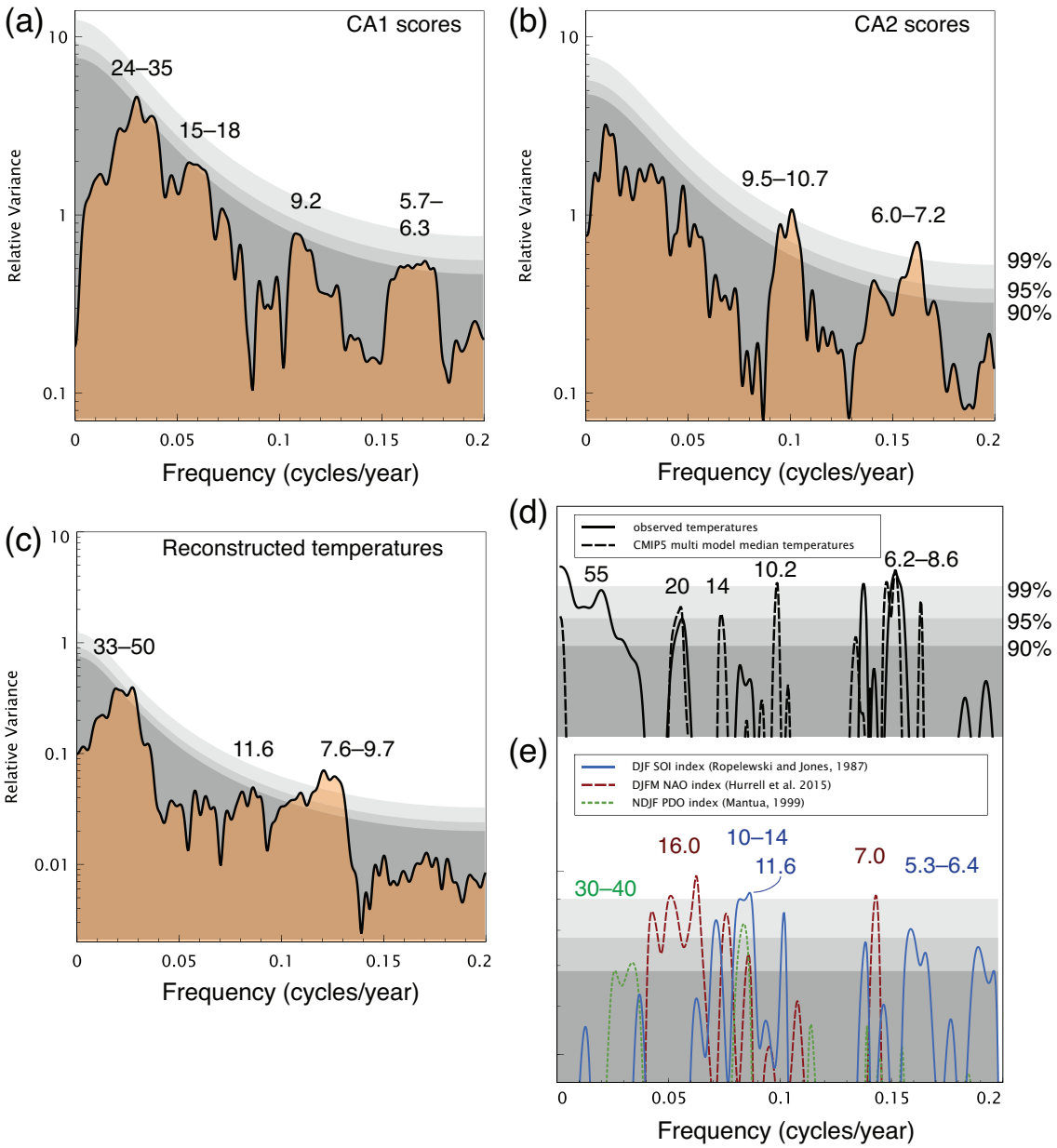

Figure I.5: Frequency spectra and coherence obtained with the multitaper method (MTM) using a red-noise null hypothesis (Ghil et al., 2002). Grey shading indicates significance levels relative to the estimated red noise background above 90%, 95% and 99%, respectively. MTM spectra and significant frequencies of CA1 scores **(a)**, CA2 scores **(b)** and the reconstructed January temperature anomalies **(c)**. Cross-power spectra and significantly coherent frequencies between reconstructed temperatures, as well as observed and simulated temperatures **(d)**, and respective circulation indices **(e)**.

eruptions. Furthermore, volcanic eruptions led to an enhancement of the hydrological cycle in monsoonal Asia (Anchukaitis et al., 2010; Cui et al., 2014). Winter temperatures in Europe were anomalously warm in the years following large volcanic explosions (Robock and Mao, 1992; Wegmann et al., 2014) while cold winter anomalies covered large parts of southern Asia (Shindell et al., 2004).

To test a potential short-lived response of winter conditions in our core to major volcanic eruptions, we compared timings of the four well documented major volcanic eruptions in the early 19th century (Schmidt et al., 2012), the two of unknown origin 1804 and 1809, the Tambora eruption in 1815, as well as two other tropical eruptions 1831 and 1835. None of those were apparently related to the first of the noticeable three cold episodes, as volcanic eruptions occurred ~5–30 years later (Figure I.4). The second cooling in the late 19th century occurred ~10 years after the Krakatoa eruption in 1883, while a possible response would be expected in the second year following the eruption (Shindell et al., 2004). Another smaller short-lived temperature anomaly in 1909, which is also evident from the instrumental temperature record, occurred 3 years earlier to the Novarupta/Katmai (Alaska) eruption in 1912. Generally, the temporal resolution of 2–3 years of our foraminiferal record could be below the detection limit needed to cover the short-lived response of atmospheric perturbations caused by major volcanic eruptions.

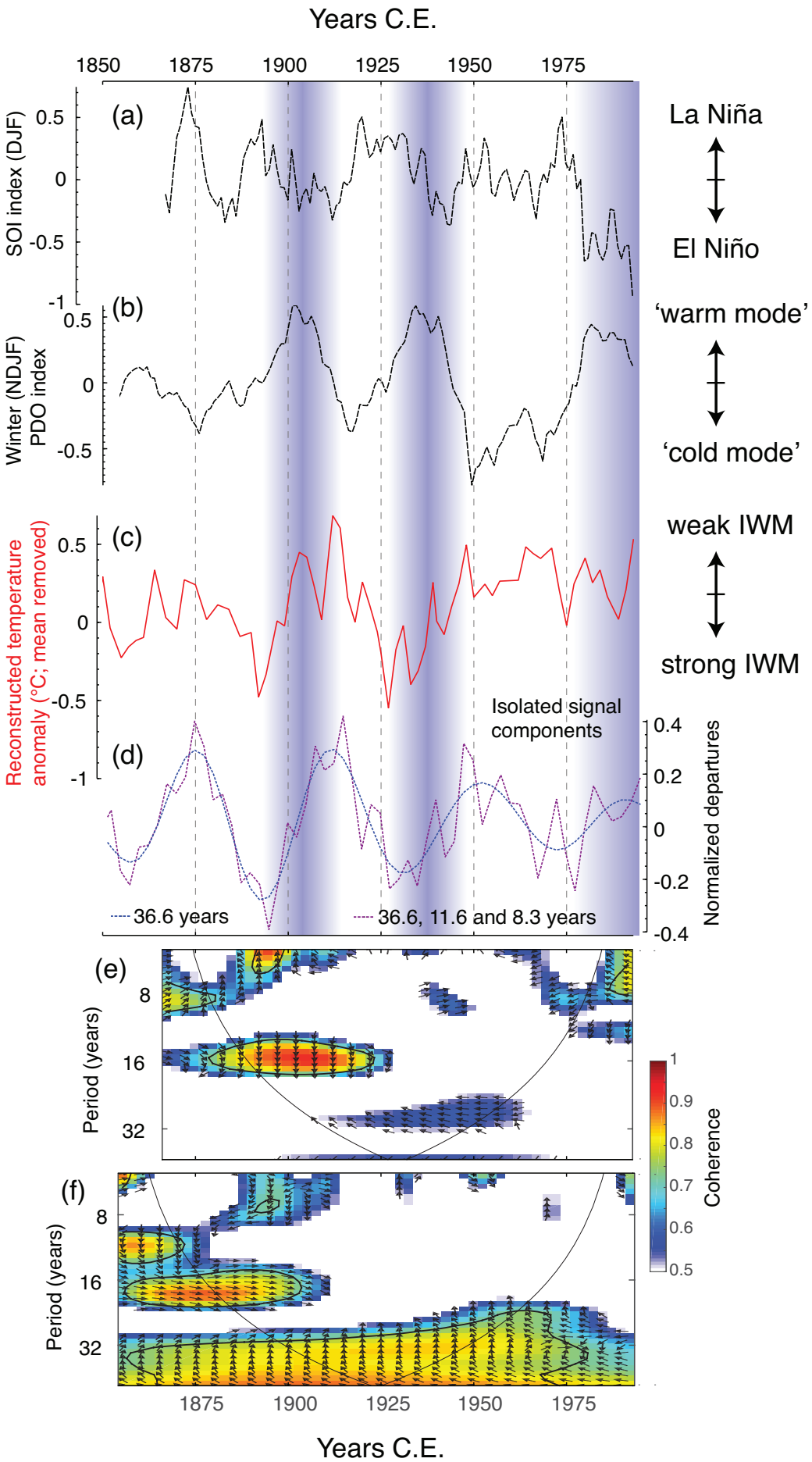
Years C.E.
1850
1875
1900
1925
1950
1975
(a)
SOI index (DJF)
0.5
0
-0.5
-1
La Niña
El Niño
(b)
Winter (NDJF)
PDO index
0.5
0
-0.5
'warm mode'
'cold mode'
(c)
Reconstructed temperature
anomaly (°C; mean removed)
0.5
0
-0.5
-1
weak IWM
strong IWM
Isolated signal
components
(d)
0.4
0.2
0
-0.2
-0.4
Normalized departures
36.6 years
36.6, 11.6 and 8.3 years
(e)
Period (years)
8
16
32
(f)
Period (years)
8
16
32
1
0.9
0.8
0.7
0.6
0.5
Coherence
1875
1900
1925
1950
1975
Years C.E.

Figure I.6: Comparison of **(a)** winter (December–February) Southern Oscillation Index (SOI; 3-year running mean), **(b)** winter (November–February) Pacific Decadal Oscillation Index (PDO; 7-year running mean) and **(c)** detrended reconstructed January temperature anomaly of 39KG between 1850 and 1993. Vertical bars indicate apparent PDO 'warm phases'. **(d)** shows a reconstruction of the isolated signal components identified from the MTM spectrum in Figure I.5c as solely decadal (blue stippling) and summarised decadal- to inter-decadal components (purple stippling). Wavelet coherence analysis of reconstructed temperature estimates with winter (DJF) SOI **(e)** and (NDJF) PDO **(f)** indices. Arrows indicating phase relationships, i.e. for (e) arrows pointing down are interpreted as a 90 ° lag of January temperatures to the anti-phase of the winter SOI index. A 90 ° lag on a 10–14-year bandwidth would convert to 3 years. For (f) the arrow pointing up on the multidecadal ~36-year periodicity can be interpreted as PDO leading January temperatures by a 90 ° phase-angle, thus 90 ° at a wavelength of 36.6 years=9.2 years. SOI is obtained from the NOAA Earth System Research Laboratory (http://www.esrl.noaa.gov/psd/gcos_wgsp/Timeseries/SOI/), PDO from http://www.ncdc.noaa.gov/teleconnections/pdo/.

Teleconnections of IWM climate variability to large-scale circulation patterns

Our temperature reconstructions vary significantly on interannual (7.6–9.7 years), interdecadal (11.6 years) and multidecal (33–50 years) time scales (Figure I.5). These cycles are reflecting the periodicities of the planktic foraminiferal fauna, captured by CA1 and CA2 scores. Reconstructed temperatures vary significantly and coherently with the observational-based Southern Oscillation index (SOI) on the 'classical' interannual ENSO bandwidth (7.6 years) and on a 11.6-year period (Figure I.5). Surprisingly, the ~12-year bandwidth also has coherencies with NAO and PDO indices, a cyclicity that was previously identified from tropical Atlantic trade wind intensity (Black et al., 1999) and Indian Ocean coral $\delta^{18}O$ (Charles et al., 1997; Cobb et al., 2001). This indicates that winter IWM intensities are modulated across seasons on decadal frequencies via a trans-regional teleconnection.
January temperatures are coherent with PDO indices on the 30–40-year cycle (Figure I.5) of PDO phase-shifts (Mantua et al., 1997). The reconstructed multidecadal 36.6-band signal component is lagging the PDO 'warm modes' by ~7 years (Figure I.6), which is also evident from a wavelet coherence analysis. Thus, strong (weak) winter monsoon conditions follow cold (warm) PDO modes on decadal time-scales. Winter temperatures are lagging the anti-phase of SOI on the 10–14 year band by ~3 years Figure I.6), indicating that ENSO and PDO are modulating winter

conditions, although on different frequency bands yet according to PDO modes. However, this relationship is apparently weakening since the beginning of the 20^{th} century, several decades earlier than it was suggested for the Indian summer monsoon (Krishna Kumar et al., 1999).
The NAO is, like ENSO, a major source of interannual global climate variability and contributes largely to Northern Hemisphere temperature patterns (Hurrell, 1996). Based on the finding that the close relationship to NAO is enhanced during the three distinct phases of colder climate (Figure I.7), we hypothesize that the atmospheric circulation over the North Atlantic is the main driver for cold perturbations of IWM climate, potentially through an amplification of the Siberian High (Wu and Wang, 2002). These linkages, as well as the observed weakening of the ENSO-IWM relationship and the general deficiency of describing ENSO and PDO properties in climate simulations (Bellenger et al., 2014) adds to the complexity of reproducing winter monsoon climatology in current state-of-the-art climate models (Gong et al., 2014). Although the simulated January temperatures are coherent with reconstructed and observed January temperatures on interdecadal- to decadal-scale frequencies (Figure I.5), models fail to reproduce the timing and temperature pattern from our record (Figure I.8).

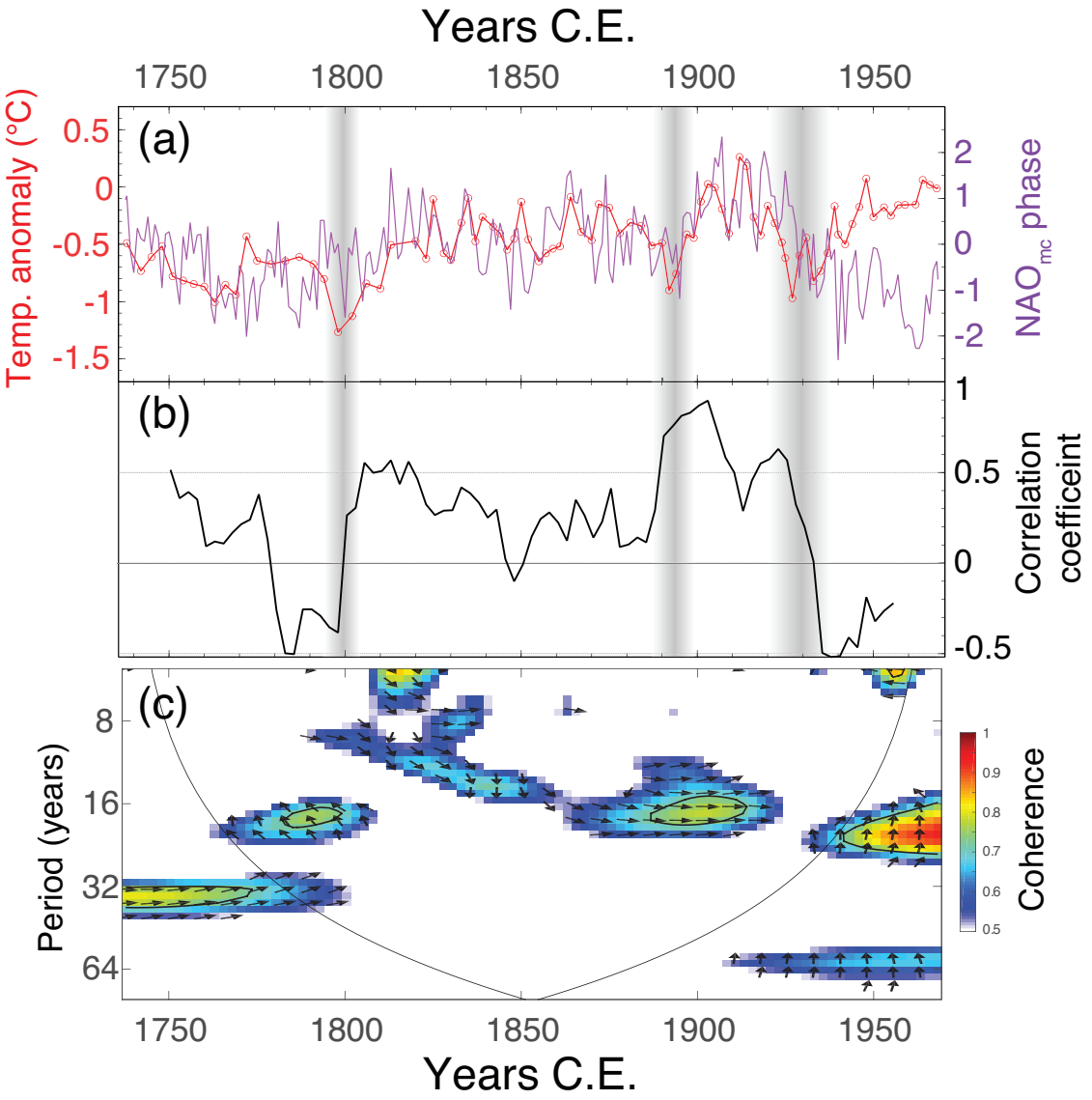

Figure I.7: (a) Time series of the reconstructed January temperature anomalies (red line) and the reconstructed model-constrained North Atlantic Oscillation (NAO_{mc}, purple line) from (Ortega et al., 2015). **(b)** Running correlation along a 25-year sliding window and **(c)** wavelet coherence analysis reveals that both records show highest correlations and coherency around the three obvious cold spells of the winter temperature record. Coherency on the 16-year bandwidth is consistent with the instrumental-based winter NAO index (Figure I.5e). Both records are negatively correlated and phase-shifted during the first cold phase around the year ~1800, but in-phase and positively correlated during the second cold phase around ~1890.

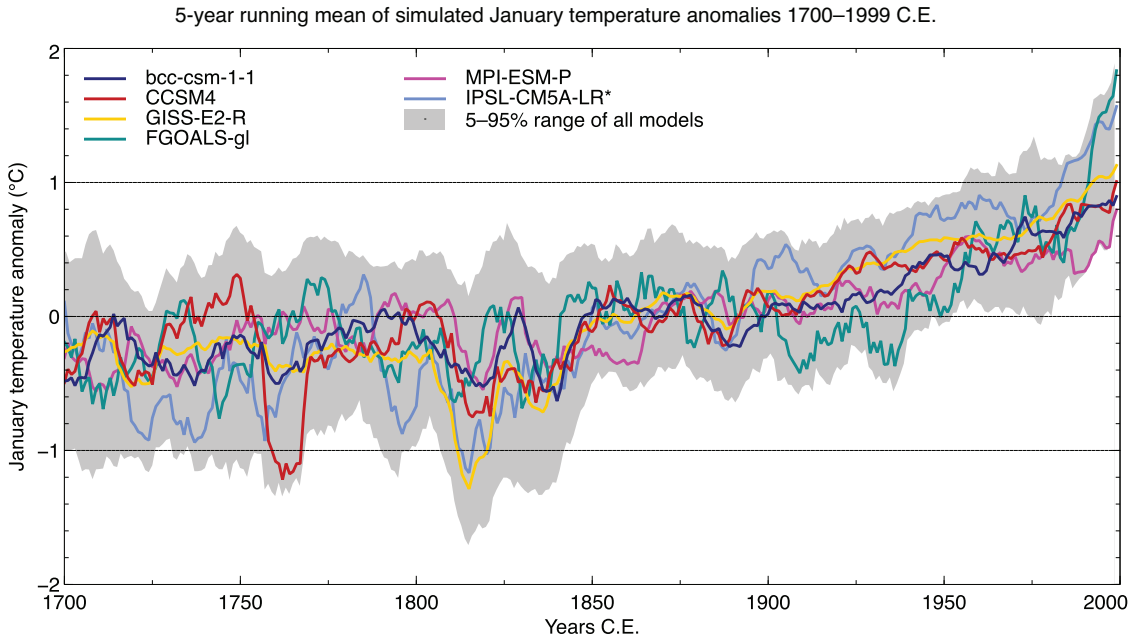

Figure I.8: Simulated January temperature anomalies (relative to the each model's average from 1700–1999 and smoothed with a 5-year running average) obtained from the Coupled Model Intercomparison Project 5 of the grid cell containing the core location of 39KG ($20-25\,^{\circ}$N; $65-70\,^{\circ}$E) covering the period 1700–1999. The 5%–95% percentile ranges of all models are plotted as grey shading. Results of the IPSL-CM5A-LR experiment (star) does only contain atmospheric output (Amon).

Summary

Our results show that winter monsoon intensities in the Arabian Sea are coupled to Pacific and North Atlantic climate, but with a complex and shifting pattern. A better understanding of extratropical and tropical influences on winter monsoon climate might help to improve model performance (Levine et al., 2013), and hence, predictability of tropical to mid-latitude winter climate conditions in the Northern Hemisphere.

References

Agnihotri, R., K. Dutta, R. Bhushan, and B. Somayajulu (2002): 'Evidence for solar forcing on the Indian monsoon during the last millennium'. *Earth and Planetary Science Letters*, vol. 198(3-4): pp. 521–527.

Anchukaitis, K. J., B. M. Buckley, E. R. Cook, B. I. Cook, R. D. D´Arrigo, and C. M. Ammann (2010): 'Influence of volcanic eruptions on the climate of the Asian monsoon region'. *Geophysical Research Letters*, vol. 37(22): p. L22703.

Anet, J. G., S. Muthers, E. V. Rozanov, C. C. Raible, A. Stenke, A. I. Shapiro, S. Brönnimann, F. Arfeuille, Y. Brugnara, J. Beer, F. Steinhilber, W. Schmutz, and T. Peter (2014): 'Impact of solar versus volcanic activity variations on tropospheric temperatures and precipitation during the Dalton Minimum'. *Climate of the Past*, vol. 10(3): pp. 921–938.

Ashok, K., Z. Guan, N. H. Saji, and T. Yamagata (2004): 'Individual and combined influences of ENSO and the Indian Ocean dipole on the Indian summer monsoon'. *Journal of Climate*, vol. 17(16): pp. 3141–3155.

Ashok, K. and N. H. Saji (2007): 'On the impacts of ENSO and Indian Ocean dipole events on sub-regional Indian summer monsoon rainfall'. *Natural Hazards*, vol. 42(2): pp. 273–285.

Barber, R. T., J. Marra, R. C. Bidigare, L. A. Codispoti, D. Halpern, Z. Johnson, M. Latasa, R. Goericke, and S. L. Smith (2001): 'Primary productivity and its regulation in the Arabian Sea during 1995'. *Deep Sea Research Part II: Topical Studies in Oceanography*, vol. 48(6-7): pp. 1127–1172.

Bellenger, H., E. Guilyardi, J. Leloup, M. Lengaigne, and J. Vialard (2014): 'ENSO representation in climate models: from CMIP3 to CMIP5'. *Climate Dynamics*, vol. 42(7-8): pp. 1999–2018.

Bhanu Kumar, O. S. R. U., C. V. Naidu, S. R. L. Rao, and B. Ravi Srinivasa Rao (2004): 'Prediction of southern Indian winter monsoon rainfall from September local upper-air temperatures'. *Meteorological Applications*, vol. 11(3): pp. 189–199.

Birks, H., O. Heiri, H. Seppä, and A. E. Bjune (2010): 'Strengths and weaknesses of quantitative climate reconstructions based on late-Quaternary biological proxies'. *Open Ecology Journal*, vol. 3: pp. 68–110.

Black, D. E., L. C. Peterson, J. T. Overpeck, A. Kaplan, M. N. Evans, and M. Kashgarian (1999): 'Eight centuries of North Atlantic Ocean atmosphere variability'. *Science*, vol. 286(5445): pp. 1709–1713.

Böll, A., H. Schulz, P. M. Munz, T. Rixen, B. Gaye, and K.-C. Emeis (2015): 'Contrasting sea surface temperature of summer and winter monsoon variability in the northern Arabian Sea over the last 25ka'. *Palaeogeography, Palaeoclimatology, Palaeoecology*, vol. 426: pp. 10–21.

Charles, C. D., D. E. Hunter, and R. G. Fairbanks (1997): 'Interaction Between the ENSO and the Asian Monsoon in a Coral Record of Tropical Climate'. *Science*, vol. 277(5328): pp. 925–928.

Clark, C. O., J. E. Cole, and P. J. Webster (2000): 'Indian Ocean SST and Indian summer rainfall: Predictive relationships and their decadal variability'. *Journal of Climate*, vol. 13(14): pp. 2503–2519.

Cobb, K. M., C. D. Charles, and D. E. Hunter (2001): 'A central tropical Pacific coral demonstrates Pacific, Indian, and Atlantic decadal climate connections'. *Geophysical Research Letters*, vol. 28(11): pp. 2209–2212.

Cowtan, K. and R. G. Way (2014): 'Coverage bias in the HadCRUT4 temperature series and its impact on recent temperature trends'. *Quarterly Journal of the Royal Meteorological Society*, vol. 140(683): pp. 1935–1944.

Crowley, T. J. and M. B. Unterman (2013): 'Technical details concerning development of a 1200 yr proxy index for global volcanism'. *Earth System Science Data*, vol. 5(1): pp. 187–197.

Cui, X., Y. Gao, and J. Sun (2014): 'The response of the East Asian summer monsoon to strong tropical volcanic eruptions'. *Advances in Atmospheric Sciences*, vol. 31(6): pp. 1245–1255.

Dimri, A. P. (2013): 'Intraseasonal oscillation associated with the Indian winter monsoon'. *Journal of Geophysical Research: Atmospheres*, vol. 118(3): pp. 1189–1198.

Doose-Rolinski, H., U. Rogalla, G. Scheeder, A. Lückge, and U. von Rad (2001): 'High-resolution temperature and evaporation changes during the late Holocene in the northeastern Arabian Sea'. *Paleoceanography*, vol. 16(4): pp. 358–367.

Ghil, M., M. Allen, M. Dettinger, K. Ide, D. Kondrashov, M. Mann, A. Robertson, A. Saunders, Y. Tian, F. Varadi, and P. Yiou (2002): 'Advanced spectral methods for climatic time series'. *Reviews of Geophysics*, vol. 40(1): pp. 3-1–3-41.

Gong, H., L. Wang, W. Chen, R. Wu, K. Wei, and X. Cui (2014): 'The Climatology and Interannual Variability of the East Asian Winter Monsoon in CMIP5 Models'. *Journal of Climate*, vol. 27(4): pp. 1659–1678.

Grinsted, A., J. C. Moore, and S. Jevrejeva (2004): 'Application of the cross wavelet transform and wavelet coherence to geophysical time series'. *Nonlinear Processes in Geophysics*, vol. 11(5-6): pp. 561–566.

Gupta, A. K., M. Das, and D. M. Anderson (2005): 'Solar influence on the Indian summer monsoon during the Holocene'. *Geophysical Research Letters*, vol. 32(17): p. L17703.

Hurrell, J. W. (1996): 'Influence of variations in extratropical wintertime teleconnections on northern hemisphere temperature'. *Geophysical Research Letters*, vol. 23(6): pp. 665–668.

Juggins, S. (2015): *rioja: Analysis of Quaternary Science Data*. R package version (0.8-7).

Juggins, S. and H. Birks (2012): 'Quantitative environmental reconstructions from biological data'. *Tracking environmental change using lake sediments*. Ed. by Birks, H. J. B., A. F. Lotter, S. Juggins, and J. P. Smol. Developments in Paleoenvironmental Research 5. Springer Netherlands.

Krishna Kumar, K., B. Rajagopalan, and M. Cane (1999): 'On the weakening relationship between the Indian monsoon and ENSO'. *Science*, vol. 284(5423): pp. 2156–2159.

Krishna Kumar, K., B. Rajagopalan, M. Hoerling, G. Bates, and M. Cane (2006): 'Unraveling the Mystery of Indian Monsoon Failure During El Nino'. *Science*, vol. 314(5796): pp. 115–119.

Krishnamurthy, L. and V. Krishnamurthy (2014): 'Decadal scale oscillations and trend in the Indian monsoon rainfall'. *Climate Dynamics*, vol. 43(1-2): pp. 319–331.

Krishnan, R. and M. Sugi (2003): 'Pacific decadal oscillation and variability of the Indian summer monsoon rainfall'. *Climate Dynamics*, vol. 21(3-4): pp. 233–242.

Kucera, M., M. Weinelt, T. Kiefer, U. Pflaumann, A. Hayes, M. Weinelt, M.-T. Chen, A. C. Mix, T. T. Barrows, E. Cortijo, J. Duprat, S. Juggins, and C. Waelbroeck (2005): 'Reconstruction of sea-surface temperatures from assemblages of planktonic foraminifera: multi-technique approach based on geographically constrained calibration data sets and its application to glacial Atlantic and Pacific Oceans'. *Quaternary Science Reviews*, vol. 24(7-9): pp. 951–998.

Levine, R. C., A. G. Turner, D. Marathayil, and G. M. Martin (2013): 'The role of northern Arabian Sea surface temperature biases in CMIP5 model simulations and future projections of Indian summer monsoon rainfall'. *Climate Dynamics*, vol. 41(1): pp. 155–172.

Liu, X. and Z.-Y. Yin (2001): 'Spatial and Temporal Variation of Summer Precipitation over the Eastern Tibetan Plateau and the North Atlantic Oscillation'. *Journal of Climate*, vol. 14(13): pp. 2896–2909.

Mann, M. E. and J. M. Lees (1996): 'Robust estimation of background noise and signal detection in climatic time series'. *Climatic change*, vol. 33(3): pp. 409–445.

Mantua, N. J., S. R. Hare, Y. Zhang, J. M. Wallace, and R. C. Francis (1997): 'A Pacific Interdecadal Climate Oscillation with Impacts on Salmon Production'. *Bulletin of the American Meteorological society*, vol. 78(6): pp. 1069–1079.

Mohtadi, M., M. Prange, D. W. Oppo, R. De Pol-Holz, U. Merkel, X. Zhang, S. Steinke, and A. Lückge (2014): 'North Atlantic forcing of tropical Indian Ocean climate'. *Nature*, vol. 509(7498): pp. 76–80.

Morice, C. P., J. J. Kennedy, N. A. Rayner, and P. D. Jones (2012): 'Quantifying uncertainties in global and regional temperature change using an ensemble of observational estimates: The HadCRUT4 data set'. *Journal of Geophysical Research*, vol. 117(D8): p. D08101.

Munz, P. M., M. Siccha, A. Lückge, A. Böll, M. Kucera, and H. Schulz (2015): 'Decadal-resolution record of winter monsoon intensity over the last two millennia from planktic foraminiferal assemblages in the northeastern Arabian Sea'. *The Holocene*, vol. 25(11): pp. 1756–1771.

Oksanen, J., F. G. Blanchet, R. Kindt, P. Legendre, P. R. Minchin, R. B. O´Hara, G. L. Simpson, P. Solymos, M. H. H. Stevens, and H. Wagner (2015): *vegan: Community Ecology Package*. R package version 2.3-1.

Ortega, P., F. Lehner, D. Swingedouw, V. Masson-Delmotte, C. C. Raible, M. Casado, and P. Yiou (2015): 'A model-tested North Atlantic Oscillation reconstruction for the past millennium'. *Nature*, vol. 523(7558): pp. 71–74.

Prasanna Kumar, S. and T. G. Prasad (1999): 'Formation and spreading of Arabian Sea high-salinity water mass'. *Journal of Geophysical Research*, vol. 104(C1): pp. 1455–1464.

R Core Team (2015): *R: A Language and Environment for Statistical Computing*. R Foundation for Statistical Computing. Vienna, Austria.

Robock, A. and J. Mao (1992): 'Winter warming from large volcanic eruptions'. *Geophysical Research Letters*, vol. 19(24): pp. 2405–2408.

Schiebel, R., A. Zeltner, U. F. Treppke, and J. J. Waniek (2004): 'Distribution of diatoms, coccolithophores and planktic foraminifers along a trophic gradient during SW monsoon in the Arabian Sea'. *Marine Micropaleontology*, vol. 51(3-4): pp. 345–371.

Schmidt, A., K. S. Carslaw, G. W. Mann, A. Rap, K. J. Pringle, D. V. Spracklen, M. Wilson, and P. M. Forster (2012): 'Importance of tropospheric volcanic aerosol for indirect radiative forcing of climate'. *Atmospheric Chemistry and Physics*, vol. 12(16): pp. 7321–7339.

Schulz, H., U. von Rad, and V. Ittekkot (2002): 'Planktic foraminifera, particle flux and oceanic productivity off Pakistan, NE Arabian Sea: modern analogues and application to the paleoclimatic record'. *The Tectonic and Climatic Evolution of the Arabian Sea Region*. Ed. by Clift, P., D. Kroon, C. Gaedicke, and J. Craig. Vol. 195. London: Geological Society Special Publications: pp. 499–516.

Shen, J., X. Wu, Z. Zhang, W. Gong, T. He, X. Xu, and H. Dong (2013): 'Ti content in Huguangyan maar lake sediment as a proxy for monsoon-induced vegetation density in the Holocene'. *Geophysical Research Letters*, vol. 40(21): pp. 5757–5763.

Shindell, D. T., G. A. Schmidt, M. E. Mann, and G. Faluvegi (2004): 'Dynamic winter climate response to large tropical volcanic eruptions since 1600'. *Journal of Geophysical Research*, vol. 109(D5): p. D05104.

Sigl, M. et al. (2015): 'Timing and climate forcing of volcanic eruptions for the past 2,500 years'. *Nature*, vol. 523(7562): pp. 543–549.

Song, F. and T. Zhou (2015): 'The Crucial Role of Internal Variability in Modulating the Decadal Variation of the East Asian Summer Monsoon–ENSO Relationship during the Twentieth Century'. *Journal of Climate*, vol. 28(18): pp. 7093–7107.

Steinhilber, F., J. Beer, and C. Fröhlich (2009): 'Total solar irradiance during the Holocene'. *Geophysical Research Letters*, vol. 36(19): p. L19704.

Telford, R. J., C. Li, and M. Kucera (2013): 'Mismatch between the depth habitat of planktonic foraminifera and the calibration depth of SST transfer functions may bias reconstructions'. *Climate of the Past*, vol. 9(2): pp. 859–870.

Ter Braak, C. J. F., S. Juggins, H. J. B. Birks, and H. van der Voet (1993): 'Weighted averaging partial least squares regression (WA-PLS): Definition and comparison with other methods for species-environment calibration'. *Multivariate Environmental Statistics*. Ed. by Patil, G. P. and C. R. Rao. Amsterdam: Elsevier Science Publishers. Chap. 25: pp. 525–560.

Terray, P., E. Guilyardi, A. S. Fischer, and P. Delecluse (2005): 'Dynamics of the Indian monsoon and ENSO relationships in the SINTEX global coupled model'. *Climate Dynamics*, vol. 24(2-3): pp. 145–168.

Tierney, J. E., N. J. Abram, K. J. Anchukaitis, M. N. Evans, C. Giry, K. H. Kilbourne, C. P. Saenger, H. C. Wu, and J. Zinke (2015): 'Tropical sea surface temperatures for the past four centuries reconstructed from coral archives'. *Paleoceanography*, vol. 30(3): pp. 226–252.

Ummenhofer, C. C., R. D. D´Arrigo, K. J. Anchukaitis, B. M. Buckley, and E. R. Cook (2013): 'Links between Indo-Pacific climate variability and drought in the Monsoon Asia Drought Atlas'. *Climate Dynamics*, vol. 40(5-6): pp. 1319–1334.

von Rad, U., M. Schaaf, K. H. Michels, H. Schulz, W. H. Berger, and F. Sirocko (1999): 'A 5000-yr record of climate change in varved sediments from the oxygen minimum zone off Pakistan, northeastern Arabian sea'. *Quaternary Research*, vol. 51(1): pp. 39–53.

von Rad, U. et al. (1995): 'Sampling the oxygen minimum zone off Pakistan: glacial-interglacial variations of anoxia and productivity (preliminary results, sonne 90 cruise)'. *Marine Geology*, vol. 125(1-2): pp. 7–19.

Wang, B., S. C. Clemens, and P. Liu (2003): 'Contrasting the Indian and East Asian monsoons: implications on geologic timescales'. *Marine Geology*, vol. 201: pp. 5–21.

Wang, L., J. Li, H. Lu, Z. Gu, P. Rioual, Q. Hao, A. W. Mackay, W. Jiang, B. Cai, B. Xu, J. Han, and G. Chu (2012): 'The East Asian winter monsoon over the last 15,000 years: its links to high-latitudes and tropical climate systems and complex correlation to the summer monsoon'. *Quaternary Science Reviews*, vol. 32: pp. 131–142.

Webster, P. J., V. O. Magaña, T. N. Palmer, J. Shukla, R. A. Tomas, M. Yanai, and T. Yasunari (1998): 'Monsoons: Processes, predictability, and the prospects for prediction'. *Journal of Geophysical Research: Oceans*, vol. 103(C7): pp. 14451–14510.

Wegmann, M., S. Brönnimann, J. Bhend, J. Franke, D. Folini, M. Wild, and J. Luterbacher (2014): 'Volcanic Influence on European Summer Precipitation through Monsoons: Possible Cause for "Years without Summer"*'. *Journal of Climate*, vol. 27(10): pp. 3683–3691.

Winter, A., D. Zanchettin, T. Miller, Y. Kushnir, D. Black, G. Lohmann, A. Burnett, G. H. Haug, J. Estrella-Martínez, S. F. M. Breitenbach, L. Beaufort, A. Rubino, and H. Cheng (2015): 'Persistent drying in the tropics linked to natural forcing'. *Nature Communications*, vol. 6(7627).

Wu, B. and J. Wang (2002): 'Winter Arctic Oscillation, Siberian High and East Asian Winter Monsoon'. *Geophysical Research Letters*, vol. 29(19): p. 1897.

Late Holocene primary productivity and sea surface temperature variations in the northeastern Arabian Sea: Implications for winter monsoon variability

Paleoceanography

Vol. 29, No. 8, p. 778–794, 2014. doi:10.1002/2013PA002579

Anna Böll[1], Andreas Lückge[2], Philipp Munz[3],Sven Forke[4], Hartmut Schulz[3], V. Ramaswamy[5], Tim Rixen[4], Birgit Gaye[1] and Kay-Christian Emeis[1,6]

[1]*Institute of Biogeochemistry and Marine Chemistry, University of Hamburg, Hamburg, Germany,;*
[2]*Bundesanstalt für Geowissenschaften und Rohstoffe, Hannover, Germany;*
[3]*Department of Geosciences, University of Tübingen, Tübingen, Germany;*
[4]*Leibniz Center for Tropical Marine Ecology, Bremen, Germany;*
[5]*National Institute of Oceanography, Goa, India;*
[6]*Institute of Coastal Research, Helmholtz Center Geesthacht, Geesthacht, Germany;*

Key Points: Winter monsoon strength influences productivity and SST off Pakistan; Late Holocene NE monsoon intensity is anticorrelated with the Asian SW monsoon The winter monsoon record is in phase with Northern Hemisphere climate periods

Abstract

Variability in the oceanic environment of the Arabian Sea region is strongly influenced by the seasonal monsoon cycle of alternating wind directions. Prominent and well studied is the summer monsoon, but much less is known about late Holocene changes in winter monsoon strength with winds from the northeast that drive convective mixing and high surface ocean productivity in the northeastern Arabian Sea. To establish a high-resolution record of winter monsoon variability for the late Holocene, we analyzed alkenone-derived sea surface temperature (SST) variations and proxies of primary productivity (organic carbon and δ^{15}N) in a well-laminated sediment core from the Pakistan continental margin. Weak winter monsoon intensities off Pakistan are indicated from 400 B.C. to 250 A.D. by reduced productivity and relatively high SST. At about 250 A.D., the intensity of the winter monsoon increased off Pakistan as indicated by a trend to lower SST. We infer that monsoon conditions were relatively unstable from ~500 to 1300 A.D., because primary production and SST were highly variable. Declining SST and elevated biological production from 1400 to 1900 A.D. suggest invigorated convective winter mixing by strengthening winter monsoon circulation, most likely a regional expression of colder climate conditions during the Little Ice Age on the Northern Hemisphere. The comparison of winter monsoon intensity with records of summer monsoon intensity suggests that an inverse relationship between summer and winter monsoon strength exists in the Asian monsoon system during the late Holocene, effected by shifts in the Intertropical Convergence Zone.

Introduction

The Asian monsoon system is one of the most important components of global climate. Although variations in the Asian monsoon have a great impact on climatological and biogeochemical processes in the ocean as well as on land, there are yet few high-resolution studies recording monsoon variability during the last 2000 years. One opportunity to establish such high-resolution records of late Holocene climate change comes from laminated sediments deposited on the Makran continental margin in the northeastern Arabian Sea (Doose-Rolinski et al., 2001; Lückge et al., 2001; von Rad et al., 1999).

Primary productivity in the Arabian Sea is high and is tightly linked to the seasonal dynamics of the Asian monsoon system. Forced by reversing atmospheric pressure

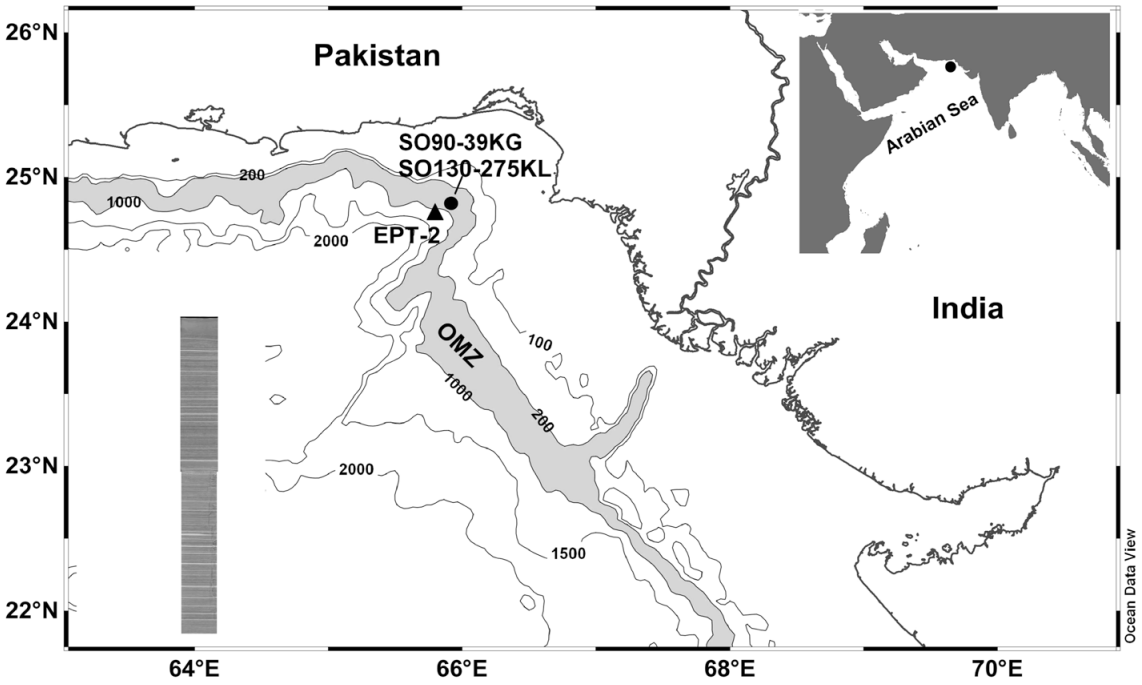

Figure II.1: Study area in the northeastern Arabian Sea off Pakistan with core locations 275KL and 39KG and sediment trap station EPT-2. The shaded area indicates OMZ impinging on the continental slope. Bathymetry is shown in meters. Inset: vertical profile of core 275KL showing varve-like lamination. This map is produced by using Ocean Data View (Schlitzer, 2013).

gradients between central Asia and the southern Indian Ocean and accompanied by shifts in the Intertropical Convergence Zone (ITCZ) (Clemens et al., 1991), low-level winds reverse direction in the course of the year. Strong southwesterly winds during the summer months caused by differential land-ocean heating in spring (Hastenrath and Lamb, 1979) induce clockwise surface water circulation in the Arabian Sea. As a consequence, upwelling of nutrient-rich waters along the coast off Somalia, Oman, and southwest India supports high biological productivity during the months June to September (Haake et al., 1993; Nair et al., 1989; Rixen et al., 1996). A secondary primary productivity peak in the northern basin is initiated when the wind direction reverses due to faster cooling of the continent in fall (Rixen et al., 2005). Prevailing moderate and dry northeasterly winds in winter drive a counterclockwise surface circulation and cool Arabian Sea surface waters (Wyrtki, 1973), thereby initiating convective winter mixing that provides nutrients for seasonally and regionally enhanced biological productivity (Banse and McClain, 1986; Madhupratap et al., 1996).

Whereas most sediment trap studies in the central Arabian Sea indeed indicate

highest biological productivity during the summer monsoon (Broerse et al., 2000; Prahl et al., 2000; Wakeham et al., 2002); highest particle fluxes in the northeastern Arabian Sea are observed during the winter monsoon season (Andruleit et al., 2000; Lückge et al., 2002; Rixen et al., 2005; Schulz et al., 2002) and are associated with sea surface cooling down to about 23 °C. Hence, periods of low sea surface temperatures (SSTs) in the northeastern Arabian Sea are linked to the cool northeast monsoonal winds during winter.

We know today that monsoon activity varied not only on Milankovitch time scales but also during the late Holocene, as evident in Arabian Sea sediments (Agnihotri et al., 2008; Anderson et al., 2010, 2002; Chauhan et al., 2010; Gupta et al., 2003, 2011; Lückge et al., 2001; von Rad et al., 1999) and in various cave records from Oman (Burns et al., 2002; Fleitmann et al., 2004), Yemen (Van Rampelbergh et al., 2013), India (Berkelhammer et al., 2010; Sinha et al., 2007, 2011), and China (Zhang et al., 2008). Similarly, primary productivity in the Arabian Sea was not uniform on time scales of a few hundred thousand years but tracked monsoon variations caused by glacial/interglacial cycles (Rostek et al., 1997; Schulte and Müller, 2001; Schulte et al., 1999; Schulz et al., 1998). Although some knowledge exists about summer monsoon-related changes in primary productivity over the last 2000 years from the Oman Margin (Anderson et al., 2010, 2002; Gupta et al., 2003) and the southwestern coast off India (Agnihotri et al., 2008), paleoceanographic responses to late Holocene winter monsoon variability in the northeastern Arabian Sea are unknown.

Here we report a high-resolution record of winter monsoon variability for the late Holocene discerned from changes in primary productivity and sea surface temperature for the mainly winter monsoon-dominated northeastern Arabian Sea. We analyzed a 188 cm long section of a well-laminated sediment core from the Pakistan Margin (Figure II.1) for bulk components (organic carbon, carbonate, and opal), stable nitrogen isotopes, and alkenone unsaturation ratios to reconstruct the productivity and monsoon variability throughout the last 2400 years. A key proxy for the winter monsoon intensity is the alkenone-derived SST estimate, which we validate by analyzing the seasonality of the alkenone-based SST signal at eastern PAKOMIN sediment trap station (EPT-2) close to our core location. Our detailed objectives are to (1) examine the relationship between SST and alkenone unsaturation ratios in sediment trap material for the northeastern Arabian Sea, (2) reconstruct late Holocene (winter monsoon-dominated) SST and

paleoproductivity changes for the northeastern Arabian Sea, (3) compare the winter monsoon-dominated record with records of summer monsoon variability to learn about the dynamics of the monsoon low-level wind system, and (4) examine possible links in the regional wind and surface ocean system to Northern Hemisphere climate change in historical time.

Study Area

Unlike offshore the coast of Somalia, Oman, and southeast India, upwelling does not occur during the southwest (SW) monsoon season on the Pakistan Margin, so that SSTs are warm during summer (27.8 to 29.3 °C). In the northeastern Arabian Sea, high productivity during the SW monsoon in summer is partly supported by the lateral advection of nutrient-rich surface waters from the upwelling area off Oman (Schulz et al., 1996). Cool winter SSTs (~23 °C) during the northeast (NE) monsoon season are accompanied by a deepening of the mixed layer through convective mixing (Figure II.2) that stimulates a second peak in primary production (Banse and McClain, 1986; Madhupratap et al., 1996). During this season, reduced solar insolation together with enhanced evaporation lead to density increase of surface waters and convective deepening of the mixed layer over the Pakistan Margin. Concentrations of nitrate and chlorophyll a and primary production in the surface layer here correlate with mixed layer depth and wind speeds (Madhupratap et al., 1996; Prasanna Kumar and Prasad, 1996; Prasanna Kumar et al., 2001). Increased particle fluxes during the months of January and February indicate even higher production during the NE monsoon season than during the SW monsoon season over the Pakistan Margin (Andruleit et al., 2000; Schulz et al., 2002, ; see Figure II.2).

In the northern Arabian Sea, a stable midwater oxygen minimum zone (OMZ) between 200 and 1200 m water depth is maintained by high organic matter fluxes and subsequent oxygen consumption during mineralization of organic matter, combined with reduced vertical mixing caused by the input of warm, saline water masses from the Persian Gulf and the Red Sea to intermediate water depths (Olson et al., 1993; Schulz et al., 1996). High organic matter fluxes from the euphotic zone raise rates of denitrification in the OMZ, which in turn raise the δ^{15}N values of thermocline nitrate mixed into the surface layer and assimilated by phytoplankton. Intensification of the OMZ thus results in high sedimentary δ^{15}N values upon burial of particulate N, whereas weakening of the OMZ and reduced

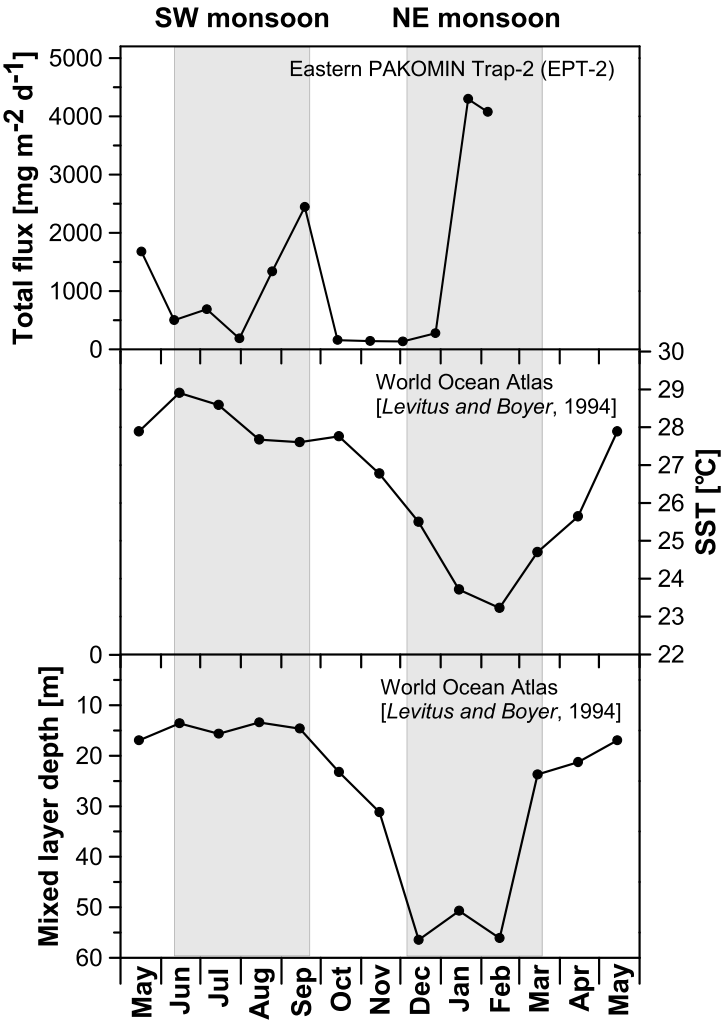

Figure II.2: Annual variability of mixed layer depth and SST for site 275KL extracted from the World Ocean Atlas (Levitus and Boyer, 1994) and total particle flux measured in sediment trap EPT-2 after Andruleit et al., (2000). Increased particle fluxes occur during the NE monsoon season when strong convective winter mixing deepens the mixed layer and SST decreases.

denitrification intensity lead to low sedimentary δ^{15}N values (e.g., Altabet et al., 1995; Gaye-Haake et al., 2005; Naqvi et al., 1998; Suthhof et al., 2001).

Sediments deposited within the OMZ depth interval on the Pakistan Margin are laminated with alternating dark and light sediment layers and record high input of lithogenic material originating from dust storms and/or river runoff (Schulz et al., 1996; von Rad et al., 1999, 1995). Lückge et al., (2002) showed that dark laminae are deposited over large parts of the year and reflect primary production of marine organic matter, whereas light-colored laminae contain almost exclusively land-

derived materials which are deposited in the winter season during short-term heavy rainfall events.

Methods

Sample Collection and Stratigraphy

In this study we investigated piston core 275KL and box core 39KG, both located within the center of the OMZ off the Pakistan coast (Figure 1). The box core 39KG (24 °50.01'N, 65 °55.01'E; 695 m water depth) was collected in 1993 during SONNE cruise 90, and results were published by Doose-Rolinski et al., (2001) and von Rad et al., (1999) and Lückge et al., (2001). The piston core 275KL was retrieved from the same position in 1998 during SONNE cruise 130 (24 °49.31'N, 65 °54.60'E; 782 m water depth). We studied the top 188 cm interval of core 275KL and the top 15 cm of core 39KG, which together yield a continuous record of environmental conditions on the Pakistan Margin over the last 2400 years. Core 275KL was continuously sampled in 0.5 cm intervals (sample resolution of 5 to 80 years) for bulk analysis (organic carbon and carbonate), and every third or fourth sample (of this sample series) was analyzed for opal concentrations and stable nitrogen isotope measurements. Alkenones were measured at continuous 2 cm intervals in core 275KL. In core 39KG, all parameters were analyzed on 1 cm intervals (6 to 8year resolution). All samples were freeze dried and homogenized with mortar and pestle prior to chemical treatment and analyses.

In addition to seasonal varves, core 275KL exhibits reddish brown silt turbidites up to 9 cm thick and light gray short event deposits (>1 mm thick) consisting of allochthonous lithotypes interpreted as "plume deposits" by episodically heavy river floods that transport mud suspensions across the narrow shelf onto the steep upper slope (Lückge et al., 2002; von Rad et al., 2002a). Sediments containing these event deposits or turbidites were excluded from our sample set.

Varves, turbidites, and event layers in our core are equivalent to the lithostratigraphy observed in core 56KA from the same position. Core 56KA has been dated by von Rad et al., (1999) by varve counting and several conventional and accelerator mass spectrometry ^{14}C datings. Our age model is based on the visual correlation of event deposit layers from both cores as stratigraphic tie points and interpolation between these tie points (Figure S1 in the supporting information).

We also analyzed alkenones and calculated alkenone fluxes as well as the $U^{K'}_{37}$ index of samples from the eastern PAKOMIN sediment trap mooring station (EPT-2; 24 °45.6'N, 65 °48.7'E; 590 m water depth) to ascertain the validity of sea surface temperatures estimated in sediment core samples. The EPT-2 trap was deployed from May 1995 to February 1996 and was previously studied by Andruleit et al., (2000) and Schulz et al., (2002).

Bulk Components (Organic Carbon, Carbonate, and Opal)

Total carbon was analyzed on a Carlo Erba 1500 elemental analyzer (Milan, Italy) with a precision of 0.2%. Total organic carbon (TOC) was measured with the same instrument after samples were treated with 1M hydrochloric acid (HCl) to remove inorganic carbon. Analytical precision for organic carbon was 0.02%. Carbonate carbon was calculated as the difference between total carbon and organic carbon.

Biogenic opal was determined by wet alkaline extraction of biogenic silica (BSi) using a variation of the DeMaster method (DeMaster, 1981). About 30g sediment per sample was digested in 40 mL of 1% sodium carbonate solution (Na_2CO_3) in a shaking bath at 85 °C. After 3 h, the supernatant was withdrawn and neutralized in 0.021 M HCl. The concentration of dissolved silica in the subsamples was determined photometrically. Biogenic opal was calculated by multiplying the BSi concentrations with a factor of 2.4. The mean standard deviation based on duplicate measurements of samples is 0.17%. To ensure that BSi is not overestimated bymineral dissolution at low BSi concentrations, we analyzed representative samples after 3, 4, and 5 h and used a slope correction for the determination of BSi concentrations (Conley, 1998). The amount of BSi was then estimated from the intercept of the line through the time course aliquots (DeMaster, 1981). Results of slope-corrected opal estimates showed that our method slightly overestimated opal concentrations by a mean of 0.13%. All bulk components are presented as weight percent.

Mass accumulation rates of organic carbon were calculated by multiplying the dry bulk densities of the sediments (measured at the Department of Geosciences, University of Tübingen) with calculated sedimentation rates and the weight fraction of organic carbon.

X-ray Elemental Analysis

X-ray fluorescence (XRF) core scanner data were collected by XRF core scanner I at MARUM–Center for Marine Environmental Sciences (University of Bremen) using a Kevex Psi Peltier cooled silicon detector and a Kevex X-ray tube with the target material molybdenum (Mo). Counts were acquired directly at the split core surface of the archive half every 2 mm downcore over an area of 0.2 cm^2 with an instrument slit size of 2 mm using a generator setting of 20 kV, 0.087 mA, and a sampling time of 30 s. The split core surface was covered with a polypropylene foil to avoid contamination of the XRF measurement unit and desiccation of the sediment.

Nitrogen Stable Isotope Ratios

The ratio of the two stable isotopes of nitrogen ($^{15}N/^{14}N$) is expressed as $\delta^{15}N$, which is given as the per mil deviation fromthe N isotope composition of atmospheric N_2 ($\delta^{15}N$=0‰): $\delta^{15}N = ((R_{Sample} - R_{Standard})/R_{Standard}) \times 1000$, where R_{Sample} is the $^{15}N/^{14}N$ ratio of the sample and $R_{Standard}$ is the $^{15}N/^{14}N$ ratio of atmospheric N_2. The $\delta^{15}N$ values were determined using a Finnigan MAT 252 gas isotope mass spectrometer after hightemperature flash combustion in a Carlo Erba NA-2500 elemental analyzer at 1100 °C. Pure tank N_2 calibrated against the International Atomic Energy Agency reference standards IAEA-N-1 and IAEA-N-2, which were, in addition to an internal sediment standard, also used as working standards. Analytical precision based on replicate measurements of a reference standard was better than 0.1‰. Duplicate measurements of samples resulted in a mean standard deviation of 0.07‰.

Alkenones

Freeze-dried and homogenized sediment samples (1 to 3 g) were extracted twice for 5 min with methylene chloride (DCM) using an accelerated solvent extractor (Dionex; temperature 75 °C, pressure 70 bar). Directly after extraction, a known amount of internal standard (14-heptacosanone) was added to the extracts. The extracts were then rotary evaporated until near dryness and saponified with 5% methanolic potassium hydroxide (KOH) solution overnight. The KOH solution was dried under a nitrogen flow, dissolved in DCM, and cleaned over a silica gel column using DCM as eluent. The clean fraction containing the alkenones was

dried under N_2 and taken up in n-hexane (50–150 µL) prior to analysis. Alkenones were analyzed by gas chromatography on an Agilent 6850 gas chromatograph (GC) equipped with a split-splitless inlet system and flame ionization detector (310 °C). Separation was achieved on a silica column (30 m × 0.1 µm film thickness × 0.32 mm ID; Optima1; Macherey–Nagel) using hydrogen as carrier gas (1 mL min^{-1}). The GC oven maintained 50 °C for the first minute and was then programmed from 50 ° to 230 °C at 20 °C min^{-1}, from 230 ° to 260 °C at 4.5 °C min^{-1}, and from 260 ° to 320 °C at 1.5 °C min^{-1} followed by an isothermal period of 15 min. $C_{37:2}$ and $C_{37:3}$ alkenones were identified by comparing peak retention times between sediment samples and a working sediment standard. Quantification of alkenones was achieved by integrating the peak areas of the C_{37} alkenones and that of the internal standard (14-heptacosanone). Since both the C_{37} alkenones and the internal standard are very similar in structure, no different response factors between the C_{27} ketone and the C_{37} alkenones are assumed. Alkenones were translated into sea surface temperature using the core top calibration for the Indian Ocean from Sonzogni et al., (1997b): SST = $(U^{K'}_{37} - 0.043)/0.033$ with $U^{K'}_{37} = C_{37:2}/(C_{32:2} + C_{37:3})$. Replicate extraction and measurement of a working sediment standard resulted in a mean standard deviation of estimated SST of 0.5 °C.

Results

Alkenone Fluxes and $U^{K'}_{37}$ in Sediment Traps

Alkenone fluxes in EPT-2 between May 1995 and February 1996 ranged from 0.15 µg m^{-2} d^{-1} to 1.21 µg m^{-2} d^{-1} (see Figure II.3a). Peak fluxes occurred in May 1995 (1.21 µg $m^{-}2$ $d^{-}1$) and during the late NE monsoon in January 1996 (0.92 µg m^{-2} d^{-1}) and February 1996 (0.94 µg m^{-2} d^{-1}). Alkenone fluxes for the months September and October could not be determined due to low amounts of sample material. Alkenone fluxes on the Pakistan continental margin track coccolith fluxes during the seasonal cycle (Andruleit et al., 2000) with maxima at the onset of the summer and of the winter monsoon. This underscores a strong link between primary and alkenone production. Alkenone (C_{37}) fluxes on the Pakistan Margin match those from the Oman Margin (Wakeham et al., 2002) but are slightly lower than the total alkenone (C_{37}, C_{38}, and C_{39}) fluxes in the central Arabian Sea (Prahl et al., 2000). Sediment trap studies from different parts of

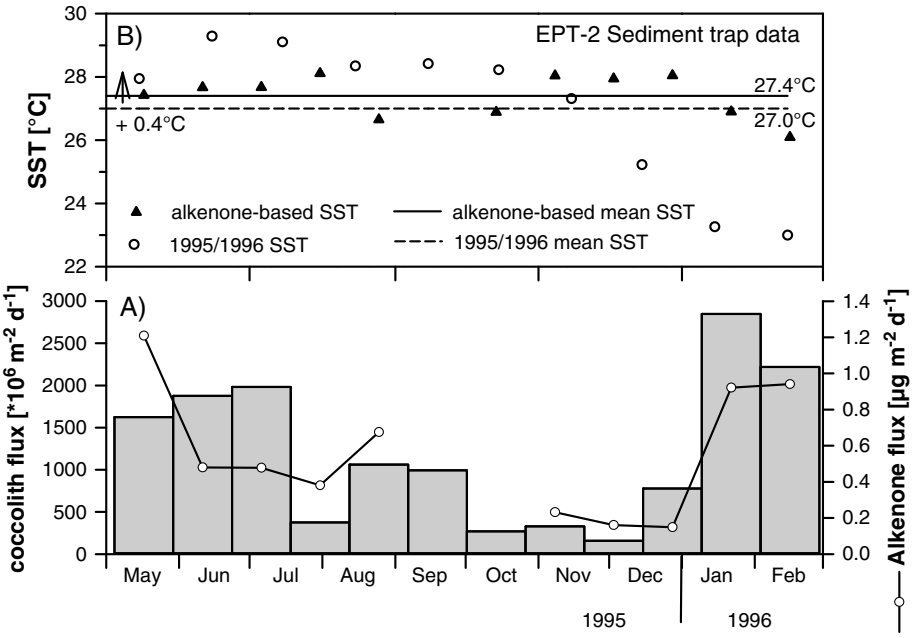

Figure II.3: (a) Total coccolith (gray bars (Andruleit et al., 2000)) and alkenone fluxes (open circles) at trap EPT-2 in the northeastern Arabian Sea off Pakistan. **(b)** Alkenone-derived SST measured in EPT-2 samples (triangle) compared to 1995/1996 monthly SST (circle; extracted from the website http://ingrid.ldgo.columbia.edu). Mean alkenone-based SST is about 0.4 °C higher than mean temperature over May 1995 to February 1996.

the Arabian Sea thus showed a strong coupling between coccolithophore (and alkenone) production and the seasonal cycle in this area (Andruleit et al., 2000; Broerse et al., 2000; Prahl et al., 2000; Wakeham et al., 2002).

This seasonality may bias the SST signal in sediments toward seasonal flux maxima, so that it may not be representative of the annual mean SST (AM-SST). In our set of trap samples covering the period from May 1995 to February 1996, the seasonal variability of alkenone-derived SST (26.1 °C to 28.1 °C; $U^{K'}_{37}$ from 0.904 to 0.971; Figure II.3b) is attenuated compared to observed SSTs which vary from 23.0 °C to 29.2 °C (Reynolds et al., 2002). The observed mismatch between alkenone-based SST in sediment trap samples and regional seasonal SST patterns seems to be a general phenomenon independent on oceanic region (central Arabian Sea (Prahl et al., 2000); Sea of Okhotsk, northwest Pacific (Seki et al., 2007), subtropical oligotrophic North Pacific (Prahl et al., 2005)). In general, these studies found that alkenone-based SST produces a warm SST bias in winter and a cold SST bias in summer concordant with our observations from the northeastern Arabian

Sea, where monthly average alkenone-based SSTs deviate most from modern observed SSTs during the cold winter months of the trapping period in 1995/1996. The overestimation of winter SST by alkenones may be explained by a change in the coccolithophore community to alkenone-producing species that exhibit a different response to growth temperature, thus altering the relationship of $U^{K'}_{37}$ ratio to SST (Prahl et al., 2005). At the Pakistan Margin, changes in the coccolithophore assemblage (including the alkenone-producing species *Emiliania huxleyi* and *Gephyrocapsa oceanica*) are mainly controlled by variations in the mean mixed layer depth and total nutrient availability (Andruleit et al., 2004). A change in the alkenone producing coccolithophore community due to mixed layer deepening at site EPT-2 is well reflected in the ratio of *G. oceanica* to *E. huxleyi* that show an increasing abundance of *G. oceanica* relative to *E. huxleyi* in winter (see Figure S2 in the supporting information; coccolithore flux data were taken from Andruleit et al., (2000)). Although relative species composition of the two alkenone-producing coccolithophorides seems to be stable in the Indian Ocean sedimentary record (spatially (Sonzogni et al., 1997b) as well as through time (Doose-Rolinski et al., 2001)), we suggest that it might be of importance for $U^{K'}_{37}$ calibration on a seasonal scale on the Pakistan continental margin. If we use a linear offset of 0.085 (instead of 0.043) to calibrate the $U^{K'}_{37}$ index to SST as suggested by Prahl et al., (2005) for the deeply mixed wintertime, alkenone-based SST were much closer to observed SST at 10 m water depth (Figure S2 in the supporting information). On the other hand, the slight cold bias of alkenone-based SST in our trap samples during summer is best explained by alkenone production in the upper mixed layer between 0 to 30 m water depths.

Albeit the complexity of processes that plays a role in seasonal alkenone-based SST estimates, we state that sedimentary $U^{K'}_{37}$ measurements on the Pakistan Margin are best approximated by AM-SST. The average alkenone-derived SST of the sampling period is 27.4 °C, which (considering an uncertainty of 0.5 °C) matches well with the mean modern SST (27.0 °C; see Figure II.3b), which in turn is very close to the average mean SST from May to February obtained fromthe Levitus climatology (26.9 °C (Levitus and Boyer, 1994)). Climatological annual mean SST (including the months missing in the trap investigation) is 26.4 °C (Levitus and Boyer, 1994). But because alkenones reflect an integrated signal of the upper 0 to 50 m of the water column (Sonzogni et al., 1997b), small deviations from actual sea surface temperature measurements are to be expected.

Our interpretation of sedimentary $U_{37}^{K'}$ measurements as an AM-SST signal is supported by $U_{37}^{K'}$ estimates for sediment trap samples from the central Arabian Sea (Prahl et al., 2000) and by a compilation of sediment trap time series distributed over different oceanic regions worldwide (Rosell-Melé and Prahl, 2013). Furthermore, measurements of sediment core tops, which were used to develop an alkenone calibration equation for the Indian Ocean, showed no significant differences between calculated production-weighted temperature and AM-SST (Sonzogni et al., 1997a,b). According to Doose-Rolinski et al., (2001), alkenone derived SSTs measured in a Holocene section of a sediment core from the Pakistan Margin were best approximated by annual mean temperature as well.

Alkenone SST Record in Core 39KG/275KL

Alkenone SST vary between 26.9 °C and 28.4 °C ($U_{37}^{K'}$ from 0.932 to 0.981) over the last 2400 years and thus lie well above the modern annual mean of 26.4 °C (Levitus and Boyer, 1994). Conte et al., (2006) stated that a positive offset of reconstructed core top temperature (27.6 °C for SO90-39KG) compared to atlas temperature is observed in several areas worldwide. It is alternatively explained by diagenetic alteration of alkenone ratios in the water column and/or surficial sediments, by lateral advection, or by variations in the seasonality and depth of alkenone production. In our view, diagenesis can be ruled out as a significant process affecting our $U_{37}^{K'}$ estimates, because the offset was also observed between trap alkenone SST and modern AM-SST and was furthermore confirmed by Mg/Ca temperatures (Dahl and Oppo, 2006). Biasing of the alkenone signal by alkenones produced and advected from the upwelling area off Oman may be a factor (Andruleit et al., 2000), but coccolithophore fluxes on the Pakistan Margin are only slightly enhanced during the SW monsoon season, and the associated bias in the alkenone signal must be of minor importance. As SSTs in the southeastern Arabian Sea remain relatively high during winter, lateral advection of water masses and alkenones from the southwest Indian coast (following the counterclockwise surface current established during the NE monsoon) on the other hand would result in a warm bias of alkenone SST on the Pakistan Margin during the winter. However, based on a comparison of coccolith fluxes with coccosphere fluxes (which should present a vertical flux signal), Andruleit et al., (2000) suggested that coccolithophore assemblages were not influenced by resuspension processes during this time of the year.

Regardless of the absolute SST, Figure II.5 illustrates relative SST variations around the overall mean of 27.7 °C over the last 2 millennia. Although the amplitude of the alkenone-derived SST signal is small in our record, our SST reconstruction exhibits statistical significant periods of long-term SST changes (see also detailed discussion of signal-to-noise ratio in the supporting information). SSTs were high at around 28.2 °C until 250 A.D., rapidly decreased and outlined a time period of low SST that lasted from 400 to 1000 A.D. After a rebound to $>$ 28 °C between 1000 and 1300 A.D., the decline in SST continued until minimum temperatures (26.9 °C) are registered during the 18th century. The minimum of our SST reconstruction at this time agrees with the results obtained from a global climate proxy network, which suggests 0.3 °C cooler SSTs than present during the Little Ice Age in the northeastern Arabian Sea (Mann et al., 2009). Our SST estimates, after this minimum, suggest a northern Arabian Sea warming tendency that persists to the present.

Records of Productivity

Our analytical approach to trace the past productivity changes were based on TOC concentrations, δ^{15}N values, and the ratio of carbonate to opal. The range of TOC concentrations (1.0 and 2.0%) and δ^{15}N values (7.1 to 8.5‰) in the sediment cores at sites 39KG/275KL (Figure II.4) is a characteristic of high-productivity areas with a well-developed OMZ and water column denitrification (e.g., Altabet et al., 1999; Gaye-Haake et al., 2005; Naqvi et al., 1998) such as the northern Arabian Sea (Cowie et al., 1999). Organic carbon concentrations in sediments on the Pakistan Margin (and elsewhere) are influenced by surface productivity but also by dilution with lithogenic material, bottom water oxygen concentrations, bulk accumulation rate, sediment texture, refractory of organic matter, and the mineral surface area (e.g., Keil and Cowie, 1999; Paropkari et al., 1992; Suthhof et al., 2000; van der Weijden et al., 1999).

At our core site, the use of organic carbon mass accumulation rates (TOC MAR) as a productivity indicator that theoretically remove an influence of dilution is complicated by strongly fluctuating sedimentation rates (SR) (ranging from 87 to 212 cm kyr^{-1}). Sediment mass accumulation rates (71 to 203 g cm^{-2} kyr^{-1}; event deposits excluded) calculated from SR and bulk densities are even higher than glacial/interglacial variations reported from the western (SR ranging from 6 to 38 cm kyr^{-1} and MAR ranging from 5 to 50 g cm^{-2} kyr^{-1} (Emeis et al., 1995)) and eastern Arabian Sea (SR ranging from 4 to 9 cm kyr^{-1} (Rostek et al., 1997)). SR and

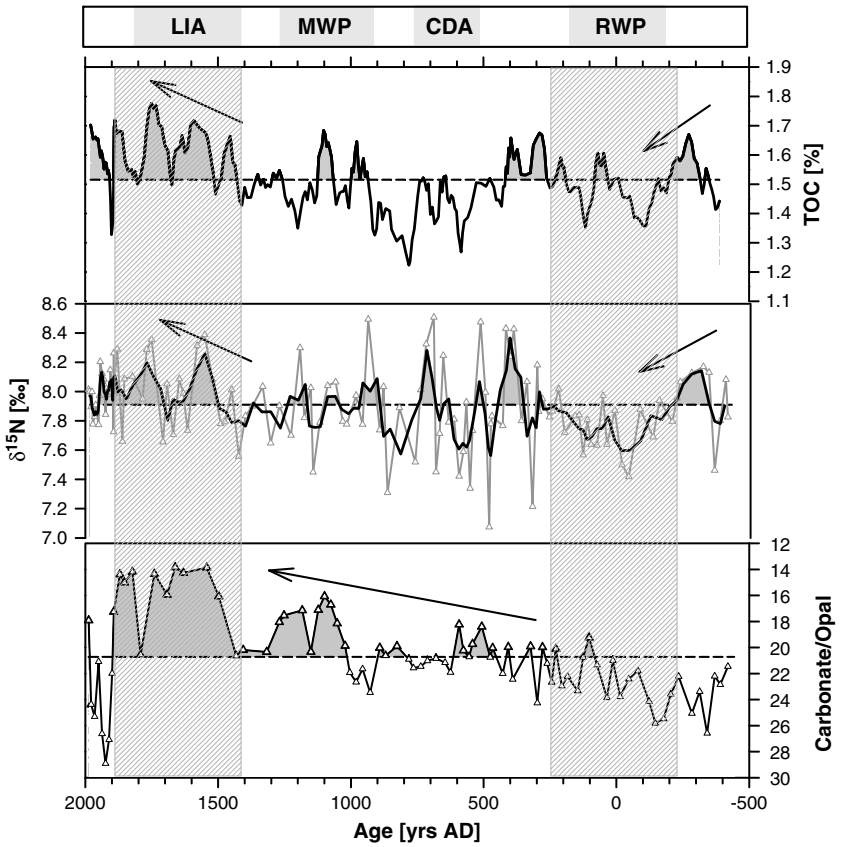

Figure II.4: Late Holocene productivity record for cores 39KG and 275KL from the northeastern Arabian Sea. Carbonate/opal ratios, δ^{15}N values (bold line: running mean of 3) and smoothed TOC contents (running average of 5) were used as productivity indicators. The gray shaded areas indicate good agreement between productivity proxies. The dashed lines indicate the respective mean over the complete data set. Further illustrated are the characteristic climate periods known from the Northern Hemisphere: Little Ice Age (LIA), Medieval Warm Period (MWP), Cold Dark Ages (CDA), and Roman Warm Period (RWP).

MAR at our study site are caused by highly variable input of lithogenic matter (range from 81 to 86%) from river runoff and/or dust storms (Schulz et al., 1996; von Rad et al., 1999). Even though sedimentary OM in our core mainly consists of marine OM ($\delta^1$3C measured in core 275KL ranges from -21.5 to -19.5‰), significant positive correlations between TOC MAR and SR (R^2 = 0.56) and TOC MAR and sedimentary mass accumulation rates (R^2 = 0.76) indicate a dominant influence of bulk MAR (and thus alternating input of organic matter transported with mineral matter on its passage across the shelf) on organic carbon accumulation rates (Emeis et al., 1995; Müller and Suess, 1979). This conclusion is supported by the good agreement between downcore variations in TOC MAR and varve thickness, which

is an indicator for precipitation and river runoff (von Rad et al., 1999, ; see Figure S3 in the supporting information). Thus, we infer that in our study area, TOC contents can be used as a tracer for the past primary productivity changes rather than the organic carbon accumulation rates. Although measured TOC contents during the period 400 to 900 A.D. might partly be affected by dilution as indicated by visual comparison of organic carbon concentrations with MAR (Figure S4 in the supporting information), no significant correlation between TOC contents and mass accumulation rates (R^2 = 0.008) could be observed indicating no significant control of the dilution on downcore variations in TOC concentrations.

Over the last 2400 years of our record, elevated TOC concentrations coincide with increased δ^{15}N values and vice versa, a relationship described for Holocene sediments (Agnihotri et al., 2003) and over glacial/interglacial cycles (Altabet et al., 1995; Ganeshram et al., 2000; Suthhof et al., 2001) in the northern Indian Ocean. Parallel changes in TOC concentrations and δ^{15}N are both related to the productivity variations caused by variable access to the subthermocline nitrate pool. That nitrate pool has a high δ^{15}N resulting from denitrification within the upper part of the OMZ (Gaye et al., 2013). Upwelling does not occur at our core location, so that variable deepening of the mixed layer due to convective winter mixing during the NE monsoon season is the most likely process transporting the ^{15}N-enriched nitrate to the ocean surface and enabling productivity. Together, δ^{15}N values and TOC concentrations in our sediment cores thus reflect productivity changes associated with mixed layer deepening due to NE monsoon conditions. A third indirect signal of productivity is the ratio of the biogenic constituents carbonate (ranging from 6 to 15.5%) and opal (ranging from 0.5 to 0.9%), because high nutrient availability induces diatom blooms and high flux rates or organic matter, whereas high carbonate rain rates indicate low nutrient availability. The carbonate to opal ratio ranges from 14 to 29 and indicates a dominance of carbonate primary producers (coccolithophores) at our study site that decreases over time relative to opal from diatoms (Ramaswamy and Gaye, 2006). In this general trend, declining carbonate to opal ratios indicate a shift to higher productivity around 1400 A.D. (Figure II.4).

As discussed above, proxies indicative of productivity changes are influenced by a lot of processes. To minimize the effect of processes not related to productivity variations and to better filter out the signal caused by productivity changes, a productivity index (combining TOC, $\delta^1$5N, and carbonate/opal) was calculated.

First, the range of values for all three parameters was standardized to values between 0 and 1, so that the respective productivity indicators were equally weighted and comparable to each other. The sum of the standardized values was calculated and again standardized to values between 0 (low productivity) and 1 (high productivity). High productivity from 1400 to 1950 A.D. and periods of decreased productivity from about 200 B.C. to 250 A.D., as recorded by all individual productivity parameters (Figure II.4, indicated by the gray shaded areas), are well reflected by our productivity index (Figure II.5, not reverse y axis). In addition, superimposed on short-term variability, the productivity index shows a gradual trend to increasing primary production in the northeastern Arabian Sea over the late Holocene.

Variability in Sr/Ca Ratios

The relationship between elevated Sr/Ca ratios and increased winter monsoon activity was first proposed for glacial/interglacial intervals by Reichart et al., (1998) and was later adapted for Holocene sediments by Lückge et al., (2001). These authors proposed that elevated Sr/Ca ratios image variations in mixed layer depths. Because aragonite has a higher Sr content than calcite, variations in Sr/Ca track the depth interval of the aragonite compensation depth (ACD), and the deepening of the ACD and higher Sr/Ca ratios indicates intensified deep winter mixing due to elevated winter monsoon activity (Reichart et al., 1998). A different mechanism for changes in Sr/Ca on millennial time scales was proposed by Böning and Bard, (2009), who attributed the variations in Sr/Ca in the northeastern Arabian Sea to changes in the formation of Antarctic Intermediate Waters. Today, Antarctic Intermediate Water in the Arabian Sea can only be traced up to 5 °N (You, 1998), so that for the 2400 year record here, this long-term variability is most likely irrelevant.

The Sr/Ca ratio in the sediment cores vary between 0.023 and 0.032 at sites 39KG/275KL (Figure II.5), which are in the range of previously measured values for Holocene sediments from the Makran area (Lückge et al., 2001). The increase in Sr/Ca ratios indicates a shift to winter monsoon conditions on the Pakistan Margin around 700 A.D.

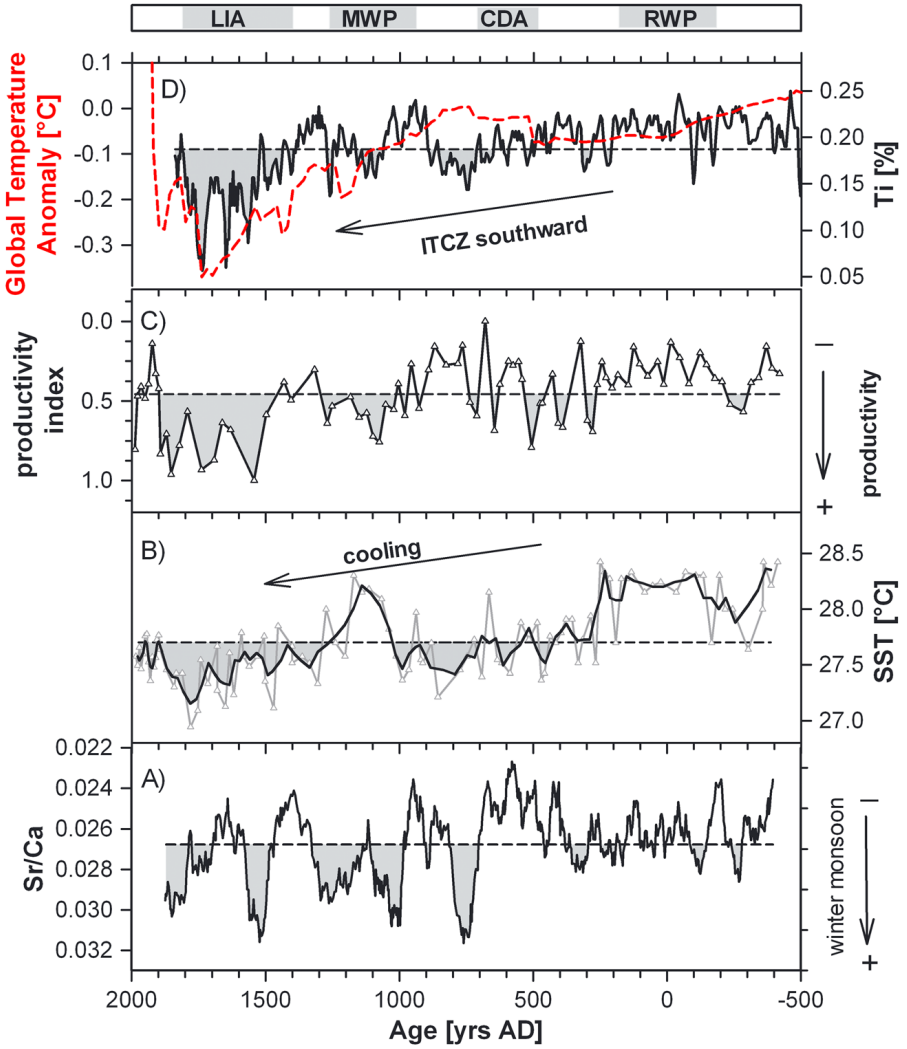

Figure II.5: Reconstruction of winter monsoon variability in the northeastern Arabian Sea over the last 2400 years compared to long-term movements of the Intertropical Convergence Zone (ITCZ). **(a)** Smoothed Sr/Ca ratios (21 point running mean), **(b)** alkenone SST record (bold line: 3 point running mean), and **(c)** productivity index for core 39KG/275KL. **(d)** Titanium content of Cariaco Basin sediments as an indicator for the latitudinal shifts in the ITCZ (Haug et al., 2001) compared to global temperature anomalies (Marcott et al., 2013). The dashed lines indicate the respective mean over the studied time interval.

Discussion

Productivity and SST Variability: Evidence for Monsoonal Change

Winter monsoon activity affects both sea surface temperature and mixed layer depth over the Pakistan Margin and thus controls the amount of thermocline nutrients entrained into the mixed layer (Figure II.2). As a result, primary productivity changes in the northeastern Arabian Sea are strongly coupled to the intensity of the NE monsoon season. Whereas primary production is unambiguously related to monsoon strength, SST in the northeastern Arabian Sea, although primarily controlled by monsoon-related processes, can also be impacted by global temperature variations. A decrease in the alkenone-based SST signal at sites 39KG/275KL can thus be caused either by local strengthening of NE monsoon conditions or by globally lowered atmospheric temperature. If SST was changing as a response to varying NE monsoon intensity, then this should also be noted in our primary productivity reconstruction because intensified NE monsoon strength induces high rates of primary production at the Pakistan continental margin. The general trend of decreasing SST and increasing productivity seen in our record over the last 2400 years (Figure II.5) confirms that alkenone SST primarily reflect changes in the NE monsoon strength. This coupling of SST and productivity is particularly pronounced during the periods from 400 B.C. to 300 A.D. and from 1400 A.D. until the present, while it is less clear between ~500 and 1300 A.D. Furthermore, alkenone SSTs follow the same pattern as reconstructed winter SSTs (based on planktic foraminifera transfer functions measured in the same sediment core; unpublished data) confirming the strong influence of the winter season on alkenone SST in this region.

A link between NE monsoon conditions, decreasing SSTs, and increasing productivity can be observed not only on a seasonal scale and over the last 2400 years but also on time scales of several hundreds of thousands of years. In the northeastern Arabian Sea, relatively high productivity and sea surface cooling appear to correspond to glacial stages due to elevated NE monsoon activity (e.g., Rostek et al., 1997; Schulte and Müller, 2001; Schulte et al., 1999).

Local Monsoon Dynamics in the Northeastern Arabian Sea During the Last 2400 Years

On the basis of the above-mentioned considerations, our multiproxy study from the northeastern Arabian Sea indicates three main periods of changing monsoon intensities throughout the late Holocene (Figure II.5). Winter monsoon intensity was low before about 250 A.D. and is recorded by high SSTs and generally low primary production due to diminished northeasterly winds and reduced convective winter mixing in the northeastern Arabian Sea. Winter monsoon mixing strengthened after 250 A.D., which caused a cooling of the sea surface and slightly increased primary production. Finally, winter monsoon conditions started to predominate off Pakistan at about 700 A.D., as indicated by a shift to higher Sr/Ca ratios in core 275KL (Figure II.5, note reverse Sr/Ca y axis). Weak correlation between SST and primary productivity from ~500 to 1300 A.D. suggests a "transition period" from weak to strengthening NE monsoon, characterized by unstable and fluctuating environmental conditions on the Pakistan Margin. Strong winter monsoon activity prevailed during the Little Ice Age (LIA) from 1400 to 1900 A.D., as indicated by low SSTs and a peak in biological productivity due to strong convective winter mixing. Low SSTs during the LIA as well as relatively high SSTs due to diminished NE monsoon conditions occurring 2000 years ago agree with another northeastern Arabian Sea (alkenone-based) SST reconstruction (Doose-Rolinski et al., 2001). Although both SST records differ in detail, possibly as a result of proxy uncertainty, they display similar trends of warming at around 0 A.D. and cooling during the LIA. This small-scale variability between both records might further be caused by the analysis of different core sections and thus variations in the time interval which is integrated by the alkenones.

The dynamics of the monsoon low-level wind system on the Pakistan Margin throughout the last 2400 years affect marine processes as well as moisture changes in this area. Variable but relatively lowsalinity values after 500 A.D. probably reflect diminished SW monsoon and/or enhanced NE monsoon conditions (Doose-Rolinski et al., 2001). Lückge et al., (2001) proposed a shift from SW monsoon-dominated precipitation to NE monsoon precipitation in the Makran area around 500 A.D. These findings match our interpretation of predominating NE monsoon conditions since ~700 A.D.

Enhanced NE monsoonal activity during the LIA was most likely induced by

an increased influence of westerlies in the Makran area during this period. Today, winter rainfall brought by westerly winds and connected to cyclonic storms originating in the Mediterranean significantly contributes to the total annual precipitation in the study area (Lückge et al., 2001; von Rad et al., 2002b, and references therein). Higher precipitation implicating stronger westerlies on the coast off Pakistan after 1600 A.D. and during the LIA was deduced from varve thickness data from the nearby cores SO90/56KA (von Rad et al., 1999) and in a cave record from the central Kumaun Himalaya (Sanwal et al., 2013). A significant feature preceding the LIA in the northeastern Arabian Sea is a distinct phase of increased SST (1050 to 1300 A.D.; see Figure II.5) that coincides with the Medieval Warm Period (MWP), a time of generally warm climate conditions observed in the Northern Hemisphere.

The response of the marine system to regional monsoon dynamics is best explained by the reactions of the surface ocean to seasonal shifts in the ITCZ. The reversal of low-level winds in the Arabian Sea during the seasonal cycle is accompanied by a shift in the location of the ITCZ. Core sites 39KG/275KL are located at the average northern latitudinal position of the ITCZ, and thus, surface ocean processes in this area are sensitive to the long-term movements of the annual mean position of the ITCZ and the associate change in prevailing low-level winds. Northward migration of the ITCZ in spring (SW monsoon) and southward retreat in autumn (NE monsoon) differentially impact on surface ocean salinity and temperature and thus thermocline depth in the northeastern Arabian Sea. At times when the northern position of the ITCZ slightly shifts south of the average position, the duration of NE monsoon influence at site 275KL during winter is prolonged. This would enhance the influence of the winter monsoon on surface ocean conditions in this area.

Different studies widely distributed over the low-latitude region (e.g., Fleitmann et al., 2007; Haug et al., 2001; Russell and Johnson, 2005) indicate a general southward shift of the annual mean position of the ITCZ over the late Holocene in response to global climate variability. We argue that long-term southward movement of the ITCZ throughout the late Holocene is responsible for the long-term trends of declining sea surface temperature and rising productivity seen in our record (Figure II.5). In this long-term trend, times of the southernmost ITCZ displacements were contemporaneous with the periods of highest primary productivity and lowest SST on the Pakistan continental margin. Both reflect an

increasing regional influence of the NE monsoon and a reaction of the surface ocean by progressive winter deepening of convective mixing. This argument is supported by Jung et al., (2004), who attributed coherent basin-wide decadal to century-scale temperature variations in the Arabian Sea during the Holocene (based on a correlation between SST variations off Somalia and Pakistan) to a shift in the mean position of the ITCZ throughout the Holocene. Such a connection between a southward migrating annual mean position of the ITCZ and monsoon as well as precipitation changes throughout the Holocene was proposed by several authors (Fleitmann et al., 2003; Fleitmann et al., 2007; Haug et al., 2001; Lückge et al., 2001; Russell and Johnson, 2005; Sinha et al., 2011; Wang et al., 2005; Yancheva et al., 2007).

Reversed Behavior Between Summer and Winter Monsoon Strength During the Late Holocene

The mechanism above argues for an inverse relationship between summer and winter monsoon strength throughout the Indian and East Asian monsoon domain in the time-variant location of the ITCZ, expressed by the decreasing summer monsoon intensity with increasing winter monsoon activity and vice versa (e.g., Reichart et al., 2002; Yancheva et al., 2007). Is this inverse relationship evident in a comparison of our winter monsoon record with records of summer monsoon strength? The regions influenced most drastically by the SW monsoon are the Oman and the Somalia upwelling systems, that both registered a gradual warming of sea surface temperatures during the last 2400 years (Huguet et al., 2006), in contrast to decreasing SST on the Pakistan Margin over this period. This points to a general antagonistic behavior in the millennial trend of summer and winter monsoon strength over the late Holocene. However, summer and winter monsoon were more variable on centennial time scales, particularly during the time intervals of greatest climate contrast over the last 2000 years on the Northern Hemisphere, namely, the MWP (950 to 1250 A.D.) and the LIA (1400 to 1800 A.D.). Evidence for increased summer monsoon intensity during the MWP comes from the northwestern Arabian Sea (Anderson et al., 2010, 2002; Gupta et al., 2003), from Oman (Fleitmann et al., 2004), India (Sinha et al., 2007, 2011), as well as from China (Zhang et al., 2008). Changes in winter monsoon strength off Pakistan during this time are less pronounced. While higher SST argues for diminished NE monsoon activity over the northeastern Arabian Sea, slightly enhanced primary

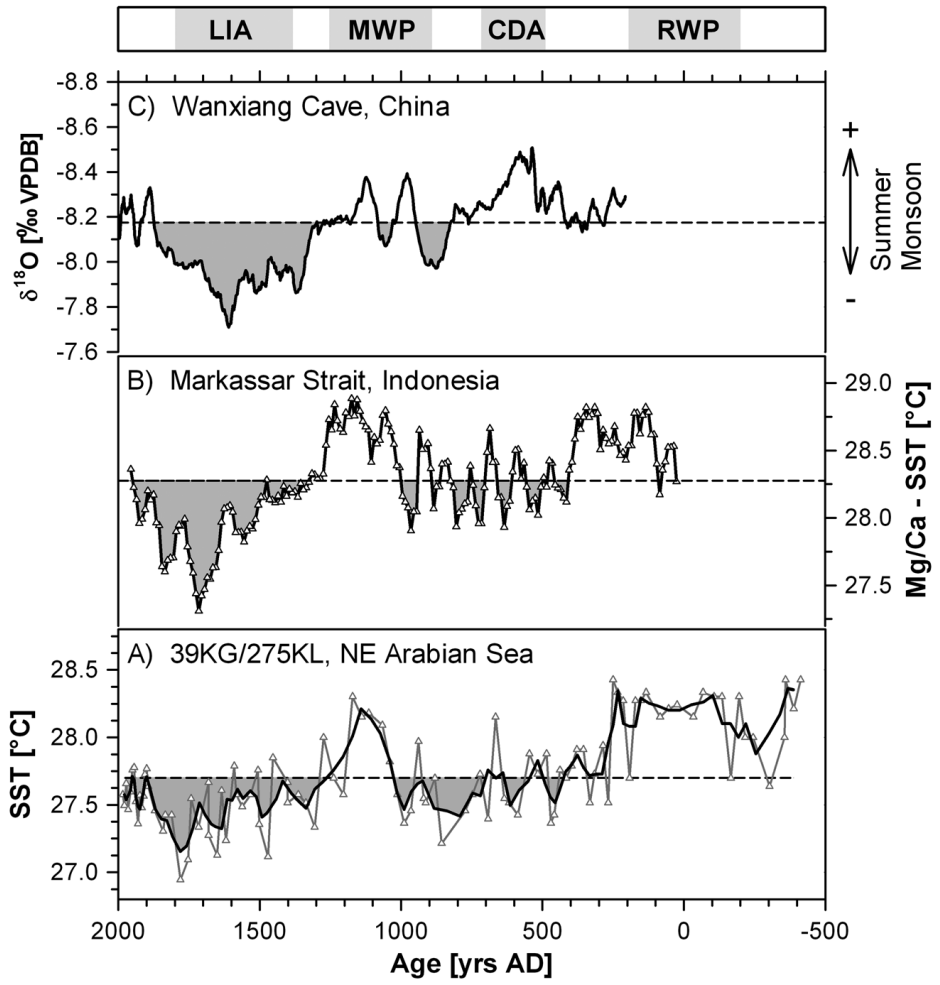

Figure II.6: (a) Late Holocene alkenone-derived SST variations (cores 39KG and 275KL) from the northeastern Arabian Sea compared to **(b)** Mg/Ca-SST variations reconstructed for the Markassar Strait (Indonesia) by Oppo et al., (2009) and **(c)** a smoothed $\delta^{18}O$ record (15 point moving average) of Wanxiang Cave (China) as an indicator for the summer monsoon intensity from Zhang et al., (2008). The dashed lines indicate the respective mean over the studied time interval.

production and relatively higher Sr/Ca ratios might be indicative of NE monsoon intensification. One possible explanation for this mismatch might be that primary productivity on the Pakistan Margin during this time is fueled by lateral advection of nutrients from the upwelling area off Oman due to intensified summer monsoon circulation. On the other hand, most studies reconstructed diminished SW monsoon strength during the LIA (Fleitmann et al., 2004; Sinha et al., 2011; Zhang et al., 2008), when our record suggests increased NE monsoon activity over the Pakistan Margin.

During the last 400 years, however, SW monsoon strengthens again in the northwestern Arabian Sea, probably as a result of a general warming trend (Anderson et al., 2002). Speleothem δ^{18}O from Kahf Defore in southern Oman indicates summer monsoon rainfall generally above the long-term average since 1660 A.D. and supports this hypothesis (Fleitmann et al., 2004). However, in the Pakistan Margin record, winter monsoon indicators continue to dominate over the last 400 years. Only most recently (since 1900 A.D.), primary productivity on the Pakistan Margin appears to decrease and SSTs increase slightly, suggestive of diminished NE monsoon conditions in the northeastern Arabian Sea. The Oman cave record on land may be more sensitive to summer monsoon changes than the marine record in the Makran area, which is dominated by winter monsoon variability.

The antagonism of SW and NE monsoon is evidenced by the comparison of our winter monsoon record with other monsoon reconstructions in the Arabian Sea and beyond. Based on the assumption that the δ^{18}O signal measured in speleothems from Wanxiang Cave is mainly influenced by summer monsoon precipitation, Zhang et al., (2008) compiled a 1810 year long record of summer monsoon intensity for central China. Their δ^{18}O variations show a strong resemblance to our reconstructed SST curve with lower SST in the northeastern Arabian Sea, coinciding with a decline in summer monsoon rainfall in central China due to weaker East Asian summer monsoon intensity (Figure II.6). Furthermore, SST variations in the northeastern Arabian Sea are not only related to changes in East Asian summer monsoon over central China but also to changes in SSTs from the Indo-Pacific warm pool (Oppo et al., 2009, , Figure II.6). In accordance with our interpretation, Oppo et al., (2009) suggested that strong sea surface cooling in the Markassar Strait during the LIA was caused by intensified winter monsoon conditions rather than by monsoon-induced upwelling. We thus conclude that a linkage between summer and winter monsoon strength exists over the whole Asian monsoon system during the late Holocene, reflecting long-term and short-term shifts in the ITCZ.

Global Connections: The LIA Climate Feature

The monsoon record from the Pakistan Margin is in phase with characteristic, northern hemispheric climate periods of the late Holocene, such as the Little Ice Age, the Medieval Warm Period, and the Roman Warm Period (RWP). It reveals a consistent pattern of diminished winter monsoon activity in the northeastern

Arabian Sea during northern hemispheric warm periods (MWP and RWP) and strengthened winter monsoon activity during hemispheric colder periods (LIA). Our high-resolution record implies that this consistent link between the North Atlantic and the Indian Ocean, which was described for glacial/interglacial (e.g., Schulte and Müller, 2001; Schulz et al., 1998; Sirocko et al., 1993) to climatological (Gupta et al., 2003) time scales, appears to operate during historical times as well. It causes the SW monsoon to weaken and the NE monsoon to gain strength during colder climate conditions over the North Atlantic.

One of the most prominent climate features in the northeastern Arabian Sea over the last 2400 years was the sharp decrease in SST due to the strengthening NE monsoon conditions between 1400 and 1850 A.D., contemporaneous with the LIA. Once described as a climate period restricted only to the northern extratropical hemisphere (e.g., Keigwin, 1996), LIA climate conditions appear to have impacted on SST in low-latitude regions as well (Black et al., 2007; DeMenocal, 2000; Oppo et al., 2009). A recently published global data set of proxy records indeed confirms a global cooling trend between 1580 and 1880 A.D. (PAGES 2k Consortium, 2013) that is preceded by a phase of low solar irradiance between 1450 and 1750 A.D. (Bard et al., 2000), suggesting that LIA climate conditions may at least partly be influenced by solar forcing. Solar radiation has been proposed as a forcing mechanism controlling both North Atlantic climate (Bond et al., 2001) as well as variations in monsoon intensity during the Holocene (Agnihotri et al., 2002; Fleitmann et al., 2003; Gupta et al., 2005; Neff et al., 2001; Wang et al., 2005). We thus infer that the decline in SST and increased NE monsoonal wind strength in the northeastern Arabian Sea during the LIA were triggered by global colder climate conditions (as a response to radiative forcing such as solar output, aerosols, and greenhouse gases), accompanied by southward displacement of the ITCZ.

Conclusions

Our high-resolution reconstruction of primary productivity and alkenone-derived SST from the northeastern Arabian Sea provides a unique record of winter monsoon variability throughout the late Holocene. In this area, primary production and sea surface temperatures are linked to winter monsoon intensity that cools the sea surface and increases its salinity so that thermocline deepening entrains more nutrients into the mixed layer and raises productivity. Because core 275KL is located in a sensitive region at the modern northern mean latitudinal position of the

ITCZ, observed changes in surface ocean properties in response to the monsoonal wind regime on the Pakistan Margin track long-term and short-term movements of the ITCZ throughout the late Holocene. Reconstructed SST decreased whereas productivity increased over the last 2400 years, imaging a long-term trend of NE monsoon strengthening in response to insolation-induced southward migration of the ITCZ. Comparison of our winter monsoon record with records of summer monsoon intensity confirms an antagonistic relationship between summer and winter monsoon strength during the last 2400 years.

Reconstructed monsoon variability supports the growing body of evidence that significant climate variability occurs not only on time scales of several hundred of thousand years but also through the late Holocene. Before 250 A.D., winter monsoon activity in the northeastern Arabian Sea was generally weak, and convective winter mixing was shallow, indicated by high SSTs (~28.3 °C) and reduced primary productivity. Winter monsoon conditions started to predominate off Pakistan at about 700 A.D., in response to the overall southward movement of average ITCZ location during the late Holocene. While winter monsoon activity was relatively unstable from ~500 to 1300 A.D., strong sea surface cooling down to 26.9 °C and a peak in primary productivity indicated strong and prevailing winter monsoon activity during the LIA from 1400 to 1900 A.D. The coherence between monsoon-induced variations over the Pakistan Margin with other monsoon records indicates a strong linkage of climate variability in the entire Asian monsoon system during the late Holocene, caused by migration of the ITCZ.

Acknowledgements

We thank S. Beckmann and F. Langenberg for their analytical support. Financial support was provided by the German Federal Ministry of Education and Research (BMBF) grant 03G0806B (CARIMA) and is gratefully acknowledged. This is a NIO contribution. Data will be available at www.pangaea.de.

References

Agnihotri, R., S. K. Bhattacharya, M. M. Sarin, and B. L. K. Somayajulu (2003): 'Changes in surface productivity and subsurface denitrification during the Holocene: A multiproxy study from the eastern Arabian Sea'. *The Holocene*, vol. 13: pp. 701–713.

Agnihotri, R., K. Dutta, R. Bhushan, and B. L. K. Somayajulu (2002): 'Evidence for solar forcing on the Indian monsoon during the last millennium'. *Earth Planet. Sci. Lett. 198*, vol. 198: pp. 521–527.

Agnihotri, R., S. Kurian, M. Fernandes, K. Reshma, W. D´Souza, and S. W. A. Naqvi (2008): 'Variability of subsurface denitrification and surface productivity in the coastal eastern Arabian Sea over the past seven centuries'. *The Holocene*, vol. 18: pp. 755–764.

Altabet, A., D. W. Murray, and W. L. Prell (1999): 'Climatically linked oscillation in Arabian Sea denitrification over the past 1 m.y. : Implications for the marine N cycle'. *Paleoceanography*, vol. 14: pp. 732–743.

Altabet, M. A., R. Francois, D. W. Murray, and W. L. Prell (1995): 'Climate-related variations in denitrification in the Arabian Sea from sediment 15N/14N ratios'. *Nature*, vol. 373: pp. 506–509.

Anderson, D. M., C. K. Baulcomb, A. K. Duvivier, and A. K. Gupta (2010): 'Indian summermonsoon during the last two millennia'. *J. Quat. Sci.* Vol. 25: pp. 911–917.

Anderson, D. M., J. T. Overpeck, and A. K. Gupta (2002): 'Increase in the Asian Southwest Monsoon during the past Four Centuries'. *Science*, vol. 297(5581): pp. 596–599.

Andruleit, H. A., U. von Rad, A. Bruns, and V. Ittekkot (2000): 'Coccolithophore fluxes from sediment traps in the northeastern Arabian Sea off Pakistan'. *Mar. Micropaleontol.* Vol. 38: pp. 285–308.

Andruleit, H., U. Rogalla, and S. Staiger (2004): 'From living communities to fossil assemblages: Origin and fate of coccolithophores in the northern Arabian Sea'. *Micropaleontology*, vol. 50: pp. 5–21.

Banse, K. and C. R. McClain (1986): 'Winter blooms of phytoplankton in the Arabian Sea as observed by the Coastal Zone Color Scanner'. *Mar. Ecol. Prog. Ser.* Vol. 34: pp. 201–211.

Bard, E., G. Raisbeck, F. Yiou, and J. Jouzel (2000): 'Solar irradiance during the last 1200 years based on cosmogenic nuclides'. *Tellus*, vol. 52B(3): pp. 985–992.

Berkelhammer, M., A. Sinha, M. Mudelsee, H. Cheng, R. L. Edwards, and K. G. Cannariato (2010): 'Persistent multidecadal power of the Indian Summer Monsoon'. *Earth Planet. Sci. Lett.* Vol. 290: pp. 166–172.

Black, D. E., M. A. Abahazi, R. C. Thunell, A. Kaplan, E. J. Tappa, and L. C. Peterson (2007): 'An 8-century tropical Atlantic SST record from the Cariaco Basin: Baseline variability, twentieth-century warming, and Atlantic hurricane frequency'. *Paleoceanography*, vol. 22: PA4204.

Bond, G., B. Kromer, J. Beer, R. Muscheler, M. N. Evans, W. Showers, S. Hoffmann, R. Lotti-Bond, I. Hajdas, and G. Bonani (2001): 'Persistent Solar Influence on North Atlantic Climate During the Holocene'. *Science*, vol. 294: pp. 2130–2136.

Böning, P. and E. Bard (2009): 'Millennial/centennial-scale thermocline ventilation changes in the Indian Ocean as reflected by aragonite preservation and geochemical variations in Arabian Sea sediments'. *Geochim. Cosmochim. Acta*, vol. 73: pp. 6771–6788.

Broerse, A. T. C., G.-J. Brummer, and J. E. Van Hinte (2000): 'Coccolithophore export production in response to monsoonal upwelling off Somalia (northwestern Indian Ocean)'. *Deep Sea Res. II*, vol. 47: pp. 2179–2205.

Burns, S. J., D. Fleitmann, M. Mudelsee, U. Neff, A. Matter, and A. Mangini (2002): 'A 780-year annually resolved record of Indian Ocean monsoon precipitation from a speleothem from south Oman'. *J. Geophys. Res.* Vol. 107(D20): p. 4434.

Chauhan, O. S., E. Vogelsang, N. Basavaiah, and U. S. A. Kader (2010): 'Reconstruction of the variability of the southwest monsoon during the past 3 ka, from the continental margin of the southeastern Arabian Sea'. *J. Quat. Sci.* Vol. 25(5): pp. 798–807.

Clemens, S., W. L. Prell, D. W. Murray, G. Shimmield, and G. Weedon (1991): 'Forcing mechanisms of the Indian Ocean monsoon'. *Nature*, vol. 353: pp. 720–725.

Conley, D. J. (1998): 'An interlaboratory comparison for the measurement of biogenic silica in sediments'. *Mar. Chem.* Vol. 63: pp. 39–48.

Conte, M. H., M.-A. Sicre, C. Rühlemann, J. C. Weber, S. Schulte, D. Schulz-Bull, and T. Blanz (2006): 'Global temperature calibration of the alkenone unsaturation index (UK '37) in surface waters and comparison with surface sediments'. *Geochem. Geophys. Geosyst.* Vol. 7: Q02005.

Cowie, G. L., S. E. Calvert, T. F. Pedersen, H. Schulz, and U. von Rad (1999): 'Organic content and preservational controls in surficial shelf and slope sediments from the Arabian Sea (Pakistan margin)'. *Mar. Geol.* Vol. 161: pp. 23–38.

Dahl, K. A. and D. W. Oppo (2006): 'Sea surface temperature pattern reconstructions in the Arabian Sea'. *Paleoceanography*, vol. 21: PA1014.

DeMaster, D. J. (1981): 'The supply and accumulation of silica in the marine environment'. *Geochim. Cosmochim. Acta*, vol. 45(10): pp. 1715–1732.

DeMenocal, P. (2000): 'Coherent High- and Low-Latitude climate variability during the Holocene Warm Period'. *Science*, vol. 288: pp. 2198–2202.

Doose-Rolinski, H., U. Rogalla, G. Scheeder, A. Lückge, and U. von Rad (2001): 'High-resolution temperature and evaporation changes during the late Holocene in the northeastern Arabian Sea'. *Paleoceanography*, vol. 16: pp. 358–367.

Emeis, K.-C., D. M. Anderson, H. Doose-Rolinski, D. Kroon, and D. Schulz-Bull (1995): 'Sea-Surface Temperatures and the History of Monsoon Upwelling in the Northwest Arabian Sea during the Last 500,000 Years'. *Quat. Res.* Vol. 43: pp. 355–361.

Fleitmann, D., S. J. Burns, M. Mudelsee, U. Neff, J. Kramers, A. Mangini, and A. Matter (2003): 'Holocene forcing of Indian Monsoon recorded in a Stalagmite from Southern Oman'. *Science*, vol. 300(5626): pp. 1737–1739.

Fleitmann, D., S. J. Burns, U. Neff, M. Mudelsee, A. Mangini, and A. Matter (2004): 'Palaeoclimatic interpretation of high-resolution oxygen isotope profiles derived from annually laminated speleothems from Southern Oman'. *Quat. Sci. Rev.* Vol. 23: pp. 935–945.

Fleitmann, D., S. J. Burns, A. Mangini, M. Mudelsee, J. Kramers, I. Villa, U. Neff, A. A. Al-Subbary, A. Buettner, D. Hippler, and A. Matter (2007): 'Holocene ITCZ and Indian monsoon dynamics recorded in stalagmites from Oman and Yemen (Socotra)'. *Quat. Sci. Rev.* Vol. 26: pp. 170–188.

Ganeshram, S., F. Pedersen, E. Calvert, W. McNeill, and M. R. Fontugne (2000): 'Glacial-interglacial variability in denitrification in the world's oceans: Causes and consequences'. *Paleoceanography*, vol. 15: pp. 361–376.

Gaye, B., B. Nagel, K. Dähnke, T. Rixen, and K.-C. Emeis (2013): 'Evidence of parallel denitrification and nitrite oxidation in the ODZ of the Arabian Sea from paired stable isotopes of nitrate and nitrite'. *Global Biogeochem. Cycles*, vol. 27: pp. 1059–1071.

Gaye-Haake, B., N. Lahajnar, K.-C. Emeis, D. Unger, T. Rixen, A. Suthhof, V. Ramaswamy, H. Schulz, A. Paropkari, M. Guptha, and V. Ittekkot (2005): 'Stable nitrogen isotopic ratios of sinking particles and sediments from the northern Indian Ocean'. *Mar. Chem.* Vol. 96: pp. 243–255.

Gupta, A. K., D. M. Anderson, and J. T. Overpeck (2003): 'Abrupt changes in the Asian southwest monsoon during the Holocene and their links to the North Atlantic Ocean'. *Nature*, vol. 421: pp. 354–356.

Gupta, A. K., M. Das, and D. M. Anderson (2005): 'Solar influence on the Indian summer monsoon during the Holocene'. *Geophys. Res. Lett*, vol. 32: p. L17703.

Gupta, A. K., K. Mohan, S. Sarkar, S. C. Clemens, R. Ravindra, and R. K. Uttam (2011): 'East-West similarities and differences in the surface and deep northern Arabian Sea records during the past 21 Kyr'. *Palaeogeogr. Palaeoclimatol. Palaeoecol.* Vol. 301: pp. 75–85.

Haake, B., V. Ittekkot, T. Rixen, V. Ramaswamy, R. R. Nair, and W. B. Curry (1993): 'Seasonality and interannual variability of particle fluxes to the deep Arabian Sea'. *Deep Sea Res. I*, vol. 40(7): pp. 1323–1344.

Hastenrath, S. and P. J. Lamb (1979): *Climate Atlas of the Indian Ocean, Surface Climate and Atmospheric Circulation*. Vol. 1. Univ. of Wisconsin Press, Madison.

Haug, G. H., K. A. Hughen, D. M. Sigman, L. C. Peterson, and U. Röhl (2001): 'Southward migration of the intertropical convergence zone through the Holocene'. *Science*, vol. 293(5533): pp. 1304–1308.

Huguet, C., J.-H. Kim, J. S. Sinninghe Damsté, and S. Schouten (2006): 'Reconstruction of sea surface temperature variations in the Arabian Sea over the last 23 kyr using organic proxies (TEX 86 and $U_{37}^{K'}$)'. *Paleoceanography*, vol. 21(3).

Jung, S. J. A., G. R. Davies, G. Ganssen, and D. Kroon (2004): 'Synchronous Holocene sea surface temperature and rainfall variations in the Asian monsoon system'. *Quat. Sci. Rev.* Vol. 23: pp. 2207–2218.

Keigwin, L. D. (1996): 'The Little Ice Age and Medieval Warm Period in the Sargasso Sea'. *Science*, vol. 274: pp. 1504–1508.

Keil, R. G. and G. L. Cowie (1999): 'Organic matter preservation through the oxygen-deficient zone of the NE Arabian Sea as discerned by organic carbon: Mineral surface area ratios'. *Mar. Geol.* Vol. 161: pp. 13–22.

Levitus, S. and T. Boyer (1994): *World Ocean Atlas 1994, Temperature, NOAA Atlas NESDIS*. Vol. 4. U.S. department of Commerce.

Lückge, A., H. Doose-Rolinski, A. A. Khan, H. Schulz, and U. von Rad (2001): 'Monsoonal variability in the northeastern Arabian Sea during the past 5000 years: Geochemical evidence from laminated sediments'. *Palaeogeogr. Palaeoclimatol. Palaeoecol.* Vol. 167: pp. 273–286.

Lückge, A., L. Reinhardt, H. Andruleit, H. Doose-Rolinski, U. von Rad, H. Schulz, and U. Treppke (2002): 'Formation of varve-like laminae off Pakistan: Decoding 5 years of sedimentation'. *The Tectonic and Climatic Evolution of the Arabian Sea Region*. Ed. by Clift, P., D. Kroon, C. Gaedicke, and J. Craig. Vol. 195. London: Geological Society Special Publications: pp. 421–431.

Madhupratap, M., S. Prasanna Kumar, P. M. A. Bhattathiri, M. Dileep Kumar, S. Raghukumar, K. K. C. Nair, and N. Ramaiah (1996): 'Mechanism of the biological response to winter cooling in the northeastern Arabian Sea'. *Nature*, vol. 384: pp. 549–552.

Mann, M. E., Z. Zhang, S. Rutherford, R. S. Bradley, M. K. Hughes, D. Shindell, C. Ammann, G. Faluvegi, and F. Ni (2009): 'Global signatures and dynamical origins of the Little Ice Age and Medieval Climate Anomaly'. *Science*, vol. 326: pp. 1256–1260.

Marcott, S. A., J. D. Shakun, P. U. Clark, and A. C. Mix (2013): 'A Reconstruction of Regional and Global Temperature for the Past 11,300 Years'. *Science*, vol. 339: pp. 1198–1201.

Müller, P. J. and E. Suess (1979): 'Productivity, sedimentation rate, and sedimentary organicmatter in the oceans-I. Organic carbon preservation'. *Deep Sea Res*, vol. 26A: pp. 1347–1362.

Nair, R. R., V. Ittekkot, S. J. Manganini, V. Ramaswamy, B. Haake, E. T. Degens, B. N. Desai, and S. Honjo (1989): 'Increased particle flux to the deep ocean related to monsoons'. *Nature*, vol. 338: pp. 749–751.

Naqvi, S. W. A., T. Yoshinari, D. A. Jayakumar, M. A. Altabet, P. V. Narvekar, A. H. Devol, J. A. Brandes, and L. A. Codispoti (1998): 'Budgetary and biogeochemical implications of N_2O isotope signatures in the Arabian Sea'. *Nature*, vol. 394: pp. 462–464.

Neff, U., S. J. Burns, A. Mangini, M. Mudelsee, D. Fleitmann, and A. Matter (2001): 'Strong coherence between solar variability and the monsoon in Oman between 9 and 6 kyr ago'. *Nature*, vol. 411: pp. 290–293.

Olson, D. B., G. L. Hitchcock, R. A. Fine, and B. A. Warren (1993): 'Maintenance of the low-oxygen layer in the central Arabian Sea'. *Deep Sea Res. II*, vol. 40(3): pp. 673–685.

Oppo, D. W., Y. Rosenthal, and B. K. Linsley (2009): '2, 000-year-long temperature and hydrology reconstructions from the Indo-Pacificwarmpool'. *Nature*, vol. 460: pp. 1113–1116.

PAGES 2k Consortium (2013): 'Continental-scale temperature variability during the past two millennia'. *Nature Geoscience*, vol. 6: pp. 339–346.

Paropkari, A. L., C. P. Babu, and A. Mascarenhas (1992): 'A critical evaluation of depositional parameters controlling the variability of organic carbon in Arabian Sea sediments'. *Mar. Geol.* Vol. 107: pp. 213–226.

Prahl, F. G., J. Dymond, and M. A. Sparrow (2000): 'Annual biomarker record for export production in the central Arabian Sea'. *Deep Sea Res. II*, vol. 47: pp. 1581–1604.

Prahl, F. G., B. N. Popp, D. M. Karl, and M. A. Sparrow (2005): 'Ecology and biogeochemistry of alkenone production at Station ALOHA'. *Deep Sea Res. I*, vol. 52: pp. 699–719.

Prasanna Kumar, S. and T. G. Prasad (1996): 'Winter cooling in the northern Arabian Sea'. *Curr. Sci.* Vol. 71(10): pp. 834–841.

Prasanna Kumar, S., N. Ramaiah, M. Gauns, V. V. S. S. Sarma, P. M. Muraleedharan, S. Raghukumar, M. Dileep Kumar, and M. Madhupratap (2001): 'Physical forcing of biological productivity in the Northern Arabian Sea during the Northeast Monsoon'. *Deep Sea Res. II*, vol. 48: pp. 1115–1126.

Ramaswamy, V. and B. Gaye (2006): 'Regional variations in the fluxes of foraminifera carbonate, coccolithophorid carbonate and biogenic opal in the northern Indian Ocean'. *Deep Sea Res. I*, vol. 53: pp. 271–293.

Reichart, G. J., L. J. Lourens, and W. J. Zachariasse (1998): 'Temporal variability in the northern Arabian Sea Oxygen Minimum Zone (OMZ) during the last 225,000 years'. *Paleoceanography*, vol. 13: pp. 607–621.

Reichart, G. J., S. J. Schenau, G. J. de Lange, and W. J. Zachariasse (2002): 'Synchroneity of oxygen minimum zone intensity on the Oman and Pakistan Margins at sub-Milankovitch time scales'. *Mar. Geol.* Vol. 185: pp. 403–415.

Reynolds, R. W., N. A. Rayner, T. M. Smith, D. C. Stokes, and W. Wang (2002): 'An improved in situ and satellite SST analysis for climate'. *J. Clim. 15*, vol. 15: pp. 1609–1625.

Rixen, T., M. V. S. Guptha, and V. Ittekkot (2005): 'Deep ocean fluxes and their link to surface ocean processes and the biological pump'. *Prog. Oceanogr.* Vol. 65: pp. 240–259.

Rixen, T., B. Haake, V. Ittekkot, M. V. S. Guptha, R. R. Nair, and P. Schlüssel (1996): 'Coupling between SW monsoon-related surface and deep ocean processes as discerned from continuous particle flux measurements and correlated satellite data'. *J. Geophys. Res.* Vol. 101: pp. 569–582.

Rosell-Melé, A. and F. G. Prahl (2013): 'Seasonality of $U^{K'}_{37}$ temperature estimates as inferred from sediment trap data'. *Quat. Sci. Rev.* Vol. 72: pp. 128–136.

Rostek, F., E. Bard, L. Beaufort, C. Sonzogni, and G. Ganssen (1997): 'Sea surface temperature and productivity records for the past 240 kyr in the Arabian Sea'. *Deep Sea Res. II*, vol. 44(6–7): pp. 1461–1480.

Russell, J. M. and T. C. Johnson (2005): 'Late Holocene climate change in the North Atlantic and equatorial Africa: Millennial-scale ITCZ migration'. *Geophys. Res. Lett*, vol. 32: p. L17705.

Sanwal, J., B. S. Kotlia, C. Rajendran, S. M. Ahmad, K. Rajendran, and M. Sandiford (2013): 'Climatic variability in Central Indian Himalaya during the last 1800 years: Evidence from a high resolution speleothem record'. *Quat. Int.* Vol. 304: pp. 183–192.

Schlitzer, R. (2013): *Ocean Data View*. http://odv.awi.de.

Schulte, S. and P. Müller (2001): 'Variations of sea surface temperature and primary productivity during Heinrich and Dansgaard-Oeschger events in the northeastern Arabian Sea'. *Geo-Mar. Lett. 21*, vol. 21: pp. 168–175.

Schulte, S., F. Rostek, E. Bard, J. Rullkötter, and O. Marchal (1999): 'Variations of oxygen-minimum and primary productivity recorded in sediments of the Arabian Sea'. *Earth Planet. Sci. Lett.* Vol. 173: pp. 205–221.

Schulz, H., U. von Rad, and H. Erlenkeuser (1998): 'Correlation between Arabian Sea and Greenland climate oscillations of the past 110,000 years'. *Nature*, vol. 393: pp. 54–57.

Schulz, H., U. von Rad, and V. Ittekkot (2002): 'Planktic foraminifera, particle flux and oceanic productivity off Pakistan, NE Arabian Sea: modern analogues and application to the paleoclimatic record'. *The Tectonic and Climatic Evolution of the Arabian Sea Region*. Ed. by Clift, P., D. Kroon, C. Gaedicke, and J. Craig. Vol. 195. London: Geological Society Special Publications: pp. 499–516.

Schulz, H., U. von Rad, and U. von Stackelberg (1996): 'Laminated sediments from the oxygen-minimum zone of the northeastern Arabian Sea'. *Paleoclimatology*

and Paleoceanography from Laminated Sediments. Ed. by Kemp, A. Vol. 116. London: Geological Society Special Publications: pp. 185–207.

Seki, O., T. Nakatsuka, K. Kawamura, S. .-.-I. Saitoh, and M. Wakatsuchi (2007): 'Time-series sediment trap record of alkenones from the western Sea of Okhotsk'. *Mar. Chem.* Vol. 104: pp. 253–265.

Sinha, A., K. G. Cannariato, L. D. Stott, H. Cheng, R. L. Edwards, M. G. Yadava, R. Ramesh, and I. B. Singh (2007): 'A 900-year (600 to 1500 A.D.) record of the Indian summer monsoon precipitation from the core monsoon zone of India'. *Geophys. Res. Lett*, vol. 34: p. L16707.

Sinha, A., L. D. Stott, M. Berkelhammer, H. Cheng, R. L. Edwards, B. Buckley, M. Aldenderfer, and M. Mudelsee (2011): 'A global context of megadroughts in monsoon Asia during the past millennium'. *Quat. Sci. Rev.* Vol. 30: pp. 47–62.

Sirocko, F., M. Sarnthein, H. Erlenkeuser, H. Lange, M. Arnold, and J. C. Duplessy (1993): 'Century-scale events in monsoonal climate over the past 24,000 years'. *Nature*, vol. 364: pp. 322–324.

Sonzogni, C., E. Bard, F. Rostek, D. Dollfus, A. Rosell-Melé, and G. Eglinton (1997a): 'Temperature and salinity effects on alkenone ratios measured in surface sediments from the Indian Ocean'. *Quat. Res.* Vol. 47: pp. 344–355.

Sonzogni, C., E. Bard, F. Rostek, R. Lafont, A. Rosell-Melé, and G. Eglinton (1997b): 'Core-top calibrations of the alkenone index vs. sea surface temperature in the Indian Ocean'. *Deep Sea Res. II*, vol. 44(6–7): pp. 1445–1460.

Suthhof, A., V. Ittekkot, and B. Gaye-Haake (2001): 'Millennial-scale oscillation of denitrification intensity in the Arabian Sea during the late Quaternary and its potential influence on atmospheric N_2O and global climate'. *Global Biogeochem. Cycles*, vol. 15: pp. 637–649.

Suthhof, A., T. C. Jennerjahn, P. Schäfer, and V. Ittekkot (2000): 'Nature of organic matter in surface sediments from the Pakistan continental margin and the deep Arabian Sea: Amino acids'. *Deep Sea Res. II*, vol. 47: pp. 329–351.

van der Weijden, C. H., G. J. Reichart, and H. J. Visser (1999): 'Enhanced preservation of organic matter in sediments deposited within the oxygen minimum zone in the northeastern Arabian Sea'. *Deep Sea Res. I*, vol. 46: pp. 807–830.

Van Rampelbergh, M., D. Fleitmann, S. Verheyden, H. Cheng, L. Edwards, P. D. Geest, D. D. Vleeschouwer, S. J. Burns, A. Matter, P. Claeys, and E. Keppens (2013): 'Mid- to late Holocene Indian Ocean Monsoon variability recorded in four speleothems from Socotra Island, Yemen'. *Quaternary Science Reviews*, vol. 65: pp. 129–142.

von Rad, U., G. Delisle, and A. Lückge (2002a): 'Comment - On the formation of laminated sediments on the continental margin off Pakistan'. *Mar. Geol.* Vol. 192: pp. 425–429.

von Rad, U., A. A. Khan, W. H. Berger, D. Rammlmair, and U. Treppke (2002b): 'Varves, turbidites and cycles in upper Holocene sediments (Makran slope, northern Arabian Sea)'. *The Tectonic and Climatic Evolution of the Arabian Sea Region*. Ed. by Clift, P., D. Kroon, C. Gaedicke, and J. Craig. Vol. 195. London: Geological Society Special Publications: pp. 387–406.

von Rad, U., M. Schaaf, K. H. Michels, H. Schulz, W. H. Berger, and F. Sirocko (1999): 'A 5000-yr record of climate change in varved sediments from the Oxygen Minimum Zone off Pakistan, Northeastern Arabian Sea'. *Quat. Res.* Vol. 51: pp. 39–53.

von Rad, U., H. Schulz, and SONNE 90 Scientific Party (1995): 'Sampling the oxygen minimum zone off Pakistan: Glacial-interglacial variations of anoxia and productivity (preliminary results, SONNE 90 cruise)'. *Mar. Geol.* Vol. 125: pp. 7–19.

Wakeham, S. G., M. L. Peterson, J. I. Hedges, and C. Lee (2002): 'Lipid biomarker fluxes in the Arabian Sea, with a comparison to the equatorial Pacific Ocean'. *Deep Sea Res. II*, vol. 49: pp. 2265–2301.

Wang, Y., H. Cheng, R. L. Edwards, Y. He, X. Kong, Z. An, J. Wu, M. J. Kelly, C. A. Dykoski, and X. Li (2005): 'The Holocene Asian monsoon: Links to solar changes and North Atlantic climate'. *Science*, vol. 308: pp. 854–857.

Wyrtki, K. (1973): 'Physical Oceanography of the Indian Ocean'. *The Biology of the Indian Ocean*. Ed. by Zeitzschel, B. Springer Berlin: pp. 18–36.

Yancheva, G., N. R. Nowaczyk, J. Mingram, P. Dulski, G. Schettler, J. F. W. Negendank, J. Liu, D. M. Sigman, L. C. Peterson, and G. H. Haug (2007): 'Influence of the intertropical convergence zone on the East Asian monsoon'. *Nature*, vol. 445: pp. 74–77.

You, Y. (1998): 'Intermediate water circulation and ventilation of the Indian Ocean derived from water-mass contributions'. *J. Mar. Res.* Vol. 56: pp. 1029–1067.

Zhang, P. et al. (2008): 'A Test of Climate, Sun, and Culture Relationships from an 1810-Year Chinese Cave Record'. *Science*, vol. 322(5903): pp. 940–942.

Decadal-resolution record of winter monsoon intensity over the last two millennia from planktic foraminiferal assemblages in the northeastern Arabian Sea

The Holocene

Vol. 25, No. 11, p. 1756–1771, 2015. doi:10.1177/0959683615591357

Philipp M. Munz[1], Michael Siccha[2], Andreas Lückge[3], Anna Böll[4], Michal Kucera[2] and Hartmut Schulz[1]

[1]*Department of Geosciences, University of Tübingen, Germany;*
[2]*MARUM – Center for Marine Environmental Sciences, Germany;*
[3]*Bundesanstalt für Geowissenschaften und Rohstoffe (BGR), Germany;*
[4]*Institute of Geology, University of Hamburg, Germany;*

Keywords: Indian paleomonsoon; late Holocene; planktic foraminifera; sea surface temperature; transfer functions; winter monsoon intensity

Abstract

The Indian monsoon system is an important climate feature of the northern Indian Ocean. Small variations of the wind and precipitation patterns have fundamental influence on the societal, agricultural and economic development of India and its neighboring countries. To understand current trends, sensitivity to forcing or natural variation, records beyond the instrumental period are needed. However, high-resolution archives of past winter monsoon variability are scarce. One potential archive of such records are marine sediments deposited on the continental slope in the NE Arabian Sea, an area where present-day conditions are dominated by the winter monsoon. In this region, winter monsoon conditions lead to distinctive changes in surface water properties, affecting marine plankton communities that are deposited in the sediment. Using planktic foraminifera as a sensitive and well-preserved plankton group, we first characterize the response of their species distribution on environmental gradients from a dataset of surface sediment samples in the tropical and subtropical Indian Ocean. Transfer functions for quantitative paleoenvironmental reconstructions were applied to a decadal-scale record of assemblage counts from the Pakistan Margin spanning the last 2000 years. The reconstructed temperature record reveals an intensification of winter monsoon intensity near the year 100 CE. Prior to this transition, winter temperatures were $> 1.5\,^{\circ}$C warmer than today. Conditions similar to the present seem to have established after 450 CE, interrupted by a ingular event near 950 CE with warmer temperatures and accordingly weak winter monsoon. Frequency analysis revealed significant 75-, 40- and 37-year cycles, which are known from decadal- to centennial-scale resolution records of Indian summer monsoon variability and interpreted as solar irradiance forcing. Our first independent record of Indian winter monsoon activity confirms that winter and summer monsoon were modulated on the same frequency bands and thus indicates that both monsoon systems are likely controlled by the same driving force.

Introduction

The monsoon climate is generally defined as the seasonal reversal of the prevailing surface winds and accompanied precipitation, driven by the migrating low surface pressure belt of the Intertropical Convergence Zone (ITCZ) and atmospheric pressure over Central Asia (Wyrtki, 1971). In the Arabian Sea region,

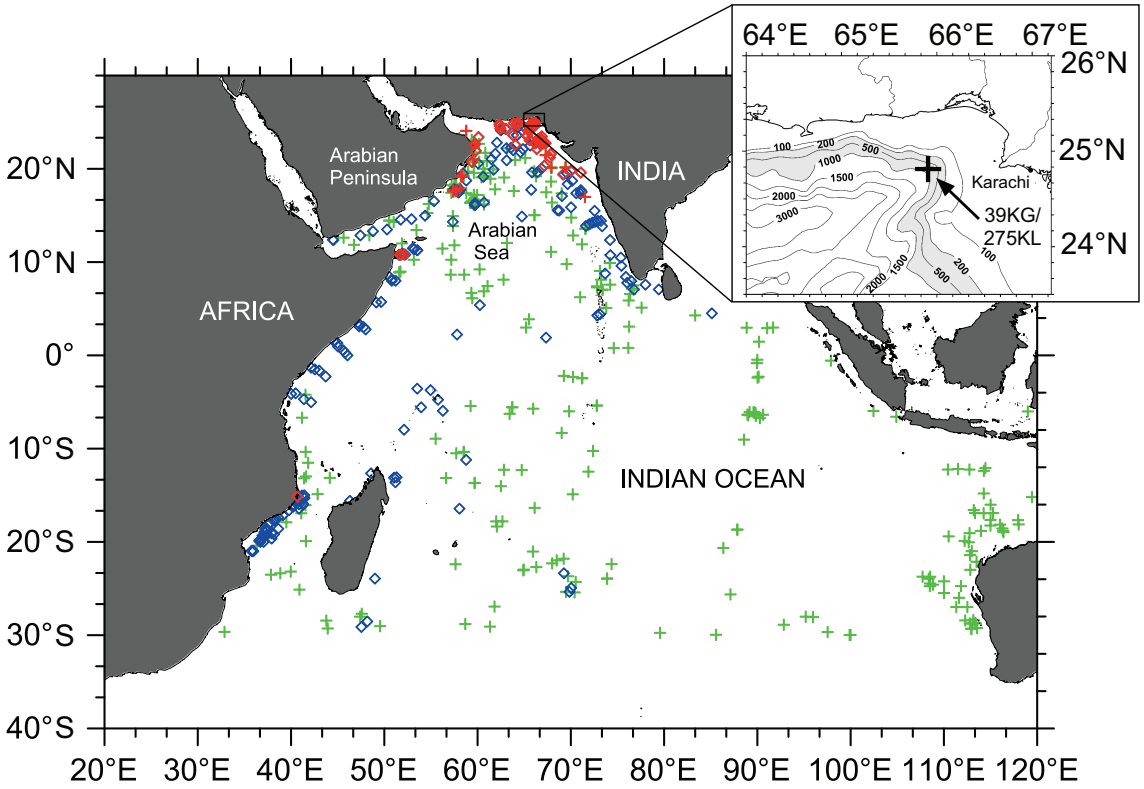

Figure III.1: Map of the Indian Ocean showing locations of coretop samples of the initial calibration dataset. Cross symbols are samples from the AUSMAT-F4 dataset compiled by the MARGO group ($n = 329$; Barrows and Juggins, 2005). Open diamond symbols are additional $n = 274$ own contributions. Red colored symbols were used for the reconstruction in the adjusted calibration dataset. Smaller map shows the location of cores 39KG/275KL on the upper continental margin off Pakistan, within the permanent oxygen minimum zone (grey shading) on the Makran accretionary wedge.

strong and moisture-laden southwesterly winds prevail during summer, when the low-pressure zone of the Hadley circulation is on the northward position over continental Asia and northern Arabia (Shetye et al., 1994). The reversed mode during winter drives dry northeasterly winds of lower velocity towards the low-pressure zone above the open ocean. Both seasonal modes of the monsoon lead to distinct hydrographic changes in the water column of the Arabian Sea, affecting the production and distribution of marine plankton, including planktic foraminifera (Curry et al., 1992; Schiebel et al., 2004; Schulz et al., 2002). Southwesterly winds during summer induce upwelling by Ekman transport along the coast of Somalia, Oman and southwestern India, resulting in enhanced primary production and surface water cooling from June to September (Colborn, 1975; Currie et al., 1973). Northeasterly winter winds cause cooling of surface waters in the northeastern

Arabian Sea and the resulting deepening of the thermocline and weakening of the thermal stratification enables convective mixing and injection of nutrients into the photic zone (Banse and McClain, 1986; Ittekkot et al., 1992; Madhupratap et al., 1996). In the northeastern Arabian Sea, these processes lead to maximum primary productivity during winter (Lückge et al., 2002; Schulz et al., 2002). Sediment trap studies revealed a conspicuous shift of the planktic foraminiferal (PF) assemblage induced by these two particular oceanic seasons (Curry et al., 1992; Schulz et al., 2002), indicating that PF may be a powerful recording system for past dynamics of the Indian monsoon.

Historical records of past Indian monsoon intensity are limited to the last 140 years (Sontakke et al., 1993), therefore limiting the accurate determination of low-frequency multi-decadal- to centennial-scale variability of the monsoon system. The time frame over the last two millennia (the Common Era, CE) provides the opportunity to disentangle natural climate variability from anthropogenic forcing (e.g., Jones and Mann, 2004) and has recently attracted broad attention of the scientific community (PAGES 2k Consortium, 2013). The dynamics of the summer monsoon over the last two millennia have been intensively studied from speleothem records on the Arabian Peninsula, Socotra and Andaman Islands (Burns et al., 2002; Fleitmann et al., 2003, 2007; Laskar et al., 2013; Neff et al., 2001), marine sediments recording upwelling intensity off Oman (Anderson et al., 2002; Gupta et al., 2003) and tree rings from localities in Central Asia and on the Indian subcontinent (Bräuning and Mantwill, 2004; Cook et al., 2013; Xu et al., 2012).

But the dynamics of the winter monsoon are virtually unknown. In theory, an anti-phase behavior to the summer monsoon intensity can be derived from the lateral migration of the annual mean position of the ITCZ. On millennial- and longer timescales, a more northward position of the ITCZ induces strengthening of the summer monsoon and weakening of the winter monsoon during interstadials, whereas the situation during stadials is reversed (Wang et al., 2005a; Yancheva et al., 2007). On decadal- to centennial timescales, however, both systems are probably controlled by the dynamics of the El Niño/Southern Oscillation (ENSO; Kumar et al., 2006; Zhou et al., 2007). To better predict how the summer and winter monsoon interact and whether they respond in-phase and coherently to external forcing, long records of the winter monsoon are needed.

The upper continental slope off Pakistan (Figure III.1) is characterized by a strong and permanent oxygen minimum zone (OMZ) between a water depth of 200 and

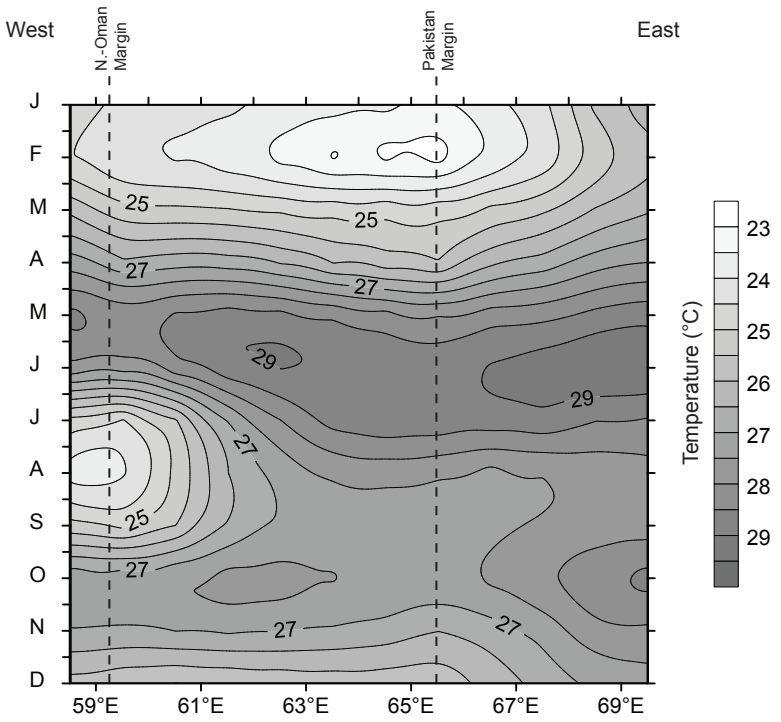

Figure III.2: Contour plot of annual (January–December) temperature evolution along an arch-shaped section in the northern Arabian Sea in the approximate depth of cores 39KG/275KL, showing lowest temperatures off Pakistan during winter and off Oman during summer.

1,200 m (Schulz et al., 1996; von Rad et al., 1995), resulting from mid-water oxygen consumption by high degradation rates of organic matter. Oxygen deficiency prevents post depositional mixing of the sediment by burrowing organisms, which enables the formation and preservation of annually resolving varve-like laminated sediments (Lückge et al., 2001; Schulz and von Rad, 2014; Schulz et al., 2002, 1996). High sedimentation rates caused by high biological productivity as well as the lateral advection and resuspension of fine-grained terrigeneous matter (Schulz and von Rad, 2014), combined with the lack of bioturbation enables the identification of interannual and even seasonal signals (Kemp, 1996). This makes marine sediments from the OMZ on the Makran accretionary wedge off Pakistan an archive of an exceptionally high-resolution chronology, providing the potential to unravel short-term climate oscillations. Compared to the northwestern Arabian Sea, where sea surface temperatures (SST) are coldest during summer upwelling, minimum SST along the coast off Pakistan occurs during the winter season (Figure III.2). This suggests, verified by satellite-derived concentrations of monthly chlorophyll α in the surface waters (Feldman and McClain, 2013), that the annual cycle of sea

surface properties in this area is dominated by winter conditions.

In a previous paper (Böll et al., 2014), we attempted to reconstruct winter monsoon intensity from regionally calibrated alkenone temperatures and stable nitrogen isotopes in laminated sediment cores (39KG/275KL) from the Pakistan margin (Figure III.1). There we identified a general cooling trend of reconstructed annual mean temperatures over the last 2,400 years together with several periods of century-scale temperature changes, that occurred largely in phase with geochemical productivity estimates. However, open questions about the response of surface water properties to winter monsoon activity remained when the general trend of decreasing temperatures and increasing productivity was reversed, e.g. during the Medieval Warm Period (950–1250 CE, Common Era; CE/BCE were used numerically equivalent to AD/BC). Furthermore, we observed a heterogeneous pattern of coccolith and alkenone fluxes from a sediment trap study over the course of one year. Because the observed seasonality greatly contributes to the general difficulty in attributing alkenone-derived annual mean temperatures to the seasonal winter component, we have used the same sediment cores in this study (39KG/275KL) and generated a high-resolution record of PF assemblages spanning the last 2,000 years. Using a new, regionally valid transfer function constrained by rigorous evaluation of potential driving forces, we convert the assemblage counts into a record of winter sea surface temperatures (wSST). This record is then used to assess the seasonal evolution of winter monsoon variability in the northeastern Arabian Sea and to allow comparison to other proxy records of winter- and summer monsoon intensity. This allows a rigorous investigation of a potential anti-phase relationship to the summer monsoon during the late Holocene.

Material and methods

Late Holocene sediment record from the Pakistan margin

In order to calculate SST variations over the last 2,000 years from foraminiferal transfer functions, we studied samples from the uppermost 15 cm of Sonne 90 box-core 39KG (von Rad et al., 1995, 1999) and the uppermost 167 cm of Sonne 130 piston-core 275KL (Böll et al., 2014; von Rad et al., 1998). Both cores were taken at the same station from the continental margin off Pakistan (Figure III.1; 24 °50′N, 65 °55′E, 695 m water depth), allowing us to achieve a continuous record over the

last 2,000 years. Correlation of both cores was enabled by a 10 cm-thick reddish-brown event layer ('F1-layer'), present in both records (Schulz and von Rad, 2014). Coarse fraction samples of boxcore 39KG above F1 were available in continuous 3 mm-intervals (n=50 samples) from a previous study (Doose-Rolinski et al., 2001). 275KL was sampled from a U-Channel below F1 in continuous 5 mm-intervals (n=332 samples) to achieve a suitable number of PF individuals from the narrower sample size.

Chronostratigraphy of both cores has been presented by von Rad et al., (1999), who established age models of Sonne 90 cores 39KG and 56KA by varve counts and conventional and AMS radiocarbon dating. Correlation between 56KA and 275KL, recovered at the same location, is based on a layer-by-layer tracking of prominent 1-30 mm-thick light colored event deposits ('C-Layers'). 39KG covers the record from retrieval in the year 1993 CE to the deposition of F1 in 1888 CE, providing an average sample resolution of 2 years for the last ~100 years. 275KL is linked to the record of 39KG below F1 and was analyzed from 1888 CE until 118 BCE with an average resolution of 9 years for the last ~2,000 years.

Samples for PF analyses were freeze-dried, wet-sieved over a 63 µm screen and oven-dried at 40 °C. Counts were conducted on a split fraction (39KG) or the whole residue (275KL) of the size fraction >150 µm, examined under a stereo-dissecting microscope. Planktic foraminifera were identified to species level, based on the taxonomic framework given by Bé and Hutson, (1977) and Bé, (1967) and Hemleben et al., (1989). For the calculation of relative assemblage compositions of 275KL, samples yielding less than 300 counted individual PF were combined with adjacent samples to achieve a minimum of 300 individuals. 89 samples were merged, representing 27% of the dataset. Merging was done when the coarse fraction of a sample was diluted by fine-grained terrigeneous matter of an event deposit ('C- or F-Layers'), thus not decreasing the actual resolution of the marine deposition.

Surface sample calibration dataset

To investigate factors affecting assemblage composition of planktic foraminifera in surface sediments in the Arabian Sea, we compiled modern coretop data consisting of a subset of the AUSMAT-F4 dataset compiled by the MARGO group ($n = 329$ samples; Barrows and Juggins, 2005), extended by $n = 274$ new samples by this study. The subset was defined to cover the tropical and sub-tropical Indian

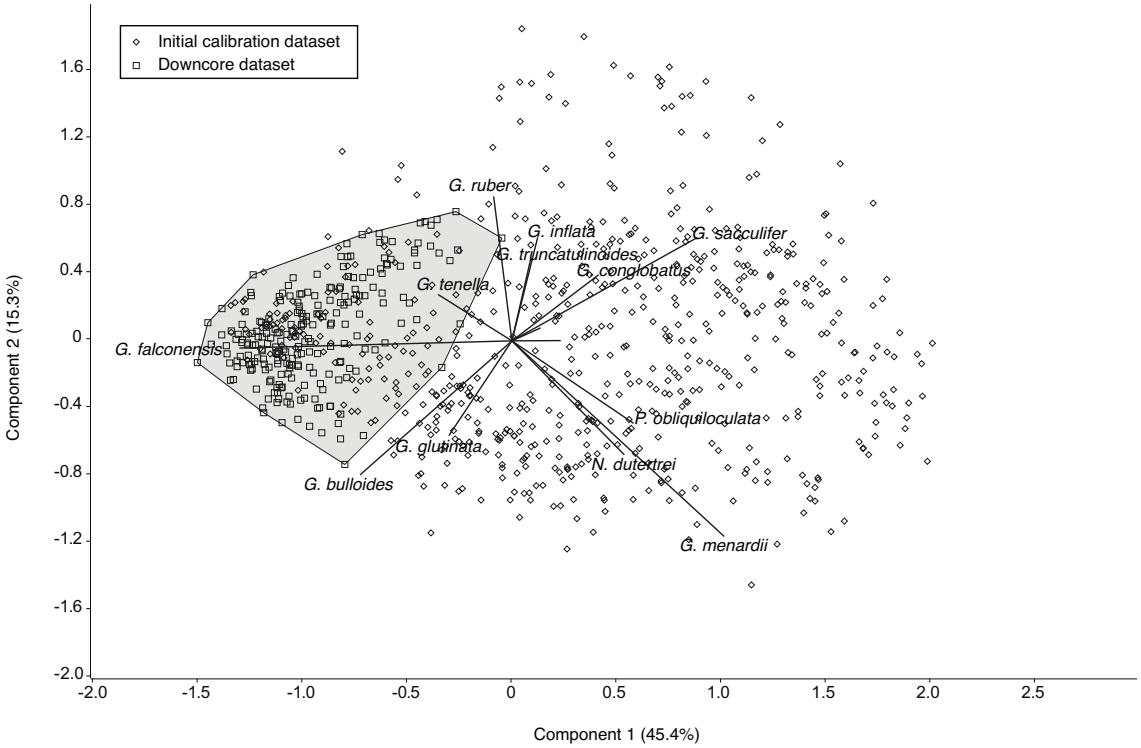

Figure III.3: Joint PCA scatter plot and species scores of the log-transformed calibration (diamond) and downcore (square) datasets. The grey shaded area marks the variability captured by the late Holocene record of cores 39KG/275KL, defining the final input for calibrating the transfer functions.

Ocean from 30 °N to 30 °S and from 30 °–120 °E, to reduce the risk of including endemic species and cryptic morphotypes from divergent oceanic environments. According to Kucera et al., (2005b), noise in the data could be introduced by a broader geographical coverage, when the genetic and ecological variation not captured by the taxonomic input variables increases, and with the increasing influence of secondary environmental gradients. Due to the unique environmental forcing in the Bay of Bengal (Murty et al., 1992; Wyrtki, 1973) and the Red Sea (Auras-Schudnagies et al., 1989; Siccha et al., 2009), samples from these basins were omitted. The $n = 274$ additional samples substantially increased the regional coverage of the eastern and northeastern Arabian Sea and along the western margins of the Indian Ocean (Figure III.1).

Both datasets were thoroughly checked for taxonomic inconsistencies and for an adequate minimum number of identified PF individuals. Assemblage alteration by carbonate dissolution was identified by unusually high numbers (>3%) of the dissolution-resistant species *Sphaeroidinella dehiscens*. To minimize a potential bias

introduced by different contributors to the dataset, taxonomic units showing a close morphological similarity, namely *Globigerinella siphonifera* and *Globigerinella calida* (Weiner et al., 2015), as well as *Globorotalia menardii* and *Globorotalia tumida*, were merged, respectively. All morphotypes of *Globigerinoides sacculifer*, with and without a sacc-form ultimate chamber, were treated as one taxonomic unit (André et al., 2013). Due to the low signal-to-noise ratio of rare species for quantitative paleoenvironmental reconstructions (Kucera et al., 2005b), the dataset was filtered to a minimum average occurrence of 0.5%. This resulted in the exclusion of 14 out of 29 species.

For the construction of an adjusted calibration dataset, a joined R-mode principal component analysis (PCA) was conducted. Since measurements of the input variables are based on the same units (relative species abundances) a covariance matrix was used to preserve the magnitude of variation between the variables. A log-ratio transformation was used to compensate for the mutual dependency of the compositional dataset (Aitchinson, 1999; Aitchinson et al., 2000). PCA was conducted on log-transformed relative abundances of the 15 species in the initial pool of tropical- and sub-tropical Indian Ocean surface samples (n=603) and the downcore faunal dataset (Figure III.4). The first two PC axes explained 61% of the variance of both datasets. $N = 103$ samples in the calibration dataset had the same range of PCA scores along the first two PC axes as the downcore samples, thus being most similar in the direction of the first two components. The remaining $n = 500$ calibration samples described assemblages not represented in the downcore dataset, most likely recording conditions outside of the range of variation of the winter monsoon region.

To investigate the species response to potential controlling environmental gradients, a redundancy analysis (RDA) was carried out using the VEGAN package (Dixon, 2003) of the R statistical program (R Core Team, 2014). Since the annual cycle of plankton productivity in the investigated area of the eastern Makran is dominated by winter conditions (Madhupratap et al., 1996), and specimens of PF deposited during winter therefore dominate the sedimentary assemblages, we calibrated the modern coretop database to variables representing the boreal winter season (J-F-M and D-J-F).

Since the Arabian Sea experiences extreme intraannual variations of biological productivity (Banse, 1987; Lal, 1994; Prasanna Kumar et al., 2001; Smith et al., 1998; Zeitschel and Gerlach, 1973), three different approaches were made to char-

acterize the primary production. As a proxy for the surface standing stock of phytoplankton, chlorophyll α measurements from NASA's SeaWiFS and MODIS sensors were used (Feldman and McClain, 2013). The December to February averages were binned over a timespan from 1998–2010. In comparison, Vertical Generalized Production Models (VGPM) calculate net primary production rates in the euphotic zone (Behrenfeld and Falkowski, 1997), taking into account the physiological variability through the water column. We employed the Eppley-version VGPM as a temperature-dependent model of photosynthetic efficiency extracted from the Oregon State University, (2014) to generate an estimate of winter productivity. As an additional approach of quantifying phytoplankton productivity we applied the updated Carbon-based Production Model (uCbPM; Oregon State University, 2014), which, compared to VGPM, calculates phytoplankton carbon biomass from particulate backscatter coefficients and is independent of standard chlorophyll measurements. Both net primary productivity estimates were calculated as January-March averages from 1998–2010. As a measure of water column stratification, the maximum Brunt-Väisälä frequency (BVF) of the top 250 m of the water column was used. The calculations were performed on the data of the World Ocean Atlas 2001 (Conkright et al., 2002) using the implemented algorithm in OceanDataView 4.5.7 (Schlitzer, 2014). Sea surface temperature (SST) is apparently the strongest determinant controlling PF species distributions in large parts of the world's oceans (Morey et al., 2005). Following the MARGO recommendations (Kucera et al., 2005a), SST values were interpolated via kriging to the coretop samples from the 10 m depth level of the World Ocean Atlas 2001 (Conkright et al., 2002). We are aware of a potential bias introduced by PF assemblages that are more sensitive to subsurface than to surface temperatures, as discussed by Telford et al., (2013). However, we do not expect large changes in the ocean thermal structure over the last 2,000 years and consider this issue to be of less importance here. In total, the PF assemblage data in the adjusted surface dataset are then analysed together with five environmental parameters, reflecting winter productivity (chlorophyll α, Eppley VGPM, uCbPM), temperature (SST) and stratification (BVF).

Design of the transfer function models

We used a suite of different transfer functions for the quantitative reconstructions of environmental variables controlling the distribution of planktic foraminifera.

There is no single 'best method' to be recommended (Juggins and Birks, 2012) and using different statistical techniques that model species response to environmental gradients in different ways allows the assessment of signals that are robust to method-specific bias (Kucera et al., 2005b), which is particularly significant in our case where we expect a relatively low signal to noise ratio. We employed the Imbrie and Kipp factor analysis- IKFA (Imbrie and Kipp, 1971), weighted averaging partial least square regression- WA-PLS (ter Braak and Juggins, 1993), the maximum likelihood response curves method- MLRC (Birks et al., 1990) and artificial neural networks- ANN (Malmgren and Nordlund, 1997). Except for ANN, we used the *R* package *rioja* ver. 0.8-7 (Juggins, 2015) to calculate the transfer functions. All methods used the relative species abundances of the adjusted calibration dataset ($n = 103$ samples). As a measure of distance to modern analogs, the Bray-Curtis dissimilarity to the samples of the adjusted calibration dataset was calculated for each fossil sample. For IKFA, the number of factors to extract was determined by the Kaiser-Guttman-Criterion and Parallel Analysis after Horn (Horn, 1965), both limiting the number of factors to five. For WA-PLS, two components performed with the lowest error during cross-validation and were thus used for the reconstruction. ANN were computed as back propagation networks using the *BioComp* software NeuroGeneticOptimizer© ver. 2.6.142. The system was configured to limit the number of neurons in multiple hidden layers to four and to optimize the network structure with 100 network populations over 30 generations, with a minimum of 100 and a maximum of 2500 passes, and a stop criterion if no improvement occurred over the last 40 passes.

Performance fitness was based on improvement of the root-mean-square-error (RMSE) of a test set, consisting of 50% of the surface sample dataset. Ten different pairs of training- and test sets were used and the average of the best of the ten resulting networks was calculated as the final output. Except for ANN, model validation and error estimates were based on bootstrapping (1000 cycles). RMSEP (root-mean-square-error of prediction) was estimated from the cross-validated average RMSE across the bootstrap cycles. The sample specific standard error of prediction was calculated as the square root of the sum of the samples squared standard error and the mean squared error across the bootstrap cycles. ANN RMSEP were calculated from the average RMSE across the ten best networks.

Results

Modern faunal distribution and multivariate analysis of the surface sample dataset

The distribution of PF species in the surface sample dataset (Figure III.4) replicates the patterns observed by Bé and Hutson, (1977) and Hutson and Prell, (1980). The increased spatial coverage in the northern Arabian Sea, along the margin off Oman and western India, as well as off Somalia and Mozambique allows for a more detailed analysis. *Globigerinoides ruber* (white), the most abundant species in the entire calibration dataset, is most frequent below the subtropical gyre of the southern Indian Ocean and south of the central Arabian Sea. Furthermore, *G. ruber* is abundant along the western coast of India outside the Gulf of Khambat. *Globigerina bulloides* shows highest abundances close to the coast of high summer upwelling areas off northern Somalia and Oman, as well as off the southwestern tip of India. Medium abundances are apparent along the entire coast off Somalia, in the Gulf of Aden, as well as in the northern and eastern Arabian Sea. *Globigerinita glutinata*, on the other hand, seems to be more abundant outside the coastal upwelling areas in the open ocean upwelling of the northern Arabian Sea. *Neogloboquadrina dutertrei*, *G. sacculifer* and *G. menardii* are typical for the central Arabian Sea and for open ocean sites along the South Equatorial Current. *N. dutertrei* occurs in low numbers along the coast of Somalia, Oman and southwest India, but is not found in the northeastern Arabian Sea. *G. sacculifer* is also absent in surface samples from the western and northeastern Arabian Sea (see also Schulz et al., 2002). *G. siphonifera/G. calida* is, like *G. sacculifer*, mostly absent from regions of intense upwelling and occurs in moderate numbers in the open equatorial and southern Indian Ocean. Very high numbers of *G. menardii/G. tumida* observed in a few open ocean sites might be an indication for calcite dissolution. *Globigerina falconensis* seems to be characteristic of the eastern and northeastern Arabian Sea.

Results of the RDA conducted on the adjusted calibration dataset with the winter constraints are illustrated as a triplot in Figure III.5. The first axis explains 38.9% of the variation in the species data and is highly correlated with temperature, stratification, chlorophyll α concentration, as well as the Eppley-VGPM productivity (Table III.1). The second axis, explaining 16.3% of the species variation, is correlated strongest with the updated Carbon-based Productivity Model.

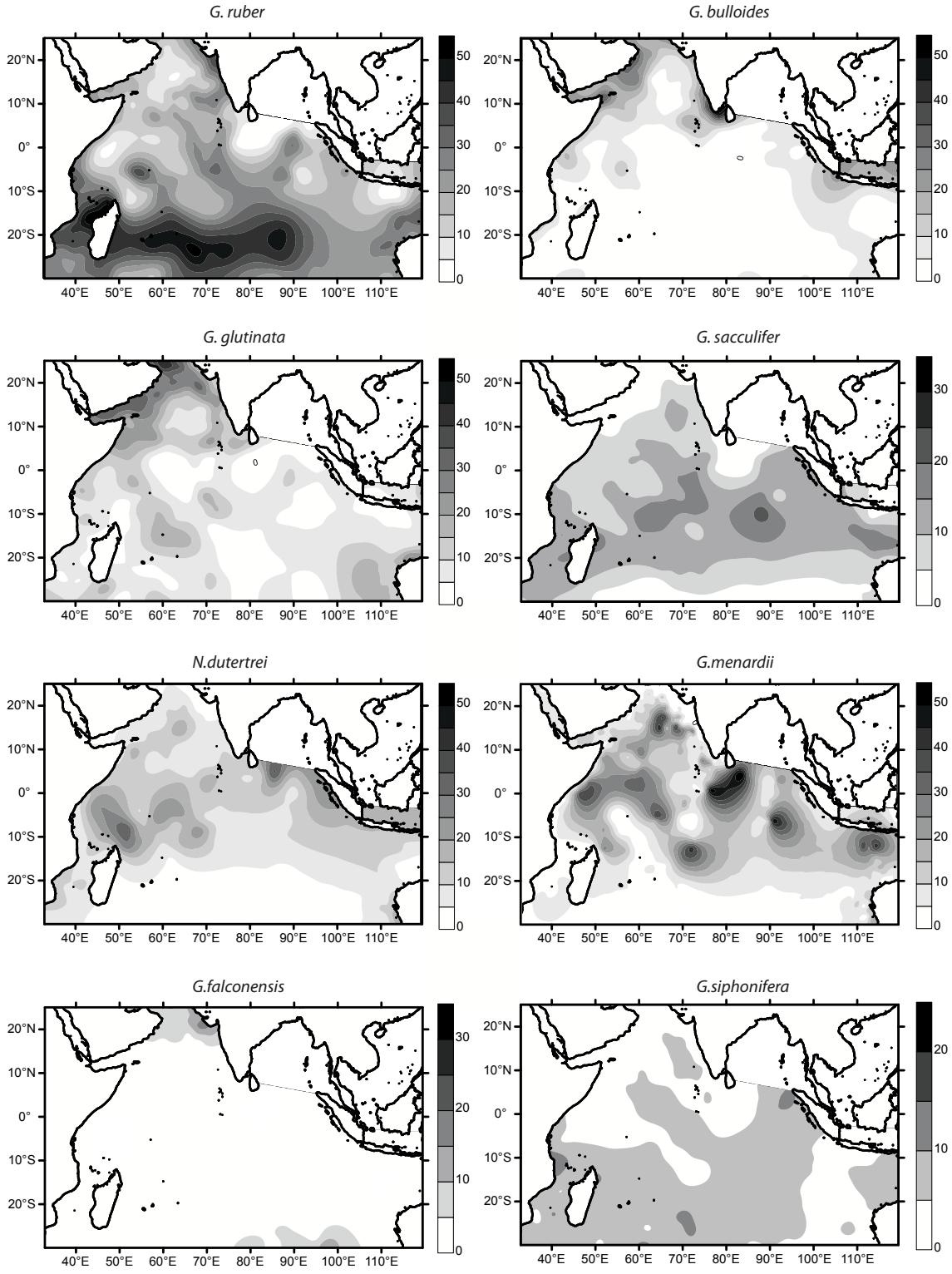

Figure III.4: Contour plot of relative frequencies of species >3% average abundance in initial coretop database spanning the Arabian Sea and Indian Ocean from 30 °N 30 °S and 30 °E – 120 °E, by omitting the Bay of Bengal and the Red Sea.

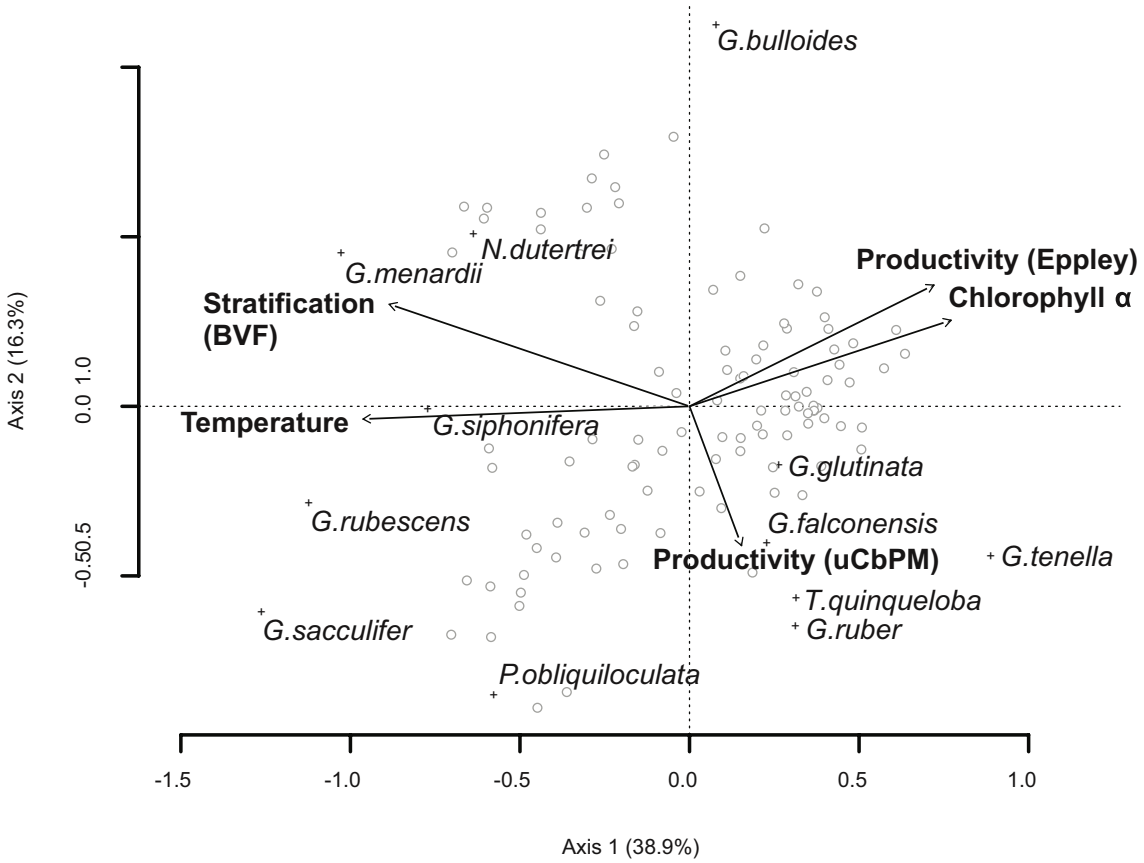

Figure III.5: Scatter triplot of redundancy analysis results computed with the species (cross symbols) and environmental data (arrows) of the winter season. Open circles indicate surface samples.

Among the environmental variables investigated by RDA, winter temperature has the highest correlation with the first axis, and thus appears to be the most important variable for the explanation of the species variation. Temperature and stratification are positively correlated with each other and the pair is negatively correlated to chlorophyll *α* and Eppley-VGPM. Relative abundances of *G. siphonifera*, *G. rubescens* and *G. sacculifer* show a positive correlation with increasing temperatures and stratification and a negative correlation with chlorophyll *α* and Eppley-VGPM. Stratification is correlated with the relative abundances of *G. menardii* and *N. dutertrei* and has a negative correlation with *G. tenella*. Interestingly, uCbPM best explains the abundance of *G. falconensis*, *T. quinqueloba* and *G. ruber*, and to a minor extent also of *G. glutinata*. *G. bulloides* plots on the positive end of the second RDA axis, implying a negative correlation with the winter productivity of the uCbPM model. Stronger winter winds cause intensified cooling, winter deep mixing and enhanced primary productivity (Banse and McClain, 1986; Mad-

Table III.1: Results of the redundancy analysis of the adjusted calibration dataset.

	RDA1	RDA2	RDA3	RDA4	RDA5	Permutation test statistics (p)
Eigenvalue	0.389	0.163	0.100	0.050	0.010	
Cumulative proportion explained	0.115	0.163	0.192	0.207	0.210	
Correlation						
Temperature	–0.982	–0.038	–0.005	0.081	0.169	<0.001
Stratification	–0.903	0.307	–0.293	–0.005	0.071	<0.001
Chlorophyll α	0.786	0.259	0.437	–0.193	0.294	<0.01
Eppley-VGPM	0.735	0.365	0.555	–0.085	0.107	<0.01
uCbPM	0.156	–0.419	–0.113	0.776	0.431	<0.01

VGPM: Vertical Generalized Production Models; uCbPM: updated Carbon-based Production Model.

hupratap et al., 1996). Accordingly, stronger winter conditions shift the faunal assemblage from *G. bulloides* to higher abundances of *G. falconensis* and *G. glutinata*.

Transfer function performance

One of the key assumptions of paleoecological transfer functions states that the environmental variable to be reconstructed is the dominant factor for the ecological changes in the fossil assemblage records (e.g., Juggins and Birks, 2012). Thus we reconstructed the gradient that performed best in explaining the species variation by RDA, which is winter sea surface temperature (wSST). In terms of reconstruction uncertainties, WA-PLS and IKFA showed similar error rates and outperformed MLRC (Table III.2). The error estimation of ANN is not based on bootstrapping and is therefore not fully comparable to the other techniques. In general, all prediction error estimates are considerably lower than the uncertainty for basin-wide foraminiferal transfer functions of $1-2\,^{\circ}$C (e.g., Kucera et al., 2005b). Error estimates represent a minimum uncertainty because the training and test sets are not fully independent and contain a certain degree of spatial autocorrelation (Telford and Birks, 2005; Telford et al., 2004). However, since the selection criterion for the final calibration dataset is based on taxonomic similarity rather than geographically or environmentally close sites, samples are distributed among different margins of the Arabian Sea (Figure III.1). To compare the absolute values of the error rate with basin-wide reconstructions, these are expressed as the percentage of the range of the target variable (Table III.2). Values range from 15.4% for ANN, 17.6% and 18.6% for WA-PLS and IKFM, respectively, to 24.9% for MLRC. This is about three to four times higher compared to basin-wide reconstructions with a target variable range of ~30 °C (e.g., Kucera et al., 2005b). This reflects the fact that basin-wide datasets have a very strong temperature dependency in the

middle part of the SST gradient, whereas our adjusted calibration dataset is at the edge of the SST gradient. The initial subset of the calibration dataset covering the tropical- and subtropical Indian Ocean exhibits a range of the wSST gradient of 18–29°C, whereas the adjusted dataset of 23–27°C.

Downcore development of planktic foraminiferal assemblages

It turned out that high species variability of the biennial resolution record of core 39KG is not comparable to the decadal-scale resolution of the longer core 275KL (Figure III.7). As a consequence, we would expect this to result in poor analogy to a calibration dataset of the same decadal- to centennial-scale resolution. For the purpose of this study we therefore achieved a spliced record of comparable temporal resolution while retaining a continuous sampling scheme by binning the PF counts from 39KG to the average resolution of the longer core 275KL.

Eight PF species occurred with average abundances of >2%, that together sum up to 96% of the total faunal composition. These are in descending order *G. falconensis*, *G. bulloides*, *G. ruber*, *G. glutinata*, *G. siphonifera*, *N. dutertrei*, *G. sacculifer* and *G. tenella* (Table III.3). A PCA conducted solely on the downcore dataset was used to investigate the major trends in the fossil fauna (Figure III.6). The first component explains 40.6% of the total variance and the second component explains 13.7%. The variance explained by the second component is lower than the variance generated by a broken-stick-model and can therefore probably be neglected (e.g., Joliffe, 2002). The first axis mainly separates *G. sacculifer* and *G. siphonifera* from *G. tenella* and *G. glutinata*. PCA time-series reveals that samples that are most associated with the former species occurred largely prior to the year 450 CE (Figure III.8), consistent with higher abundances of *G. sacculifer* and *G. siphonifera*. Downcore development of PF species distribution is given in Figure III.8. The most noticeable feature from the dataset is the occurrence of *G. sacculifer* between 250–450 CE and 100 BCE–100 CE, together with higher abundances of *G. siphonifera* and *O. universa*. Whereas *G. sacculifer* is mostly absent after 450 CE, this species is reaching more than 25% prior to 450 CE. Simultaneously, G. tenella is rare or completely absent prior to 450 CE and *G. falconensis* shows lower abundances during the interval 100 BCE–100 CE.

A positive correlation among reconstructed wSST from all transfer function techniques and with the PC1 scores (Table III.2) indicates that the ecological changes in the species assemblages are interpreted coherently by all methods and reflect

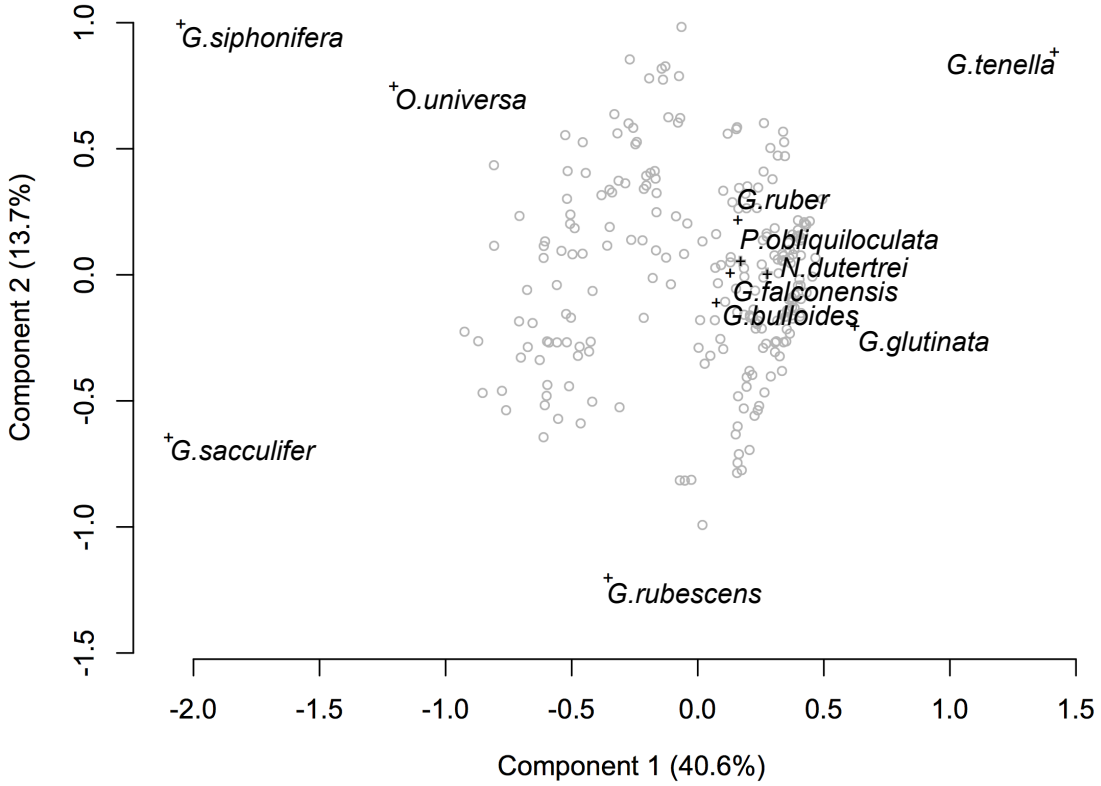

Figure III.6: Scatterplot of the downcore principal component analysis and the variance explained by each axis. The first principal component (PC1) mainly separates *G. siphonifera* and *G. sacculifer* from *G. tenella* and *G. glutinata*.

the strongest gradient in the data. It is therefore very likely, that the reconstruction is primarily driven by the changes of the reconstructed environmental variable (Juggins and Birks, 2012).

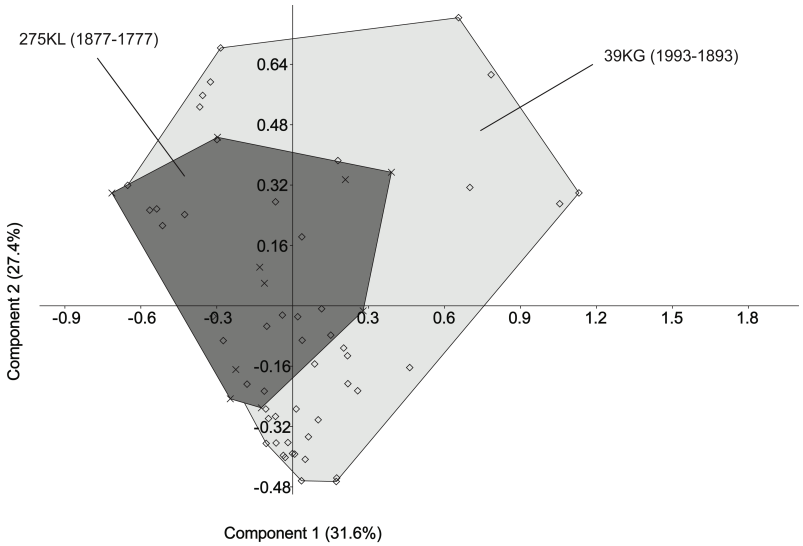

Figure III.7: Joint R-mode PCA scatterplot of the log-transformed species abundance data covering a 100-years period from core 39KG (1993–1893 CE) and 275KL (1877–1777 CE). The area covered by PCA scores scores along the first and second PC-axes illustrates the higher variance of species abundance data of core 39KG (light grey) compared to 275KL (dark grey). To enable comparison and splicing of both records the abundance data of core 39KG were downscaled to the same 9-years continuous sampling resolution of core 275KL prior to the transfer function approach.

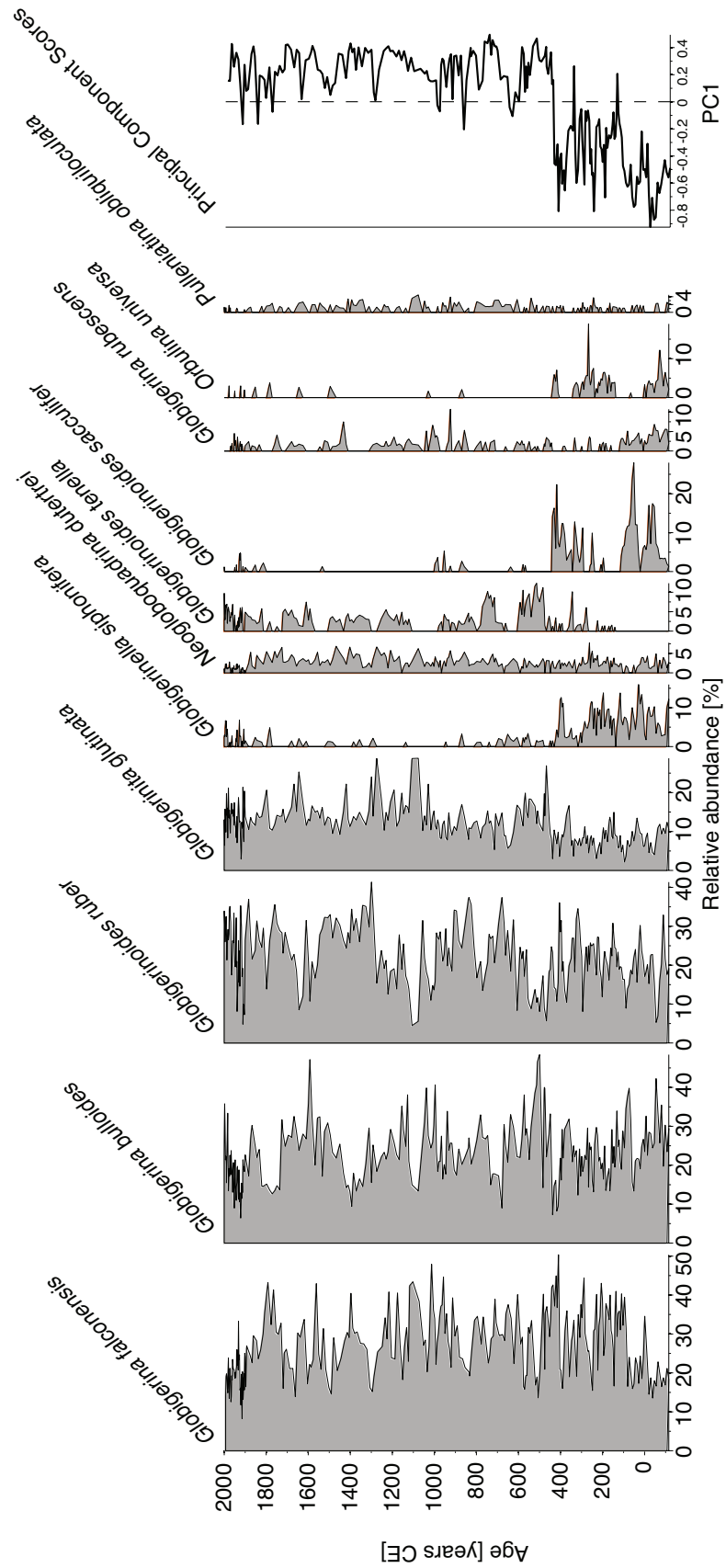

Figure III.8: Changes in relative abundance of the planktic foraminiferal taxa and first principal component scores (from Figure III.6) during the last ~2000 years in cores 39KG/275KL. The abrupt change at 450 CE is associated with the sudden occurrence of *G.sacculifer* and *G.siphonifera*, mainly on the expense of *G.tenella* and *G.glutinata*.

Table III.2: (a) Error estimates for the individual transfer functions reconstructing wSST and **(b)** correlation table among the individual reconstructions and with PC1 scores (lower left corner shows in bold numbers the linear correlation value r, upper right corner represents the respective p value).

	(a) Error estimates for transfer functions				(b) Correlation among reconstructions				
	RMSE	RMSEP (bootstrap)	R^2	Range fraction of the target variable (%)	WA-PLS	IKFM	MLRC	ANN	PC1 scores
WA-PLS	0.545	0.632	0.505	17.55		2.04E-53	1.84E-67	4.50E-77	9.91E-16
IKFM	0.597	0.671	0.360	18.63	**0.39**		4.68E-47	1.57E-29	3.87E-65
MLRC	0.786	0.896	0.326	24.87	**0.62**	**0.77**		1.16E-45	8.45E-51
ANN	0.556		0.606	15.44	**0.92**	**0.65**	**0.77**		4.34E-37
PC1 scores	–	–	–	–	**–0.50**	**–0.85**	**–0.79**	**–0.71**	

RMSE: root mean square error; RMSEP: root mean square error of prediction; WA-PLS: weighted averaging partial least square regression; MLRC: maximum likelihood response curves method; ANN: artificial neural networks.

Table III.3: Summary statistics of planktic foraminiferal abundances in the fossil record of cores 39KG/275KL.

Species	Mean	Minimum	Maximum	Standard deviation	Occurrence (total $n = 382$)
Globigerina falconensis (Blow, 1959)	26.65	11.24	49.33	7.73	362
Globigerina bulloides (d'Orbigny, 1829)	23.07	7.17	47.24	7.11	356
Globigerinoides ruber white (d'Orbigny, 1839)	22.86	4.36	48.20	7.92	345
Globigerinita glutinata (Egger,1895)	12.13	2.16	30.83	4.96	358
Globigerinella siphonifera (d'Orbigny, 1839)	2.80	0	15.61	3.31	255
Globigerinella claida (Parker, 1962)	0.19	0	2.43	0.27	56
Globoturborotalita tenella (Parker, 1958)	2.50	0	12.11	2.69	233
Neogloboquadrina dutertrei (d'Orbigny, 1839)	2.45	0	7.50	1.35	344
Globigerinoides sacculifer (Brady, 1877)	2.22	0	27.58	4.12	179
Globoturborotalita rubescens (Hofker, 1956)	1.41	0	10.53	1.50	232
Pulleniatina obliquiloculata (Parker and Jones, 1865)	1.10	0	4.39	0.80	272
Orbulina universa (d'Orbigny, 1839)	1.07	0	18.50	2.09	107
Globorotalia menardii (Jones and Brady, 1865)	0.69	0	3.24	0.58	195
Neogloboquadrina pachyderma (Ehrenberg, 1861)	0.21	0	2.09	0.35	55
Turborotalita quinqueloba (Natland, 1938)	0.18	0	2.73	0.42	43
Dentigloborotalia anfracta (Parker, 1967)	0.13	0	1.88	0.28	41
Beella digitata (Brady, 1879)	0.10	0	2.10	0.29	25
Globigerinoides conglobatus (Brady, 1879)	0.05	0	1.16	0.14	17
Tenuitella iota (Parker, 1962)	0.07	0	1.08	0.16	15
Globorotaloides hexagonus (Natland, 1938)	0.03	0	1.21	0.10	2
Globorotalia theyeri (Fleisher, 1974)	0.02	0	0.60	0.07	2
Hasitgerina plagica (d'Orbigny, 1839)	0.01	0	1.28	0.09	1
Globoquadrina conglomerata (Schwager, 1866)	0	0	0.42	0.03	1

Discussion

Environmental control on species distribution

The results of RDA on the adjusted dataset of modern samples revealed a strong relationship along the first component between temperature and stratification on the one side and the chlorophyll-based productivity estimates on the other side (Figure III.5). This might be explained by the mutual dependency of thermocline deepening and strength of surface cooling during the winter season. Stronger and colder surface winds lead to more severe cooling of surface waters and thus enhance convective winter deepening of the mixed layer. The less stratified water column enables nutrients from deeper waters to be mixed into the euphotic zone, nourishing primary productivity. As a result, both effects cannot be fully disentangled. However, the positive correlation of *G. falconensis*, a species considered as typical for the deep thermocline mixing during winter monsoon conditions (Peeters and Brummer, 2002; Schulz et al., 2002), and other productivity-indicating species with increasing uCbPM productivity could indicate that these model data are a useful representation of nutrient conditions during winter monsoon. *G. bulloides* is considered as an indicator of summer upwelling conditions in the western Arabian Sea (Curry et al., 1992; Gupta et al., 2003; Naidu and Malmgren, 1996). The strong negative correlation of *G. bulloides* with winter productivity, especially uCbPM, reveals an antiphase relationship of this species to winter conditions in this part of the basin. Possible lateral advection of nutrient-rich surface waters originating in the upwelling areas of the northwestern Arabian Sea (Schulz et al., 1996) could lead to higher accumulation rates of *G. bulloides* during summer. If *G. bulloides* is related to summer conditions, the response of this species could not be explained by the winter constraints of the analysis. The constrained variation explained by the second RDA component is, however, small compared to the total unconstrained variance, which makes to refrain from an attempt to construct a transfer function for winter productivity. *G. siphonifera* and *G. sacculifer* are associated with warmer temperatures and accordingly weaker winter conditions. Both species are spinose macroperforate, symbiont-bearing and mainly occur in warm tropical- and sub-tropical waters with low seasonality (Fraile et al., 2008; Hemleben et al., 1989). In the Arabian Sea, *G. sacculifer* and *G. siphonifera* are typical for non-upwelling areas of low nutrient concentrations (Cayre et al., 1999; Peeters and Brummer, 2002; Schiebel et al., 2004).

G. glutinata is common in coastal- and open-ocean upwelling areas (Naidu and Malmgren, 1996) and known to feed mainly on diatom prey (Hemleben et al., 1989). In sediment trap studies of the northeastern Arabian Sea, *G. tenella* occurs together with *G. rubescens* during late winter and spring (Schulz et al., 2002). The negative association of the samples of this interval in the PCA of the downcore dataset with productivity-related species (*G. falconensis, G. bulloides, G. glutinata*) and the positive association with temperature-related *G. sacculifer* and *G. siphonifera* suggest diminished influence of winter monsoon conditions. After 450 CE, *G. sacculifer* occurs only sporadically in very small numbers, indicating a sudden faunal shift in the planktic foraminiferal assemblage.

Decadal-scale variability of foraminiferal assemblages and winter monsoon intensity over the last two millennia

Given the relatively short period covered by the two core profiles 39KG and 275KL, most species show a comparatively high variability in their abundances (Table III.3). A sampling interval of 5 mm corresponds to an average sediment accumulation time of ~10 years. Occasional sampling of an unequal number of summer- and winter layers could potentially lead to an irregular distribution of each season, which might introduce a noisy sampling bias of up to 10% disparity compared to a signal of equal seasons. If this were the case for our dataset, the similarity of the adjacent samples would be lower than the similarity to samples of increasing distance. For 66% of the dataset, the Bray-Curtis similarity to the closest sample is, however, higher compared to the similarity of the next-but-one sample. We therefore conclude that the observed variability of species abundances is not affected by an unequal contribution of the seasonal signals, but rather attests to the success of the sampling scheme, which yielded decadal-scale data not affected by bioturbational mixing in the laminated sediments.

The high variability within the species dataset is also obvious from the scatterplot of the joint PCA of the downcore- and entire initial calibration dataset (Figure III.4). The latter is spanning a wide ecological range of the tropical- and subtropical Indian Ocean, thus contains most of the species variance. The downcore dataset covers approximately one fourth of the variance captured by the initial calibration dataset. This suggests that short-term interannual fluctuations in PF relative abundances and production rates are underestimated by potentially bioturbated coretop samples, often carrying an integrated signal over several decades to

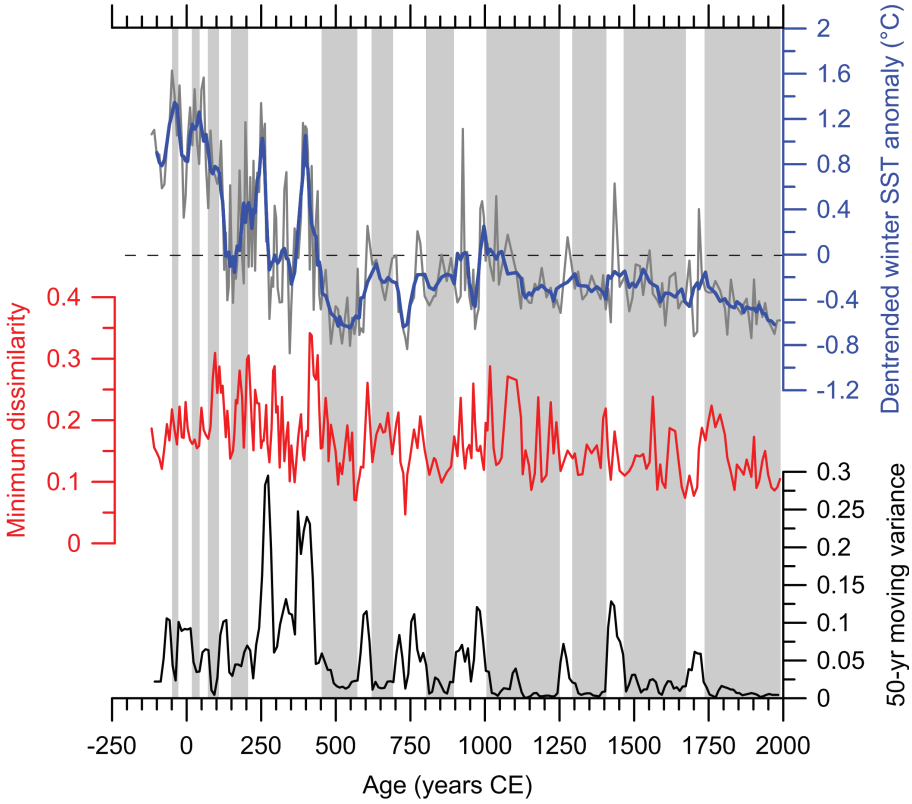

Figure III.9: Temporal evolution of the wSST variance time series calculated within an overlapping 50-year moving window on the detrended time series filtered with a 30-year low-pass Butterworth filter. Grey bars indicate periods of low variance. Minimum Bray-Curtis dissimilarity between the fossil samples and the adjusted calibration dataset as a measure of analogy. Changes of winter monsoon intensity are shown as the detrended winter SST anomaly.

millennia (Kucera et al., 2005b).

The multi-decadal evolution of the wSST variance and detrended temperature anomaly (Figure III.9) reveals that winter monsoon variability shows three stages of changing strength and frequency. Whereas during the periods prior to 250 CE and after 450 CE changes are relatively small, wSST variance during the period 250–450 CE was considerably higher. To further explore the decadal- to centennial-scale variability of the wSST record, we computed the spectral peaks with the Multitaper Method (MTM) implemented in the *SpectraWorks* software kSpectra© ver. 3.4.2 (Ghil et al., 2002) with the default settings ($p = 2$, $K = 3$ tapers). Figure III.10 shows the MTM frequency spectrum of the detrended wSST time series, smoothed with a low-pass Butterworth filter with a 30-year cutoff frequency. Multi-decadal variability of winter monsoon intensity was found on 75-, 40–37- and 31-year cycles. Several recent studies based on observational data (e.g., Kim et al., 2014;

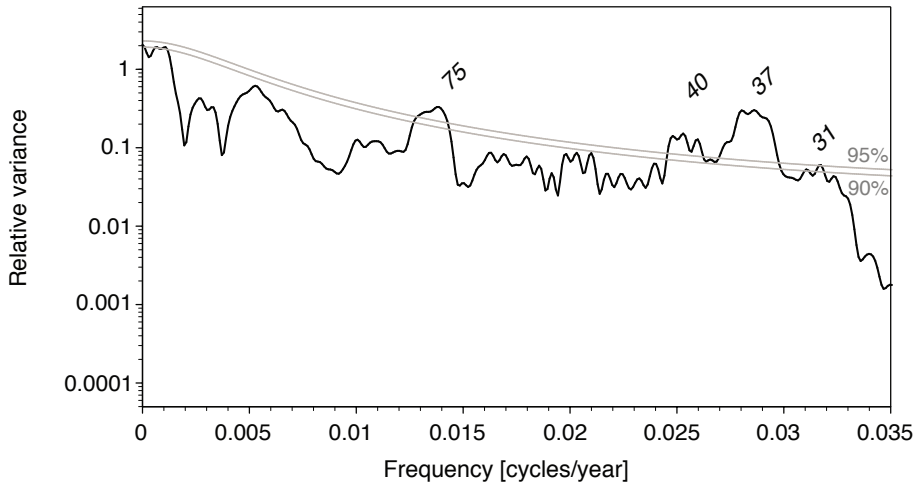

Figure III.10: Results of a multitaper method (MTM) spectral analysis of the wSST record of winter monsoon variability over the last ~2000 years with a red noise null hypothesis (90%- and 95% confidence levels are indicated as grey lines). Significant peaks are attributed to harmonic 75-, 40- and 37-year cycles (bold), as well as to a 31-year cycle.

Krishnamurthy and Krishnamurthy, 2014; Webster et al., 1998; Zhou et al., 2007) indicated that the monsoon-ENSO relationship is modulated on low-frequency inter-decadal timescales according to regime shifts of the Pacific Decadal Oscillation (PDO). The PDO, defined as the leading mode of monthly SST anomalies in the extratropical North Pacific (Mantua et al., 1997), shifts its phase with periods from 20–30 years (Mantua and Hare, 2002). The potential to resolve meaningful winter monsoon variability within this frequency range with our record is, however, limited by the 9-year resolution and requires records capable of resolving inter-decadal signals. The multi-decadal cycles estimated by MTM are close to the 78- and 35-year periodicities found by Neff et al., (2001) for the Hoti cave (H5) δ^{18}O stalagmite record from northern Oman. Their record spans the early- to mid Holocene evolution of the Indian summer monsoon precipitation and the decadal-scale variability is interpreted to controlled by solar irradiance forcing. The 75-year periodicity is also very close to the ~79-year cycle found in the Oman upwelling record, implied by Gupta et al., (2005) to be coherent with a sunspot cycle. In the eastern Arabian Sea, Agnihotri et al., (2002) found a dominant 60–70-year periodicity in a record of Indian summer monsoon variability over the last millennium that appears to be solar forcing. From a study of coastal climate proxies in Sri Lanka that are interpreted to be controlled by winter monsoon variability, ~64- and 28–32-year periodicities were found (Ranasinghe et al., 2013). These findings

suggest that summer and winter monsoon modulated on the same decadal-scale frequency bands are most likely driven by changes of solar irradiance. Furthermore, early- to mid Holocene periodicities (Neff et al., 2001) also existed during the late Holocene.

Implications for late Holocene SST variability and monsoon evolution

Our 2,000-year-record of wSST in the northeastern Arabian Sea shows three stages of winter monsoon evolution. The first interval until 100 CE is marked by a relatively stable period of temperatures warmer than average (Figure III.9), implying weak winter monsoon conditions. The subsequent stage, between 100 and 450 CE is characterized by high winter monsoon variability where highly fluctuating wSST suggests a transition phase of winter monsoon strength until after 450 CE when a sudden cooling marks the onset of persistently enhanced winter monsoon conditions. During the relatively stable but colder third phase from 450 CE onwards, the most obvious feature is a gradual warming towards 950 CE, where winter monsoon conditions are weakest within that interval, and a gradual strengthening thereafter.

In a previous paper (Böll et al., 2014), we also found three distinct phases of changing monsoon intensities during the last ~2400 years, although the timing compared to the present study is slightly different. The most obvious features of the alkenone record are an abrupt decrease of annual mean temperatures (AM-SST) around 250 CE and a persistent warming around 1050–1150 CE (Figure III.11). In contrast to our newly developed record of foraminiferal-based wSST, the former shift occurred between the end of stable weak winter monsoon conditions at 100 CE and the onset of intensified winter conditions after 450 CE, during the transition phase. The warming phase around 1050–1150 CE occurs apparently ~100 years later in the alkenone record and shows also a longer duration as in the wSST record. This might indicate that the observed three distinct climate phases of colder and warmer temperatures had a different impact on the respective seasonal cycles and that changes during the inter-monsoon season did not occur simultaneously to variations of winter monsoon intensity. These phases could have been amplified in the AM-SST record, because especially during intervals of weak winter monsoon intensity and accordingly warmer wSST, the contribution of the warmer inter-monsoon signal (cf. Figure III.2, warmest modern SST $> 27\,^{\circ}$C occur from April–November) to annual mean temperatures must have been increased. Our data do

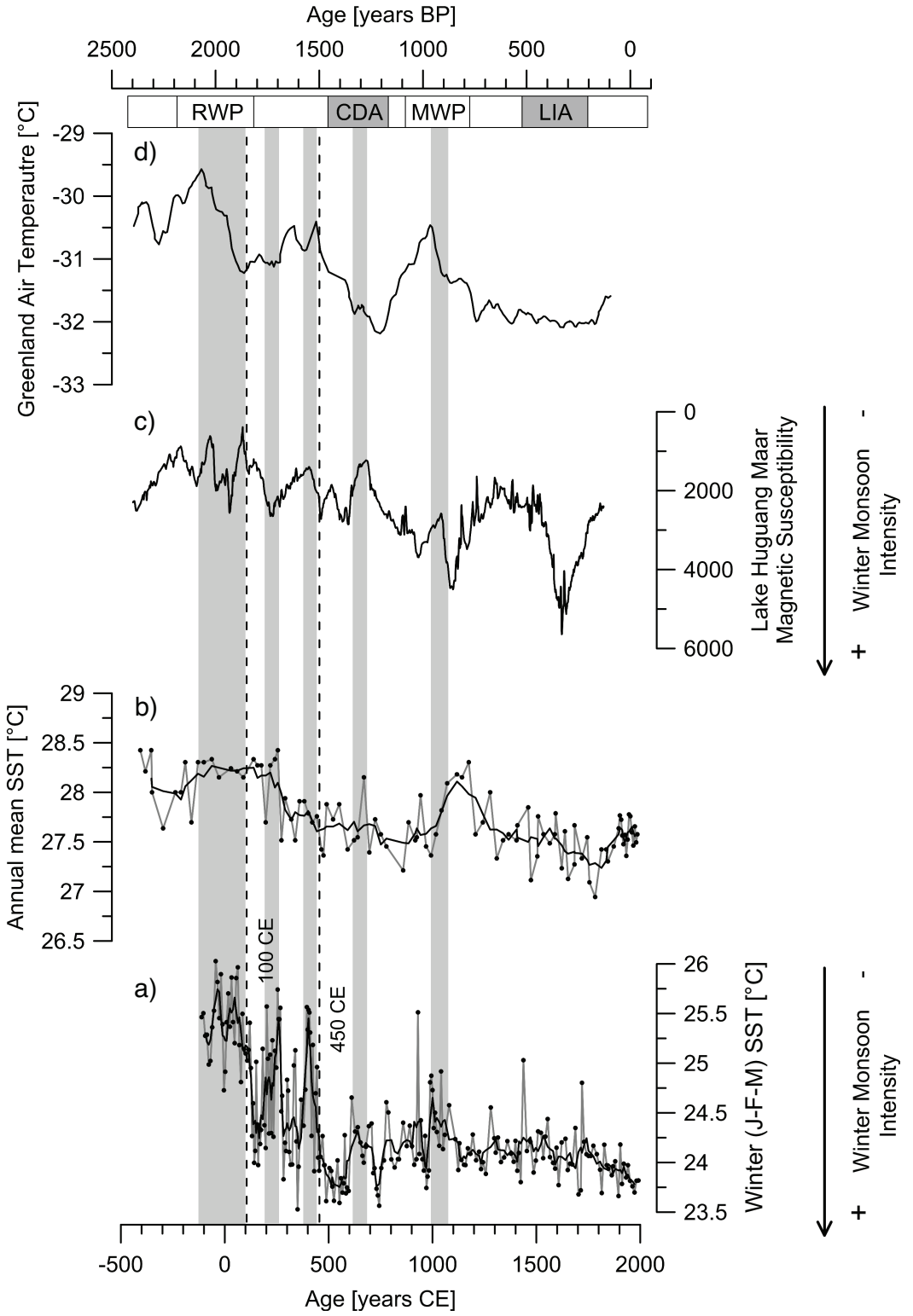

Figure III.11: Reconstructed winter sea surface temperatures from cores 39KG/275KL during the last ~2000 years as the consensus from all transfer function methods (black line as 3-pt running mean) and alkenone-derived annual mean temperatures co-registered in the same sediment core (Böll et al., 2014). Magnetic susceptibility of Lake Huguang Maar (Yancheva et al., 2007) indicates East Asian winter monsoon intensity. Northern Hemisphere climate epochs are derived from Greenland air temperatures (Alley, 2000). Conspicuous temperature changes occurred around 100 CE and 450 CE (stippled). Intervals of diminished winter monsoon intensity are grey shaded.

also not indicate that winter conditions were substantially stronger at ~1800 CE, as it is evident from alkenone-derived AM-SST on the Pakistan Margin (Böll et al., 2014; Doose-Rolinski et al., 2001), a feature that was suggested to be linked to the Little Ice Age (LIA). Apparently, the colder LIA climate only affected the inter-monsoon- or summer temperatures in the northeastern Arabian Sea, without enhancing winter monsoon intensity. Furthermore, the observed difference of both climate series might, apart from a potentially different control mechanism on the respective proxies, also be owed to the different sampling scheme of both records. Alkenone-derived AM-SST and foraminiferal-based wSST are co-registered in the same sediment core, but the record of AM-SST uses a continuous 25-year resolution, whereas the record of wSST is based on a continuous 9-year resolution. This especially explains the observed amplitudinal difference of both SST time series, as the lower sampling resolution integrates almost three samples of the higher resolution record. However, resampling of both records to the lower sampling resolution following AM-SST by linear interpolation reveals a positive correlation ($r = 0.60$, $p = 4.44\text{E} - 09$), indicating that winter temperatures must have a strong control on AM-SST.

One yet unresolved question about the regional monsoon systems exists as to how the Indian and East Asian monsoon systems are related on decadal- to centennial timescales during the late Holocene (e.g., Wang et al., 2014; Wang et al., 2005a). The Indian and East Asian monsoon systems react to different forcing mechanisms and are thus expected to reveal dissimilar variability of their proxy records (Wang et al., 2003). Due to the scarcity of high-resolution winter monsoon records, the relationship of both winter monsoon systems remains unclear. Although the temperature range of the wSST record of this study after 450 CE is mostly within the reconstruction uncertainty of ~1°C, persistent cold spells around 450–600 CE and 750 CE, as well as warmer intervals between 600–700 CE, around 950 CE, 1300 CE and 1450 CE, are consistent with the Lake Huguang Maar magnetic susceptibility record of East Asian winter monsoon intensity (Figure III.11). This relationship is further investigated by wavelet coherence analysis (Figure III.12), that measures the coherency of two cross wavelet transforms in time frequency space (Grindsted et al., 2004), using the MATLAB package available on the website of the National Oceanography Centre (http://noc.ac.uk/using-science/crosswavelet-wavelet-coherence). A broad significant interval with the same phase angle shows a strong coherency between 100 BCE and 1000 CE at a period of 300–400 years.

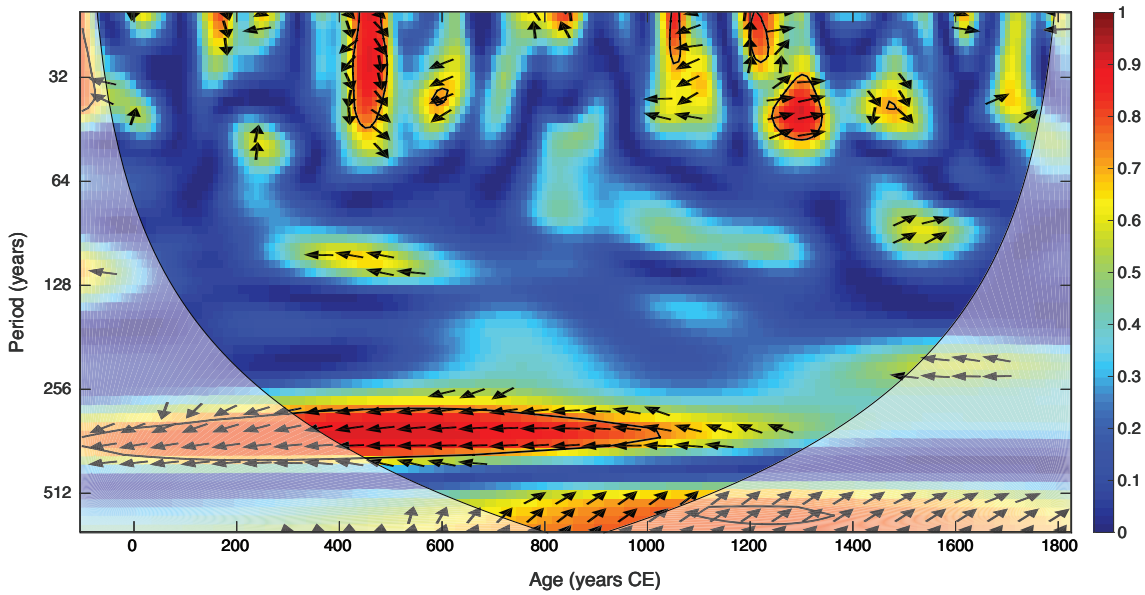

Figure III.12: Wavelet coherency between the wSST record and magnetic susceptibility of the Lake Huguang Maar record (Yancheva et al., 2007) indicates areas in the time-frequency space where both time series co-vary. Thick black contour shows the 5% significance level against red noise. The phase shift between the components of both time series is indicated within the significant areas by arrows (pointing right=in-phase, pointing left=anti-phase, up=wSST leading Lake Huguang Maar by 90 °, down=Lake Huguang Maar leading wSST by 90 °). Note that anti-phase behavior of both proxies means in-phase response to monsoon intensity, as increasing intensity is relative to opposite scaling. The cone of influence where edge artifacts might be introduced is indicated as white shading.

Further significant coherency on shorter wavelengths around 30–50 years occurs in disconnected intervals and shows either in-phase (around 1300 CE) or phase-shifted (around 500 CE) relationships between the two records. Periodicities on these frequency bands are also evident from the MTM power spectrum of wSST variability (Figure III.10). This implies that a persistent centennial-scale relationship between the variation of the Indian winter monsoon and the East Asian winter monsoon existed until 1000 CE.

Our data indicate that the Indian winter monsoon intensity shifted rapidly during the last two millennia. The shift from persistent weak to highly variable winter conditions at 100 CE is concomitant with the end of the Northern Hemisphere Roman Warm Period (RWP). This is followed by strongest winter conditions at ~500–600 CE, concomitant with the onset of the Cold Dark Ages (CDA) and Bond event 1 in the North Atlantic (Bond et al., 2001). Several studies of late Holocene monsoon activity indicate changing conditions around that time. A persistent link

between warmer North Atlantic climate and weaker winter monsoon on centennial timescales during the late Holocene was also suggested by Böll et al., (2014). Lückge et al., (2001) proposed the "transition phase" of highly fluctuating wSST after 100 CE to be an interval of summer-monsoon domination while the winter monsoon was diminished. Stalagmite records from Qunf cave in southern Oman show a prominent hiatus until ~550 CE, which potentially indicates very low summer monsoon precipitation (Fleitmann and Matter, 2009; Fleitmann et al., 2007). Very low summer monsoon-induced upwelling off the Oman coast at ~550 CE is also evidenced by Gupta et al., (2003) and Anderson et al., (2010). This finding may suggest that strongest winter monsoon conditions were contemporaneous with phases of weakened summer monsoon, indicating an anti-phase relationship between summer and winter monsoon intensity.

Slightly weakened winter monsoon intensities at 950 CE might be related to the Medieval Warm Period (MWP) of the Northern Hemisphere. A gradual weakening of the winter monsoon towards 950 CE is compatible to a broad increase of Oman upwelling intensity at 750–1350 CE (Gupta et al., 2003), whereas the picture is less clear for the cave records (e.g., Fleitmann and Matter, 2009; Wang et al., 2005b). If an anti-phase relationship persisted during the late Holocene until present, we would also expect to see the same major change for the last 400 years as implied by Anderson et al., (2002). But during that period wSST are very stable, indicating even a very recent strengthening of winter conditions from 1800 CE onwards. Changing conditions during the last 400 years are, however, also not evident from the records of Böll et al., (2014) and Yancheva et al., (2007), suggesting that an inverse relationship between Indian summer- and winter monsoon is not persistent to the present.

Conclusions

We analyzed planktic foraminiferal species compositions from an optimized dataset, adjusted to the reconstruction of the decadal-scale variability of fossil assemblages from the northeastern Arabian Sea. Redundancy analysis revealed that winter sea surface temperature has the strongest effect on the explanation of the modern planktic foraminiferal species variation. Winter monsoon induced hydrographic conditions are revealed by a strong negative relationship between temperature and chlorophyll-based productivity estimates. The updated Carbon-based Productivity Model (uCbPM) is a useful representation of the nutrient

conditions during winter deep mixing.

Reconstruction outcomes for the last two millennia show a consistent pattern among the techniques, indicating that ecological changes of the fossil assemblages are primarily caused by the reconstructed variable. The most obvious feature from the record of reconstructed winter monsoon intensity is a sudden change from warm temperatures around 25 °C prior to 450 CE towards temperatures below 24 °C thereafter. This shift is contemporaneous with the end of the Roman Warm Period on the Northern Hemisphere and mainly associated with a shift in the faunal assemblage caused by the occurrence of *G. sacculifer* and *G. siphonifera*.

Our record can be divided into three main phases:

1. Prior to 100 CE, warm and stable temperatures above 25 °C were found, representing diminished winter monsoon conditions.
2. From 100 to 450 CE, highly variable temperatures indicate a transition phase.
3. After 450 CE, winter temperatures are constantly lower. Highest temperatures during this interval occurred around 950 CE concomitant with the Medieval Warm Period.

These phases can be paralleled to changes in records of late Holocene summer monsoon intensity. Frequency analysis revealed that winter monsoon intensity was modulated on decadal-scale periodicities that are known from proxy records of Indian summer monsoon and interpreted to be solar irradiance forcing. An inverse relationship of winter and summer monsoon intensity during the last two millennia is indicated by simultaneous prominent phase shifts, but is not persistent during the last 400 years.

Acknowledgements

The following institutions and colleagues have provided untreated core top material for foraminiferal analyses: BGR Hannover (U von Stackelberg, U von Rad, A Lückge), IOW Warnemünde (R Endler), Univ. Kharagpur (AK Gupta), NIO Goa (A Paropkari), Univ. Cambridge (T Kiefer), Univ. Hamburg (Ch Betzler), Univ. Mainz (F Sirocko), Univ. Tübingen (Ch Hemleben, P Heinz), Univ. Utrecht (JW Zachariasse). T Epp, D Mosandl and P Schwarz are thankfully acknowledged for lab assistance. We thank two anonymous reviewers for their constructive comments that helped to improve the manuscript. Funding was provided by the

German Ministry of Education and Research (BMBF) grant 03G0806C (CARIMA). The data will be available at www.pangaea.de.

References

Agnihotri, R., K. Dutta, R. Bhushan, et al. (2002): 'Evindence for solar forcing on the Indian monsoon during the last millennium'. *Earth and Planetary Science Letters*, vol. 198(3–4): pp. 521–527.

Aitchinson, J. (1999): 'Logratio and natural laws in compositional data analysis'. *Mathematical Geology*, vol. 31: pp. 563–580.

Aitchinson, J., C. Barcelo-Vidal, J. Martin-Fernandez, et al. (2000): 'Logratio analysis and compositional distance'. *Mathematical Geology*, vol. 32(3): pp. 271–275.

Alley, R. (2000): 'Ice-core evidence of abrupt climate changes'. *Proceedings of the National Academy of Sciences*, vol. 97: pp. 1331–1334.

Anderson, D., J. Overpeck, and A. Gupta (2002): 'Increase in the Asian southwest monsoon during the past four centuries'. *Science*, vol. 297: pp. 596–599.

Anderson, D., C. Baulcomb, A. Duvivier, et al. (2010): 'Indian summer monsoon during the last two millennia'. *Journal of Quaternary Science*, vol. 25: pp. 911–917.

André, A., A. Weiner, F. Quillévéré, et al. (2013): 'The cryptic and the apparent reversed: lack of genetic differentiation within the morphologically diverse plexus of the planktic foraminifer *Globigerinoides sacculifer*'. *Paleobiology*, vol. 39(1): pp. 21–39.

Auras-Schudnagies, A., D. Kroon, G. Ganssen, et al. (1989): 'Distributional pattern of planktonic foraminifers and pteropods in surface waters and top core sediments of the Red Sea, and adjacent areas controlled by the monsoonal regime and other ecological factors'. *Deep Sea Research*, vol. 36: pp. 1515–1533.

Banse, K. (1987): 'Seasonality of phytoplankton chlorophyll in the central and northern Arabian sea'. *Deep Sea Research Part A*, vol. 34: pp. 713–723.

Banse, K. and C. McClain (1986): 'Winter blooms of phytoplankton in the Arabian Sea as observed by the Coastal Zone Color Scanner'. *Marine Ecology - Progress Series*, vol. 34: pp. 201–211.

Barrows, T. and S. Juggins (2005): 'Sea-surface temperatures around the Australian margin and Indian Ocean during the Last Glacial Maximum'. *Quaternary Science Reviews*, vol. 24(7): pp. 1017–1047.

Bé, A. W. H. and W. H. Hutson (1977): 'Ecology of Planktonic Foraminifera and Biogeographic Patterns of Life and Fossil Assemblages in the Indian Ocean'. *Micropaleontology*, vol. 23(4): p. 369.

Bé, A. (1967): 'Foraminifera families: *Globigerinidae* and *Globorotalidae*'. *Fiches d´Identification du Zooplankton*. Ed. by Fraser, J. H. Vol. Sheet 108. Charlottenlund, Denmark: Conseil Perm. Internat. Explor. Mer: pp. 1–8.

Behrenfeld, M. and P. Falkowski (1997): 'Photosynthetic rates derived from satellite-based chlorophyll concentration'. Vol. 42: pp. 1–20.

Birks, H., J. Line, S. Juggins, et al. (1990): 'Diatoms and pH reconstruction'. *Philosophical Transactions of the Royal Society B*, vol. 327: pp. 263–278.

Böll, A., A. Lückge, P. Munz, et al. (2014): 'Late Holocene primary productivity and sea surface temperature variations in the northeastern Arabian Sea: implications for winter monsoon variability'. *Paleoceanography*, vol. 29: pp. 1–17.

Bond, G., B. Kromer, J. Beer, et al. (2001): 'Persistent Solar Influence on North Atlantic Climate During the Holocene'. *Science*, vol. 294: pp. 2130–2136.

Bräuning, A. and B. Mantwill (2004): 'Summer temperature and summer monsoon history on the Tibetan plateau during the last 400 years recorded by tree rings'. *Geophysical Research Letters*, vol. 31: p. L24205.

Burns, S., D. Fleitmann, M. Mudelsee, et al. (2002): 'A 780-year annually resolved record of Indian Ocean monsoon precipitation from a speleothem from south Oman'. *Journal of Geophysical Research-Atmospheres*, vol. 107(D20): p. 4434.

Cayre, O., L. Beaufort, and E. Vincent (1999): 'Paleoproductivity in the equatorial Indian Ocean for the last 260, 000 yr: A transfer function based on planktonic foraminifera'. *Quaternary Science Reviews*, vol. 18: pp. 839–857.

Colborn, J. (1975): 'The Thermal Structure of the Indian Ocean'. *International Indian Ocean Expedition oceanographic monographs 2*. Honolulu, Hawaii: University of Hawaii Press: p. 173.

Conkright, M., R. Locarnini, H. Garcia, et al. (2002): *World Ocean Atlas 2001: Objective analyses, data statistics, and figures. CD-ROM Documentation*. Silver Spring, MD.: National Oceanographic Data Center.

Cook, E., P. Krusic, K. Anchukaitis, et al. (2013): 'Tree-ring reconstructed summer temperature anomalies for temperate East Asia since 800 C.E.' *Climate Dynamics*, vol. 41: pp. 2957–2972.

Currie, R., A. Fisher, and P. Hargraves (1973): 'Arabian Sea upwelling'. *The Biology of the Indian Ocean*. Ed. by B, Z. and G. SA. Berlin: Springer-Verlag: pp. 37–52.

Curry, W., D. Ostermann, M. Guptha, et al. (1992): 'Foraminiferal production and monsoonal upwelling in the Arabian Sea: evidence from sediment traps'. *Upwelling Systems: Evolution Since the Early Miocene*. Ed. by Summerhayes CP, P. W. and K. Emeis. Vol. 64. London: Geological Society Special Publication: pp. 93–106.

Dixon, P. (2003): 'VEGAN, a package of R functions for community ecology'. *Journal of Vegetation Science*, vol. 14: pp. 927–930.

Doose-Rolinski, H., U. Rogalla, G. Scheeder, et al. (2001): '(2001) High-resolution temperature and evaporation changes during the late Holocene in the northeastern Arabian Sea'. *Paleoceanography*, vol. 16: pp. 358–367.

Feldman, G. and C. McClain (2013): 'Ocean Color Web, SeaWiFS, AquaMODIS-/Chlorophyll a concentration, 09/1997-06/2013'. *NASA Goddard Space Flight Center*. Ed. by Kuring, N., S. Bailey, B. Franz, G. Meister, P. Werdell, and R. Eplee. http://oceancolor.gsfs.nasa.gov/.

Fleitmann, D. and A. Matter (2009): 'The speleothem record of climate variability in Southern Arabia'. *Comptes Rendus Geoscience*, vol. 341: pp. 633–642.

Fleitmann, D., S. Burns, M. Mudelsee, et al. (2003): 'Holocene forcing of the Indian monsoon recorded in a stalagmite from southern Oman'. *Science*, vol. 300: pp. 1737–1739.

Fleitmann, D., S. Burns, A. Mangini, et al. (2007): 'Holocene ITCZ and Indian monsoon dynamics recorded in stalagmites from Oman and Yemen (Socotra)'. *Quaternary Science Reviews*, vol. 26: pp. 170–188.

Fraile, I., M. Schulz, S. Mulitza, et al. (2008): 'Predicting the global distribution of planktonic foraminifera using a dynamic ecosystem model'. *Biogeosciences*, vol. 5: pp. 891–911.

Ghil, M., R. Allen, M. Dettinger, et al. (2002): 'Advanced spectral methods for climatic time series'. *Reviews of Geophysics*, vol. 40: pp. 1–41.

Grindsted, A., J. Moore, and S. Jevrejeva (2004): 'Application of the cross wavelet transform and wavelet coherence to geophysical time series'. *Nonlinear Processes in Geophysics*, vol. 11: pp. 561–566.

Gupta, A., D. Anderson, and J. Overpeck (2003): 'Abrupt changes in the Asian southwest monsoon during the Holocene and their links to the North Atlantic Ocean'. *Nature*, vol. 421: pp. 354–357.

Gupta, A., M. Das, and D. Anderson (2005): 'Solar influence on the Indian summer monsoon during the Holocene'. *Geophysical Research Letters*, vol. 32: p. L17703.

Hemleben, C., M. Spindler, and R. Anderson (1989): *Modern Planktonic Foraminifera*. New York: Springer-Verlag: p. 363.

Horn, J. (1965): 'A rationale and test for the number of factors in factor analysis'. *Psychometrika*, vol. 30: pp. 179–185.

Hutson, W. and W. Prell (1980): 'A paleoecological transfer function, FI-2, for Indian Ocean planktonic foraminifera'. *Journal of Paleontology*, vol. 54: pp. 381–399.

Imbrie, J. and N. Kipp (1971): 'A new micropaleontological method for quantitative paleoclimatology: application to a late Pleistocene Caribbean core'. *Late Cenozoic Glacial Ages*. Ed. by Turekian, K. New Haven: Yale University Press.

Ittekkot, V., B. Haake, M. Bartsch, R. Nair, and V. Ramaswamy (1992): 'Organic carbon removal in the sea: the continental connection'. *Upwelling systems: Evolution since the Early Miocene*. Ed. by Summerhayes, C., W. Prell, and K. Emeis. Vol. 64. Geological Society Special Publication: pp. 167–176.

Joliffe, T. (2002): *Principal Component Analysis*. New York: Springer.

Jones, P. and M. Mann (2004): 'Climate over the past millennia'. *Reviews of Geophysics*, vol. 42(2): RG2002.

Juggins, S. (2015): *rioja: Analysis of Quaternary Science Data*. R package version (0.8-7).

Juggins, S. and H. Birks (2012): 'Quantitative environmental reconstructions from biological data'. *Tracking environmental change using lake sediments*. Ed. by Birks, H. J. B., A. F. Lotter, S. Juggins, and J. P. Smol. Developments in Paleoenvironmental Research 5. Springer Netherlands.

Kemp, A. (1996): *Paleoclimatology and Paleoceanography from Laminated Sediments*. Vol. 116. Geological Society, London, Special Publication: p. 258.

Kim, J.-W., S.-W. Yeh, and E.-C. Chang (2014): 'Combined effect of El Niño-Southern Oscillation and Pacific Decadal Oscillation on the East Asian winter monsoon'. *Climate Dynamics*, vol. 42: pp. 957–971.

Krishnamurthy, L. and V. Krishnamurthy (2014): 'Influence of PDO on South Asian summer monsoon and monsoon–ENSO relation'. *Climate Dynamics*, vol. 42: pp. 2397–2410.

Kucera, M., A. Rosell-Melé, R. Schneider, et al. (2005a): 'Multiproxy approach for the reconstruction of the glacial ocean surface (MARGO)'. *Quaternary Science Reviews*, vol. 24(7–9): pp. 813–819.

Kucera, M., M. Weinelt, T. Kiefer, et al. (2005b): 'Reconstruction of sea-surface temperatures from assemblages of planktonic foraminifera: multi-technique approach based on geographically constrained calibration data sets and its application to glacial Atlantic and Pacific Oceans'. *Quaternary Science Reviews*, vol. 24(7–9): pp. 951–998.

Kumar, K., B. Rajagopalan, M. Hoerling, et al. (2006): 'Unraveling the Mystery of Indian Monsoon Failure During El Niño'. *Science*, vol. 314: pp. 115–119.

Lal, D. (1994): *Biogeochemistry of the Arabian Sea*. Vol. 103. 2. Bangalore: Proceedings, Indian Academy of Sciences: p. 253.

Laskar, A., M. Yadava, R. Ramesh, et al. (2013): 'A 4 kyr stalagmite oxygen isotopic record of the past Indian Summer Monsoon in the Andaman Islands'. *Geochemistry, Geophysics, Geosystems*, vol. 14: pp. 3555–3566.

Lückge, A., H. Doose-Rolinski, A. Khan, et al. (2001): 'Monsoonal variability in the northeastern Arabian Sea during the past 5000 years: geochemical evidence from laminated sediments'. *Palaeogeography, Palaeoclimatology, Palaeoecology*, vol. 167: pp. 273–286.

Lückge, A., L. Reinhardt, H. Andruleit, et al. (2002): 'Formation of varve-like laminae off Pakistan: decoding 5 years of sedimentation'. *The Tectonic and Climatic Evolution of the Arabian Sea Region*. Ed. by Clift, P. D., D. Kroon, C. Gaedicke, and J. Craig. Vol. 195. London: Geological Society Special Publications: pp. 421–431.

Madhupratap, M., S. Prasanna Kumar, P. Bhattathiri, et al. (1996): 'Mechanism of the biological response to winter cooling in the northeastern Arabian Sea'. *Nature*, vol. 384: pp. 549–552.

Malmgren, B. and U. Nordlund (1997): 'Application of artificial neural networks to paleoceanographic data'. *Palaeogeography, Palaeoclimatology, Palaeoecology*, vol. 136: pp. 359–373.

Mantua, N. and S. Hare (2002): 'The Pacific decadal oscillation'. *Journal of Oceanography*, vol. 58: pp. 35–44.

Mantua, N., S. Hare, Y. Zhang, et al. (1997): 'A Pacific interdecadal climate oscillation with impacts on salmon production'. *Bulletin of the American Meteorological Society*, vol. 78: pp. 1069–1079.

Morey, A., A. Mix, and N. Pisias (2005): 'Planktonic foraminiferal assemblages preserved in surface sediments correspond to multiple environmental variables'. Vol. 24: pp. 925–950.

Murty, V., Y. Sarma, D. Rao, et al. (1992): 'Water characteristics, mixing and circulation in the Bay of Bengal during southwest monsoon'. *Journal of Marine Research*, vol. 50: pp. 207–228.

Naidu, P. and B. Malmgren (1996): 'A high-resolution record of late Quaternary upwelling along the Oman Margin, Arabian Sea based on planktonic foraminifera'. *Paleoceanography*, vol. 11: pp. 129–140.

Neff, U., S. Burns, A. Mangini, et al. (2001): 'Strong coherence between solar variability and the monsoon in Oman between 9 and 6 kyr ago'. *Nature*, vol. 411: pp. 290–293.

Oregon State University (2014): *Ocean Productivity Site*. http://www.science.oregonstate.edu/ocea

PAGES 2k Consortium (2013): 'Continental-scale temperature variability during the past two millennia'. *Nature Geoscience*, vol. 6: pp. 339–346.

Peeters, F. and G.-J. Brummer (2002): 'The seasonal and vertical distribution of living planktic foraminifera in the NW Arabian Sea'. *The tectonic and climatic evolution of the Arabian Sea Region*. Vol. 195. London: Geological Society Special Publications: pp. 463–498.

Prasanna Kumar, S., N. Ramaiah, M. Gauns, et al. (2001): 'Physical forcing of biological productivity in the Northern Arabian Sea during the Northeast Monsoon'. *Deep Sea Research Part II: Topical Studies in Oceanography*, vol. 48: pp. 1115–1126.

R Core Team (2014): *R: A language and environment for statistical computing*. R Foundation for Statistical Computing. Vienna, Austria: http://www.R-project.org.

Ranasinghe, P., J. Ortiz, A. Smith, et al. (2013): 'Mid- to late- Holocene Indian winter monsoon variability from a terrestrial record in eastern and southeastern coastal environments of Sri Lanka'. *The Holocene*, vol. 23(7): pp. 945–960.

Schiebel, R., A. Zeltner, U. Treppke, et al. (2004): 'Distribution of diatoms, coccolithophores and planktic foraminifers along a trophic gradient during SW monsoon in the Arabian Sea'. *Marine Micropaleontology*, vol. 51: pp. 345–371.

Schlitzer, R. (2014): *Ocean Data View*. http://odv.awi.de.

Schulz, H. and U. von Rad (2014): 'Vertical and lateral flux on the continental slope off Pakistan: correlation of sediment core and trap results'. *Biogeosciences*, vol. 11: pp. 3107–3120.

Schulz, H., U. von Rad, and V. Ittekkot (2002): 'Planktic foraminifera, particle flux and oceanic productivity off Pakistan, NE Arabian Sea: modern analogues and application to the paleoclimatic record'. *The Tectonic and Climatic Evolution of the*

Arabian Sea Region. Ed. by Clift, P., D. Kroon, C. Gaedicke, and J. Craig. Vol. 195. London: Geological Society Special Publications: pp. 499–516.

Schulz, H., U. von Rad, and U. von Stackelberg (1996): 'Laminated sediments from the oxygen-minimum zone of the northeastern Arabian Sea'. *Paleoclimatology and Paleoceanography from Laminated Sediments*. Ed. by Kemp, A. Vol. 116. London: Geological Society Special Publications: pp. 185–207.

Shetye, S., A. Gouveia, and S. Shenoi (1994): 'Circulation and water masses of the Arabian Sea'. *Biogeochemistry of the Arabian Sea*. Ed. by Lal, D. Vol. 103. 2. Proceedings, Indian Academy of Sciences: pp. 9–25.

Siccha, M., G. Trommer, H. Schulz, et al. (2009): 'Factors controlling the distribution of planktonic foraminifera in the Red Sea and implications for the development of transfer functions'. *Marine Micropaleontology*, vol. 72: pp. 146–156.

Smith, S., M. Roman, I. Prusova, et al. (1998): 'Seasonal response of zooplankton to monsoonal reversals in the Arabian Sea'. *Deep Sea Research Part II*, vol. 45: pp. 2369–2403.

Sontakke, N., G. Pant, and N. Singh (1993): 'Construction of all-India summer monsoon rainfall series for the period 1844–1991'. *Journal of Climate*, vol. 6: pp. 1807–1811.

Telford, R. and H. Birks (2005): 'The secret assumption of transfer functions: problems with spatial autocorrelation in evaluating model performance'. *Quaternary Science Reviews*, vol. 24: pp. 2173–2179.

Telford, R., C. Li, and M. Kucera (2013): 'Mismatch between the depth habitat of planktonic foraminifera and the calibration depth of SST transfer functions may bias reconstructions'. *Climate of the Past*, vol. 9: pp. 859–870.

Telford, R., C. Andersson, H. Birks, et al. (2004): 'Biases in the estimation of transfer function prediction errors'. *Paleoceanography*, vol. 19: PA4014.

ter Braak, C. and S. Juggins (1993): 'Weighted averaging partial least squares regression (WA-PLS): an improved method for reconstructing environmental variables from species assemblages'. *Hydrobiologia*, vol. 269/270: pp. 485–502.

von Rad, U., H. Doose, and cruise participants (1998): *SONNE Cruise SO 130 Cruise Report MAKRAN II*. Hannover: Bundesanstalt für Geowissenschaften und Rohstoffe.

von Rad, U., H. Schulz, and SONNE 90 Scientific Party (1995): 'Sampling the oxygen minimum zone off Pakistan: glacial-interglacial variations of anoxia and productivity (preliminary results SONNE 90 cruise)'. *Marine Geology*, vol. 125: pp. 7–19.

von Rad, U., M. Schaaf, K. Michels, et al. (1999): 'A 5000-yr Record of Climate Change in Varved Sediments from the Oxygen Minimum Zone off Pakistan, Northeastern Arabian Sea'. *Quaternary Research*, vol. 51: pp. 39–53.

Wang, B., S. Clemens, and P. Liu (2003): 'Contrasting the Indian and East Asian monsoons: implications on geologic timescales'. *Marine Geology*, vol. 201: pp. 5–21.

Wang, P., B. Wang, H. Cheng, et al. (2014): 'The global monsoon across timescales: coherent variability of regional monsoons'. *Climate of the Past*, vol. 10: pp. 2007–2052.

Wang, P., S. Clemens, L. Beaufort, et al. (2005a): 'Evolution and variability of the Asian monsoon system: state of the art and outstanding issues'. *Quaternary Science Reviews*, vol. 24(5–6): pp. 595–629.

Wang, Y., H. Cheng, R. Edwards, et al. (2005b): 'The Holocene Asian monsoon: links to solar changes and North Atlantic climate'. *Science*, vol. 308: pp. 854–857.

Webster, P., V. Magaña, T. Palmer, et al. (1998): 'Monsoons: Processes, predictability, and the prospects for prediction'. *Journal of Geophysical Research: Oceans*, vol. 103(C7): pp. 14451–14510.

Weiner, A., M. Weinkauf, A. Kurasawa, et al. (2015): 'Genetic and morphometric evidence for parallel evolution of the *Globigerinella calida* morphotypes'. *Marine Micropaleontology*, vol. 114: pp. 19–35.

Wyrtki, K. (1971): *Oceanographic Atlas of the International Indian Ocean Expedition*. Washington: National Science Foundation.

Wyrtki, K. (1973): 'Physical oceanography of the Indian Ocean'. *The Biology of the Indian Ocean*. Ed. by Zeitschel, B. and S. Gerlach. New York: Springer.

Xu, H., Y. Hong, and B. Hong (2012): 'Decreasing Asian summer monsoon intensity after 1860 AD in the global warming epoch'. *Climate Dynamics*, vol. 39: pp. 2079–2088.

Yancheva, G., N. Nowaczyk, J. Mingram, et al. (2007): 'Influence of the intertropical convergence zone on the East Asian monsoon'. Vol. 445: pp. 74–77.

Zeitschel, B. and S. Gerlach (1973): *The Biology of the Indian Ocean*. Berlin: Springer-Verlag: p. 549.

Zhou, W., X. Wang, T. Zhou, et al. (2007): 'Interdecadal variability of the relationship between the East Asian winter monsoon and ENSO'. *Meteorology and Atmospheric Physics*, vol. 98(3–4): pp. 283–293.

Variability of the Indian summer monsoon during early- to mid Holocene and its relation to bottom-water conditions at the northern Oman margin

In preparation

Philipp M. Munz[1], Stephan Steinke[2, 5], Anna Böll[3], Andreas Lückge[4], Jeroen Groeneveld[5], Michal Kucera[5] and Hartmut Schulz[1]

[1]*Department of Geosciences, University of Tübingen, Germany;*
[2]*Department of Geological Oceanography, Xiamen University, China;*
[3]*Institute of Geology, University of Hamburg, Germany;*
[4]*Bundesanstalt für Geowissenschaften und Rohstoffe (BGR), Germany;*
[5]*MARUM – Center for Marine Environmental Sciences, Germany;*

Abstract

The Indian summer monsoon (ISM) brings most of the annual precipitation to the densely populated region in southern Asia. It is therefore vital to assess the variability of the monsoon system on societal relevant decadal- to centennial time scales, which might help to better understand how potential driving forces might be controlling it. Here we present a study of a sediment core from the northern Oman margin, revealing early- to mid Holocene ISM conditions on a near 20-year resolution. We assess multiple independent proxies indicative of sea surface temperatures (SST) during the upwelling season together with bottom water conditions during the early- to mid Holocene epoch. We use geochemical parameters, transfer functions of planktic foraminiferal assemblages and Mg/Ca paleothermometry and find evidence corroborating previous studies that upwelling intensity varies significantly in coherence to solar sunspot cycles. The dominant ~80–90-year Gleissberg cycle was apparently also affecting bottom water oxygen conditions. Although the interval from 8.4 to 5.8 ka B.P. is relatively short, the gradually decreasing trend of summer monsoon conditions was interrupted by short events of intensified ISM conditions. Results from both independent SST proxies are linked to phases of weaker OMZ conditions and enhanced carbonate preservation. This indicates that surface water properties were the main driver for bottom water conditions and state of the OMZ on decadal time scales.

Introduction

The Indian summer monsoon (ISM) is the dominant driver for intraseasonal changes of wind directions and precipitation patterns in one of the world's most densely populated regions. To precisely determine possible changes under climatic conditions in response to anthropogenic impact, it is vital to understand how ISM variability is modulated on societal relevant decadal- to centennial time scales. In comparison to modern times, the early- to mid Holocene is marked by different orbital configurations, affecting Northern Hemisphere insolation (Berger, 1978a) and monsoon circulations (Kutzbach and Street-Perrott, 1985). This period was marked by a steep decline of solar insolation changes whilst climatic conditions were largely unaffected by human induced greenhouse gas emissions. Furthermore, climatic conditions during the early- to mid-Holocene have been attributed to cultural and societal turnover in Africa (Kuper and Kröpelin, 2006)

and Mesopotamia (Kennett and Kennett, 2007).

Monsoonal winds develop when summer (July to September) heating over the continent forms a low-pressure zone over continental Asia, which then interacts with the high-pressure zone over the southern Indian Ocean and drives strong, moisture-laden southwesterly winds. Along the eastern coast off Somalia and Oman, the alongshore winds induce coastal upwelling of cold and nutrient-rich deeper water layers, which cool surface water temperatures and fuel biological productivity within the euphotic zone (Findlater, 1969; Wyrtki, 1973). Below the photic zone, remineralisation of sinking organic matter consumes oxygen, which leads in combination with the lateral supply of low-oxygenated intermediate water masses (You and Tomczak, 1993), to the formation of a pronounced mid-depth oxygen minimum zone (OMZ). Upwelling and OMZ intensity, together with the biological uptake/release of carbon dioxide (CO_2), nitrous oxide (N_2O) and other greenhouse gases from/into the atmosphere (Farías et al., 2009; Paulmier et al., 2011; Ward et al., 2009), play a critical role for the global climate system.

Quantitative reconstructions of upwelling intensity have the advantage of being directly related to wind strength and thus ISM intensity (Murtugudde et al., 2007). Numerous studies attempted to quantitatively reconstruct sea surface temperatures (SST) in the northwestern Arabian Sea to study changes in upwelling intensity and thus ISM intensity (Anand et al., 2008; Clemens et al., 1991; Dahl and Oppo, 2006; Emeis et al., 1995; Godad et al., 2011; Huguet et al., 2006; Naidu and Malmgren, 1996). Accordingly, ISM variations are modulated by Northern Hemisphere summer insolation changes controlled by orbital parameters of the earths' precessional cycle. However, previous reconstructions did not resolve SST variations on societal relevant decadal- to centennial timescales. Here, we present a high-resolution study of early- to mid Holocene ISM variability based on a multi-proxy study comprising of SST fluctuations and OMZ intensity. Reconstructions are based on a comparison of Mg/Ca measurements of the upwelling-related species *Globigerina bulloides* and on transfer functions based on planktic foraminiferal (PF) census counts. To this end we first evaluate species response to potential ecological driving parameters and convert fossil assemblage counts of summer SST using a regionally validated transfer function (Munz et al., 2015). We test the ecological importance and statistical significance of the reconstructions and evaluate summer SST variability in comparison to other proxy records. We further assess the influence of surface parameters, upwelling

SST and primary productivity, on variations of OMZ intensity and deep-water carbonate preservation.

Modern oceanographic setting

Hydrographic conditions in the Arabian Sea today are dominated by the seasonal monsoon cycle. During boreal summer (June-September), strong southwestern monsoonal winds drive surface currents in the western Arabian Sea, the East Arabian Current as the northward extension of the Somali Current, promoting an overall anti-cyclonic circulation pattern (Shetye et al., 1994; Tomczak and Godfrey, 1994). The alongshore surface currents induce an offshore-directed deflection of surface waters and upwelling of deeper, cold and nutrient-rich subsurface waters through the process of Ekman-pumping. During boreal winter (December-March), weaker, dry and cold northeasterly winds (IWM; Indian Winter Monsoon) lead to increased surface water cooling and evaporation, especially in the northeastern part of the basin, where it enables deep convective mixing and a second productivity peak during winter (Madhupratap et al., 1996; Schulz et al., 2002).

Enhanced nutrient availability during summer upwelling nourishes primary productivity within the photic zone near the Somali- and Omani coast. This promotes OMZ conditions at intermediate water levels (~100–1000 m) (Figure IV.1). The water masses in the Arabian Sea are derived from several major sources. High evaporation leads to highly saline surface water, which is therefore often named Arabian Sea High Salinity Water — ASHSW (Prasanna Kumar and Prasad, 1999; Shetye et al., 1994). Thermocline waters are mainly sourced by an intermediate water mass (500–1500 m water depth) that originates in the central Indian Ocean (Indian Ocean Central Water, IOCW) as a mixture of Antarctic Intermediate Water (AAIW) and Indonesian Intermediate Water (IIW) (Emery and Meincke, 1986; You, 1998). Although these waters have a relatively low pre-formed oxygen saturation when they arrive in the Arabian Sea, the Subantarctic Mode and Antarctic Intermediate Waters (SAMW-AAIW) exert a strong influence on the OMZ of the Arabian Sea (Böning and Bard, 2009). Additionally, intermediate waters are sourced by the inflow of highly saline waters forming through excess evaporation over precipitation in the Persian Gulf and Red Sea. This leads to the formation of high salinity subsurface waters and subduction under less saline waters after entering the Arabian Sea. The Persian Gulf Water (PGW) shows a pronounced salinity

maximum at 200–400 m water depth, whereas the Red Sea Water (RSW) has an equilibrium depth of 500m at its maximum northward extent at ~18°N (Shetye et al., 1994). Although the PGW is a relatively young water mass and originates from a closer source region compared to the other intermediate water masses, the high-salinity tongue of modern PGW increases the oxygen concentration at mid-depth by less than 0.5 ml/l (Figure IV.1).

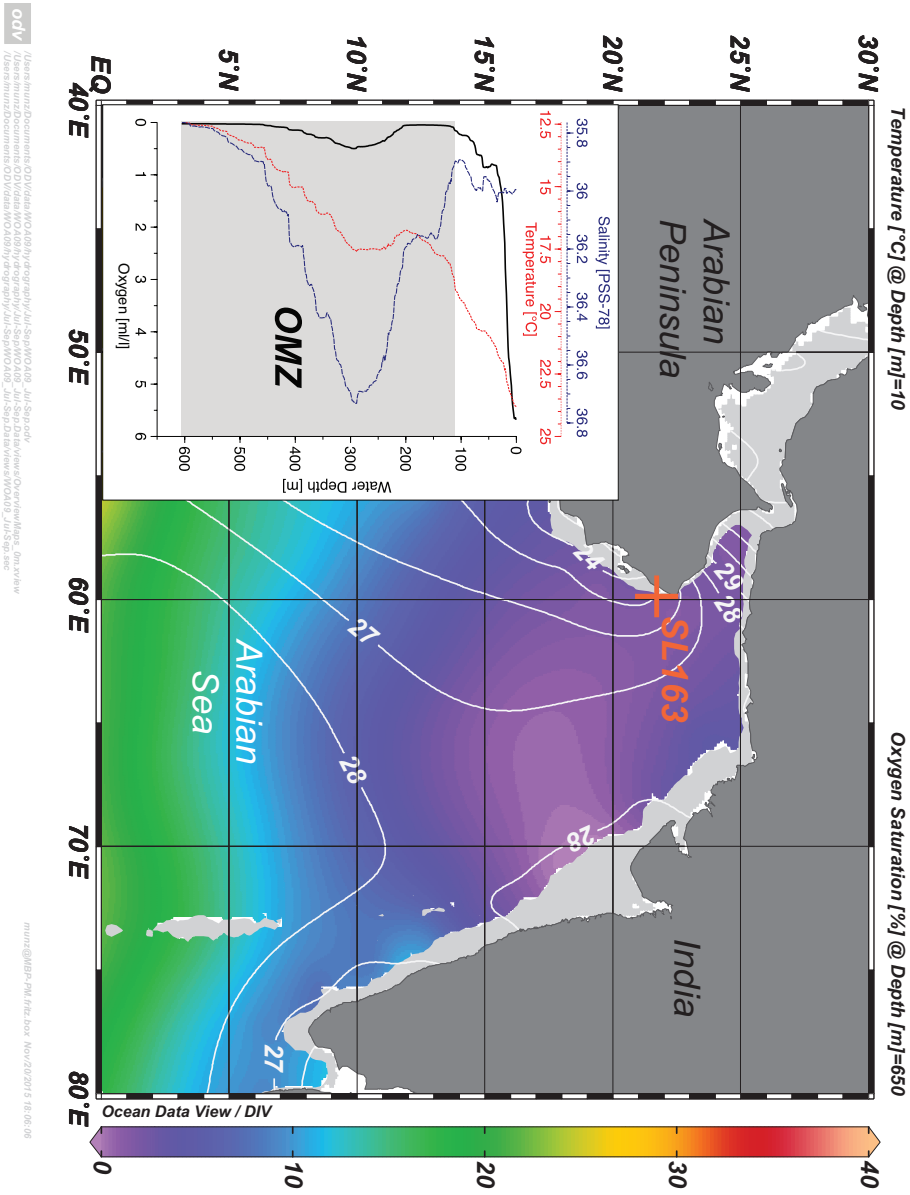

Figure IV.1: Map of the Arabian Sea, showing the location of core SL163 (red cross) at the northern Oman Margin (21°55.97'N; 059°48.15'E) in 650 m water depth. White contour lines refer to the summer (July to September) sea surface temperature (SST) in 10 m water depth. Color shading indicates oxygen saturation (%) in 650 m water depth, indicating a strong oxygen deficiency in the modern depth of the sampled sediment core. SST (Locarnini et al., 2010) and oxygen saturation data (Garcia et al., 2010) are from World Ocean Atlas 2009. Inset figure shows the depth profile of the CTD data measured during cruise M74/1b at the station of core SL163. Grey shading refers to the location of the modern oxygen minimum zone (OMZ). A subsurface salinity maximum in 200–400m water depth indicates the location of Persian Gulf Water (PGW).

Material and methods

Samples and chronology

During R/V METEOR cruise M74 on Leg 1b in September 2007 (Bohrmann et al., 2010), piston core SL163 recovered the uppermost 955 cm of the sedimentary sequence from 650 m water depth within the central part of the present-day OMZ (Figure IV.1) at the northern Oman Margin (21°55.97'N; 059°48.15'E). Multicorer MC681 recovered the undisturbed uppermost 53 cm of near-surface sediments at the same position. The sedimentary sequence from the intervals 1–56 cm of core SL163 and 1–53 cm of MC681 is considerably different from the topmost 1 cm and the deeper intervals of SL163. From smear-slide analysis and scanning electron microscopy the sediment can be described as faintly bioturbated, olive-brown organic-rich diatomaceous nannofossil silty clay. The uppermost 1 cm from both cores as well as the deposition below 56 cm of SL163 is described as olive foraminiferal nannofossil ooze. Core SL163 was sampled in continuous 1–2.5 cm intervals and for this study only samples from the foraminiferal nannofossil ooze between 56cm and 400 cm of SL163 and the core top (0–1 cm) of MC681 were investigated.

The age model of core SL163 and the core top sample of MC681 is based on fourteen AMS ^{14}C datings (Table IV.1), measured at Beta Analytics, Miami/USA and the Leibniz Laboratory in Kiel/Germany. Datings of core SL163 were mostly based on a monospecific analysis of handpicked individuals of *Neogloboquadrina dutertrei* (Table IV.1). This species is commonly known to thrive at thermocline depths (e.g., Fairbanks et al., 1982), but in the western Arabian Sea it shows a shallow habitat within the upper 35 m of the water column (Peeters and Brummer, 2002). For two samples (52.5 cm and 58.5 cm) with insufficient foraminiferal carbonate content, the bulk organic fraction was dated. To avoid a potential bias introduced by dating different organic compounds that might have been produced during different seasons or within different water masses, the core top sample of MC681 was sampled twice using mixed planktic foraminifera and bulk organic fraction. Both analyses yielded comparable results (Table IV.1), indicating a similar synthesis and general comparability of both dating methods.

Radiocarbon dates were calibrated to calendar years using the MARINE13 calibration curve (Reimer et al., 2013) within the program clam ver. 2.2 (Blaauw, 2010) for the statistical software environment *R* ver. 3.2.1 (R Core Team, 2015).

We assume a regional reservoir correction of $\Delta R = 231 \pm 31$ years, which is the weighted mean of the four closest (max. distance ~700 km) ΔR determination points from the 14CHRONO Database (http://calib.qub.ac.uk/marine/). Added to the global marine reservoir age of 400 years, this correction factor is consistent with the recent age of our undisturbed core top sample of MC681 (Table IV.1). An age-depth model was then built for SL163 using a smooth spline regression with a mixed effect model (10,000 iterations) within clam.

Planktic foraminiferal faunal analyses and transfer function approach

Samples were freeze-dried, washed with tap water over a 63 µm-screen, oven-dried at 40 °C and dry-sieved into the size fractions 150–250 µm, 250–315 µm and >315 µm. Planktic foraminifera (PF) were identified according to the taxonomic framework of Bé and Hutson, (1977a), Bé, (1967), and Hemleben et al., (1989). Following the procedure of Pflaumann et al., (1996), PF counts were conducted on a sub-split of each size fraction that contained a minimum of 100 PF individuals, yielding a summed fraction (>150µm) to contain >300 identified PF individuals. Relative species abundances were calculated on the summed fraction >150 µm after multiplying each size fraction with the respective split factor. To evaluate the secondary influence of calcite dissolution we calculated fragmentation indices following Le and Shackleton, (1992). The plankton to benthos ratio (%B, benthos) was calculated following Arrhenius, (1952) as a proxy for surface water productivity.

Quantitative reconstructions from PF faunal abundances were based on a modern calibration dataset of $n = 603$ surface samples spanning the Indian Ocean from 30 °S to 25 °N and 33 °E to 119 °E recently compiled by Munz et al., (2015). To enhance the signal-to-noise ratio, rare species <0.5% average abundance were removed from the calibration dataset prior to further analyses (Kucera et al., 2005), which resulted in the exclusion of 16 rare species out of 33 taxa. The dataset was then further subsampled to contain only samples most similar with the fossil assemblages of core SL163. This removes noisy effects introduced by modern samples covering ecological conditions outside the range of the fossil samples (Kucera et al., 2005). We followed the approach presented in Munz et al., (2015) and restricted the calibration dataset to samples that had the same range along the first and second axis of a joint principal component analysis (using square-root transformed species abundances to dampen the effect of a few dominant taxa) together with the fossil dataset (Figure IV.2). The resulting subsampled dataset

used for further analyses contained $n = 96$ modern surface samples.

Environmental gradient analysis was carried out on the 96 subsampled calibration samples using the package vegan ver 2.3-1 (Oksanen et al., 2015) for *R* . An initial detrended correspondence analysis (DCA) revealed a short gradient length (0.75 for the longest gradient on DCA axis 1), suggesting an ordination method based on linear species response (Birks, 1998). Redundancy analysis (RDA) was therefore chosen for the construction of an ordination model, to examine species response to several potential controlling environmental gradients. Because of the extreme seasonality of surface water productivity owed to the monsoonal circulation, four different approaches were used to assess modern productivity values. Net primary productivity estimates from the Vertically Generalized Production Model (VGPM), the Eppley-VGPM and the Carbon-based Productivity Model (CbPM) were accessed through the Ocean Productivity Home Page (http://www.science.oregonstate.edu/ocean.productivity/). Satellite-derived chlorophyll α measurements of SeaWiFS and Aqua MODIS sensors averaged over the period 1998–2010 were obtained from NASA Ocean Biology (http://oceancolor.gsfc.nasa.gov/cms/). Sea surface salinity (SSS) and sea surface temperature (SST) were extracted from the 10 m depth level of the World Ocean Atlas 1998 (Conkright et al., 1998).

Transfer function analysis and statistical significance tests of the reconstructions were performed with the *R* packages rioja ver 0.9-5 (Juggins, 2015) and palaeoSig ver. 1.1-3 (Telford, 2015). We used two common techniques for paleoenvironmental reconstructions, the Imbrie-and-Kipp method — IK (Imbrie and Kipp, 1971) and weighted averaging partial least squares regression — WA-PLS (ter Braak and Juggins, 1993) to reconstruct SST from the fossil samples. The number of factors to extract for IK was based on the Kaiser-Guttman criterion, the Parallel Analysis after Horn, (1965) and the analysis of optimal coordinates (reviewed by Courtney and Gordon, 2013). WA-PLS model complexity was evaluated from the model of lowest root mean squared error of prediction (RMSEP) using bootstrapping cross-validation ($n = 999$ cycles).

Mg/Ca analyses and paleothermometry of *G. bulloides*

For Mg/Ca analyses approximately 30 individuals of *G. bulloides* were picked from the size fraction 250–315µm, gently crushed between two glass plates under the microscope to open the chambers and cleaned following the protocol of

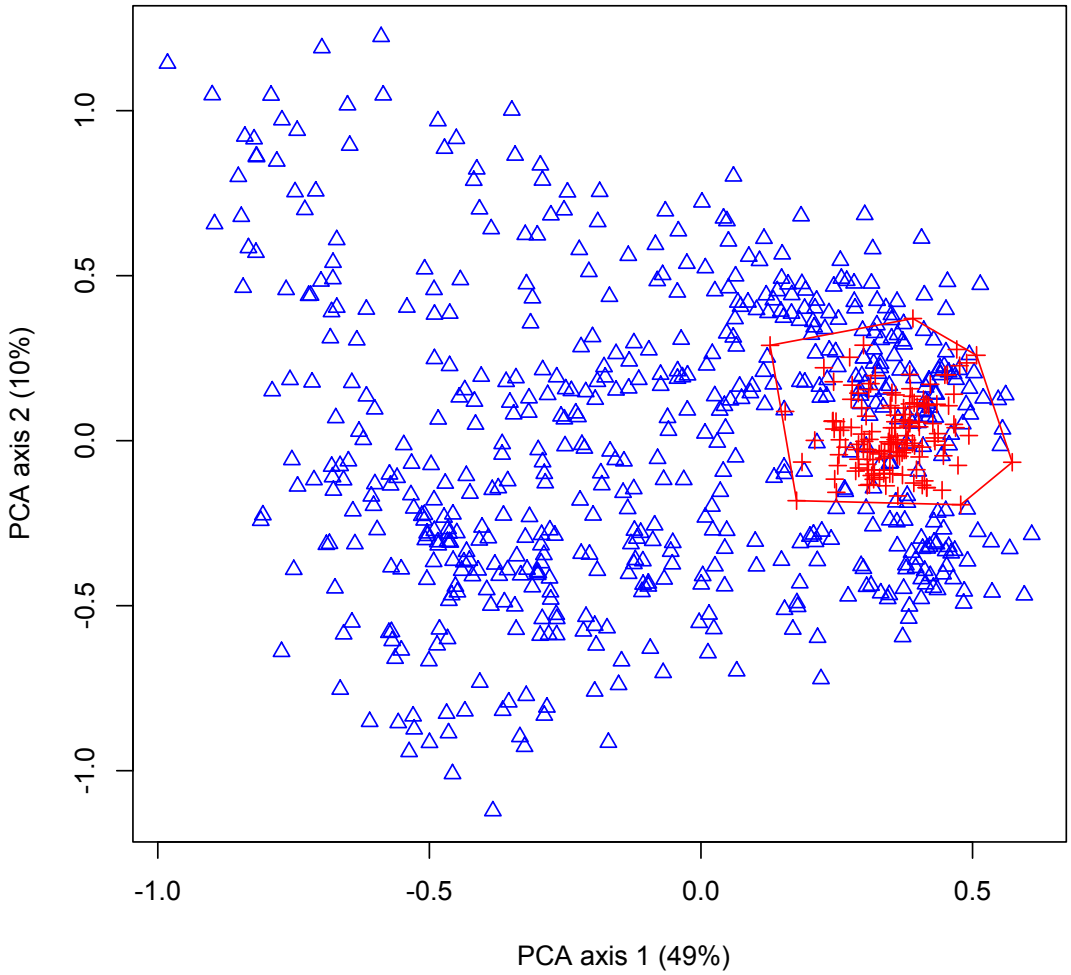

Figure IV.2: Scatterplot of the joint principal component analysis (PCA) of $n = 603$ modern calibration samples (blue triangles) and fossil downcore samples of SL163 (red crosses). The variance of the first and second PCA axis is indicated. $N = 96$ modern samples within the red polygon are most similar to the fossil samples along the first and second PCA axis, and were used for the calibration of transfer functions.

Barker et al., (2003). Trace elemental measurements were performed with an inductively coupled plasma optical emission spectrometer (ICP-OES) using an Agilent Technologies 700 Series with autosampler ASX-520 Cetac and micro-nebulizer at the MARUM-Center for Marine Environmental Sciences, University of Bremen/Germany. Precision of ICP-OES measurements was determined using an in-house standard with a Mg/Ca ratio of 2.93 mmol/mol after every five samples. The average relative standard deviation from $n = 55$ measurements was 0.155% ($1\sigma = 0.005$). As a standard reference material, we analysed the international limestone standard ECRM752-1 with an Mg/Ca ratio of 3.75 mmol/mol (Greaves et al., 2008) prior to every batch of 50 samples. In addition, an in-house standard solution with a Mg/Ca of 2.93 mmol/mol was measured after every five samples. Average Mg/Ca values over all ECRM752-1 measurements was 3.714 ($n = 8$; $1\sigma = 0.041$). Three replicate measurements of every sample were used to estimate analytical precision and yielded an average relative standard deviation of 0.068% ($n = 702$ measurements, $1\sigma = 0.004$). To estimate SST from Mg/Ca we used the species-specific calibration equation $T = 1/0.102 \times LN(\mathrm{Mg/Ca}/0.528)$ published by Elderfield and Ganssen, (2000) for *G. bulloides*. This Mg/Ca-temperature relationship was previously used for calibrating Mg/Ca measurements of *G. bulloides* in the Arabian Sea (Anand et al., 2008; Ganssen et al., 2011).

Samples were screened for a potential contamination by iron-manganese coatings and clay minerals not successfully removed by the cleaning technique (Barker et al., 2003). Ten out of 142 samples showed Fe/Ca or Mn/Ca values of more than 0.1 mmol/mol and were excluded prior to further analyses. Paleotemperature estimates based on trace elemental concentrations in foraminiferal calcite can potentially suffer from post-depositional dissolution and preferential removal of more solution susceptible Mg-rich calcite (e.g., Brown and Elderfield, 1996; Dekens et al., 2002). We therefore tested a systematic dissolution bias of samples from core SL163 using a cross correlation of Mg/Ca ratios and the fragmentation index of Le and Shackleton, (1992). If Mg/Ca measurements were affected by carbonate dissolution, a strong negative relationship between Mg/Ca ratios and fragmentation indices would be expected, which is not the case for our samples ($r = -0.07$, $p = 0.43$). Furthermore, the presence of pteropods suggests that carbonate dissolution did not systematically alter Mg/Ca-ratios.

Bulk geochemical analyses

Bulk geochemical analyses of the sediment were performed on average every 5 cm with X-ray fluorescence (XRF). Concentrations of manganese (Mn) and vanadium (V) were quantitatively analysed as an indicator for bottom water redox conditions and state of the OMZ. After fusion of the samples with lithium metaborate at 1200 °C for 20 minutes (sample/$LiBO_2$ = 1/5) samples were measured using Philips PW 2400 and PW 1480 wavelength dispersive spectrometers at the Federal Institute for Geosciences and Natural Resources, Hannover/Germany. Instrumental precision of the results was controlled with certified reference materials (CRM) (i.e., BCR, Community Bureau of Reference, Brussels). The precision for major elements was generally better than $\pm$0.5% and better than 5% for trace elements. Biogenic opal was determined photometrically after wet alkaline extraction of biogenic silica (BSi) using a modification of the DeMaster method (DeMaster, 1981). About 30 g dry sediment per sample was digested in 40 mL of 1% sodium carbonate solution (Na_2CO_3) in a shaking bath at 85 °C. After treatment with 0.021 M HCl, the neutralized supernatant was analyzed after 3, 4 and 5 hours and the amount of BSi was estimated from the linear intercept through the time course aliquots. This slope correction was used to prevent an overestimation of BSi by dissolution of clay minerals at low BSi concentrations (Conley, 1998). Biogenic opal was determined by multiplying the BSi concentrations with a factor of 2.4. A mean standard deviation of 0.13% was determined by duplicate measurements.

Spectral analyses

Spectral analyses on the proxy records from planktic foraminiferal transfer functions, Mg/Ca-SST and OMZ intensity with the multi-taper method (MTM; Mann and Lees, 1996) were computed with the SpectraWorks software kSpectra©ver. 3.4.5 and a red noise null hypothesis (Ghil et al., 2002) using the default setting of $p = 2$ and $K = 3$ tapers. A cross wavelet transform (XWT; Grindsted et al., 2004) of both temperature proxy time series was calculated with the biwavelet package ver. 0.17.10 for *R*. MTM and XWT analyses were conducted on trend-removed time series interpolated to regular average sample spacings using piecewise cubic polynomial interpolation (function 'pchip' of the signal package ver. 0.7-6 for *R*). To estimate a linear relationship of the low-frequency signals between the differently spaced time series, a new common time axis was produced where signals were consecutively averaged into 60-year long bins with a 20-year

overlap.

Results

Age control

Table IV.1: Samples for radiocarbon dating with the organic compound used, dating results and calibrated ages using the MARINE13 calibration curve (Reimer et al., 2013) and a reservoir correction of $\Delta R = 231 \pm 31$years. Analyses were conducted at Beta Analytics in Miami/FL, U.S.A. (Beta) and the Leibniz Laboratory in Kiel, Germany (KIA).

Lab Code	Core	Sample Type	Depth (cm)	Conventional ^{14}C age (years)	Error	δ^{13}C (‰)	cal. min (95%)	cal. max (95%)
Beta342813	MC681	mixed PF	1	650	30	–2.4		
Beta342812	MC681	bulk org.	1	630	30	–20.4		
Beta346603	SL163	bulk org.	52.5	2100	30	–19.4	1329	1505
Beta346604	SL163	bulk org.	58.5	5740	30	–19.3	5788	5973
KIA47119	SL163	*N. dutertrei*	77.75	5760	30	+0.24	5841	5987
Beta319751	SL163	*N. dutertrei*	141.25	5990	30	–0.5	6095	6266
Beta319752	SL163	*N. dutertrei*	193.75	6350	40	+0.5	6436	6646
KIA47120	SL163	*N. dutertrei*	252.75	6715	35	+0.48	6878	7114
Beta319753	SL163	*N. dutertrei*	278.75	6670	40	+0.8	6790	7043
Beta319754	SL163	*N. dutertrei*	295.0	7030	40	+0.3	7246	7407
Beta319755	SL163	*N. dutertrei*	326.25	6990	40	+0.4	7193	7386
KIA47121	SL163	*N. dutertrei*	353.75	7420	40	+1.59	7568	7737
KIA47122	SL163	*N. dutertrei*	392.5	8090	40	+1.42	8211	8396
Beta319756	SL163	*N. dutertrei*	395.0	8090	40	+0.8	8211	8396
Beta342816	SL163	*N. dutertrei*	417.5	8500	40	–0.4	8647	8957

mixed PF=mixed planktic foraminifera; bulk org.=bulk organic fraction

The 1–2.5 cm sample spacing yielded an average temporal sampling distance of ~19 years over the entire interval. We observed two samples where the age-depth relationship is reversed within the lower half of the core (Figure IV.3). However, the maximum age deviation is lower than the 2σ probability of both dating points, enabling to fit a smooth spline model with continuous deposition rates and continuously increasing ages. The sharp lithofacies change at 56 cm core depth is marked by a sedimentation hiatus of ~3600 years (Table IV.1). Based on the accumulation rates above and below the unconformity, this corresponds to a thickness of the missing sedimentary sequence of ~1.5 m. One possible reason for this might be that the high water content of the organic-rich diatomaceous nannofossil silty clay deposited above the foraminiferal nannofossil ooze led to gravitational instability at the steeply inclined northern Oman margin.

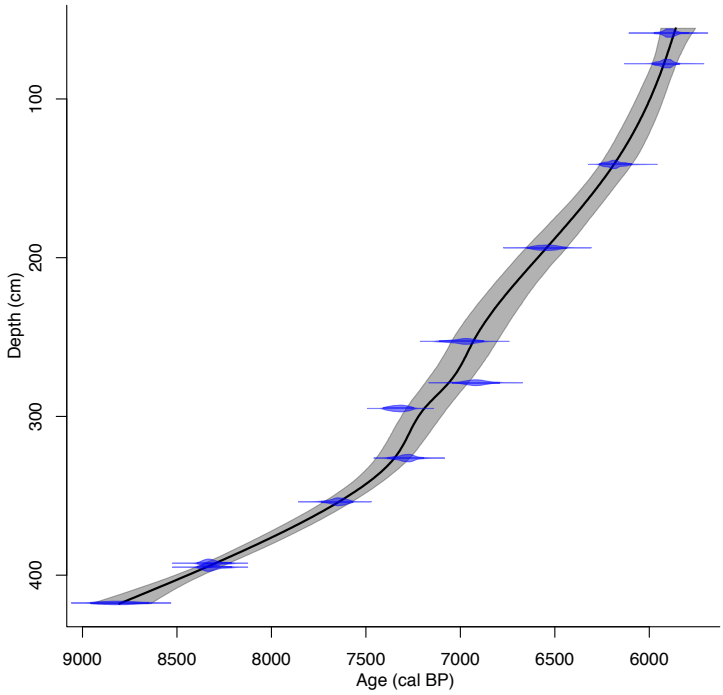

Figure IV.3: Age-depth relationship of the early- to mid Holocene section of core SL163 (55–400 cm). Blue areas indicate the conventional ^{14}C calibrated ages, the black line indicates the interpolation between the dated samples using a smooth spline fit and the 95% confidence level (grey shading).

PF faunal analyses of core SL163 and paleothermometry

A total of 29 PF morphospecies were identified in core SL163, whereof six species showed a total average abundance of >5% (Figure IV.4). The overall PF fauna is dominated by *Globigerina bulloides* (39.2%), followed by *Globigerinita glutinata* (11.5%), *Globigerinoides ruber* (11.2%), *Globigerina falconensis* (9.2%), *Globigerinoides sacculifer* (8.3%) and *Globigerinella siphonifera* (7.4%). Core top studies (Bé and Hutson, 1977b; Hutson and Prell, 1980; Prell and Curry, 1981), plankton tow casts (Peeters and Brummer, 2002) and sediment trap studies (Conan et al., 2002; Conan and Brummer, 2000; Curry et al., 1992; Mohan et al., 2006) in the Arabian Sea indicate that *G. bulloides* is the dominant species during upwelling season. Relative abundances of *G. bulloides* were used in a number of studies to express upwelling and ISM intensity (Anderson et al., 2002; Gupta et al., 2005; Naidu and Malmgren, 1996). The very high numbers of *G. bulloides* throughout the studied interval of core SL163 suggests highly elevated primary productivity during the early- to mid Holocene summer upwelling at this station.

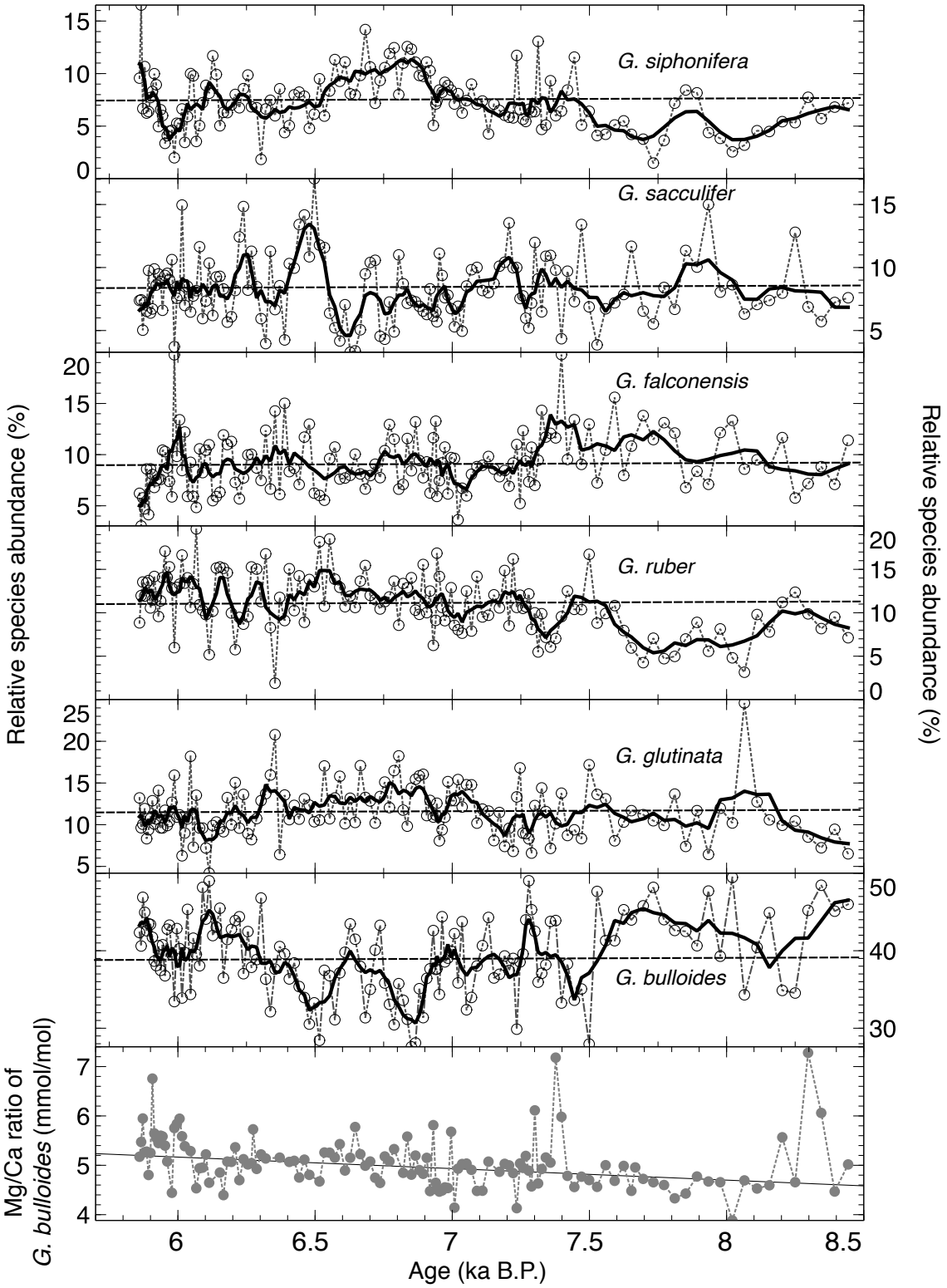

Figure IV.4: Time series of the six most common planktic foraminiferal species (>5% average abundance) and Mg/Ca measurements of *G. bulloides* from the studied interval in core SL163. Dashed lines are the real data, thick solid lines give the 3-pt running average.

Modern surface water properties and plankton productivity at the northern Oman margin are dominated by the seasonal upwelling during boreal summer. Because PF assemblages are dominated by species produced during the upwelling season (Curry et al., 1992), we investigated the environmental control on the PF fauna during summer (July to September; J-A-S). RDA results indicate, that summer SST correlates best with the first RDA axis and is the strongest determinant in the explanation of PF assemblages among the investigated parameters (Table IV.2). Transfer functions were therefore calibrated to summer SST.

Table IV.2: Results of the redundancy analysis of the adjusted calibration dataset. Highest correlation with RDA1 axis and highest explanation of the PF assemblage variance is shown by temperature (bold numbers).

	RDA1	RDA2	RDA3		
Eigenvalue	1.763	0.185	0.097		
Cumulative proportion variance explained (%)	35.9	39.6	41.6	Captured variance of species data	**Proportion (%)**
Correlation					
Temperature	**–0.93**	–0.07	0.15	1.55	**31.5**
Salinity	–0.87	0.47	–0.05	0.24	5.0
Eppley-VGPM	0.33	0.75	0.26	0.19	4.0
uCbPM	–0.02	–0.65	0.32	0.07	1.5
Chlorophyll α	0.39	0.36	–0.18	0.05	1.0

VGPM=Vertical Generalized Production Models; uCbPM=updated Carbon-based Production Model.

The three methods used for determining the factor numbers to retain for the IK transfer function approach suggested a number of $n = 4$ factors. For WA-PLS, a two component model showed best model performance ($r^2 = 0.65$) and lowest cross-validated error estimates (RMSEP $= 0.95\,^{\circ}$C). Performance estimates for both methods are given in Table IV.3. Statistical significance of the reconstructions was tested using a novel method of random forest reconstructions (Telford and Birks, 2011). The analysis shows that summer SST can be reconstructed from fossil PF assemblages of core SL163 with a high statistical significance (Table IV.3; Figure IV.5). Reconstructed summer SST from both techniques (IK and WA-PLS) show a high linearity ($r = 0.82$; $p < 2.2\text{E}-16$), indicating a low model-specific bias (Kucera et al., 2005). The resulting consensus of reconstructed summer SST from the transfer function techniques ranges between 23.3 °C and 25.8 °C (Figure IV.6b). Compared to modern summer (J-A-S) SST (10 m depth interval), which is 25.8 °C at this station (Conkright et al., 1998), reconstructed early- to mid Holocene summer SST are thus <2.5 °C colder.

Measured Mg/Ca values range between 3.9 mmol/mol and 7.3 mmol/mol (Figure IV.4), corresponding to water temperatures ranging from 19.6 °C to 25.7 °C.

The Mg/Ca value of 6.66 mmol/mol of the core top sample at this station (MC681) yields SST estimates ($T = 24.85\,^{\circ}$C) close to modern summer SST of the upper 50 m of the water column (WOA1998 $= 24.81\,^{\circ}$C), indicating that the calibration equation of Elderfield and Ganssen, (2000) is applicable to the Mg/Ca–temperature dependence of *G. bulloides* at the northern Oman margin.

Proxies of OMZ conditions and carbonate preservation

Trace-element distributions of manganese (Mn) and vanadium (V) were used as an indicator for bottom water redox conditions and state of the OMZ, following (Tribovillard et al., 2006). The values were expressed as enrichment to average shale (Wedepohl, 1971). V is enriched throughout the studied interval and enrichment relative to average shale ranges from 1.0 to 1.7. With average values of 0.92, Mn is mostly depleted except for four short phases centered at 6.0, 6.3, 7.2 and 8.4 ka B.P. (Figure IV.6g). The concentration of pteropod fragments ranges from 0 (pteropod-barren) to $5.2x10^3$ numbers per gram dry weight and PF fragmentation ranges between 0.1% and 12.2% (Le and Shackleton, 1992).

Table IV.3: Cross-validated root mean squared error of prediction (RMSEP) as absolute values and relative to the range of the target variable, as well as the coefficient of determination. The results of the significance analysis after Telford and Birks, (2011) from both transfer function methods are given, p indicates the statistical significance against the null distribution of 999 random reconstructions.

	RMSEP	RMSEP (% of target range	R^2	SST $p =$	Eppley-VGPM $p =$
Imbrie-Kipp	0.92	15.72	0.67	0.015	0.758
WA-PLS	0.95	16.20	0.65	0.007	0.160

WA-PLS=weighted averaging partial least squares method.

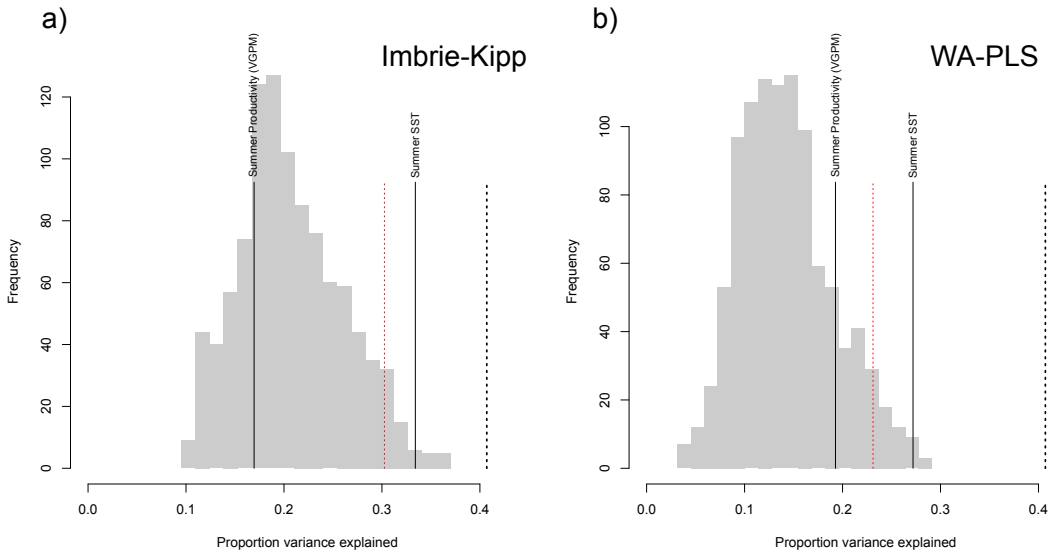

Figure IV.5: Results of the significance test of assemblage-based paleoenvironmental reconstructions using the R package palaeoSig (Telford, 2015). The null distribution is produced by generating 999 random environmental variables and reconstruct these variables from PF assemblages of core SL163 using **(a)** the Imbrie-and-Kipp method (IK) and **(b)** the weighted averaging partial least squares (WA-PLS) method. Grey shaded histograms indicate the amount of variance of the fossil data explained by the 999 random environmental variables, whereas the black vertical lines indicate the variance explained by the reconstruction of summer productivity (VGPM) and summer SST with the respective method. The red dashed line represents the 95^{th} percentile of the null distribution, the black dashed line the variance explained by the first RDA axis. Thus, the proportion of variance explained by the IK method for the reconstruction of summer SST from the fossil dataset is higher than 95% ($p = 0.015$) of reconstructions of 999 random environmental variables. The summer SST reconstruction from the WA-PLS method is higher than 99% of the random reconstructions ($p = 0.007$). The VGPM-based reconstruction of summer surface primary productivity is not significant (IK: $p = 0.76$; WA-PLS: $p = 0.16$).

Discussion

Interpretation of the two independent planktic foraminiferal SST proxies

A direct comparison of the Mg/Ca-SST of *G. bulloides* and assemblage-based (consensus of IK and WA-PLS) summer SST reveals no linear relationship ($r = 0.02$, $p = 0.91$), although the binned time series show a weak positive linearity ($r = 0.24$, $p < 0.06$). This indicates that the low frequency signals of both time series are linearly related. Furthermore, the time series of both proxy records reveal a common trend of overall increasing temperatures over the record (Figure IV.6a-b)

and are coherent on a wide range of frequencies. Significant (>95% confidence) coherence was found on ~1300, ~110 and ~60 year periods, as well as on ~150, ~90 and ~40 year periods (>99% confidence). Both SST records are thus in good general agreement, but Mg/Ca SST are on average 2.3 °C colder. This relative offset of the SST reconstructions might be attributed to timing differences during the recording of the respective proxy signal. *G. bulloides* is interpreted to carry the upwelling signal during peak production of this species (Anand et al., 2008; Peeters et al., 2002). Highest flux rates of *G. bulloides* are found from May to October, but with a clear maximum from late July to September (Conan and Brummer, 2000; Curry et al., 1992; Peeters et al., 2002). Furthermore, several studies in the Arabian Sea (Friedrich et al., 2012; Peeters et al., 2002; Schiebel et al., 2004) and in the Java upwelling region (Mohtadi et al., 2011) indicate that *G. bulloides* thrives in coastal upwelling areas mostly within the mixed-layer and upper thermocline waters in the uppermost 50-60 m of the water column. Assemblage-based SST reconstructions are calibrated to the 10 m depth level of summer temperatures. We therefore interpret Mg/Ca values of *G. bulloides* to represent calcification temperatures of mixed-layer and upper thermocline waters during peak production of the late summer upwelling and assemblage-based SST reconstructions to represent a shallower SST average from July to September.

Evidence for early- to mid Holocene monsoon variability

The range of reconstructed water temperatures of 6.1 °C from Mg/Ca measurements of *G. bulloides* suggests that upwelling temperatures at the northern Oman Margin fluctuated strongly and rapidly during the relatively short interval of the early- to mid Holocene covered by SL163. The amplitude of temperature fluctuations recorded by *G. bulloides* is approximately twice as high compared to oxygen isotope temperatures of the same species at the Somali Margin during the early Holocene (Jung et al., 2002). Consistently low SST suggest upwelling and ISM intensity was strongest during the intervals ~7.5–8.1 ka, followed by events around ~7.0–7.3 and 6.1 ka B.P. (Figure IV.6a). Weaker ISM conditions are reflected by warmer-than-average SST values around 6, 6.5–6.9, 7.4 and 8.2 ka B.P. Supporting evidence for decreased ISM intensity during these intervals comes from a stalagmite record from the nearby Hoti and Qunf caves (Figure IV.6i-j), indicating low monsoonal precipitation around 6.3, 7.4 and 8.3 ka BP (Fleitmann et al., 2007; Neff et al., 2001). Records from the Arabian Sea revealed, that strongest

ISM conditions occurred during the early Holocene around 8–11 ka B.P. (Gupta et al., 2003; Staubwasser et al., 2002; Thamban et al., 2007), followed by a gradual weakening around 7 ka B.P., which is concomitant with the time period of relatively warm assemblage-based SST. However, the overall trend in our record is not consistent and rather indicates that gradual weakening of ISM conditions established as early as 8 ka B.P.

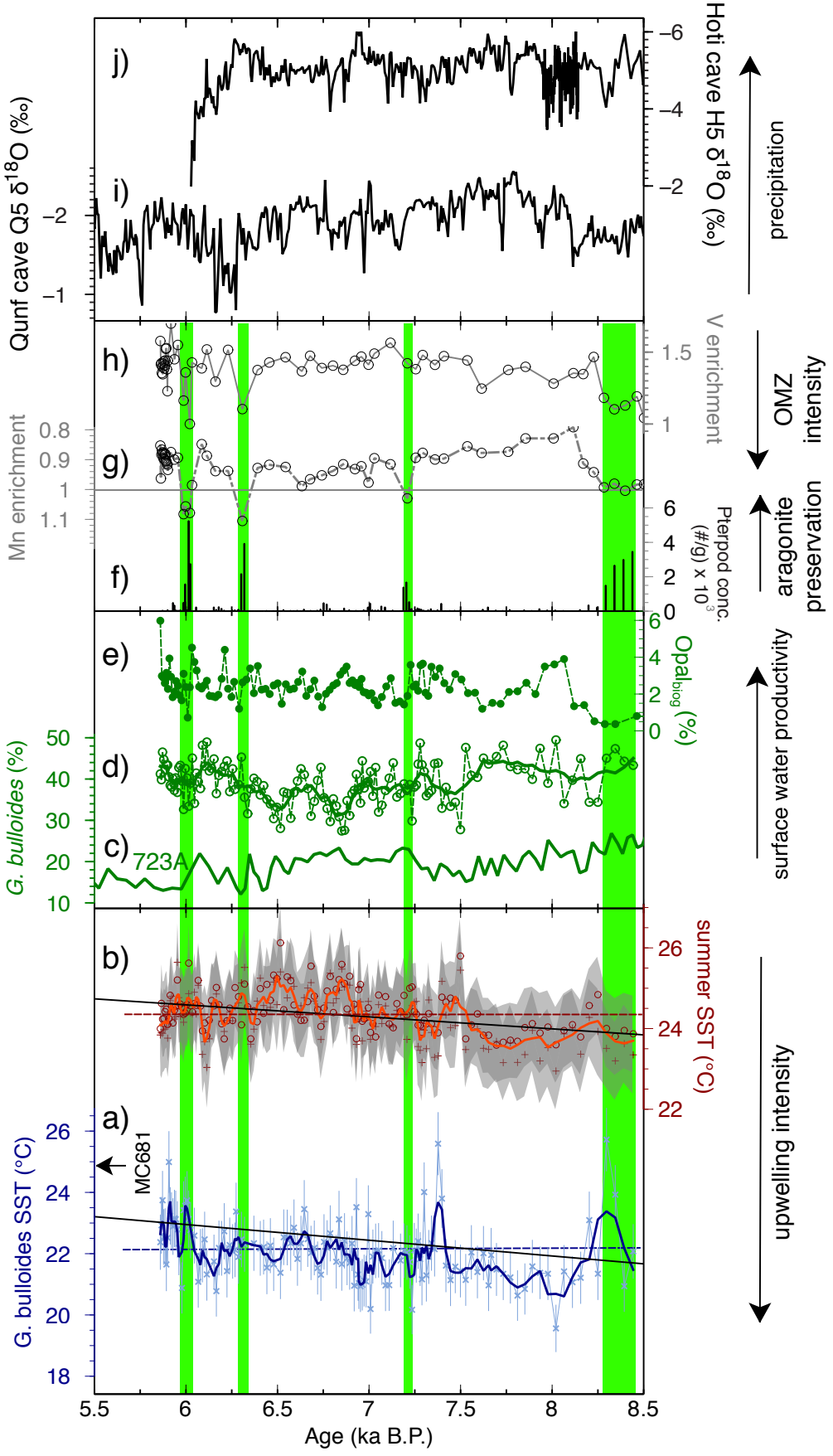
j)
i)
h)
g)
f)
e)
d)
c)
b)
a)
Qunf cave Q5 δ18O (‰)
Hoti cave H5 δ18O (‰)
precipitation
V enrichment
Mn enrichment
OMZ intensity
Pterpod conc. (#/g) x 10^3
aragonite preservation
Opalbiog (%)
G. bulloides (%)
723A
surface water productivity
summer SST (°C)
MC681
G. bulloides SST (°C)
upwelling intensity
Age (ka B.P.)

Figure IV.6: Time series of reconstructed SST from **(a)** the Mg/Ca ratio of *G. bulloides* (blue) indicating upwelling SST and **(b)** the consensus from the assemblage-based transfer function methods, IK and WA-PLS (red) indicating average summer SST (July–September). Thin lines represent real data, thick dashed lines the 3-pt running averages. Relative abundance of *G. bulloides* from ODP site 723A from Gupta et al., (2005) **(c)** and SL163 **(d)**, together with biogenic opal content **(e)**, indicates phases of increased surface water productivity. Aragonite preservation is indicated by the concentration of pteropod fragments **(f)**, bottom-water oxygen conditions and state of the oxygen minimum zone (OMZ) is shown with relative enrichment or depletion of manganese **(g)** and vanadium **(h)**. Note the inverse relationship of both elements, as explained in the text. Stable oxygen isotopes of **(i)** Qunf cave (Fleitmann et al., 2007) and **(j)** Hoti cave stalagmites (Neff et al., 2001) expressing precipitation in Oman. Vertical solid green bars indicate periods of low biogenic opal content, concomitant with decreased OMZ intensity and increased aragonite preservation. Error bars for (a) were calculated by propagating the errors introduced by the Mg/Ca measurements and the Mg/Ca-temperature calibration (Gaussian error propagation, see Mohtadi et al., 2014). Grey shading gives the uncertainty estimates for the transfer functions in (b), based on the sample specific root mean square error of prediction (RMSEP) using bootstrapping cross-validation.

MTM analysis revealed statistically significant periodicities of assemblage-based summer SST at ~1300 and 75–95 years per cycle (Figure IV.7a). Mg/Ca-SST of *G. bulloides* are modulated on frequencies at 110–130, 80–90 and ~40 years (Figure IV.7b). The longer ~110–130 year cycle was previously found in a number of records from the Asian monsoon realm (Berger and Rad, 2002; Dykoski et al., 2005; Gupta et al., 2005) and is close to the 132-year sunspot cycle previously identified to be modulating the Oman upwelling system during the Holocene (Gupta et al., 2005). The ~80–90-year cycle has been observed in several studies of ISM variability (Dykoski et al., 2005; Fleitmann et al., 2003; Gupta et al., 2005; Neff et al., 2001) and was interpreted to be most likely influenced by the 88-year solar Gleissberg cycle. We tested a possible solar component on the decadal-scale forcing of our SST records by evaluating the coherence of both time series with the record of reconstructed sunspot numbers (Solanki et al., 2004). The coherence pattern reveals, that both SST records and sunspot numbers are coherent on a wide range of periodicities (630, 190–230, 160, 110–130, 80–90, ~70, ~50 and ~40- years per cycle, Fig. 6d and e). This observation further strengthens the hypothesis, that ISM variability is not only controlled by orbital forcing, indicated by the long-term trend of warming temperatures, but also by solar forcing.

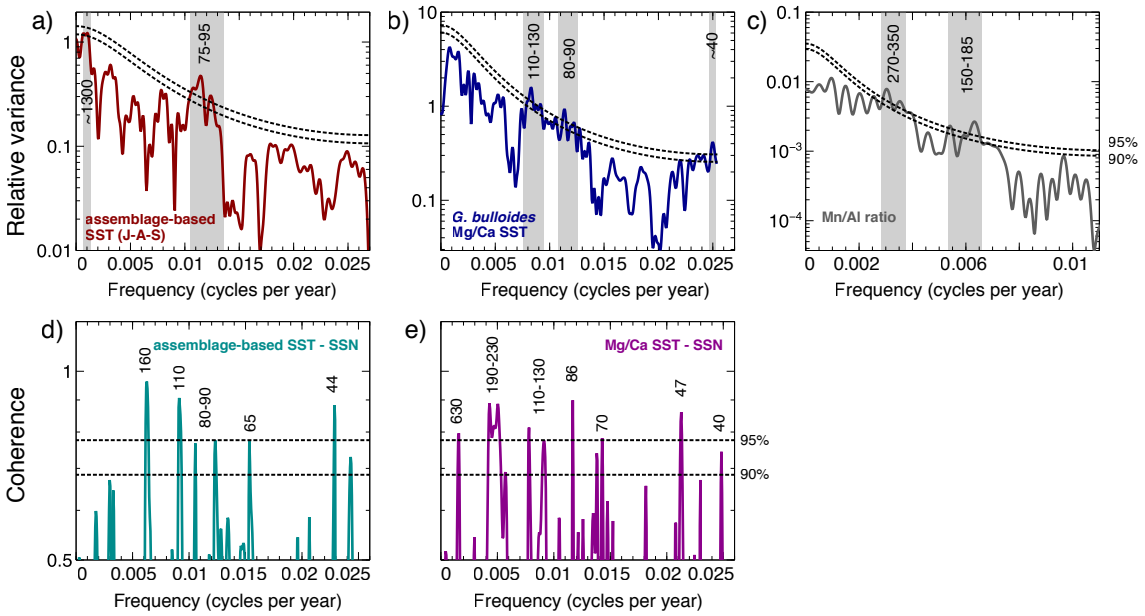

Figure IV.7: Results of the MTM spectral analysis show the frequency distribution and identified significant periodicities of the **(a)** assemblage-based SST record, **(b)** the SST record using Mg/Ca ratios of *G. bulloides* and **(c)** the Mn/Al ratio as a proxy for OMZ conditions. Black lines indicate 90% and 95% significance levels against red noise. Cross-spectral coherence of both SST records (**d** and **e**) with the record of sunspot numbers (Solanki et al., 2004) indicates that both records significantly covary on a wide range of frequencies. All time series were trend-removed prior to the analyses.

Carbonate preservation and bottom water redox conditions

In order to study the interplay of ISM intensity and OMZ fluctuations, we compared our new multi-proxy reconstruction of summer SST to OMZ reconstructions of Böll, (2015). This study previously evaluated ISM intensity and OMZ conditions during the deposition of SL163 in a spatial context using alkenone-derived annual mean SST, stable nitrogen isotopes and published OMZ reconstructions, concluding that changes of OMZ intensity were linked to variability of intermediate water ventilation and monsoon strength. Our new multi-proxy records primarily responding to summer upwelling conditions enables to study the interplay of ISM intensity and OMZ fluctuations during the early- to mid Holocene in more detail. Under oxic bottom-water conditions, Mn is precipitated as Mn oxy-hydroxides, which is reduced to soluble Mn^{2+} under suboxic conditions (Böning et al., 2004; Calvert et al., 1996; Calvert and Pedersen, 1993; Schnetger et al., 2000). Mn is mostly depleted in core SL163, indicating Mn-loss through the OMZ, except for

three short intervals of Mn enrichment centered at ~6.0, 6.3 and 7.2 ka B.P., as well as from 8.3 ka B.P. to the end of the record (Figure IV.6g). This finding is partly contradictory to Böll, (2015) who found increased denitrification indicating more intense OMZ conditions during the intervals 5.9, 6.1, 6.4 and 7.2 ka B.P. (based on the same age model). V is precipitated under anoxic conditions (Emerson and Huested, 1991) and constant enrichment values between 1.0 and 1.7 relative to average shale, however, indicate permanent anoxic bottom water conditions during the deposition of core SL163.

Carbonate preservation was assessed by PF fragmentation indices and the abundance of pteropod fragments in the sieve fraction >150µm. Pteropod shells primarily consist of aragonite, the less stable polymorph of calcium carbonate as compared to calcite (Morse et al., 1980). In the northern Arabian Sea, aragonite has a modern compensation depth (ACD) of ~500 m (Berger, 1978b; Böning and Bard, 2009) and a lysocline at ~1km water depth (Böning and Bard, 2009), thus approximately 350 m below the station of core SL163. However, in high-productivity environments supra-lysoclinal dissolution can occur well above this depth, induced by respiration of organic matter and metabolic release of CO_2 (e.g., Milliman et al., 1999). Thus, enhanced pteropod preservation indicates either ACD deepening (Reichart et al., 2002) or less supra-lysoclinal dissolution due to decreased production of organic matter. Phases of increased concentrations of pteropod fragments are linked to the short intervals of slightly enriched Mn values (Figure IV.6f-g). This indicates short phases of less corrosive bottom waters due to potentially weaker OMZ conditions. Furthermore, the variability of Mn/Al values (expressed as Mn enrichment) is modulated on dominant ~170- and ~310-year cycles (Figure IV.7c), which is approximately half (170) and one fourth (340) of the ~80–90-year frequency of the Gleissberg cycle. This suggests that bottom water oxygenation state is modulated on the same frequencies as SST variability and upwelling intensity.

The intervals of increased pteropod concentration and lower OMZ intensity at ~6, 6.3, 7.2 and 8.3–8.5 ka B.P. are linked to intervals of low biogenic opal and thus occurred when surface water productivity was diminished. The former three of these intervals also correspond to low abundances of the upwelling indicator species *G. bulloides* (Figure IV.4), but during the latter interval at 8.3–8.5 ka B.P. *G. bulloides* abundances are high (>45%). In addition, Mg/Ca measurements of *G. bulloides* at 8.3 ka B.P. are >7 mmol/mol and inferred SST are >25.5 °C. A similar feature of a very short warm excursion of Mg/Ca temperatures from *G. bulloides*

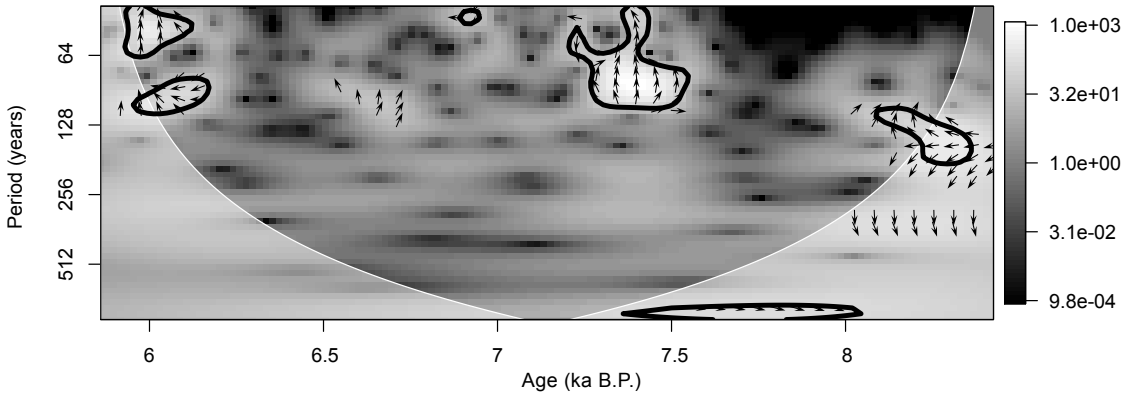

Figure IV.8: Cross wavelet transform (XWT) of the trend-removed Mg/Ca-based and assemblage-based SST time series. The 5% significance level is shown as thick contours. Relative phasing of both records is indicated by arrows. Arrows within the significant intervals pointing mostly upwards, which indicates a consistent phase-shift of both records by 90° or 270°, respectively, of assemblage-based SST relative to Mg/Ca-based SST. The cone of influence, where edge artefacts might be introduced, is indicated by white shading.

with concomitantly high abundances of this species around 8 ka B.P. was observed by Anand et al., (2008) in their record from the Somali upwelling system.
Cross wavelet transform (XWT) reveals three distinct intervals, two in the ~40–90-year band (6–6.2, 7.2–7.6 ka B.P.) and one in the ~110–130-year band (8.1–8.4 ka B.P.), where both records show significant common power (Figure IV.8). The intervals correspond well to the phases of enhanced pteropod preservation and lower OMZ intensity. The cross wavelet phase angle of XWT further indicates that both SST records are phase-shifted during these intervals. The arrows in Figure IV.8 within the significant areas are pointing mostly upwards, which indicates either that assemblage-based SST are leading Mg/Ca-SST by $\pi/2$, i.e. 90°, or that assemblage-based SST are lagging Mg/Ca-SST by $3\pi/2$, i.e. 270°. Although these phases are relatively short-lived and both scenarios seem reasonable from the visual comparison of the two SST time series, a systematic lead of faunal SST reconstructions compared to alkenone-derived SST was previously found by Cayre and Bard, (1999) in a study from the eastern Arabian Sea. However, their study observed a delay of several ka, which was potentially produced by strong productivity changes (Bard, 2001). It should be noted that the phase relationships at the longer wavelength could be erroneous, as the behaviour is not consistent

and partly truncated by edge effects below the cone of influence.
Several studies in the Arabian Sea indicate an alternating influence of different water masses during the deglacial and early Holocene (Gupta et al., 2008; Jung et al., 2001; Jung et al., 2009; Schmiedl and Leuschner, 2005; Zahn and Pedersen, 1991). The site of core SL163 is within the modern range of intermediate water masses, that form a mixture of RSW, PGW and IOCW down to ~1500 m water depth (Emery and Meincke, 1986; Shetye et al., 1994). During the last glacial stage, the outflow from the two mediterranean basins connected to the Arabian Sea (Red Sea and Persian Gulf) was highly suppressed due to lowering of the global sea level potentially close to or even below the respective sill depths (Rohling and Zachariasse, 1996). Gupta et al., (2008) discussed that ventilation changes at the northern Oman Margin during the early Holocene are distant to RSW and more likely attributed to an alternating contribution of NADW to the deeper water masses. In comparison to their study site, our core site is further north, close to the modern Ras-al-Hadd frontal zone, where PGW enters the Arabian Sea. At the station of SL163, modern PGW reaches down to 400 m (Figure IV.1). During phases of more restricted water exchange and increased evaporation, subsurface salinities in the Gulf might have been higher, which could have enabled PGW to reach the core site at deeper depth. However, the modern oxygen input of PGW is very low and OMZ conditions at this depth are still fully hypoxic. Moreover, the concomitant occurrence of high common cross wavelet power of the SST records with less corrosive bottom waters indicates that deep water conditions are instead linked to SST variations. This relationship might be derived from a secondary effect of pH on Mg/Ca ratios (e.g., Lea et al., 1999). Phases of low surface water productivity and increased carbonate preservation could have led to a better preservation of Mg-rich calcite, shifting the SST estimates to warmer values. Although a regression analysis of pteropod concentration and Mg/Ca measurements (Figure IV.9) shows that a linear relationship is rather weak, it suggests that SST and productivity variations are primarily controlling OMZ conditions at decadal time scales.

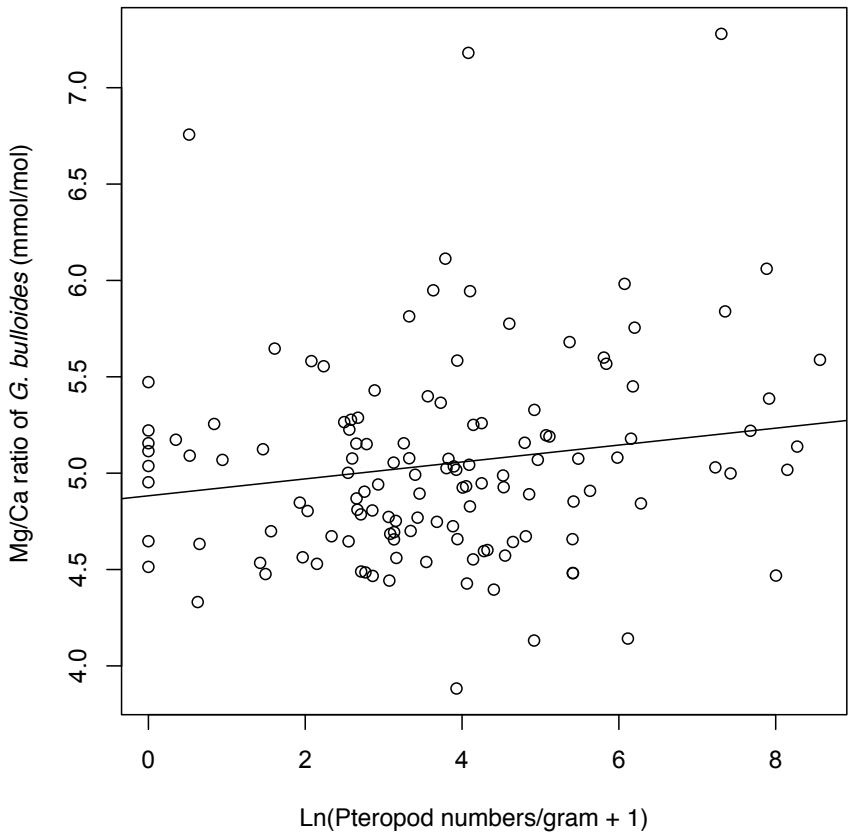

Figure IV.9: Cross plot showing the ln transformed concentration of pteropods (numbers/gram) and the Mg/Ca ratio of *G. bulloides*. A linear regression indicates, although weak, a systematic relationship of higher pteropod concentration and increased Mg/Ca ratios ($r = 0.17$, $p = 0.06$).

Conclusions

Among the environmental variables investigated, summer SST is primarily controlling the underlying variability of PF assemblages from the NW Arabian Sea. Statistically significant reconstructions of summer SST from PF assemblages and Mg/Ca-SST from *G. bulloides* are colder than present summer temperatures, indicating vigorous monsoonal winds and upwelling intensity during the early- to mid Holocene. ISM conditions were generally strongest around 8 ka$_{B.P.}$ and gradually decreased towards 5.8 ka$_{B.P.}$ The trend of weakening monsoon conditions was interrupted by decadal-scale episodes of intensified ISM around ~7 and 6.2 ka$_{B.P.}$, which is concomitant to pluvial episodes indicated by the Oman

speleothem records. Summer SST fluctuations furthermore reveal, that upwelling intensity was coupled to decadal- to centennial-scale sunspot cycles.
Low monsoonal conditions, indicated by warm upwelling and summer SST, as well as enhanced surface water productivity, are associated with enhanced pteropod preservation and weaker OMZ conditions. Enrichment of Manganese as a proxy for bottom-water oxygenation varies on multiples of the dominant ~80–90-year Gleissberg cycle, suggesting that upwelling intensity and OMZ conditions are modulated by solar activity. We therefore conclude that, instead of intermediate water mass changes, surface water processes are the main driver of OMZ conditions.

References

Anand, P., D. Kroon, A. D. Singh, and G. Ganssen (2008): 'Coupled sea surface temperature-seawater δ^{18}O reconstructions in the Arabian Sea at the millennial scale for the last 35 ka'. *Paleoceanography*, vol. 23: PA4207.

Anderson, D. M., J. T. Overpeck, and A. K. Gupta (2002): 'Increase in the Asian Southwest Monsoon During the Past Four Centuries'. *Science*, vol. 297(5581): pp. 596–599.

Arrhenius, G. (1952): 'Sediment cores from the East Pacific'. *Reports of the Swedish Deep-Sea Expedition 1947–1948*, vol. 5: pp. 1–228.

Bard, E. (2001): 'Comparison of alkenone estimates with other paleotemperature proxies'. *Geochemistry, Geophysics, Geosystems*, vol. 2(1).

Barker, S., M. Greaves, and H. Elderfield (2003): 'A study of cleaning procedures used for foraminiferal Mg/Ca paleothermometry'. *Geochemistry, Geophysics, Geosystems*, vol. 4(9).

Bé, A. W. H. and W. H. Hutson (1977a): 'Ecology of Planktonic Foraminifera and Biogeographic Patterns of Life and Fossil Assemblages in the Indian Ocean'. *Micropaleontology*, vol. 23(4): p. 369.

Bé, A. (1967): 'Foraminifera families: *Globigerinidae* and *Globorotalidae*'. *Fiches d´Identification du Zooplankton*. Ed. by Fraser, J. H. Vol. Sheet 108. Charlottenlund, Denmark: Conseil Perm. Internat. Explor. Mer: pp. 1–8.

Bé, A. and W. H. Hutson (1977b): 'Ecology of planktonic foraminifera and biogeographic patterns of life and fossil assemblages in the Indian Ocean'. *Micropaleontology*, vol. 23(4): p. 369.

Berger, A. L. (1978a): 'Long-term variations of daily insolation and Quaternary climatic changes'. *J. Atmos. Sci.* Vol. 35: pp. 2362–2367.

Berger, W. H. (1978b): 'Deep-sea carbonate: Pteropod distribution and the aragonite compensation depth'. *Deep Sea Research*, vol. 25: pp. 447–452.

Berger, W. H. and U. von Rad (2002): 'Decadal to millennial cyclicity in varves and turbidites from the Arabian Sea: hypothesis of tidal origin'. *Global and Planetary Change*, vol. 34(3): pp. 313–325.

Birks, H. (1998): 'Numerical tools in palaeolimnology–Progress, potentialities, and problems'. *Journal of Paleolimnology*, vol. 20: pp. 307–322.

Blaauw, M. (2010): 'Methods and code for 'classical'age-modelling of radiocarbon sequences'. *Quaternary Geochronology*, vol. 5(5): pp. 512–518.

Bohrmann, G., N. Lahajnar, B. Gaye, V. Spiess, and C. Betzler (2010): *Nitrogen Cycle, Cold Seeps, Carbonate Platform Development in the Northwestern Indian Ocean, Cruise No.74, August 31 - December 22, 2007*. 10-3. University of Hamburg. Hamburg.

Böll, A. (2015): 'Arabian Sea sediments as a monitor of the Asian monsoon system: Paleoproductivity and its influence on the coupled carbon and nitrogen cycle'. PhD thesis. University of Hamburg.

Böning, P., H. J. Brumsack, and M. E. Böttcher (2004): 'Geochemistry of Peruvian near-surface sediments'. *Geochimica et Cosmochimica Acta*, vol. 68(21): pp. 4429–4451.

Böning, P. and E. Bard (2009): 'Millennial/centennial-scale thermocline ventilation changes in the Indian Ocean as reflected by aragonite preservation and geochemical variations in Arabian Sea sediments'. *Geochimica et Cosmochimica Acta*, vol. 73(22): pp. 6771–6788.

Brown, S. J. and H. Elderfield (1996): 'Variations in Mg/Ca and Sr/Ca ratios of planktonic foraminifera caused by postdepositional dissolution: Evidence of shallow Mg-dependent dissolution'. *Paleoceanography*, vol. 11(5): pp. 543–551.

Calvert, S. E., R. M. Bustin, and E. D. Ingall (1996): 'Influence of water column anoxia and sediment supply on the burial and preservation of organic carbon in marine shales'. *Geochimica et Cosmochimica Acta*, vol. 60(9): pp. 1577–1593.

Calvert, S. E. and T. F. Pedersen (1993): 'Geochemistry of Recent oxic and anoxic marine sediments: Implications for the geological record'. *Marine Geology*, vol. 113(1): pp. 67–88.

Cayre, O. and E. Bard (1999): 'Planktonic foraminiferal and alkenone records of the last deglaciation from the Eastern Arabian Sea'. *Quat. Res.* Vol. 52: pp. 337–342.

Clemens, S., W. Prell, D. Murray, G. Shimmield, and G. Weedon (1991): 'Forcing Mechanisms of the Indian-Ocean Monsoon'. *Nature*, vol. 353(6346): pp. 720–725.

Conan, S. M. H., E. M. Ivanova, and G. J. A. Brummer (2002): 'Quantifying carbonate dissolution and calibration of foraminiferal dissolution indices in the Somali Basin'. *Marine Geology*, vol. 182(3): pp. 325–349.

Conan, S. and G. Brummer (2000): 'Fluxes of planktic foraminifera in response to monsoonal upwelling on the Somalia Basin margin'. *Deep Sea Research Part II: Topical Studies in ...* Vol. 47(9-11): pp. 2207–2227.

Conkright, M. E., S. Levitus, T. OBrien, T. P. Boyer, C. Stephens, D. Johnosn, L. Stathoplos, O. Baranova, J. Antonov, R. Gelfeld, J. Burney, J. Rochester, and C. Forgy (1998): *World Ocean Database 1998 Documentation and Quality Control*. Silver SPring, MD.

Conley, D. J. (1998): 'An interlaboratory comparison for the measurement of biogenic silica in sediments'. *Marine chemistry*, vol.

Courtney, M. and M. Gordon (2013): 'Determining the number of factors to retain in EFA: Using the SPSS R-Menu v2. 0 to make more judicious estimations'. *Practical Assessment*, vol. 18(8).

Curry, W. B., D. R. Ostermann, M. V. S. Guptha, and V. Ittekkot (1992): 'Foraminiferal production and monsoonal upwelling in the Arabian Sea: evidence from sediment traps'. *Upwelling Systems Evolution Since the Early Miocene*. Ed. by Summerhayes, C. P., W. L. Prell, and K. C. Emeis. London: pp. 93–106.

Dahl, K. A. and D. W. Oppo (2006): 'Sea surface temperature pattern reconstructions in the Arabian Sea'. *Paleoceanography*, vol. 21(1).

Dekens, P. S., D. W. Lea, D. K. Pak, and H. J. Spero (2002): 'Core top calibration of Mg/Ca in tropical foraminifera: Refining paleotemperature estimation'. *Geochemistry, Geophysics, Geosystems*, vol. 3(4): pp. 1–29.

DeMaster, D. J. (1981): 'The supply and accumulation of silica in the marine environment'. *Geochimica et Cosmochimica acta*, vol. 45(10): pp. 1715–1732.

Dykoski, C. A., R. L. Edwards, H. Cheng, and D. Yuan (2005): 'A high-resolution, absolute-dated Holocene and deglacial Asian monsoon record from Dongge Cave, China'. *Earth and Planetary Science Letters*, vol. 233(1-2): pp. 71–86.

Elderfield, H. and G. Ganssen (2000): 'Past temperature and delta18O of surface ocean waters inferred from foraminiferal Mg/Ca ratios.' *Nature*, vol. 405(6785): pp. 442–445.

Emeis, K.-C., D. M. Anderson, D. Kroon, and D. Schulz-Bull (1995): 'Sea-surface temperatures and history of monsoon upwelling in the Northeastern Arabian Sea during the last 500,000 years'. *Quat. Res.* Vol. 43: pp. 355–361.

Emerson, S. R. and S. S. Huested (1991): 'Ocean anoxia and the concentrations of molybdenum and vanadium in seawater'. *Marine Chemistry*, vol. 34(3-4): pp. 177–196.

Emery, W. J. and J. Meincke (1986): 'Global Water Masses - Summary and Review'. *Oceanologica Acta*, vol. 9(4): pp. 383–391.

Fairbanks, R. G., M. Sverdlove, R. Free, P. H. Wiebe, and A. Bé (1982): 'Vertical-Distribution and Isotopic Fractionation of Living Planktonic-Foraminifera From the Panama Basin'. *Nature*, vol. 298(5877): pp. 841–844.

Farías, L., C. Fernández, J. Faúndez, et al. (2009): 'Chemolithoautotrophic production mediating the cycling of the greenhouse gases N_2O and CH_4 in an upwelling ecosystem'. *Biogeosciences*, vol. 6: pp. 3053–3069.

Findlater, J. (1969): 'A major low-level air current near the Indian Ocean during the northern summer'. *Quarterly Journal of the Royal Meteorological Society*, vol. 95: pp. 362–380.

Fleitmann, D., S. J. Burns, A. Mangini, and M. Mudelsee (2007): 'Holocene ITCZ and Indian monsoon dynamics recorded in stalagmites from Oman and Yemen (Socotra)'. *Quaternary Science Reviews*, vol. 26(1-2): pp. 170–188.

Fleitmann, D., S. J. Burns, M. Mudelsee, U. Neff, J. Kramers, A. Mangini, and A. Matter (2003): 'Holocene forcing of the Indian monsoon recorded in a stalagmite from Southern Oman'. *Science*, vol. 300(5626): pp. 1737–1739.

Friedrich, O., R. Schiebel, P. A. Wilson, and S. Weldeab (2012): 'Influence of test size, water depth, and ecology on Mg/Ca, Sr/Ca, δ 18 O and δ 13 C in nine modern species of planktic foraminifers'. *Earth an Planetary Science Letters*, vol. 319-320: pp. 133–145.

Ganssen, G. M., F. J. C. Peeters, B. Metcalfe, P. Anand, S. J. A. Jung, D. Kroon, and G. J. A. Brummer (2011): 'Quantifying sea surface temperature ranges of the Arabian Sea for the past 20 000 years'. *Climate of the Past*, vol. 7(4): pp. 1337–1349.

Garcia, H. E., R. A. Locarini, T. P. Boyer, and J. I. Antonov (2010): 'World Ocean Atlas 2009, Volume 3: Dissolved Oxygen, Apparent Oxygen Utilization and Oxygen Saturation'. *A. Mishonov Technical Ed.* Ed. by Levitus, S. U.S. Government Printing Office, Washington D.C.: p. 40.

Ghil, M., R. Allen, M. Dettinger, et al. (2002): 'Advanced spectral methods for climatic time series'. *Reviews of Geophysics*, vol. 40: pp. 1–41.

Godad, S. P., P. D. Naidu, and B. A. Malmgren (2011): 'Sea surface temperature changes during May and August in the western Arabian Sea over the last 22kyr: Implications as to shifting of the upwelling season'. *Marine Micropaleontology*, vol. 78(1): pp. 25–29.

Greaves, M. et al. (2008): 'Interlaboratory comparison study of calibration standards for foraminiferal Mg/Ca thermometry'. *Geochemistry, Geophysics, Geosystems*, vol. 9(8): n/a–n/a.

Grindsted, A., J. Moore, and S. Jevrejeva (2004): 'Application of the cross wavelet transform and wavelet coherence to geophysical time series'. *Nonlinear Processes in Geophysics*, vol. 11: pp. 561–566.

Gupta, A. K., D. M. Anderson, and J. T. Overpeck (2003): 'Abrupt changes in the Asian southwest monsoon during the Holocene and their links to the North Atlantic Ocean'. *Nature*, vol. 421: pp. 354–357.

Gupta, A. K., S. C. Clemens, M. Das, and B. Mukherjee (2008): 'Benthic foraminiferal faunal and isotopic changes as recorded in Holocene sediments of the northwest Indian Ocean'. *Paleoceanography*, vol. 23(2): PA2214.

Gupta, A. K., M. Das, and D. M. Anderson (2005): 'Solar influence on the Indian summer monsoon during the Holocene'. *Geophysical Research Letters*, vol. 32(17): p. L17703.

Hemleben, C., M. Spindler, and O. R. Anderson (1989): *Modern planktonic foraminifera*. Springer Berlin Heidelberg.

Horn, J. L. (1965): 'A rationale and test for the number of factors in factor analysis'. *Psychometrika*, vol. 30: pp. 179–185.

Huguet, C., J.-H. Kim, J. S. Sinninghe Damsté, and S. Schouten (2006): 'Reconstruction of sea surface temperature variations in the Arabian Sea over the last 23 kyr using organic proxies (TEX 86 and $U_{37}^{K'}$)'. *Paleoceanography*, vol. 21(3).

Hutson, W. H. and W. L. Prell (1980): 'A paleoecological transfer function, FI-2, for Indian Ocean planktonic foraminifera'. *Journal of Paleontology*, vol. 54: pp. 381–399.

Imbrie, J. and N. G. A. Kipp (1971): 'New micropaleontologic method for quantitative paleoclimatology: application to Late Pleistocene Carribean core'. *The Late Cenozoic Glacial Ages*. Ed. by Turekian, K. K. New Haven, Conn.: pp. 71–182.

Juggins, S. (2015): *rioja: Analysis of Quaternary Science Data*. R package version (0.8-7).

Jung, S. J. A., G. R. Davies, G. Ganssen, and D. Kroon (2002): 'Decadal-centennial scale monsoon variations in the Arabian Sea during the Early Holocene'. *Geochemistry, Geophysics, Geosystems*, vol. 3(10): pp. 1–10.

Jung, S. J. A., G. M. Ganssen, and G. R. Davies (2001): 'Multidecadal variations in the Early Holocene outflow of Red Sea water into the Arabian Sea'. *Paleoceanography*, vol. 16(6): pp. 658–668.

Jung, S., D. Kroon, G. Ganssen, and F. Peeters (2009): 'Enhanced Arabian Sea intermediate water flow during glacial North Atlantic cold phases'. *Earth and Planetary Science Letters*, vol. 280(1-4): pp. 220–228.

Kennett, D. J. and J. P. Kennett (2007): 'Influence of Holocene marine transgression and climate change on cultural evolution in southern Mesopotamia'. *Climate Change and Cultural Dynamics A Global Perspective on Mid-Holocene Transitions*. Ed. by Anderson, D. G., K. A. Maasch, and D. H. Sandweiss. Climate change and ...

Kucera, M., M. Weinelt, T. Kiefer, U. Pflaumann, A. Hayes, M. Weinelt, M.-T. Chen, A. C. Mix, T. T. Barrows, E. Cortijo, J. Duprat, S. Juggins, and C. Waelbroeck (2005): 'Reconstruction of sea-surface temperatures from assemblages of planktonic foraminifera: multi-technique approach based on geographically constrained calibration data sets and its application to glacial Atlantic and Pacific Oceans'. *Quaternary Science Reviews*, vol. 24(7-9): pp. 951–998.

Kuper, R. and S. Kröpelin (2006): 'Climate-Controlled Holocene Occupation in the Sahara: Motor of Africa's Evolution'. *Science*, vol. 313: pp. 803–807.

Kutzbach, J. E. and F. A. Street-Perrott (1985): 'Milankovitch forcing of fluctuations in the level of tropical lakes from 18 to 0 kyr BP'. *Nature*, vol. 317: pp. 130–134.

Le, J. and N. J. Shackleton (1992): 'Carbonate dissolution fluctuations in the western Equatorial Pacific during the late Quaternary'. *Paleoceanography*, vol. 7: pp. 21–42.

Lea, D. W., T. A. Mashiotta, and H. J. Spero (1999): 'Controls on magnesium and strontium uptake in planktonic foraminifera determined by live culturing'. *Geochimica et Cosmochimica Acta*, vol. 63(16): pp. 2369–2379.

Locarnini, R. A., A. V. Mishonov, J. I. Antonov, T. P. Boyer, and H. E. Garcia (2010): 'World Ocean Atlas 2009, Volume 1: Temperature'. *A. Mishonov Technical Ed.* Ed. by Levitus, S. U.S. Government Printing Office, Washington D.C.: p. 40.

Madhupratap, M., S. Prasanna Kumar, P. M. A. Bhattathiri, M. Dileep Kumar, S. Raghukumar, K. K. C. Nair, and N. Ramaiah (1996): 'Mechanism of the biological response to winter cooling in the northeastern Arabian Sea'. *Nature*, vol. 384: pp. 549–552.

Mann, M. E. and J. M. Lees (1996): 'Robust estimation of background noise and signal detection in climatic time series'. *Climatic change*, vol. 33(3): pp. 409–445.

Milliman, J. D., P. J. Troy, W. M. Balch, and A. K. Adams (1999): 'Biologically mediated dissolution of calcium carbonate above the chemical lysocline?' *Deep Sea Research Part I: Oceanographic Research Papers*, vol. 46(10): pp. 1653–1669.

Mohan, R., K. Verma, Mergulhao, L. P., D. K. Sinha, S. Shanvas, and M. V. S. Guptha (2006): 'Seasonal variation of pteropods from the Western Arabian Sea sediment trap'. *Geo-Marine Letters*, vol. 26(5): pp. 265–273.

Mohtadi, M., D. W. Oppo, A. Lückge, R. DePol-Holz, S. Steinke, J. Groeneveld, N. Hemme, and D. Hebbeln (2011): 'Reconstructing the thermal structure of the upper ocean: Insights from planktic foraminifera shell chemistry and alkenones in modern sediments of the tropical eastern Indian Ocean'. *Paleoceanography*, vol. 26(3): PA3219.

Mohtadi, M., M. Prange, D. W. Oppo, R. De Pol-Holz, U. Merkel, X. Zhang, S. Steinke, and A. Lückge (2014): 'North Atlantic forcing of tropical Indian Ocean climate'. *Nature*, vol. 509(7498): pp. 76–80.

Morse, J. W., A. Mucci, and F. J. Millero (1980): 'The solubility of calcite and aragonite in seawater at various salinities, temperatures and atmosphere total pressure'. *Geochimica et Cosmochimica Acta*, vol. 44: pp. 85–94.

Munz, P. M., M. Siccha, A. Lückge, A. Böll, M. Kucera, and H. Schulz (2015): 'Decadal-resolution record of winter monsoon intensity over the last two millennia from planktic foraminiferal assemblages in the northeastern Arabian Sea'. *The Holocene*, vol. 25(11): pp. 1756–1771.

Murtugudde, R., R. Seager, and P. Thoppil (2007): 'Arabian Sea response to monsoon variations'. *Paleoceanography*, vol. 22: PA4217.

Naidu, P. D. and B. A. Malmgren (1996): 'A High-resolution record of Late Quaternary upwelling along the Oman Margin, Arabian Sea based on planktonic foraminifera'. *Paleoceanography*, vol. 11(1): pp. 129–140.

Neff, U., S. J. Burns, A. Mangini, M. Mudelsee, D. Fleitmann, and A. Matter (2001): 'Strong coherence between solar variability and the monsoon in Oman between 9 and 6 kyr ago.' *Nature*, vol. 411(6835): pp. 290–293.

Oksanen, J., F. G. Blanchet, R. Kindt, P. Legendre, P. R. Minchin, R. B. O´Hara, G. L. Simpson, P. Solymos, M. H. H. Stevens, and H. Wagner (2015): *vegan: Community Ecology Package*. R package version 2.3-1.

Paulmier, A., D. Ruiz-Pino, and V. Garçon (2011): 'CO_2 maximum in the oxygen minimum zone (OMZ)'. *Biogeosciences*, vol. 8: pp. 239–252.

Peeters, F. J. C. and G. J. A. Brummer (2002): 'The seasonal and vertical distribution of living planktic foraminifera in the NW Arabian Sea'. *Geological Society, London, Special Publications*, vol. 195(1): pp. 463–497.

Peeters, F. J. C., G.-J. A. Brummer, and G. Ganssen (2002): 'The effect of upwelling on the distribution and stable isotope composition of< i> Globigerina bul-

loides</i> and< i> Globigerinoides ruber</i>(planktic foraminifera) in modern surface waters of the NW Arabian Sea'. *Global and Planetary Change*, vol. 34(3): pp. 269–291.

Pflaumann, U., J. Duprat, C. Pujol, and L. Labeyrie (1996): 'SIMMAX: A modern analog technique to deduce Atlantic sea surface temperatures from planktonic foraminifera in deep-sea sediments'. *Paleoceanography*, vol. 11: pp. 15–35.

Prasanna Kumar, S. and T. G. Prasad (1999): 'Formation and spreading of Arabian Sea high-salinity water mass'. *Journal of Geophysical Research*, vol. 104(C1): pp. 1455–1464.

Prell, W. L. and W. B. Curry (1981): 'Faunal and isotopic indices of monsoonal upwelling-western arabian sea'. *Oceanologica Acta*, vol.

R Core Team (2015): *R: A Language and Environment for Statistical Computing*. R Foundation for Statistical Computing. Vienna, Austria.

Reichart, G.-J., S. J. Schenau, G. J. De Lange, and W. J. Zachariasse (2002): 'Synchroneity of oxygen minimum zone intensity on the Oman and Pakistan Margins at sub-Milankovitch time scales'. *Marine Geology*, vol. 185(3): pp. 403–415.

Reimer, P. J. et al. (2013): 'IntCal13 and Marine13 radiocarbon age calibration curves 0-50,000 years cal BP'. *Radiocarbon*, vol. 55(4): pp. 1869–1887.

Rohling, E. J. and W. J. Zachariasse (1996): 'Red Sea outflow during the last glacial maximum'. *Quaternary International*, vol. 31: pp. 77–83.

Schiebel, R., A. Zeltner, U. F. Treppke, and J. J. Waniek (2004): 'Distribution of diatoms, coccolithophores and planktic foraminifers along a trophic gradient during SW monsoon in the Arabian Sea'. *Marine Micropaleontology*, vol. 51(3-4): pp. 345–371.

Schmiedl, G. and D. C. Leuschner (2005): 'Oxygenation changes in the deep western Arabian Sea during the last 190,000 years: Productivity versus deepwater circulation'. *Paleoceanography*, vol. 20(2): PA2008.

Schnetger, B., H. J. Brumsack, H. Schale, and J. Hinrichs (2000): 'Geochemical characteristics of deep-sea sediments from the Arabian Sea: a high-resolution study'. *Deep Sea Research*, vol. 47(14): pp. 2735–2768.

Schulz, H., U. von Rad, and V. Ittekkot (2002): 'Planktic foraminifera, particle flux and oceanic productivity off Pakistan, NE Arabian Sea: modern analogues and application to the paleoclimatic record'. *The Tectonic and Climatic Evolution of the Arabian Sea Region*. Ed. by Clift, P., D. Kroon, C. Gaedicke, and J. Craig. Vol. 195. London: Geological Society Special Publications: pp. 499–516.

Shetye, S. R., A. D. Gouveia, and S. Shenoi (1994): 'Circulation and water masses of the Arabian Sea'. *Proc. Indian Acad. Sci. (Earth Planet. Sci.)* Vol. 103(2): pp. 107–123.

Solanki, S. K., I. G. Usoskin, B. Kromer, M. Schüssler, and J. Beer (2004): 'Unusual activity of the Sun during recent decades compared to the previous 11,000 years.' *Nature*, vol. 431(7012): pp. 1084–1087.

Staubwasser, M., F. Sirocko, P. M. Grootes, and H. Erlenkeuser (2002): 'South Asian monsoon climate change and radiocarbon in the Arabian Sea during early and middle Holocene'. *Paleoceanography*, vol. 17(4): pp. 15–1–15–12.

Telford, R. (2015): *palaeoSig: Significance Tests of Quantitative Palaeoenvironmental Reconstructions*. R package version 1.1-3.

Telford, R. J. and H. J. B. Birks (2011): 'A novel method for assessing the statistical significance of quantitative reconstructions inferred from biotic assemblages'. *Quaternary Science Reviews*, vol. 30(9): pp. 1272–1278.

ter Braak, C. J. F. and S. Juggins (1993): 'Weighted averaging partial least squares regression (WA-PLS): An improved method for reconstructing environmental variables from species assemblages'. *Hydrobiologia*, vol. 269–270: pp. 485–502.

Thamban, M., H. Kawahata, and V. P. Rao (2007): 'Indian summer monsoon variability during the holocene as recorded in sediments of the Arabian Sea: Timing and implications'. *Journal of oceanography*, vol. 63(6): pp. 1009–1020.

Tomczak, M. and J. S. Godfrey (1994): *Regional Oceanography*. Oxford, U.K.: Pergamon.

Tribovillard, N., T. J. Algeo, T. Lyons, and A. Riboulleau (2006): 'Trace metals as paleoredox and paleoproductivity proxies: An update'. *Chemical Geology*, vol. 232(1-2): pp. 12–32.

Ward, B. B., A. H. Devol, J. J. Rich, et al. (2009): 'Denitrification as the dominant nitrogen loss process in the Arabian Sea'. *Nature*, vol. 461: pp. 78–81.

Wedepohl, K. H. (1971): 'Environmental influences on the chemical composition of shales and clays'. *Physics and Chemistry of the Earth*. Ed. by Ahrens, L. H., F. Press, S. K. Runcorn, and H. C. Urey. Oxford: pp. 307–331.

Wyrtki, K. (1973): 'Physical Oceanography of the Indian Ocean'. *The Biology of the Indian Ocean*, vol.: pp. 18–36.

You, Y. (1998): 'Intermediate water circulation and ventilation of the Indian Ocean derived from water-mass contributions'. *Journal of Marine Research*, vol. 56: pp. 1029–1067.

You, Y. and M. Tomczak (1993): 'Thermocline circulation and ventilation in the Indian Ocean derived from water mass analysis'. *Deep-Sea Research Part I: Oceanographic Research Papers*, vol. 40: pp. 13–56.

Zahn, R. and T. F. Pedersen (1991): *Late Pleistocene evolution of surface and mid depth hydrography at the Oman Margin: planktonic and benthic isotope records at Site 724*. Proc. Ocean Drilling Program.